

**FIELD SOLUTION FOR
DIELECTRIC AND RING
LOADED ANNULAR SLOT
ARRAY ANTENNAS**

by

Sima Noghanian

Advisor: Professor L. Shafai

A Thesis
Submitted to the Faculty of Graduate Studies
in Partial Fulfilment of the Requirements
for the Degree of

DOCTOR OF PHILOSOPHY

**Department of Electrical and Computer Engineering
University of Manitoba
Winnipeg, Manitoba, Canada**

© January, 2001



National Library
of Canada

Acquisitions and
Bibliographic Services

395 Wellington Street
Ottawa ON K1A 0N4
Canada

Bibliothèque nationale
du Canada

Acquisitions et
services bibliographiques

395, rue Wellington
Ottawa ON K1A 0N4
Canada

Your file Votre référence

Our file Notre référence

The author has granted a non-exclusive licence allowing the National Library of Canada to reproduce, loan, distribute or sell copies of this thesis in microform, paper or electronic formats.

The author retains ownership of the copyright in this thesis. Neither the thesis nor substantial extracts from it may be printed or otherwise reproduced without the author's permission.

L'auteur a accordé une licence non exclusive permettant à la Bibliothèque nationale du Canada de reproduire, prêter, distribuer ou vendre des copies de cette thèse sous la forme de microfiche/film, de reproduction sur papier ou sur format électronique.

L'auteur conserve la propriété du droit d'auteur qui protège cette thèse. Ni la thèse ni des extraits substantiels de celle-ci ne doivent être imprimés ou autrement reproduits sans son autorisation.

0-612-62661-X

Canada

**THE UNIVERSITY OF MANITOBA
FACULTY OF GRADUATE STUDIES

COPYRIGHT PERMISSION PAGE**

Field Solution for Dielectric and Ring Loaded Annular Slot Array Antennas

BY

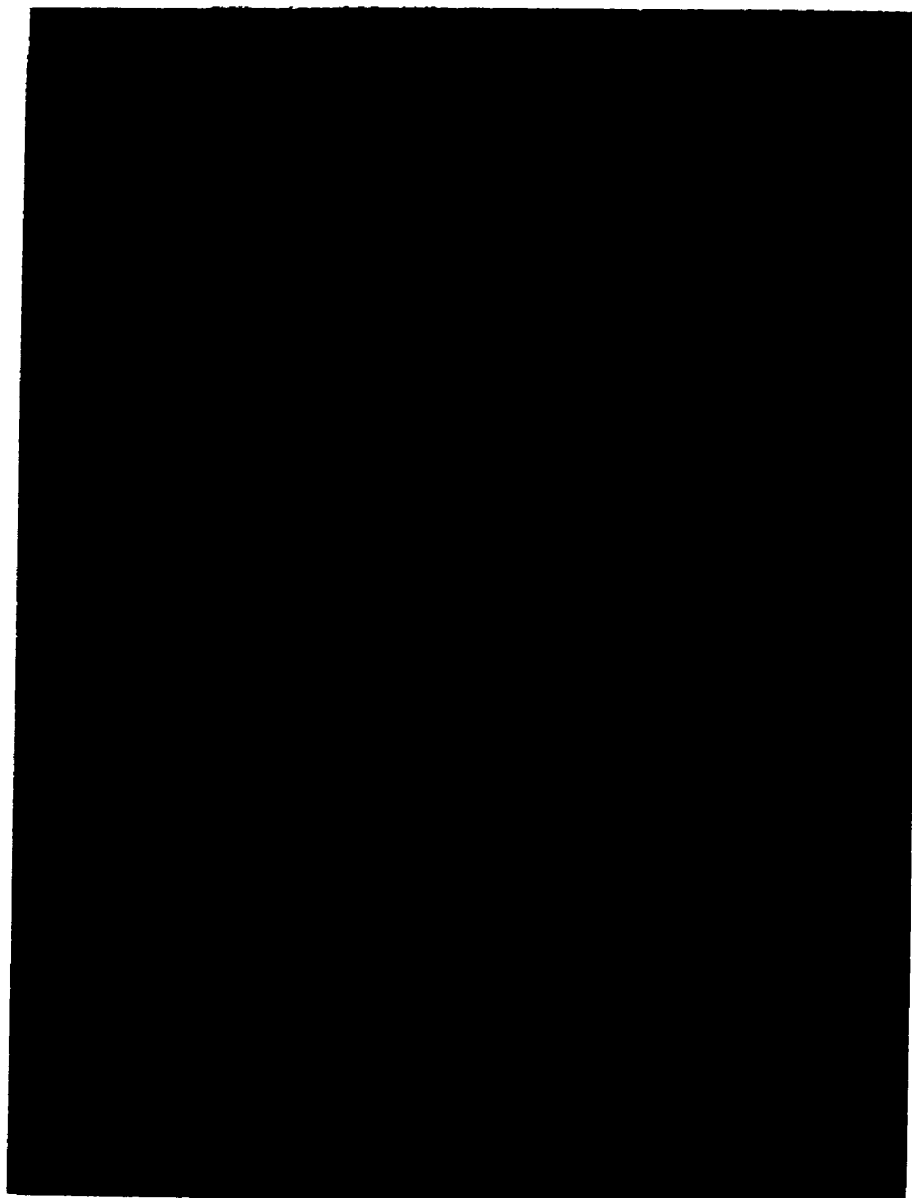
Sima Noghanian

**A Thesis/Practicum submitted to the Faculty of Graduate Studies of The University
of Manitoba in partial fulfillment of the requirements of the degree
of
Doctor of Philosophy**

SIMA NOGHANIAN © 2001

Permission has been granted to the Library of The University of Manitoba to lend or sell copies of this thesis/practicum, to the National Library of Canada to microfilm this thesis/practicum and to lend or sell copies of the film, and to Dissertations Abstracts International to publish an abstract of this thesis/practicum.

The author reserves other publication rights, and neither this thesis/practicum nor extensive extracts from it may be printed or otherwise reproduced without the author's written permission.



to my dearest

Reza and Vahid Fazel-Rezai

and to the memory of

Farangiz Rahnavardi Azari

for all her devotion and sacrifice

Abstract

An analytical method based on the boundary value method is presented, which gives the field solution for annular slot array antennas fed by a radial waveguide or cavity, and loaded by dielectric layers and array of conducting rings. The appropriate Green's functions for different regions of the antenna due to magnetic and electric current rings are obtained. Then, the induced magnetic current over the slots and electric current on the conducting rings are expanded into a Fourier series with unknown coefficients. The final formulation is achieved by employing the Green's functions and applying the boundary conditions. The result is a linear system of equations. The unknown coefficients of Fourier series are obtained by solving this system of equations. Then, the electric field just above the last layer is found and the induced magnetic current is written in terms of the electric field. The far field formulation is derived using this magnetic current. The method is confirmed through comparison of its results with those of available numerical methods and good agreement is obtained. In comparison to these numerical methods, the proposed method is more efficient in computation time and memory requirement.

The formulation is used to study the effects of dielectric loading and conducting ring loading. It is shown that both methods can improve the annular slot array antenna performance. The benefits and problems associated with each configuration are discussed and the effects of various parameters are investigated. Finite structures are also investigated, where open cavities with and without chokes and dielectric cover are used to shape the radiation patterns and improve the performance.

Acknowledgements

This thesis would have never been done without the generous help and support that I received from numerous people along the way. I would like to take this opportunity to express my sincerest thanks to these individuals.

First, and most of all, I would like to express my sincere appreciation and gratitude to Professor *L. Shafai*, for seeing potential in me, having confidence in me and my abilities, and giving me the opportunity to work with one of the best in the field. His patience, invaluable guidance, and constant encouragement made this research interesting and enjoyable. His devotion to his students and his endless energy and enthusiasm have always been a source of inspiration to me.

It is my pleasure to thank the advisory committee members, Professor *P. N. Shivakumar* and Professor *A. Sebak*, for their support and advice during all the phases of this work. Also extended thanks to Professor *S. Safavi-Naeini* for agreeing to review my thesis and serving on my defence committee as external examiner. Also gratefully acknowledged are the *University of Manitoba*, through a graduate fellowship, and of the *Natural Sciences and Engineering Research Council of Canada*, through a grant to Professor *L. Shafai*.

I would like to express my deep appreciation to my colleagues, Dr. *Derek Gray* and Dr. *Michel Clenet*, who helped me with some of the simulations and gave me good ideas along the way. Special thanks also goes to Dr. *Zahra Moussavi* and Ms. *Shelly Girardin* for all their kindness and help whenever I needed them. I am also indebted to Mr.

ACKNOWLEDGEMENTS

Brad Tabachnick, Mr. Mount-first Ng and Mr. Guy Jonatschick for all their assistance with my computer and computer lab. I would like to express my gratitude to *Ms. Lori Ruther* and *Ms. Marlynn Raven* from *Playcare* day care centre, for patiently and passionately taking good care of my son, *Vahid*. In addition, I would also like to thank them for their friendship and support during difficult stages of my research.

This work would not have been possible without the constant support, forbearance and understanding of my family, especially my husband *Dr. Reza Fazel-Rezai*. He always was ready to help me. His valuable review of the entire manuscript led to a number of improvements. I have been lucky to have his friendship and unlimited patience and support. I also would like to remember my mother, *Farangiz Rahnavardi Azari*, who passed away during my course of study. Whenever I was ready to give up, her memory and all her devotion and love made me stand up again and feel stronger.

I am also indebted to my beloved motherland, *Iran*, and her loving people. Finally, I am grateful to **Almighty God**, who provided me with all the opportunity and ability to live in the best way and let me know all these kind people.

Table of Contents

Abstract	i
Acknowledgements	ii
Table of Contents	iv
List of Figures	vii
List of Tables	xvii
Chapter 1 Introduction and Motivation	1
1.1 Preface.....	1
1.2 Statement of the Problem.....	2
1.3 Thesis Organization	6
Chapter 2 Literature Review	8
2.1 Introduction.....	8
2.2 Annular Slot Antenna	8
2.3 Dielectric Loading	17
2.4 Radial Line Slot Antenna.....	22
2.5 Summary	24
Chapter 3 Green's Functions Formulation	26
3.1 Introduction.....	26
3.2 Radial Waveguide	27
3.3 Cavity.....	31
3.4 Partially Filled Waveguide or Cavity.....	33
3.5 One Layer of Dielectric and Free Space.....	34

3.6	Conducting Ring on One Layer of Dielectric	38
3.7	Two Layers of Dielectric.....	46
3.8	Singularity and Branch Points	50
3.9	Summary	52
 Chapter 4 Annular Slot Array Antenna Formulation		53
4.1	Introduction.....	53
4.2	Antenna with One Layer of Dielectric.....	54
4.3	Conducting Ring Loaded Antenna Covered with One Layer of Dielectric.	63
4.4	Antenna Covered with Two Layers of Dielectric	70
4.5	Calculation of Infinite Integrals	72
4.6	Far-Field Calculation for Antenna Loaded with One Layer of Dielectric...	73
4.7	Far-Field Calculation for Antenna Loaded with One Layer of Dielectric and Conducting Rings	
4.8	Far-Field Calculation for Antenna Loaded with Two Layers of Dielectric.	77
4.9	Excitation of Higher Order Modes	78
4.10	Summary	82
 Chapter 5 Results and Discussion		83
5.1	Introduction.....	83
5.2	Confirmation of Boundary Value Method.....	84
5.2.1	Dielectric Covered Annular Slot Array Antenna.....	84
5.2.2	Conducting Ring Loaded Annular Slot Array Antenna.....	94
5.2.3	Input Impedance.....	98
5.2.4	Computation Time	100
5.3	Effect of Various Parameters for Infinite Structure.....	103
5.3.1	Cavity Radius.....	103
5.3.2	Cavity Height.....	110
5.3.3	Slots Locations.....	112
5.3.4	Slots Separation	118

5.3.5	Dielectric Thickness.....	120
5.3.6	Dielectric Spacing.....	125
5.3.7	Dielectric Constant.....	127
5.3.8	Conducting Ring Width	134
5.3.9	Conducting Ring Height	136
5.4	Comparison Between Dielectric and Conducting Ring Loading.....	138
5.5	Finite Structures Parametric Study	142
5.5.1	Antenna Structure	142
5.5.2	Cavity Size and Slot Location.....	144
5.5.3	Conducting Ring and Dielectric Loading	145
5.5.4	Extra Central Slot.....	153
5.5.5	Open Cavity	155
5.5.6	Frequency Bandwidth	160
5.6	Summary.....	161
Chapter 6	Conclusion and Recommendation	164
6.1	Conclusion	164
6.2	Recommendations for Future Research.....	167
Appendix A	Boundary Conditions Implementation	168
Appendix B	Derivation of Magnetic Surface Currents	171
Appendix C	Derivation of Infinite Integrals for Far-Field Calculation	177
References		180

List of Figures

Chapter 1

- Fig.1.1 Configuration of “Annular Slot Array Antenna” with two layers of dielectric.....3

Chapter 2

- Fig.2.1 “Single Annular Slot Antenna” (top view) [7].....9
- Fig.2.2 Annular slot antenna geometry [13].11
- Fig.2.3 Typical annular slot array fed by a radial waveguide [3].....12
- Fig.2.4 Directional cavity-backed annular slot antenna [16].13
- Fig.2.5 Annular slot antenna [18].....14
- Fig.2.6 Configuration of the triplate-fed annular ring slot antenna [19].....15
- Fig.2.7 Dual fed annular slot [25].16
- Fig.2.8 Geometry of multi-frequency antenna [26].16
- Fig.2.9 Geometry of the dielectric loaded annular slot antenna [39].....20
- Fig.2.10 Annular slot antenna on extended hemispherical dielectric lens [42]. ...21
- Fig.2.11 Structure of Radial Line Slot Antennas [55].....23
- Fig.2.12 Single Layer Radial Slot Line Antenna designed by Davis and Bialkowski [57].....24

Chapter 3

- Fig.3.1 Current ring in an infinite radial waveguide.27
- Fig.3.2 Current ring in a cylindrical cavity.31
- Fig.3.3 Partially filled radial waveguide.....33
- Fig.3.4 Magnetic current ring covered with one layer of dielectric.35
- Fig.3.5 Magnetic and electric sources representation of conducting rings loaded annular slot.....39

Fig.3.6	Magnetic current ring loaded with two layers of dielectric.	46
---------	--	----

Chapter 4

Fig.4.1	Slot array antenna on top of radial waveguide and loaded with one layer of dielectric.	56
Fig.4.2	Annular slot array antenna loaded with conducting rings and covered with one layer of dielectric.	64
Fig.4.3	Annular slot array antenna covered with two layers of dielectric.....	70
Fig.4.4	Probe configuration for radial waveguide excitation.	79

Chapter 5

Fig.5.1	Configuration of dielectric covered antenna for comparison with IE3D.	85
Fig.5.2	Radiation patterns for dielectric covered single slot antenna shown in Fig.5.1, comparison between BVM and IE3D, dimensions as group (a) in Table (5-1).....	86
Fig.5.3	Radiation pattern for dielectric covered double slot antenna shown in Fig.5.1, comparison between BVM and IE3D, dimensions as group (a) in Table (5-1).....	87
Fig.5.4	Radiation patterns for dielectric covered single slot antenna shown in Fig.5.1, when the first slot was moved toward the centre, dimensions as group (b) in Table (5-1).....	87
Fig.5.5	Radiation patterns for dielectric covered double slot antenna shown in Fig.5.1, when the first slot was moved toward the centre, dimensions as group (b) in Table (5-1).....	88
Fig.5.6	Radiation patterns for dielectric covered three slot antenna shown in Fig.5.1, when the first slot was moved toward the centre, dimensions as group (b) in Table (5-1).....	88
Fig.5.7	Radome covered three slot antenna configuration for comparison	

	between BVM and IE3D.....	90
Fig.5.8	Radiation patterns for three slot antenna without dielectric radome, comparison between BVM and IE3D.....	90
Fig.5.9	Radiation patterns for three slot antenna covered with dielectric radome as shown in Fig.5.7, comparison between BVM and IE3D.....	91
Fig.5.10	Cavity fed radome covered three slot antenna configuration for comparison between BVM and MBES.....	92
Fig.5.11	Radiation patterns for cavity fed three slot antenna without dielectric radome, comparison between BVM and MBES.....	92
Fig.5.12	Radiation patterns for dielectric covered, cavity fed three slot antenna shown in Fig.5.10, comparison between BVM and MBES.....	93
.Fig.5.13	Radiation patterns for dielectric covered, cavity fed three slot antenna shown in Fig.5.10, when the first slot was moved toward the centre, $\rho_1=0.45\lambda_0$, $\rho_c=\lambda_0$, $\epsilon_{r2}=2.5$, $h_2=0.158\lambda_0$	94
Fig.5.14	Conducting ring loaded annular slot array antenna fed through radial waveguide.	95
Fig.5.15	Radiation patterns for conducting ring loaded single slot antenna as shown in Fig.5.14, comparison among BVM, IE3D and MBES, dimensions as Table (5-3).	96
Fig.5.16	Radiation patterns for conducting ring loaded two slot antenna as shown in Fig.5.14, comparison among BVM, IE3D and MBES.	96
Fig.5.17	Radiation pattern comparison between BVM and experimental data taken from [68], ' pr ' is the power ratio for the TM_{01}/TM_{03} modes.....	97
Fig.5.18	S_{11} for single slot antennas, with and without dielectric cover and conducting rings, dimensions as given in Table (5-1) and Table (5-3)...	99
Fig.5.19	S_{11} for double slot antennas, with and without dielectric cover and conducting rings, dimensions as given in Table (5-1) and Table (5-3)...	99
Fig.5.20	S_{11} for three slot antennas, with and without dielectric cover, dimensions as given in Table (5-2).....	100

Fig.5.21 Cavity radius (ρ_c) effects on the directivity of unloaded annular slot array antennas, n =number of slots, $\rho_I=0.45\lambda_0$, $x=\lambda_0$, $\delta_p=0.1\lambda_0$, $\epsilon_{rI}=1$, $h_I=0.1\lambda_0$ 104

Fig.5.22 Cavity radius (ρ_c) effects on the aperture efficiency of unloaded annular slot array antennas, dimensions as Fig.5.21..... 104

Fig.5.23 Cavity radius (ρ_c) effects on the E-plane side lobe level of unloaded annular slot array antennas, dimensions as Fig.5.21..... 105

Fig.5.24 Cavity radius (ρ_c) effects on the directivity of dielectric covered three slot antennas, when dielectric thickness is ($h_2=0.8\lambda_d$), number of slots=3, $\rho_I=0.95\lambda_0$, $x=\lambda_0$, $\delta_p=0.1\lambda_0$, $\epsilon_{rI}=1$, $\epsilon_{r2}=\epsilon_r$, $h_I=0.36\lambda_0$ 106

Fig.5.25 Cavity radius (ρ_c) effects on the aperture efficiency of dielectric covered three slot antennas, when dielectric thickness is ($h_2=0.8\lambda_d$), dimensions as Fig.5.24..... 106

Fig.5.26 Cavity radius (ρ_c) effects on the E-plane side lobe level of dielectric covered three slot antennas, when dielectric thickness is ($h_2=0.8\lambda_d$), dimensions as Fig.5.24..... 107

Fig.5.27 Cavity radius (ρ_c) effects on the directivity of dielectric covered three slot antennas, when dielectric thickness is ($h_2=0.25\lambda_d$), dimensions as Fig.5.24. 107

Fig.5.28 Cavity radius (ρ_c) effects on the E-plane side lobe level of dielectric covered three slot antennas, when dielectric thickness is ($h_2=0.25\lambda_d$), dimensions as Fig.5.24..... 108

Fig.5.29 Cavity radius (ρ_c) effects on the directivity slot antennas, with and without conducting rings, n =number of slots, $\rho_I=0.45\lambda_0$, $x=\lambda_0$, $\delta_p=0.1\lambda_0$, $\epsilon_{r1,2}=1$, $h_I=0.1\lambda_0$ and for the conducting ring $h_2=0.05\lambda_0$, $L=0.5\lambda_0$ 109

Fig.5.30 Cavity radius (ρ_c) effects on the aperture efficiency of slot antennas, with and without conducting rings, n =number of slots, dimensions the same as Fig.5.29. 109

Fig.5.31 Cavity radius (ρ_c) effects on the E-plane side lobe level of slot antennas,

	with and without conducting rings, n =number of slots, dimensions the same as Fig.5.29.....	110
Fig.5.32	Cavity height (h_1) effects on the directivity, n =number of slots, $\rho_1=0.45\lambda_0$, $x=\lambda_0$, $(\rho_c-\rho_n)=0.05\lambda_0$, $\delta_p=0.1\lambda_0$, $\epsilon_{r1,2}=1$, $h_2=0.5\lambda_0$, for dielectric layer $d=0.25\lambda_d$, $\epsilon_{r3}=2.5$	111
Fig.5.33	Cavity height (h_1) effects on the aperture efficiency, n =number of slots, dimensions the same as Fig.5.32.....	111
Fig.5.34	Cavity height (h_1) effects on the E-plane side lobe level, n =number of slots, dimensions the same as Fig.5.32.	112
Fig.5.35	Effect of first slot location (ρ_1) on the directivity of dielectric covered three and five slot antennas, $x=\lambda_0$, $(\rho_c-\rho_n)=0.05\lambda_0$, $\delta_p=0.1\lambda_0$, $\epsilon_{r1,2}=1$, $h_1=0.1\lambda_0$, $h_2=0.5\lambda_0$, for dielectric layer $d=0.25\lambda_d$	114
Fig.5.36	Effect of first slot location (ρ_1) on the aperture efficiency of dielectric covered three and five slot antennas, parameters were the same as Fig.5.35.	115
Fig.5.37	Effect of first slot location (ρ_1) on the E-plane side lobe level of dielectric covered three and five slot antennas, parameters were the same as Fig.5.35.	116
Fig.5.38	Effect of first slot location (ρ_1) on the directivity of conducting ring loaded antennas, n =number of slots, $x=\lambda_0$, $(\rho_c-\rho_n)=0.05\lambda_0$, $\delta_p=0.1\lambda_0$, $\epsilon_{r1,2}=1$, $h_1=0.1\lambda_0$, $h_2=0.05\lambda_0$, conducting ring width $L=0.5\lambda_0$	117
Fig.5.39	Effect of first slot location (ρ_1) on the aperture efficiency of conducting ring loaded antennas, n =number of slots, parameters the same as Fig.5.38.	117
Fig.5.40	Effect of first slot location (ρ_1) on the E-plane side lobe level of conducting ring loaded antennas, n =number of slots, parameters the same as Fig.5.38.....	118
Fig.5.41	Slot separation (x) effects on the directivity of three and five slot antennas with and without dielectric radome, n =number of slots, $\rho_1=0.45$, $(\rho_c-$	

$\rho_n)=0.05\lambda_0, \delta_\rho=0.1\lambda_0, x=\lambda_0, \epsilon_{r1,2}=1, h_1=0.1\lambda_0, h_2=0.5\lambda_0,$
for dielectric layer $d=0.25\lambda_d, \epsilon_{r3}=2.5$119

Fig.5.42 Slot separation (x) effects on the aperture efficiency of three and five slot antennas with and without dielectric radome, n =number of slots, parameters as given in Fig.5.41.119

Fig.5.43 Slot separation (x) effects on the E-plane side lobe level of three and five slot antennas with and without dielectric radome, n =number of slots, parameters as given in Fig.5.41.120

Fig.5.44 Dielectric thickness (h_2) effects for different dielectric constants ($\epsilon_r=\epsilon_{r2}$) on the directivity of dielectric covered single and double slot antennas, $\rho_l=0.95, \delta_\rho=0.1\lambda_0, x=\lambda_0, \epsilon_{rl}=1, h_l=0.36\lambda_0$121

Fig.5.45 Dielectric thickness (h_2) effects for different dielectric constants ($\epsilon_r=\epsilon_{r2}$) on the aperture efficiency of dielectric covered single and double slot antennas, parameters as given in Fig.5.44.121

Fig.5.46 Dielectric thickness (d) effects for different dielectric constants ($\epsilon_r=\epsilon_{r3}$) on the directivity of single and double slot cavity backed antennas, $\rho_l=0.95\lambda_0, (\rho_c-\rho_n)=0.05\lambda_0, \delta_\rho=0.1\lambda_0, x=\lambda_0, \epsilon_{r1,2}=1, h_l=0.36\lambda_0$122

Fig.5.47 Dielectric thickness (d) effects for different dielectric constants ($\epsilon_r=\epsilon_{r3}$) on the aperture efficiency of single and double slot cavity backed antennas, parameters as given in Fig.5.46.123

Fig.5.48 Dielectric thickness (d) effects for different dielectric constants ($\epsilon_r=\epsilon_{r3}$) on the E-plane side lobe level of single and double slot cavity backed antennas, parameters as given in Fig.5.46.123

Fig.5.49 Dielectric thickness (d) effects for different dielectric constants ($\epsilon_r=\epsilon_{r3}$) on the directivity of single and double slot cavity backed antennas, $\rho_l=0.45\lambda_0, (\rho_c-\rho_n)=0.05\lambda_0, \delta_\rho=0.1\lambda_0, x=\lambda_0, \epsilon_{r1,2}=1, h_l=0.36\lambda_0, \epsilon_{r1,2}=1$ 124

Fig.5.50 Dielectric thickness (d) effects for different dielectric constants ($\epsilon_r=\epsilon_{r3}$) on the aperture efficiency of single and double slot cavity backed

	antennas, parameters are given in Fig.5.49.....	124
Fig.5.51	Dielectric thickness (d) effects for different dielectric constants ($\epsilon_r=\epsilon_{r3}$) on the E-plane side lobe level of single and double cavity backed antennas, parameters are given in Fig.5.49.....	125
Fig.5.52	Effect of spacing between radome and slot plane (h_2) on the directivity, n =number of slots, $\rho_l=0.45\lambda_0$, $(\rho_c-\rho_n)=0.05\lambda_0$, $\delta_\rho=0.1\lambda_0$, $x=\lambda_0$, $\epsilon_{r1,2}=1$, $h_l=0.1\lambda_0$, for dielectric layer $d=0.25\lambda_0$, $\epsilon_{r3}=2.5$	126
Fig.5.53	Effect of spacing between radome and slot plane (h_2) on the aperture efficiency, n =number of slots, other parameters as given in Fig.5.52...	126
Fig.5.54	Effect of spacing between radome and slot plane (h_2) on the E-plane side lobe level, n =number of slots, parameters are given in Fig.5.49.	127
Fig.5.55	Radiation patterns for three slot antennas covered with different dielectric materials, dimensions are given in Table (5-7).	130
Fig.5.56	Radiation patterns for five slot antennas covered with different dielectric materials, dimensions are given in Table (5-7).	131
Fig.5.57	Radiation patterns for single slot antennas covered with different dielectric materials, dimensions are given in Table (5-10)	133
Fig.5.58	Conducting ring width effects on the directivity of cavity backed antennas, dimensions were as given in Table (5-12), n = number of slots and conducting rings.	135
Fig.5.59	Conducting ring width effects on the aperture efficiency of cavity backed antenna, dimensions were as given in Table (5-12), n =number of slots and conducting rings.	136
Fig.5.60	Conducting ring width effects on the E-plane side lobe level of cavity backed antennas, dimensions were as given in Table (5-12), n =number of slots and conducting rings.....	136
Fig.5.61	Conducting ring height (h_2) effect on the directivity of cavity backed antennas, $L=0.5\lambda_0$, other antenna dimensions were as given in Table (5-12), n =number of slots and conducting rings.	137

Fig.5.62 Conducting ring height (h_2) effect on the aperture efficiency of cavity backed antennas, $L=0.5\lambda_0$, other antenna dimensions were as given in Table (5-12), n =number of slots and conducting rings137

Fig.5.63 Conducting ring height (h_2) effect on the E-plane side lobe level of cavity backed antennas, $L=0.5\lambda_0$, other antenna dimensions were as given in Table (5-12), n =number of slots and conducting rings.138

Fig.5.64 Radiation patterns comparison for the original and improved three slot antennas, (a) $\rho_I=0.45\lambda_0$, (b) $\rho_I=0.95\lambda_0$, other parameters: (ρ_C - ρ_n)= $0.05\lambda_0$, $\delta_p=0.1\lambda_0$, $x=\lambda_0$, $\epsilon_{r1,2}=1$, $h_I=0.1\lambda_0$, for dielectric: $h_2=0.5\lambda_0$, $d=0.25\lambda_0$, $\epsilon_{r3}=\epsilon_r$ for conducting ring: $h_2=0.05\lambda_0$, $L=0.5\lambda_0$141

Fig.5.65 Structure of annular slot antenna with finite ground plane.....143

Fig.5.66 Radiation patterns for annular slot antenna of Table (5-15).144

Fig.5.67 Radome covered annular slot antenna with conducting ring added.....146

Fig.5.68 Effect of conducting ring width (L) on the (a) directivity and (b) E-plane side lobe level of the antenna without and with dielectric radome ($R=1.7\lambda_0$, $d=0.15\lambda_0$, $\epsilon_r=2.5$, $h=0.05\lambda_0$).147

Fig.5.69 Effect of conducting ring height (h_I) on the (a) directivity and (b) E-plane side lobe level of the antenna without and with dielectric radome ($R=1.7\lambda_0$, $d=0.15\lambda_0$, $\epsilon_r=2.5$, $L=0.7\lambda_0$).148

Fig.5.70 Radiation patterns for three antennas with and without a conducting ring, Directivity: without conducting ring = 13.40dBi, with conducting ring with ($h=0.05\lambda_0$) = 16.318, and with ($h=0.03\lambda_0$) = 16.085dBi.....148

Fig.5.71 Radiation patterns for three antennas with and without a conducting ring and covered with dielectric ($R=1.7\lambda_0$, $d=0.15\lambda_0$, $\epsilon_r=2.5$) Directivity: without conducting ring = 15.566dBi, with conducting ring with ($h=0.05\lambda_0$) = 17.471, and with ($h=0.03\lambda_0$) = 16.996dBi.....149

Fig.5.72 Effect of dielectric thickness (d) on the antenna directivity nc: No conducting ring is added, wc: with conducting ring ($L=0.75\lambda_0$, $h=0.05\lambda_0$ 150

Fig.5.73 Effect of dielectric radius (R) on the directivity of the antenna without and with a conducting ring ($L=0.75\lambda_0$, $h=0.05\lambda_0$, $d=0.15\lambda_0$)..... 150

Fig.5.74 Effects of dielectric constant on the radiation when there was no conducting ring above the slot. 152

Fig.5.75 Effects of dielectric constant when a conducting ring with the width of $L=0.7\lambda_0$ was located at the height of $h=0.05\lambda_0$ above the slot. 153

Fig.5.76 Radiation patterns for annular slot antenna loaded with dielectric and conducting ring and with one extra slot above the probes, $R=1.7\lambda_0$, $d=0.15\lambda_0$, $\epsilon_r=2.5$, $w=0.04\lambda_0$, $\rho_e=0.20\lambda_0$, $h=0.05\lambda_0$, (a) $L=0.7\lambda_0$, Directivity = 17.409dBi, (b) $L=0.5\lambda_0$, Directivity = 17.897dBi. 156

Fig.5.77 Structure of annular slot antenna covered with dielectric and with open cavity and choke..... 156

Fig.5.78 Effect of open cavity wall size on the directivity of the antenna without dielectric and with dielectric layer ($R=1.15\lambda_0$, $d=0.15\lambda_0$, $\epsilon_r=2.5$), antenna had a conducting ring ($L=0.5\lambda_0$, $h=0.05\lambda_0$) and extra central slot ($w=0.04\lambda_0$, $\rho_e=0.2\lambda_0$), cavity radius (ρ_c)= $1.5\lambda_0$ 156

Fig.5.79 Effect of open cavity wall size on the side and back lobe level of the antenna with configuration given in Fig.5.78. 157

Fig.5.80 Radiation patterns for the antenna with and without open cavity and covered with dielectric ($R=1.15\lambda_0$, $d=0.15\lambda_0$, $\epsilon_r=2.5$) and with conducting ring ($L=0.5\lambda_0$, $h=0.05\lambda_0$) Directivity: without cavity= 16.924dBi , with open cavity= 17.628dBi 157

Fig.5.81 Radiation patterns for the antenna with double choke, Directivity= 18.117dBi , $R=1.15\lambda_0$, $d=0.15\lambda_0$, $\epsilon_r=2.5$, $h_{ck}=0.25\lambda_0$, $t_{ck}=0.06\lambda_0$, $h_{oc}=0.9\lambda_0$ 158

Fig.5.82 Configuration of the antenna with microstrip patch. 159

Fig.5.83 Radiation patterns for the antenna with circular and ring patch added to the dielectric radome, Directivity= 17.531dBi , $d=0.55\lambda_0$, $r_p=0.136\lambda_0$, $r_a=0.9\lambda_0$, $r_b=\lambda_0$, other dimension the same as Fig.5.81. 159

LIST OF FIGURES

Fig.5.84 Radiation patterns for the antenna with circular and ring path added to the dielectric radome, Directivity=16.564dBi, $d=0.55\lambda_0$, $r_p=0.136\lambda_0$, $r_a=0.35\lambda_0$, $r_b=0.45\lambda_0$, other dimensions the same as Fig.5.81.160

Fig.5.85 Frequency bandwidth of three antennas, antenna (a) is shown in Fig.5.65, antenna (b) is shown in Fig.5.67, and antenna (c) is shown in Fig.5.82.161

List of Tables

Table (5-1)	Dimensions for antenna covered with one layer of dielectric.....	86
Table (5-2)	Dimensions for antenna covered with two layers of dielectric.....	89
Table (5-3)	Dimensions for conducting ring loaded antenna.	95
Table (5-4)	Dimensions for double layer microstrip array antenna.....	98
Table (5-5)	Comparison of memory and CPU time requirement between IE3D and BVM.....	101
Table (5-6)	Comparison of memory and CPU time requirement between MBES and BVM.....	102
Table (5-7)	Antenna dimensions for the study of dielectric constant effects, structure the same as shown in Fig.5.10.	128
Table (5-8)	Dielectric constant effects on the directivity, aperture efficiency and E-plane side lobe level of three slot antennas, dimensions are given in Table (5-7).....	129
Table (5-9)	Dielectric constant effects on the directivity, aperture efficiency and E-plane side lobe level of five slot antennas, dimensions are given in Table (5-7).....	129
Table (5-9)	Dielectric constant effects on the directivity, aperture efficiency and E-plane side lobe level of five slot antennas, dimensions are given in Table (5-7).....	129
Table (5-10)	Single slot antenna dimensions for the study of dielectric constant effects, structure the same as shown in Fig.5.10.....	132
Table (5-11)	Dielectric constant effects on the directivity, aperture efficiency and E-plane side lobe level of single slot antennas, dimensions are given in Table (5-10).....	132
Table (5-12)	Dimensions of conducting ring loaded annular slot array antennas.	135

Table (5-13)	Summary of comparison between dielectric and conducting ring loading effects on the annular slot array antenna performance.	139
Table (5-14)	Radiation characteristics for three slot sample antennas loaded with dielectric or ring shown in Fig.5.64.	140
Table (5-15)	Antenna dimensions with finite ground plane.	143
Table (5-16)	Effect of slot location on the directivity.	145
Table (5-17)	Directivity and side lobe level improvement for antennas in Fig.5.70 and Fig.5.71.	147
Table (5-18)	Directivity, E-plane side lobe and back lobe levels for antennas with different dielectric covers ($R=1.15\lambda_0$, $d=0.25\lambda_d$, $L=0.7\lambda_0$, $h=0.05\lambda_0$).	152
Table (5-19)	Effect of narrow central slot on radiation characteristics of the original annular slot antenna, slot location $\rho_e=0.18\lambda_0$	154

Chapter 1

INTRODUCTION AND MOTIVATION

1.1. PREFACE

Wireless and satellite communications are becoming increasingly important for business and private use. Wireless communication has changed our way of life and work. In recent years, internet has also become another means of communication and transfer of information. However, the connection for business and homes is not wide-band and cannot provide high and rapid data rates. This issue can be resolved using wireless technology. However, wireless systems require efficient and high gain antennas at low cost.

Reflector antennas have been used for high gain applications for many years, but they can be expensive and usually very bulky. Recently, printed antennas such as microstrip patch and slot antennas became very attractive in wireless communication, because of their low profile and lightweight. However, they have limited applications because of their low gain and narrow bandwidth. Phased array antennas are another candidate for high gain applications, but as the number of elements increases the feeding

systems become very complex. In addition, there is a drop in efficiency when required gain value is high. This drop is due to the losses in the feed network. In fact, it is difficult to obtain high gain for frequencies higher than 10GHz due to feed networks losses in microstrip array antennas.

The purpose of this work is to study and develop a planar antenna that is easy to fabricate and can be made at low cost. "*Annular Slot Array Antenna*" enjoys a low weight and low profile structures, while it has a simple feeding system. Because of its planar structure, it can be integrated with printed circuits. This kind of antenna systems may be used quite efficiently as a radiating element for mobile communication system especially in the cases where the volume and size of radiator are crucial parameters. Annular slot antenna has also applications as the airborne antenna and radiator for locally induced hyperthermia in cancer treatment.

In general, an array of narrow slots, fed by a radial waveguide, is not a good radiator. When the radial waveguide is air filled, the antenna yields low aperture efficiency. In addition, the E-plane patterns have very high side lobes. The current work is an attempt to improve the antenna aperture efficiency through dielectric loading and some modifications in the structure. An analytical solution based on the boundary value method was developed to formulate the antenna problem. The method was compared with numerical methods and good agreement was achieved.

1.2. STATEMENT OF THE PROBLEM

The basic element of annular slot array antenna, as shown in Fig.1.1, is a slotted

radial waveguide. Slots are co-centered and continues. The radial waveguide is used as the feeding system. The excitation source is located in the central region of the radial waveguide and its field is expressed by a summation of the radial waveguide modes. The waveguide can be partially or fully filled by a dielectric. Therefore, slots can be etched on one side of a dielectric substrate.

Backing the slots with a cavity not only prevents power loss in the parallel-plate region, but also helps to shield the antenna and to suppress unwanted radiation via the substrate edge. Depending on the excitation, the antenna is capable of radiation in broadside or off axis directions.

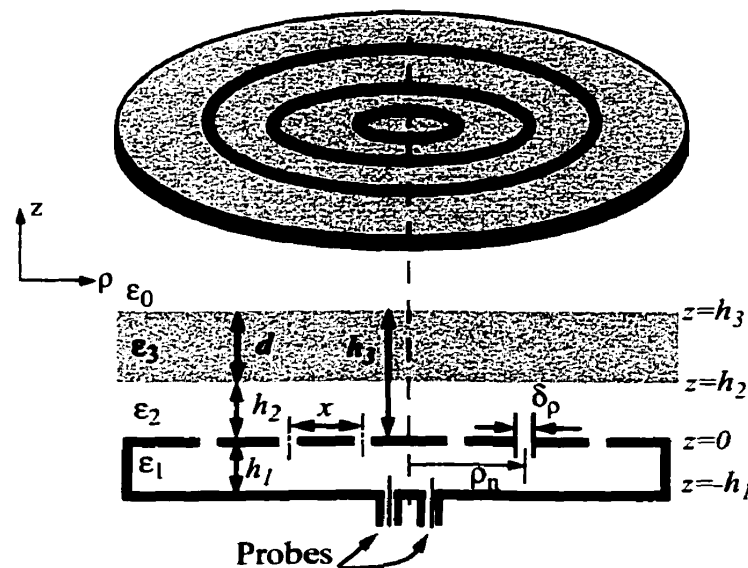


Fig.1.1. Configuration of "Annular Slot Array Antenna" with two layers of dielectric.

In this work, infinite ground plane has been assumed in all cases of analytical solution. To include the effect of finite ground plane, one has to perform analysis using Geometrical Theory of Diffraction (GTD) which is suggested as future work.

Dielectric loading has been used in controlling the radiation properties of dipole and printed antennas during the last few years. Numerous numerical techniques have been proposed and refined in the field of computational electromagnetics, such as Finite Difference Time Domain (FDTD), Finite Element (FE), the Transmission Line Method (TLM) and Method of Moments (MoM). These methods are developed based on recent advances in parallel computing techniques which allow for the implementation of algorithms. They are efficient in terms of computational cost, in order to solve general electromagnetic problems of significant complexity. On the other hand, for special problems with simpler structures such as annular slot array antennas, analytical methods which are fast and need less computational facilities seem to be more efficient. Most of the existing analytical approaches to the problem of annular slot antenna are based on simplified models. Majority of the methods assume that the aperture field distribution is equal to unperturbed field of the feeding waveguide. This means that the effect of all the higher order modes that are excited due to discontinuity on the slots is neglected. Furthermore, most of the existing methods do not consider more than one slot in the structure. However, the efficient radiator is generally formed by more than a single slot. The number of slots and their relative location are the key parameters in pattern shaping. This means that effective solution must take into account the mutual coupling between the slots.

The present work is an extension of the work done by Azarbar and Shafai [1]-[4]. The boundary value method suggested by them is extended for the case of antenna covered with dielectric and loaded with conducting rings. The method was used to

improve the antenna radiation characteristics. In spite of most of the pervious studies, which assume TEM mode as the only excited mode, there is no restriction on the excitation. In fact excitation can be presented as the summation of different radial waveguide modes. The boundary condition on slots and dielectric layer were applied to create a system of equation in matrix form, which can be solved numerically.

This method is much faster and more efficient than numerical methods and since unknowns are only considered on the slots, the number of segments are considerably smaller than numerical methods. In fact numerical tools such as Multi-Body Electromagnetic Scattering (MBES) package which uses method of moments for bodies of revolution and IE3D Zeland Software were used to solve the problem of dielectric loaded annular slot array antennas, at first. But due to some limitations these packages were unable to efficiently solve the problem with cavity-backed and multi-layers of dielectric. The number of unknowns in Boundary Value Method (BVM) are in the order of number of slots, i.e. for the single slot antennas there is only one unknown for both original and dielectric loaded antennas. When the conducting ring is added on the top depending on the ring width one unknown per 0.1 wavelength of the ring width will be added. While for MBES the number of unknowns depends on the structure. For original antenna, this is about 50 per slot. By adding the dielectric layer it increases to about 100-120 per slot. Adding the conducting rings adds about 2 unknowns per 0.1 wavelength for ring width. For IE3D there are about 300 unknowns for a single dielectric loaded slot antenna, and by adding the ring this increases to 900. For IE3D the number of unknowns does not increase linearly by adding the slots. These numbers are for waveguide fed

antennas and by adding the cavity the number of unknowns increases.

However, because of the generality of numerical methods, and their ability to model finite structures, they were used later to investigate the effect of finite dielectric and some innovations and modifications in the structure which are suggested to improve circular polarization and reduce the back radiation.

1.3. THESIS ORGANIZATION

A review of existing methods for formulation of structures similar to annular slot array antennas is presented in Chapter 2. The proposed method for field solution for dielectric loaded annular slot array antenna is described in Chapter 3 and Chapter 4. The first part of Chapter 3 is a review of Green's functions for radial waveguide and cavity with annular slots, derived by Azarbar and Shafai [1]. The second part is dedicated to derivation of Green's functions for three different new structures:

1. Magnetic current ring covered with one layer of dielectric
2. Magnetic current ring covered with one layer of dielectric in combination with an electric current ring.
3. Magnetic current ring covered with two layers of dielectric

Then branch points and singularities are discussed.

Using the results from Chapter 3, the problems of annular slot array antenna for structures containing dielectric layers or conducting rings are formulated in Chapter 4. Then, the far-field formulation is carried out. Finally, The excitation of higher order modes is discussed at the end of this chapter.

Chapter 5 presents some numerical results. The first part describes the numerical simulation programs which were used to confirm the results from proposed method. The numerical and analytical methods are used for similar problems and the results are compared. The effects of various parameters of the antenna on the radiation characteristics are examined using both numerical and analytical methods. New structures are also suggested to improve antenna efficiency and circular polarization. The dielectric and conducting ring loading effects on the frequency bandwidth are discussed as well.

Finally, Chapter 6 summarizes the results and presents concluding remarks and recommendations for future work.

Chapter 2

LITERATURE REVIEW

2.1. INTRODUCTION

In this chapter a review of prior art is given. It is divided into three sub-sections. The first section summarizes the research on the antennas which include annular slots in their structure. In the next section pervious work on dielectric loading for slot antennas in general is reviewed and the third section is dedicated to the literature about radial slot line antenna.

2.2. ANNULAR SLOT ANTENNA

The problem of circular diffraction antenna, which consists of a coaxial waveguide fitted in an infinite-plane conducting baffle and open to free space, was considered by Levine and Papas in 1950 [5]. The antenna was assumed to operate with a single propagation mode (the principle mode) in coaxial region. The principle mode of coaxial waveguide has no angular variation in any plane normal to its propagation direction.

In search for new antennas, at the end of the 1950s, Kelly introduced the concept of *annular slot planar antenna* [6]. Goebels and Kelly demonstrated the use of this kind of antenna in the early 60's in [7] and [8]. In [7], the analysis and design of antennas which can radiate circular, linear or elliptical polarization by adjustment of feed circuit were discussed. The slots were located on upper plates of radial waveguide and were composed of annular slots, with each annulus consisting of a discrete number of crossed slots (Fig.2.1). Both standing wave (cavity-backed) and travelling wave antennas (with match absorber at the end) were discussed. Only single mode (TM_{01}) was considered and magnetic fields in the radial waveguide were taken as the excitation, then the location of the slots were defined so that radial and angular component of magnetic fields were equal. This would give the linear polarization. To radiate arbitrary elliptical polarization, two TM_{01} modes of the appropriate amplitude and phase are required. The arbitrary polarization, however, is achievable only in the region of the main beam and nearin lobes. For standing wave antenna, the cavity was fed at its centre from a circular waveguide.

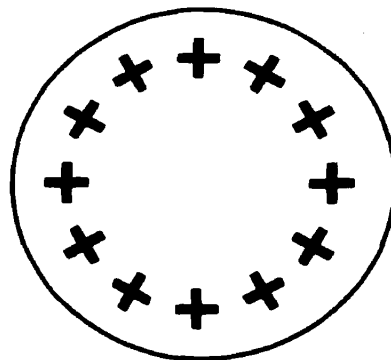


Fig.2.1. "Single Annular Slot Antenna" (top view) [7].

Based on this antenna a monopulse antenna was proposed [8]. Monopulse operation was obtained by dividing the transmission line into four independently excited quadrants, each of which was propagating a field configuration identical to the dominant TE_{10} radial waveguide mode. Again the field on the slots were assumed to be the dominant propagating mode inside the radial waveguide and the far fields were approximated by the far fields for continuous annular slot. Slots were tilted such that gain became maximum.

Cavity-backed annular slot antenna has also been studied in [9]. Both cylindrical and coaxial cavity were considered and variational techniques were used to solve the problem. An idealized source with no azimuthal variation was assumed. The method is not applicable for higher order modes and deep cavities. The numerical calculation emphasizes narrow slots and shallow cavities. Dielectric cavity loading was also found to decrease the size of resonant cavity in the price of decreasing the bandwidth.

The problem of a flush-mounted annular slot antenna, driven by an incident current wave in a coaxial line, was studied by Chang [10]. In his study, he considered the effect of higher order TM_{0n} modes to the admittance and near field distribution. The analytical and closed form expressions for the input admittance and the near field distribution were obtained by approximating the integral equation for aperture field and subsequently solving the equation indirectly with conformal transform technique. The method is only applicable to problems involving narrow apertures.

Theory of the annular slot antenna was developed based on the principle of duality in [11]. The electric field in the slot was replaced by the magnetic current. Then the image

theorem was used. The magnetic vector potential was written in terms of this magnetic current. It was assumed that the electric field on the slot was due to TEM mode in the coaxial line.

An analysis of the radiation pattern produced by the open-ended radial waveguide with Transverse Magnetic (TM) mode excitation was presented by Holst [12]. The fields inside the waveguide for TM modes were replaced by equivalent magnetic and electric currents and the far-field was determined using these currents.

The problem of a TEM excited annular slot antenna embedded in an infinite perfectly conducting ground plane (Fig.2.2) was solved using a boundary value treatment in [13]. The effect of higher order TM modes which exist in the vicinity of aperture was included in the solution. A closed form solution for the antenna admittance was given.

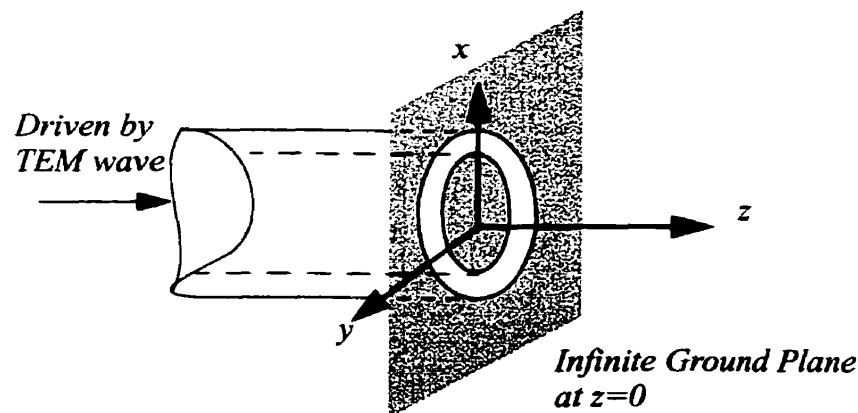


Fig.2.2. Annular slot antenna geometry [13].

Azarbar and Shafai [1]-[4] developed a boundary value method for the annular slot array antenna (Fig.2.3). In spite of most of the previous studies, which assume TEM mode as the only excited mode, there was no restriction on the excitation. Excitation can be

presented as the summation of different radial waveguide modes. The effect of all the higher order modes, which are excited in the vicinity of slots, and also mutual coupling between the slots were included in the solution. The result of applying boundary condition on the tangential magnetic field on slots, was a system of equation, which can be solved using the Galerkin's method. The only assumption made was that the slot width is electrically small enough to suppress the azimuthally directed induced currents over their surfaces.

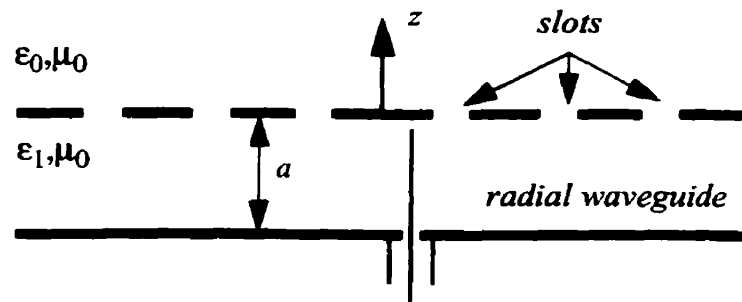


Fig.2.3. Typical annular slot array fed by a radial waveguide [3].

Butler and Keshavamurthy [14] developed an integral equation for annular slot antenna on radial waveguide. Excitation was assumed to have no angular dependency (TEM mode). Green's function for inside the waveguide was obtained, and by enforcing of continuity of magnetic field on the slots the integral equation was found and solved numerically using the method of moments. The pulse functions were used as basis functions. Similar method was used by Nevels *et al.* [15] to form and solve an integral equation for a coaxially fed annular aperture antenna. Both the coaxial probe opening into a ground plane and extending into biological tissue type were studied. In the second case

the exterior region consisted of air, fat, bone or muscle. The basis functions used in this paper were in the form of $1/r$, where r was the radial co-ordinate.

A cavity-backed annular slot array directional antenna was patented by Luedtke and Bentley [16] for radio directional finding applications. A single cavity of this shape was suggested as an antenna for large aperture array. The second and third cavities with slots were added concentric with the first one to extend the range.

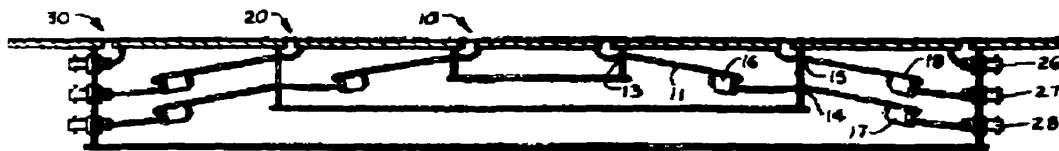


Fig.2.4. Directional cavity-backed annular slot antenna [16].

Analysis of a cavity-backed slot antenna with one point shorted was performed by Morishita *et al.* [17]. The Green's function for cavity was derived and the magnetic current on the slot was found using the method of moments. The current was expanded by piecewise sinusoidal functions. The slot aperture was shorted at one point to obtain a wide bandwidth or variation in the radiation pattern. It was shown that the polarization can be changed from linear to circular, depending upon the position of the short on the slot.

Munson and Schentzer [18] introduced a slot-type antenna with unidirectional sensitivity. Antenna feed, as shown in Fig.2.5, was in a form of corporate feed, consisting of two non-resonant cavities. The lower cavity had the height of half a wavelength and the upper cavity had the height of a quarter of wavelength. In the same reference, they also presented an antenna with four annular slots with the feeding network of three cavities.

They also suggested adding polarizers, which cross the slots at an angle, to suppress cross polarization and enhance the directivity.

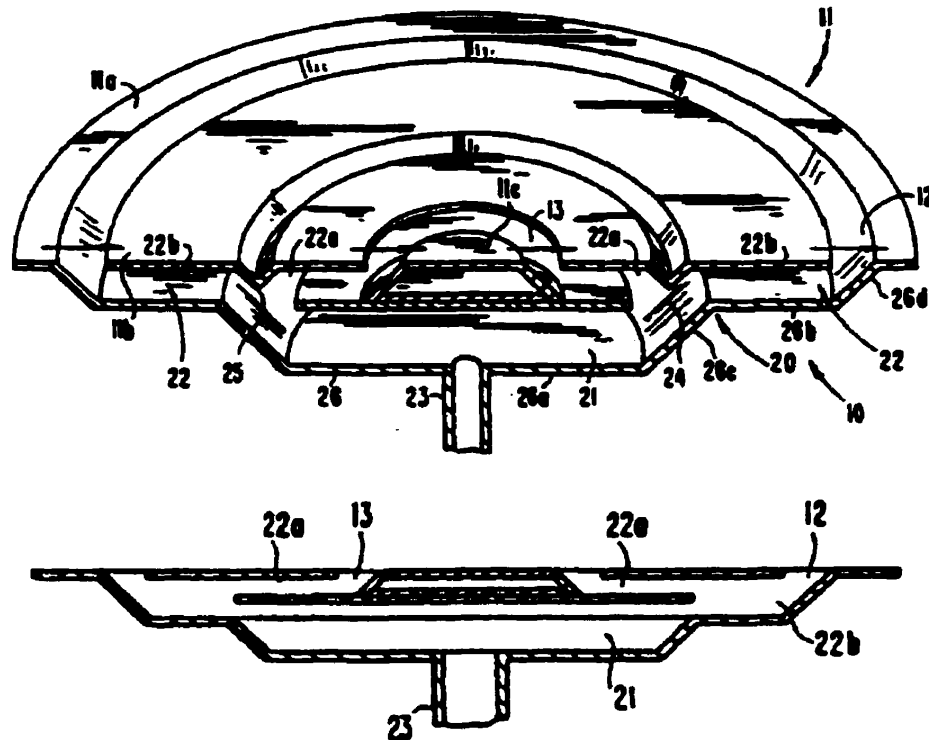


Fig.2.5. Annular slot antenna [18].

Chen *et al.* [19] modeled the stripline-fed planar printed aperture antenna elements including annular-ring slot antennas. They used triangular-patch basis functions and built upon the Mixed Potential Integral Equation (MPIE) formulation which accounts for all mutual coupling effects between the stripline and the aperture. The MPIE was solved with Galerkin's method. They used this method to investigate the triplate-fed annular ring slot antenna (Fig.2.6). They shaped the ring by adding two stubs to control the resonance frequency. They studied the effect of stub dimension on the Circular Polarization (CP).

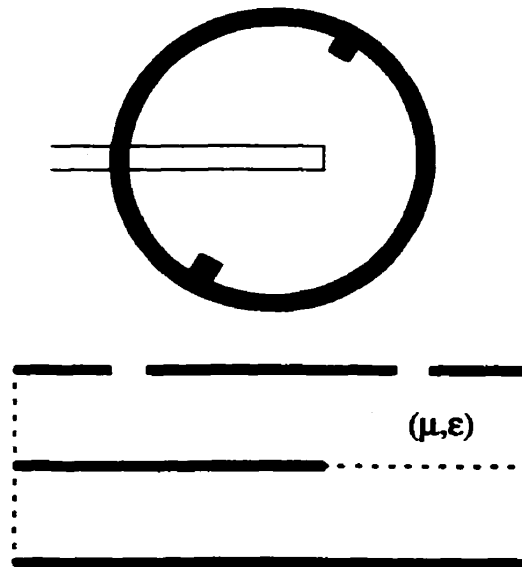


Fig.2.6. Configuration of the triplate-fed annular ring slot antenna [19].

Nikolic [20] developed an empirical model of the annular slot antenna. She derived the antenna parameters assuming an electric field of $1/r$ form in the slot region. Her analysis was based on a transmission line representation of the slot antenna. She included the effect of finite ground plane by the use of Geometrical Theory of Diffraction (GTD). Later, Nikolic *et al.* ([21]-[22]) solved the cavity backed annular slot antenna using the Magnetic Field Integral Equation (MFIE) with considering inhomogeneously filled cavity. The integral equation was solved by variational method. They also used this method to solve the coaxial array of annular slots ([23]-[24]), using separate feeds for each slot.

Zeilinger and Sengupta presented analysis of the dual-fed annular slot antenna based on MFIE in [25]. The annular slot was fed via two delta gap feeds with an amplitude of unity (Fig.2.7). The slot was resonant and phase difference between two feeds was set

to excite only the resonant mode. The dual fed annular slot showed improved uniformity of the magnetic current distribution.

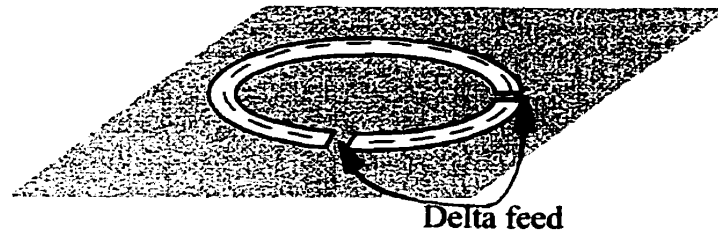


Fig.2.7. Dual fed annular slot [25].

The annular slot antenna was also used as multi-frequency antenna. Tehrani and Chang analyzed a single feed multi-frequency annular slot antenna with the method of moments [26]. They proposed the structure shown in Fig.2.8. A microstrip line was coupled electromagnetically to the slot ring, extended to the centre and coupled to the slot ring again at 235 degrees. Microstrip line is left open at the end. The frequency ratio was 1.3.

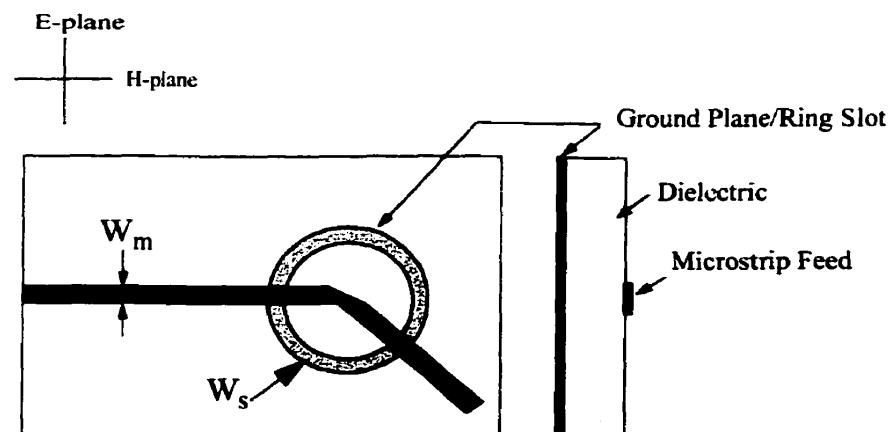


Fig.2.8. Geometry of multi-frequency antenna [26].

2.3. DIELECTRIC LOADING

The effect of dielectric loading as a radome cover has been investigated by several authors. Radome was mainly used for streamlining and protection from the external environment, but dielectric loading is also considered for modeling the lossy environment for biomedical applications or improving the antenna characteristics. Lens and dielectric resonator excited by slot antennas were also modeled as a dielectric cover in some literature.

As an early work, Jones [27] considered the problem of dielectric coated, TEM mode excited parallel-plate aperture. He determined the input impedance of the structure by using the Fourier transform theory, convolution theorem and appropriate boundary conditions in the aperture plane. Two cases were considered: 1) effect of the air gap on the admittance of dielectric coated aperture antenna, and 2) the admittance of an aperture antenna coated with an under dense plasma slab. He found that the most significant changes in input impedance occur whenever the thickness of the first layer of dielectric was less than quarter wavelength in dielectric. Also input impedance was more sensitive when the permittivity of the dielectric layer was increased or the slot width was reduced.

Baily and Calvin [28] derived the input impedance of a circular waveguide opening onto a dielectric coated ground plane. It was assumed that only the dominant mode, TE_{11} mode, was excited at the aperture. Baily [29] also investigated the input impedance of dielectric loaded narrow slot in the broad face of a rectangular waveguide, when the dominant mode was excited. He used extended Oliner's equivalent circuit for

rectangular waveguide with a narrow slot in the board wall to dielectric coated slot.

Nevels and Butler [30] formulated the problem of an infinite slot in a conducting screen situated between two dielectric slabs with different electromagnetic properties. The slot was illuminated by Transverse Electric field (TE mode). They derived an integral equation in terms of transverse component of the electric field in the slot or equivalently the slot magnetic current. Method of moments with pulse basis functions was used to solve this equation. In [31] the same approach was used to solve the problem of slot in a parallel-plate waveguide covered by a dielectric slab with incident TEM wave. Nevels and Butler compared the radiation pattern properties of two cases with and without dielectric slab. They reported considerable improvement in directivity and recommended devising a method of reducing or eliminating the effect of surface wave edge diffraction when the ground plane is finite. In [32], Butler developed analytical solution for electric field in a narrow slot in a conducting screen between two half-spaces. The solution was obtained for both TE and TM excitations and expressed as the product of a weight function and a series of Chebyshev polynomials.

Kishk and Shafai [33] studied the problem of gain enhancement for an electric dipole above finite ground plane and covered with finite dielectric sheet numerically. They used method of moments for bodies of revolution to investigate the effect of different parameters and concluded that for finite structures the gain enhancement is more than that for infinite structures. They indicated that the best spacing between dielectric layer and ground plane is half a wavelength and the optimum thickness of dielectric was quarter wavelength in dielectric.

Sugio *et al.* studied dielectric loading of slot antennas both theoretically and experimentally. In [34], the problem was analyzed using variational technique for both finite and infinite dielectric sheets. The problem of dielectric loading for rectangular and circular slots were investigated numerically in [35] and [36] respectively. In [37] Sugio *et al.* studied triplate type dielectric loaded patch experimentally. In the case of rectangular slot they showed that a beam tilt is achieved with deviation of the center positions of the dielectric. They indicated that dielectric loading spreads the frequency bandwidth for the case of finite dielectric. In the array of circular slots loaded with circular cylindrical dielectric loads, they were able to reduce the grating lobes even when the spacing was wider than a wavelength.

Tong and Blundell [38] analyzed the radiation properties of annular slot antenna on a dielectric half-space using Galerkin's method applied in the Hankel transform. The dielectric half-space was considered as a lens. Since the lens is electrically large, the radiating element acts as if it is radiating into half-space. By the use of Equivalence Principle they replaced the electric field on the slot by a magnetic current and applied the boundary condition to form the system of equations in terms of the magnetic current. Then the magnetic current was expanded as Fourier series. They introduced double fed annular slot as magic slot radiator. By changing the feed configuration, the dominant polarization was changed.

Kaklamani *et al.* [39]-[40] investigated the radiation properties of various types of dielectrically loaded radiators including an annular slot antenna of infinitesimal aperture, cut in an infinite ground plane and covered by dielectric cylinder of finite height (Fig.2.9).

The excitation was assumed to be circumstantially constant voltage at the slot opposite edges. The unknown electromagnetic field was expressed using the mixed mode spectrum of a radial dielectric waveguide. Then by enforcing the appropriate boundary conditions, an integral equation was derived in term of unknown electric field. This equation was solved using the Galerkin's technique (using Laguerre polynomial as basis functions).

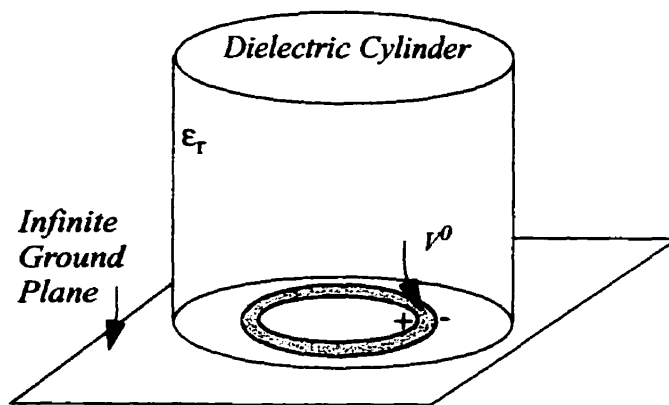


Fig.2.9. Geometry of the dielectric loaded annular slot antenna [39].

Wheeler and Nevels [41] studied the annular slot covered by dielectric hemisphere. The structure consisted of a coaxial line flush mounted on an infinite ground plane and covered by a dielectric hemisphere. Assuming TEM mode propagation inside the coaxial line, the wave equation was solved for TM_r mode. The Green's functions for the dielectric region were expressed in terms of their separated homogeneous and particular solutions. The unknown coefficients for these expansions were found by applying the continuity of tangential electric and magnetic fields. Their results showed that radiation efficiency significantly improved by adding the dielectric hemisphere on top of coaxial line. This was due to improvement in impedance matching. Also the beamwidth

was notably less than the case of homogeneous free space region.

Colomb *et al.* [42] carried out a full wave analysis in the spectral domain for modeling the fields of annular slot covered by one layer of dielectric and a lens as shown in Fig.2.10. Their analysis indicated that the E and H-plane beamwidths can be adjusted by varying the thickness of the dielectric layer. The analysis was done at 35GHz and 94GHz for mm-wave quasi-optical applications and as primary feed in reflector antenna.

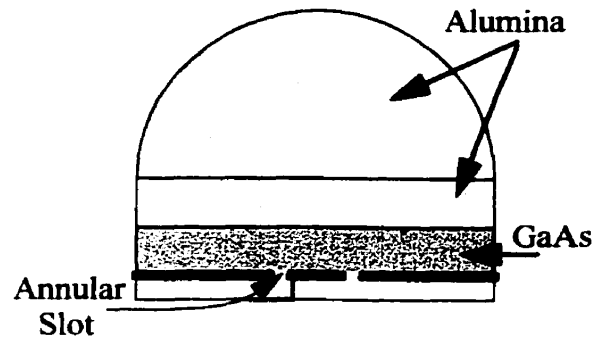


Fig.2.10. Annular slot antenna on extended hemispherical dielectric lens [42].

Different combinations of annular slot and dielectric resonator were also investigated in the literature. Michalski *et al.* [43] considered the problem of a cylindrical dielectric-post resonator with an annular slot in the upper plate. Their analysis was based on integral equation for the electric field in the slot which was solved numerically by the method of moments. They limited the solution to the axis-symmetric TM_{0n} modes. They showed that the complex resonant frequency could vary by changing the slot location and width. Leung *et al.* [44] investigated the slot coupled dielectric resonator antenna experimentally. Similar to previous work, the resonant frequency could be tuned by changing the slot width and radius.

2.4. RADIAL LINE SLOT ANTENNA

There has been extensive effort to investigate and improve a group of antennas called “Radial Line Slot Antenna” (RLSA). Basically two groups; Ando *et al.*, and Davis and Bialkowski; have worked on this kind of antenna. The idea was taken from Goebels and Kelly [7] and first published by Ando *et al.* [45]. The antenna was designed for circular polarization for the application in receiving direct broadcast from a satellite (DBS). As it is shown in Fig.2.11.(a), a three plate waveguide was used to compose a twofold radial line waveguide. The slots were on the top plate. Feeding was located at the centre of the lower waveguide and a radially outward traveling wave mode was generated. At the outer edge of the waveguide, it was transferred into a radially inward traveling-wave mode in the upper waveguide. The angle of each slot was designed such that they gave correct phase for circular polarization. The effect of coupling between slots and waveguide was discussed in [46]-[48]. Single layered RLSA was introduced in [49]-[51]. To achieve uniform distribution in single layered RLSA, the length of the slots must vary. The application of RLSA in millimeter frequency like wireless Local Area Network (LAN) was discussed in [52]. Linear polarization was achieved using RLSA with concentric slot arrangement [53]. The main problem with linearly polarized RLSA (LP-RLSA) was high return loss. A method of reflection cancelling was given in [54] by using the additional slot sets. In [55] slot parameters optimization for concentric array RLSA was discussed.

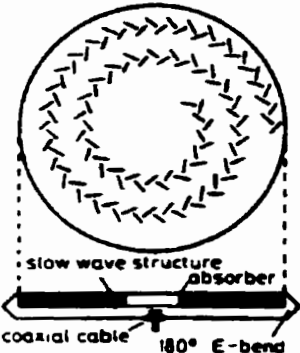
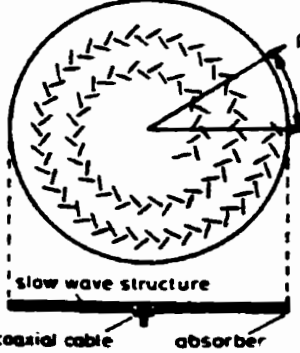
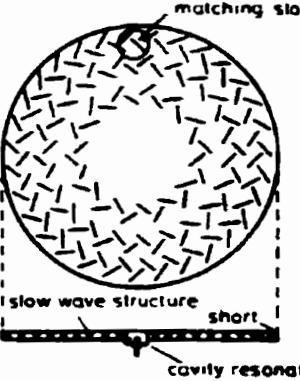
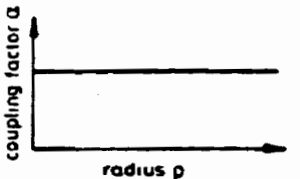
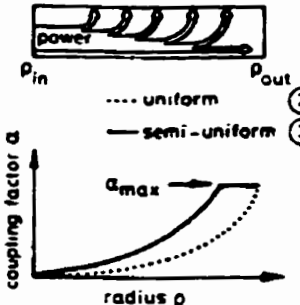
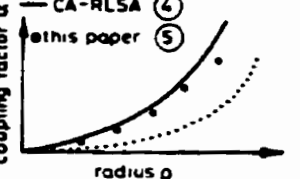
	DL-RLSA	SL-RLSA	CA-RLSA
structure			
layer	double layer	single layer	single layer
slot arrangement	spiral	spiral	concentric
aperture illumination synthesis	uniform coupling distribution ① 	continuous source model  coupling factor α vs radius p --- uniform ② — semi-uniform ③ α_{max}	conventional continuous source model ($\alpha_{max} = \infty$) this paper discrete source --- SL-RLSA ② — CA-RLSA ④ ● this paper ⑤ 
slot coupling analysis	experimental analysis (a)	waveguide region --- fig. 3 (a) (b)	conventional inner slots --- fig. 3 (a) matching slots --- fig. 3 (b) this paper --- fig. 3 (c) (c)

Fig.2.11. Structure of Radial Line Slot Antennas [55].

Davis and Bialkowski mainly worked on single layered linearly polarized RLSA [56]-[58] (Fig.2.12). They used different feed system and reflection cancelling slots. They also proposed the beam squinting method to reduce the return loss.

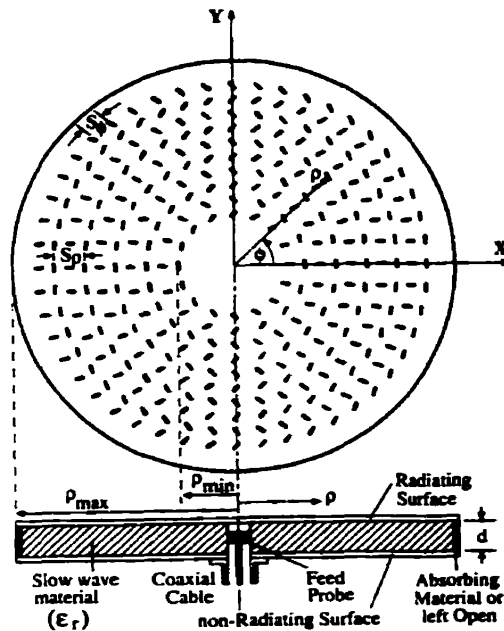


Fig.2.12. Single Layer Radial Slot Line Antenna designed by Davis and Bialkowski [57].

2.5. SUMMARY

From the literature review the following remarks can be concluded

- In most of the investigations only TEM mode was assumed. This means there was no angular variation in the excitation. The effect of the higher order modes in the vicinity of slots was mostly ignored.
- When the higher order modes were considered, problem was solved numerically, that required solving complicated matrix equations.
- To improve annular slot antennas efficiency complicated feeding systems and slot shapes were proposed.

- Dielectric loading was considered as a method to improve efficiency and other antennas characteristics for similar structures.

This thesis is an attempt to investigate the problem of “dielectric and conducting ring loaded annular slot array antenna” in an analytical approach. The analytical approach has the advantage of simplicity for user to set up the problem and efficiency over the numerical methods. The expressions for the fields on the surface of the antenna and far radiation are in closed form. This gives a physical sense of how the field changes in space and gives an easy and fast way to calculate the field values at any point in space. Both TE and TM modes are considered and the effect of mutual coupling between the slots is also included in the solution.

In the next chapter, Green’s functions for dielectric loaded annular slot are derived. These will be used to formulate and solve the wave equation for dielectric loaded annular slot array antenna.

Chapter 3

GREEN'S FUNCTIONS FORMULATION

3.1. INTRODUCTION

Generally the annular slot array antenna consists of two parts: 1) radial waveguide or cavity for feeding the slots, and 2) the upper side which consists of free space, dielectric layers and conducting rings. The first step to formulate the problem is to derive the Green's functions for each part. Green's function is simply the field solution when the slot is replaced by a thin ring of magnetic current. The Green's functions for the first part of the antenna was derived by Azarbar and Shafai [2] and a review of their results is given in 3.2 and 3.3. The modification for partially filled cavity is added to this formulation (3.4).

In Azarbar and Shafai's work slots are opened to free-space. Because of the assumption of narrow slots, electric field on the slots has only the radial component. This causes a poor aperture distribution and low aperture efficiency. To improve the aperture distribution, adding the dielectric and conducting ring is proposed, in this thesis, and the Green's functions are derived in the rest of this chapter. In order to formulate the Green's

functions for structures containing the dielectric and rings, three different cases are considered for the upper side of the antenna. First the Green's functions for a magnetic current ring with one layer of dielectric on top are found. The next step is adding the conducting ring as the second source. At last two layers of dielectric on top of the magnetic current ring is studied. The development of the Green's functions for these three cases are discussed in details in this chapter. In the next chapter these Green's functions are used to formulate the annular slot array antenna loaded with one or two layers of dielectric or one layer of dielectric and array of conducting rings.

3.2. RADIAL WAVEGUIDE

Consider the case when the radial waveguide is feeding an annular slot of zero width. It is assumed that the guide is of infinite extent in ρ (radial) direction (Fig.3.1). In practice this condition may be simulated by adding the absorbers.

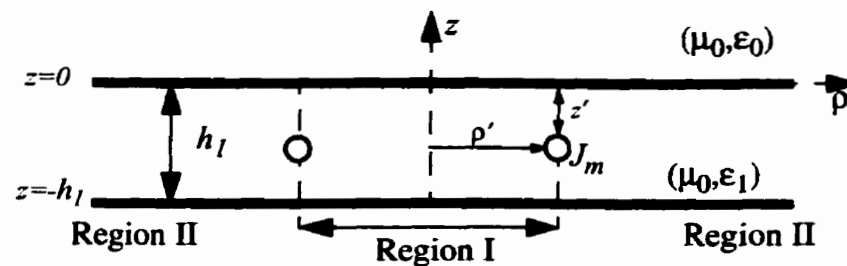


Fig.3.1. Current ring in an infinite radial waveguide.

The Green's functions, in fact, describe the impulse response to the magnetic current ring of strength $I_m(\phi')$, located at a radius $\rho = \rho'$ (Fig.3.1) and characterized by

$$\vec{J}_m = I_m(\phi')\delta(\rho - \rho')\delta(z - z')\hat{\phi}' \quad (3-1)$$

where $I_m(\phi')$ is a piece-wise continuous function of the azimuthal angle ϕ' , and (ρ', ϕ', z') are the source coordinates. $\hat{\phi}'$ is a unit vector tangent to the current source and representing the direction of the current flow. A time variation of $\exp(j\omega t)$ is assumed and suppressed throughout. The source function may be expanded in a Fourier series of the following form

$$I_m(\phi') = \sum_{n=0}^{\infty} (a_n \cos n\phi' + b_n \sin n\phi') \quad 0 \leq \phi' \leq 2\pi \quad (3-2)$$

where

$$\begin{aligned} a_n &= \frac{\epsilon_n}{2\pi} \int_0^{2\pi} I_m(\phi') \cos n\phi' d\phi' \\ b_n &= \frac{\epsilon_n}{2\pi} \int_0^{2\pi} I_m(\phi') \sin n\phi' d\phi' \\ \epsilon_n &= \begin{cases} 1 & n = 0 \\ 2 & n > 0 \end{cases} \end{aligned} \quad (3-3)$$

The source singularity suggests dividing the medium between the conductors into two distinct regions, namely region I for $\rho < \rho'$ and region II for $\rho > \rho'$. An arbitrary electromagnetic field in a homogeneous cylindrical region can be expressed as the sum of the TM and TE fields to the z -direction. The total electric and magnetic fields can then be calculated from [59]

$$\begin{aligned}\vec{E} &= -\nabla \times (\Psi^h \hat{z}) + \frac{1}{j\omega\epsilon} \nabla \times \nabla \times (\Psi^e \hat{z}) \\ \vec{H} &= \nabla \times (\Psi^e \hat{z}) + \frac{1}{j\omega\mu} \nabla \times \nabla \times (\Psi^h \hat{z})\end{aligned}\quad (3-4)$$

where Ψ^e and Ψ^h are the solutions of the wave equation. The set of equations (3-4) in cylindrical coordinates are represented by [59]

$$\begin{aligned}E_\rho &= \frac{1}{j\omega\epsilon} \frac{\partial^2 \Psi^e}{\partial \rho \partial z} - \frac{1}{\rho} \frac{\partial \Psi^h}{\partial \phi} & H_\rho &= \frac{1}{\rho} \frac{\partial \Psi^e}{\partial \phi} + \frac{1}{j\omega\mu} \frac{\partial^2 \Psi^h}{\partial \rho \partial z} \\ E_\phi &= \frac{1}{j\omega\epsilon \rho} \frac{\partial^2 \Psi^e}{\partial \phi \partial z} + \frac{\partial \Psi^h}{\partial \rho} & H_\phi &= -\frac{\partial \Psi^e}{\partial \rho} + \frac{1}{j\omega\mu \rho} \frac{\partial^2 \Psi^h}{\partial \phi \partial z} \\ E_z &= \frac{1}{j\omega\epsilon} \left(\frac{\partial^2}{\partial z^2} + k^2 \right) \Psi^e & H_z &= \frac{1}{j\omega\mu} \left(\frac{\partial^2}{\partial z^2} + k^2 \right) \Psi^h\end{aligned}\quad (3-5)$$

The next step is to expand the wave functions in terms of appropriate mode functions with unknown coefficients. To satisfy the finiteness condition of the field due to the magnetic current ring in region I and the radiation condition in region II, Bessel and Hankel functions of second kind are chosen to represent the radial dependent parts of mode functions, respectively.

$$\begin{aligned}\Psi_1^e &= \sum_{n=0}^{\infty} \sum_{m=0}^{\infty} (a_n \cos n\phi + b_n \sin n\phi) \cos\left(\frac{m\pi}{h_1} z\right) R_{1R}^e(\rho) \\ \Psi_1^h &= \sum_{n=0}^{\infty} \sum_{m=0}^{\infty} n(b_n \cos n\phi - a_n \sin n\phi) \sin\left(\frac{m\pi}{h_1} z\right) R_{1R}^h(\rho)\end{aligned}\quad (3-6)$$

where subscript 1R denotes the radial waveguide region and

$$R_{1R}^e(\rho) = \begin{cases} u_{1mn}^e(\rho', z') J_n(k_{\rho m} \rho) & \rho \leq \rho' \\ U_{1mn}^e(\rho', z') H_n^{(2)}(k_{\rho m} \rho) & \rho > \rho' \end{cases} \quad (3-7)$$

$$R_{1R}^h(\rho) = \begin{cases} u_{1mn}^h(\rho', z') J_n(k_{\rho m} \rho) & \rho \leq \rho' \\ U_{1mn}^h(\rho', z') H_n^{(2)}(k_{\rho m} \rho) & \rho > \rho' \end{cases}$$

$$k_{\rho m} = \sqrt{k_1^2 - \left(\frac{m\pi}{h_1}\right)^2} \quad (3-8)$$

$$k_1 = \omega \sqrt{\mu_0 \epsilon_1}$$

u_{1mn} and U_{1mn} are unknown functions. J_n is the Bessel function of the first kind and n th order and $H_n^{(2)}$ is the Hankel function of the second kind and n th order. An application of the Lorentz Reciprocity theorem and enforcing the continuity condition of magnetic and electric field give these unknown functions as follows [1]

$$u_{1mn}^e(\rho', z') = \frac{\pi \omega \epsilon_1 \rho'}{2 k_{\rho m} h_1} \epsilon_m \cos\left(\frac{m\pi}{h_1} z'\right) H_n^{(2)'}(k_{\rho m} \rho')$$

$$U_{1mn}^e(\rho', z') = \frac{\pi \omega \epsilon_1 \rho'}{2 k_{\rho m} h_1} \epsilon_m \cos\left(\frac{m\pi}{h_1} z'\right) J_n'(k_{\rho m} \rho')$$

$$u_{1mn}^h(\rho', z') = -j \frac{m\pi^2}{2(k_{\rho m} h_1)^2} \epsilon_m \cos\left(\frac{m\pi}{h_1} z'\right) H_n^{(2)}(k_{\rho m} \rho')$$

$$U_{1mn}^h(\rho', z') = -j \frac{m\pi^2}{2(k_{\rho m} h_1)^2} \epsilon_m \cos\left(\frac{m\pi}{h_1} z'\right) J_n(k_{\rho m} \rho')$$
(3-9)

3.3. CAVITY

Now consider the problem of magnetic current ring inside a cavity of radius ρ_c (Fig.3.2). The ground plane is assumed to be of infinite extent.

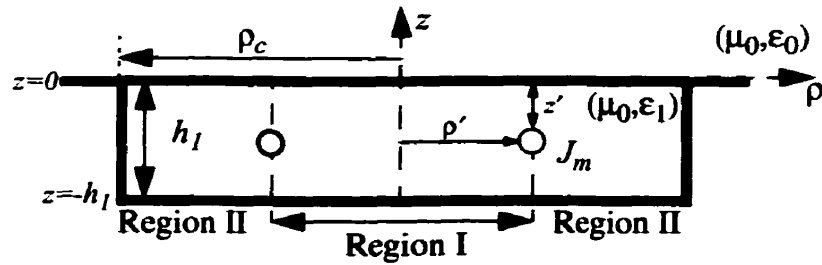


Fig.3.2. Current ring in a cylindrical cavity.

The existence of the conducting cylindrical wall at $\rho = \rho_c$ imposes the following conditions on the tangential electric field on the surface of the cylinder

$$E_z = E_\phi = 0 \quad \begin{cases} \rho = \rho_c \\ -h_1 \leq z \leq 0 \\ 0 \leq \phi \leq 2\pi \end{cases} \quad (3-10)$$

and the wave equations for this problem, Ψ_{1C}^e, Ψ_{1C}^h , are similar to those for radial waveguide case. Subscript 1C refers to the cavity region. The only part which is changed is the radial variation part.

$$R_{1C}^e(\rho) = \begin{cases} u_{1Cmn}^e(\rho', z') J_n(k_{\rho m} \rho) & \rho \leq \rho' \\ U_{1Cmn}^e(\rho', z') J_n(k_{\rho m} \rho) + V_{1Cmn}^e(\rho', z') N_n(k_{\rho m} \rho) & \rho > \rho' \end{cases} \quad (3-11)$$

$$R_{1C}^h(\rho) = \begin{cases} u_{1Cmn}^h(\rho', z') J_n(k_{\rho m} \rho) & \rho \leq \rho' \\ U_{1Cmn}^h(\rho', z') J_n(k_{\rho m} \rho) + V_{1Cmn}^h(\rho', z') N_n(k_{\rho m} \rho) & \rho > \rho' \end{cases}$$

where N_n is the Bessel function of the second kind and n th order and u_{1Cmn} , U_{1Cmn} and V_{1Cmn} are unknown functions which are determined from the boundary conditions as

$$u_{1Cmn}^e(\rho', z') = \frac{j\pi\omega\epsilon_1\rho'}{2k_{\rho m}h_1} \epsilon_m \cos\left(\frac{m\pi}{h_1}z'\right) \left[\frac{N_n(k_{\rho m}\rho_c)}{J_n(k_{\rho m}\rho_c)} J_n'(k_{\rho m}\rho') - N_n'(k_{\rho m}\rho') \right]$$

$$U_{1Cmn}^e(\rho', z') = \frac{j\pi\omega\epsilon_1\rho'}{2k_{\rho m}h_1} \epsilon_m \cos\left(\frac{m\pi}{h_1}z'\right) \left[\frac{N_n(k_{\rho m}\rho_c)}{J_n(k_{\rho m}\rho_c)} J_n'(k_{\rho m}\rho') \right]$$

$$V_{1Cmn}^e(\rho', z') = \frac{-j\pi\omega\epsilon_1\rho'}{2k_{\rho m}h_1} \epsilon_m \cos\left(\frac{m\pi}{h_1}z'\right) [J_n'(k_{\rho m}\rho')]$$

$$u_{1Cmn}^h(\rho', z') = \frac{-m\pi^2}{2(k_{\rho m}h_1)^2} \epsilon_m \cos\left(\frac{m\pi}{h_1}z'\right) \left[\frac{N_n'(k_{\rho m}\rho_c)}{J_n'(k_{\rho m}\rho_c)} J_n(k_{\rho m}\rho') - N_n(k_{\rho m}\rho') \right] \quad (3-12)$$

$$U_{1Cmn}^h(\rho', z') = \frac{-m\pi^2}{2(k_{\rho m}h_1)^2} \epsilon_m \cos\left(\frac{m\pi}{h_1}z'\right) \left[\frac{N_n'(k_{\rho m}\rho_c)}{J_n'(k_{\rho m}\rho_c)} J_n(k_{\rho m}\rho') \right]$$

$$V_{1Cmn}^h(\rho', z') = \frac{m\pi^2}{2(k_{\rho m}h_1)^2} \epsilon_m \cos\left(\frac{m\pi}{h_1}z'\right) [J_n(k_{\rho m}\rho')]$$

Note that there is no steady-state solution to the problem when the frequency of the source is the same as any of the resonant frequencies of the cavity, which occurs when $k_{\rho m}\rho_c$ equals to zeros of $J_n(x)$ or $J_n'(x)$.

3.4. PARTIALLY FILLED WAVEGUIDE OR CAVITY

If the radial waveguide or cavity is partially filled with dielectric as it is shown in Fig.3.3, the continuity of tangential electric field must be satisfied at the common boundary of two dielectric layers

$$\begin{cases} E_{\rho 1} = E_{\rho 4} \\ E_{\phi 1} = E_{\phi 4} \end{cases} \quad z = -h_4 \quad (3-13)$$

In addition, the electric field must satisfy the conditions $E_{\rho} = E_{\phi} = 0$ at $z = 0, -h_1$. The angular and radial dependent parts of wave functions are still the same as before, but for z -dependent part, the characteristic equation, which is obtained from the boundary condition at $z = -h_4$, must be solved.

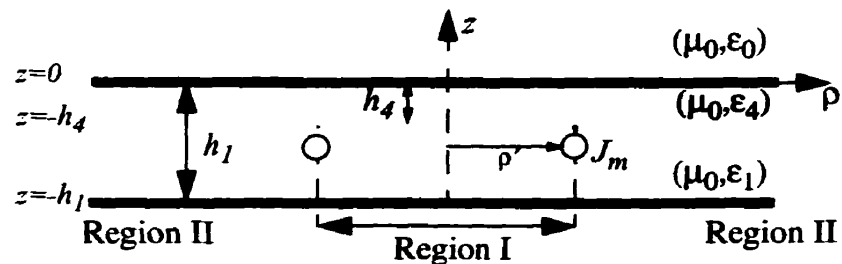


Fig.3.3. Partially filled radial waveguide.

For example the wave function for partially filled waveguide are

$$\Psi_{11}^e = \sum_{n=0}^{\infty} \sum_{m=0}^{\infty} \beta_1 (a_n \cos n\phi + b_n \sin n\phi) \cos(k_{z1}(z + h_1)) R_1^e(\rho) \quad -h_1 \leq z \leq -h_4$$

$$\Psi_{12}^e = \sum_{n=0}^{\infty} \sum_{m=0}^{\infty} \beta_2 (a_n \cos n\phi + b_n \sin n\phi) \cos(k_{z2}z) R_1^h(\rho) \quad -h_4 \leq z \leq 0$$
(3-14)

where Ψ_{11}^e is the wave function in the lower part of waveguide and Ψ_{12}^e is the wave function in the upper part. k_{z1} and k_{z2} must satisfy the relationships

$$k_{\rho m}^2 + k_{z1}^2 = \omega^2 \mu_0 \epsilon_0$$

$$k_{\rho m}^2 + k_{z2}^2 = \omega^2 \mu_0 \epsilon_4$$
(3-15)

To evaluate the constants β_1 , β_2 and $k_{\rho m}$, the boundary conditions at $z = -h_4$ must be satisfied. The results of applying these conditions are [59]

$$\frac{k_{z1} \beta_1}{\epsilon_1} \sin k_{z1}(h_1 - h_4) = -\frac{k_{z2} \beta_2}{\epsilon_4} \sin(k_{z2} h_4)$$

$$\frac{k_{z1}}{\epsilon_1} \tan k_{z1}(h_1 - h_4) = -\frac{k_{z2}}{\epsilon_4} \tan(k_{z2} h_4)$$
(3-16)

From these equations, $k_{\rho m}$ and the ratio of β_1/β_2 are determined. For partially filled cavity, one must replace $R_1^e(\rho)$ and $R_1^h(\rho)$ by $R_{1C}^e(\rho)$ and $R_{1C}^h(\rho)$, respectively.

3.5. ONE LAYER OF DIELECTRIC AND FREE SPACE

Consider one layer of dielectric on top of an infinite ground plane. To find the Green's functions, a magnetic current ring as characterized in equation (3-1) is assumed as the impulse source (Fig.3.4). The wave functions can be determined by an application of

the Hankel transform. The transform pairs of order n of each wave function is defined as

$$\begin{aligned}\bar{\Psi}(\alpha, \phi, z) &= \int_0^{\infty} \Psi(\rho, \phi, z) J_n(\alpha\rho) \rho d\rho \\ \Psi(\rho, \phi, z) &= \int_0^{\infty} \bar{\Psi}(\alpha, \phi, z) J_n(\alpha\rho) \alpha d\alpha\end{aligned}\quad (3-17)$$

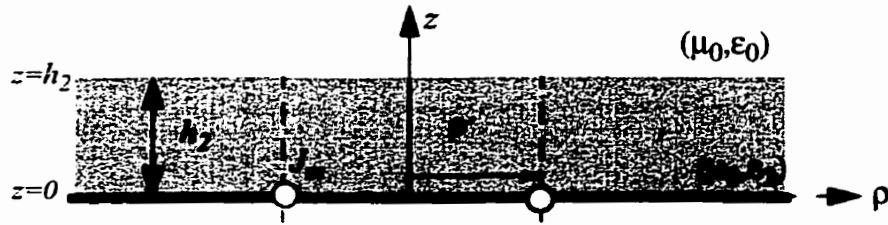


Fig.3.4. Magnetic current ring covered with one layer of dielectric.

The wave equation in cylindrical coordinates is expressed as [59]

$$\frac{\partial^2 \Psi}{\partial \rho^2} + \frac{1}{\rho} \frac{\partial \Psi}{\partial \rho} - \frac{n^2}{\rho^2} \Psi + \frac{\partial^2 \Psi}{\partial z^2} + k^2 \Psi = 0 \quad (3-18)$$

where $k = \omega \sqrt{\mu \epsilon}$. Taking Hankel transform of both sides and using the following expression available for the derivative of a function $R(\rho)$ [60]

$$\int_0^{\infty} \left(\frac{d^2 R}{d\rho^2} + \frac{1}{\rho} \frac{dR}{d\rho} - \frac{n^2}{\rho^2} R \right) J_n(\alpha\rho) \rho d\rho = -\alpha^2 \bar{R} \quad (3-19)$$

the wave equation can be expressed as follows

$$\left(\frac{\partial^2}{\partial z^2} - \gamma^2 \right) \bar{\Psi}(\alpha, \phi, z) = 0 \quad (3-20)$$

where

$$\gamma^2 = \alpha^2 - k^2 \quad (3-21)$$

This means that γ is a double valued function of α . The branch which gives stable answer should be determined by invoking the physical constrains of the problem.

The Hankel transform of the wave functions for dielectric and free space can be expressed as

$$\begin{cases} \overline{\Psi}_2^e(\alpha, \phi, z) = \sum_{n=0}^{\infty} (a_n \cos n\phi + b_n \sin n\phi)(F_n^e(\alpha)e^{-\gamma z} + f_n^e(\alpha)e^{\gamma z}) \\ \overline{\Psi}_2^h(\alpha, \phi, z) = \sum_{n=0}^{\infty} n(b_n \cos n\phi - a_n \sin n\phi)(F_n^h(\alpha)e^{-\gamma z} + f_n^h(\alpha)e^{\gamma z}) \end{cases} \quad 0 \leq z \leq h_2 \quad (3-22)$$

$$\begin{cases} \overline{\Psi}_0^e(\alpha, \phi, z) = \sum_{n=0}^{\infty} (a_n \cos n\phi + b_n \sin n\phi)G_n^e(\alpha)e^{-\delta z} \\ \overline{\Psi}_0^h(\alpha, \phi, z) = \sum_{n=0}^{\infty} n(b_n \cos n\phi - a_n \sin n\phi)G_n^h(\alpha)e^{-\delta z} \end{cases} \quad z > h_2 \quad (3-23)$$

where:

$$\begin{aligned} \gamma^2 &= \alpha^2 - k_2^2 & k_2 &= \omega \sqrt{\mu_0 \epsilon_2} \\ \delta^2 &= \alpha^2 - k_0^2 & k_0 &= \omega \sqrt{\mu_0 \epsilon_0} \end{aligned} \quad (3-24)$$

and f_n , F_n and G_n are unknown functions to be determined. The subscript 2 refers to dielectric region and subscript 0 refers to free space region. It should be noted that, one can take different variables for the Hankel transforms in dielectric and free space, i.e. α_1, α_2 . After applying the continuity conditions and orthogonality of the function in $0 \leq \alpha \leq \infty$, it can be proved that α_1 and α_2 are equal. This is discussed at the end of Appendix A. The boundary conditions used to find the unknown functions, are those on

conducting surface of ground plane ($z = 0$) and also those on the upper surface of dielectric layer ($z = h_2$)

$$\begin{cases} E_{\phi 2} = 0 \\ E_{\rho 2} = I_m(\phi)\delta(\rho - \rho') \end{cases} \quad z = 0 \quad (3-25)$$

$$\begin{cases} E_{\phi 2} = E_{\phi 0} \\ E_{\rho 2} = E_{\rho 0} \\ H_{\phi 2} = H_{\phi 0} \\ H_{\rho 2} = H_{\rho 0} \end{cases} \quad z = h_2 \quad (3-26)$$

Using a method explained in Appendix A, the following system of equations is obtained from the boundary conditions

$$\begin{aligned} -\frac{1}{j\omega\epsilon_2}\gamma\alpha[F_n^e(\alpha) - f_n^e(\alpha)] + n\alpha[F_n^h(\alpha) + f_n^h(\alpha)] &= \rho'J_{n-1}(\alpha\rho') \\ \frac{1}{j\omega\epsilon_2}\gamma\alpha[F_n^e(\alpha) - f_n^e(\alpha)] + n\alpha[F_n^h(\alpha) + f_n^h(\alpha)] &= \rho'J_{n+1}(\alpha\rho') \\ \frac{\delta e^{-\delta h_2}}{\epsilon_0}G_n^e(\alpha) &= \frac{\gamma}{\epsilon_2}[e^{-\gamma h_2}F_n^e(\alpha) - e^{\gamma h_2}f_n^e(\alpha)] \\ e^{-\delta h_2}G_n^h(\alpha) &= e^{-\gamma h_2}F_n^h(\alpha) + e^{\gamma h_2}f_n^h(\alpha) \\ e^{-\delta h_2}G_n^e(\alpha) &= e^{-\gamma h_2}F_n^e(\alpha) + e^{\gamma h_2}f_n^e(\alpha) \\ \delta e^{-\delta h_2}G_n^h(\alpha) &= \gamma[e^{-\gamma h_2}F_n^h(\alpha) - e^{\gamma h_2}f_n^h(\alpha)] \end{aligned} \quad (3-27)$$

The unknown functions can be found by solving this system of equations.

$$\begin{aligned}
F_n^e(\alpha) &= -j\omega\epsilon_2\rho' \frac{J_n'(\alpha\rho')}{\alpha\gamma} \left[\frac{1}{1 - k^e e^{-2\gamma h_2}} \right] \\
f_n^e(\alpha) &= -j\omega\epsilon_2\rho' \frac{J_n'(\alpha\rho')}{\alpha\gamma} \left[\frac{k^e e^{-2\gamma h_2}}{1 - k^e e^{-2\gamma h_2}} \right] \\
G_n^e(\alpha) &= -j\omega\epsilon_0\rho' \frac{J_n'(\alpha\rho')}{\alpha\delta} \left[\frac{(1 - k^e) e^{-\gamma h_2} e^{\delta h_2}}{1 - k^e e^{-2\gamma h_2}} \right] \\
F_n^h(\alpha) &= \frac{J_n(\alpha\rho')}{\alpha^2} \left[\frac{1}{1 + k^h e^{-2\gamma h_2}} \right] \\
f_n^h(\alpha) &= \frac{J_n(\alpha\rho')}{\alpha^2} \left[\frac{k^h e^{-2\gamma h_2}}{1 + k^h e^{-2\gamma h_2}} \right] \\
G_n^h(\alpha) &= \frac{J_n(\alpha\rho')}{\alpha^2} \left[\frac{(1 + k^h) e^{-\gamma h_2} e^{\delta h_2}}{1 + k^h e^{-2\gamma h_2}} \right]
\end{aligned} \tag{3-28}$$

where

$$\begin{aligned}
k^e &= \frac{\gamma/\epsilon_2 - \delta/\epsilon_0}{\gamma/\epsilon_2 + \delta/\epsilon_0} \\
k^h &= \frac{\gamma - \delta}{\gamma + \delta}
\end{aligned} \tag{3-29}$$

3.6. CONDUCTING RING ON ONE LAYER OF DIELECTRIC

In this section the Green's functions are derived for the case when a conducting ring is added on top of the ground plane containing an annular slot. The region between the plane of slot and the plane of conducting rings can be filled with a dielectric. As shown in Fig.3.5, two sources of magnetic and electric rings are assumed to be located at two different radii from the centre.

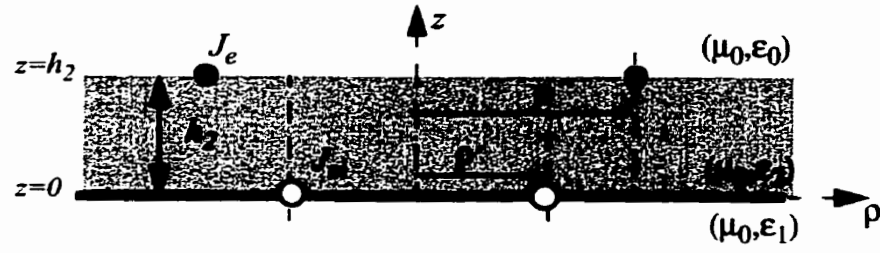


Fig.3.5. Magnetic and electric sources representation of conducting rings loaded annular slot.

These sources can be characterized as

$$\begin{aligned}\vec{J}_m &= I_m(\phi)\delta(\rho - \rho')\delta(z)\hat{a}_\phi \\ \vec{J}_e &= I_e(\phi)\delta(\rho - \rho'')\delta(z - h_2)\hat{a}_\rho\end{aligned}\quad (3-30)$$

$$\begin{aligned}I_m(\phi) &= \sum_{n=0}^{\infty} a_{1n}\cos n\phi' + a_{2n}\sin n\phi' \\ I_e(\phi) &= \sum_{n=0}^{\infty} b_{1n}\cos n\phi' + b_{2n}\sin n\phi'\end{aligned}\quad (3-31)$$

The boundary conditions that must be satisfied are

$$\begin{cases} E_{\phi 2} = 0 \\ E_{\rho 2} = I_m(\phi)\delta(\rho - \rho') \end{cases} \quad \begin{array}{l} z = 0 \\ 0 \leq \rho < \infty \\ 0 \leq \phi \leq 2\pi \end{array} \quad (3-32)$$

$$\begin{cases} E_{\phi 2} = E_{\phi 0} \\ E_{\rho 2} = E_{\rho 0} \\ H_{\phi 2} - H_{\phi 0} = I_e(\phi)\delta(\rho - \rho'') \\ H_{\rho 2} = H_{\rho 0} \end{cases} \quad \begin{array}{l} z = h_2 \\ 0 \leq \rho < \infty \\ 0 \leq \phi \leq 2\pi \end{array} \quad (3-33)$$

Using similar approach to that one for dielectric loaded slot, the Hankel transform of the

wave functions can be written as:

$$\left\{ \begin{array}{l} \overline{\Psi}_{2L}^e(\alpha, \phi, z) = \sum_{n=0}^{\infty} \left(\begin{array}{l} ((A_{1n}^e(\alpha)e^{-\gamma z} + B_{1n}^e(\alpha)e^{\gamma z}) \cos n\phi) + \\ ((A_{2n}^e(\alpha)e^{-\gamma z} + B_{2n}^e(\alpha)e^{\gamma z}) \sin n\phi) \end{array} \right) \\ \overline{\Psi}_{2L}^h(\alpha, \phi, z) = \sum_{n=0}^{\infty} n \left(\begin{array}{l} ((A_{2n}^h(\alpha)e^{-\gamma z} + B_{2n}^h(\alpha)e^{\gamma z}) \cos n\phi) - \\ ((A_{1n}^h(\alpha)e^{-\gamma z} + B_{1n}^h(\alpha)e^{\gamma z}) \sin n\phi) \end{array} \right) \end{array} \right. \quad 0 \leq z \leq h_2 \quad (3-34)$$

$$\left\{ \begin{array}{l} \overline{\Psi}_{0L}^e(\alpha, \phi, z) = \sum_{n=0}^{\infty} (C_{1n}^e(\alpha) \cos n\phi + C_{2n}^e(\alpha) \sin n\phi) e^{-\delta z} \\ \overline{\Psi}_{0L}^h(\alpha, \phi, z) = \sum_{n=0}^{\infty} n (C_{2n}^h(\alpha) \cos n\phi - C_{1n}^h(\alpha) \sin n\phi) e^{-\delta z} \end{array} \right. \quad h_2 \leq z \quad (3-35)$$

where γ and δ are the same as (3-24). By applying the inverse of Hankel transform the wave functions for each region will be found.

$$\left\{ \begin{array}{l} \overline{\Psi}_{2L}^e(\alpha, \phi, z) = \int_0^{\infty} \sum_{n=0}^{\infty} (A_{1n}^e(\alpha)e^{-\gamma z} + B_{1n}^e(\alpha)e^{\gamma z}) \cos n\phi J_n(\alpha\rho) \alpha d\alpha + \\ \int_0^{\infty} \sum_{n=0}^{\infty} (A_{2n}^e(\alpha)e^{-\gamma z} + B_{2n}^e(\alpha)e^{\gamma z}) \sin n\phi J_n(\alpha\rho) \alpha d\alpha \\ \overline{\Psi}_{2L}^h(\alpha, \phi, z) = \int_0^{\infty} \sum_{n=0}^{\infty} n (A_{2n}^h(\alpha)e^{-\gamma z} + B_{2n}^h(\alpha)e^{\gamma z}) \sin n\phi J_n(\alpha\rho) \alpha d\alpha - \\ \int_0^{\infty} \sum_{n=0}^{\infty} n (A_{1n}^h(\alpha)e^{-\gamma z} + B_{1n}^h(\alpha)e^{\gamma z}) \cos n\phi J_n(\alpha\rho) \alpha d\alpha \end{array} \right. \quad (3-36)$$

$$0 \leq z \leq h_2$$

$$\left\{ \begin{aligned} \Psi_{0L}^e(\alpha, \phi, z) &= \int_0^\infty \sum_{n=0}^\infty (C_{1n}^e(\alpha) \cos n\phi + C_{2n}^e(\alpha) \sin n\phi) e^{-\delta z} J_n(\alpha\rho) \alpha d\alpha \\ \Psi_{0L}^h(\alpha, \phi, z) &= \int_0^\infty \sum_{n=0}^\infty n(C_{2n}^h(\alpha) \cos n\phi - C_{1n}^h(\alpha) \sin n\phi) e^{-\delta z} J_n(\alpha\rho) \alpha d\alpha \end{aligned} \right. \quad h_2 \leq z \quad (3-37)$$

Now using (3-5) all the components of the electric and magnetic fields can be written in terms of unknown functions of α , $A_{in}^e(\alpha)$, $A_{in}^h(\alpha)$, $B_{in}^e(\alpha)$, $B_{in}^h(\alpha)$, $C_{in}^e(\alpha)$, and $C_{in}^h(\alpha)$, where $i = 1$ or 2 . To determine the unknown functions, the boundary conditions in (3-32) and (3-33) must be applied. The results of applying boundary condition and orthogonality of sinusoidal functions are as follows

$$\left\{ \begin{aligned} E_{\phi 2} &= 0 \quad z = 0 \\ \frac{-1}{j\omega\epsilon_2\rho} \int_0^\infty (A_{in}^e(\alpha) - B_{in}^e(\alpha)) \alpha \gamma J_n(\alpha\rho) d\alpha + \int_0^\infty (A_{in}^h(\alpha) + B_{in}^h(\alpha)) \alpha^2 J'_n(\alpha\rho) d\alpha &= 0 \end{aligned} \right. \quad (3-38)$$

$$\left\{ \begin{aligned} E_{\rho 2} &= \sum_{n=0}^\infty I_n(\phi) \delta(\rho - \rho') \quad z = 0 \\ \frac{-1}{j\omega\epsilon_2} \int_0^\infty (A_{in}^e(\alpha) - B_{in}^e(\alpha)) \alpha^2 \gamma J'_n(\alpha\rho) d\alpha + \\ \frac{n^2}{\rho} \int_0^\infty (A_{in}^h(\alpha) + B_{in}^h(\alpha)) \alpha J_n(\alpha\rho) d\alpha &= a_{in} \delta(\rho - \rho') \end{aligned} \right. \quad (3-39)$$

$$\left\{ \begin{array}{l} E_{\phi 2} = E_{\phi 0} \quad z = h_2 \\ \frac{-1}{j\omega\epsilon_2\rho} \int_0^{\infty} (A_{in}^e(\alpha)e^{-\gamma h_2} - B_{in}^e(\alpha)e^{\gamma h_2}) \alpha \gamma J_n(\alpha\rho) d\alpha + \\ \int_0^{\infty} (A_{in}^h(\alpha)e^{-\gamma h_2} + B_{in}^h(\alpha)e^{\gamma h_2}) \alpha^2 J'_n(\alpha\rho) d\alpha = \\ \frac{-1}{j\omega\epsilon_0\rho} \int_0^{\infty} C_{in}^e(\alpha)e^{-\delta h_2} \alpha \delta J_n(\alpha\rho) d\alpha + \int_0^{\infty} C_{in}^h(\alpha)e^{-\delta h_2} \alpha^2 J'_n(\alpha\rho) d\alpha \end{array} \right. \quad (3-40)$$

$$\left\{ \begin{array}{l} E_{\rho 2} = E_{\rho 0} \quad z = h_2 \\ \frac{-1}{j\omega\epsilon_2} \int_0^{\infty} (A_{in}^e(\alpha)e^{-\gamma h_2} - B_{in}^e(\alpha)e^{\gamma h_2}) \alpha^2 \gamma J'_n(\alpha\rho) d\alpha + \\ \frac{n^2}{\rho} \int_0^{\infty} (A_{in}^h(\alpha)e^{-\gamma h_2} + B_{in}^h(\alpha)e^{\gamma h_2}) \alpha J_n(\alpha\rho) d\alpha = \\ \frac{-1}{j\omega\epsilon_0} \int_0^{\infty} C_{in}^e(\alpha)e^{-\delta h_2} \alpha^2 \delta J'_n(\alpha\rho) d\alpha + \frac{n^2}{\rho} \int_0^{\infty} C_{in}^h(\alpha)e^{-\delta h_2} \alpha J_n(\alpha\rho) d\alpha \end{array} \right. \quad (3-41)$$

$$\left\{ \begin{array}{l} H_{\phi 2} - H_{\phi 0} = I_e(\phi) \delta(\rho - \rho'') \quad z = h_2 \\ - \int_0^{\infty} (A_{in}^e(\alpha)e^{-\gamma h_2} + B_{in}^e(\alpha)e^{\gamma h_2} - C_{in}^e(\alpha)e^{-\delta h_2}) \alpha^2 J'_n(\alpha\rho) d\alpha + \\ \frac{n^2}{j\omega\mu_0\rho} \int_0^{\infty} (\gamma(A_{in}^h(\alpha)e^{-\gamma h_2} - B_{in}^h(\alpha)e^{\gamma h_2}) - \delta C_{in}^h(\alpha)e^{-\delta h_2}) \alpha J_n(\alpha\rho) d\alpha = b_{in} \delta(\rho - \rho'') \end{array} \right. \quad (3-42)$$

$$\left\{ \begin{array}{l} H_{\rho 2} = H_{\rho 0} \quad z = h_2 \\ \frac{n}{\rho} \int_0^{\infty} (A_{in}^e(\alpha) e^{-\gamma h_2} + B_{in}^e(\alpha) e^{\gamma h_2}) \alpha J_n(\alpha \rho) d\alpha - \\ \frac{n}{j\omega\mu_0} \int_0^{\infty} (A_{in}^h(\alpha) e^{-\gamma h_2} - B_{in}^h(\alpha) e^{\gamma h_2}) \alpha^2 \gamma J'_n(\alpha \rho) d\alpha = \\ \frac{n}{\rho} \int_0^{\infty} C_{in}^e(\alpha) e^{-\delta h_2} \alpha J_n(\alpha \rho) d\alpha - \frac{n}{j\omega\mu_0} \int_0^{\infty} C_{in}^h(\alpha) e^{-\delta h_2} \alpha^2 \delta J'_n(\alpha \rho) d\alpha \end{array} \right. \quad (3-43)$$

Using the approach described in Appendix A, the system of equations will be found as follows

$$\left\{ \begin{array}{l} \frac{-1}{j\omega\epsilon_2} \gamma \alpha (A_{in}^e(\alpha) - B_{in}^e(\alpha)) + n\alpha (A_{in}^h(\alpha) + B_{in}^h(\alpha)) = a_{in} \rho' J_{n-1}(\alpha \rho') \\ \frac{1}{j\omega\epsilon_2} \gamma \alpha (A_{in}^e(\alpha) - B_{in}^e(\alpha)) + n\alpha (A_{in}^h(\alpha) + B_{in}^h(\alpha)) = a_{in} \rho' J_{n+1}(\alpha \rho') \end{array} \right. \quad (3-44)$$

$$\left\{ \begin{array}{l} \frac{-1}{j\omega\epsilon_2} \gamma \alpha (A_{in}^e(\alpha) e^{-\gamma h_2} - B_{in}^e(\alpha) e^{\gamma h_2}) + n\alpha (A_{in}^h(\alpha) e^{-\gamma h_2} + B_{in}^h(\alpha) e^{\gamma h_2}) = \\ \frac{-1}{j\omega\epsilon_0} \delta \alpha C_{in}^e(\alpha) e^{-\delta h_2} + n\alpha C_{in}^h(\alpha) e^{-\delta h_2} \\ \frac{1}{j\omega\epsilon_2} \gamma \alpha (A_{in}^e(\alpha) e^{-\gamma h_2} - B_{in}^e(\alpha) e^{\gamma h_2}) + n\alpha (A_{in}^h(\alpha) e^{-\gamma h_2} + B_{in}^h(\alpha) e^{\gamma h_2}) = \\ \frac{1}{j\omega\epsilon_0} \delta \alpha C_{in}^e(\alpha) e^{-\delta h_2} + n\alpha C_{in}^h(\alpha) e^{-\delta h_2} \end{array} \right. \quad (3-45)$$

$$\left\{ \begin{array}{l}
 \alpha(A_{in}^e(\alpha)e^{-\gamma h_2} + B_{in}^e(\alpha)e^{\gamma h_2} - C_{in}^e(\alpha)e^{-\delta h_2}) - \\
 \frac{1}{j\omega\mu_0}n\alpha(\gamma(A_{in}^h(\alpha)e^{-\gamma h_2} - B_{in}^h(\alpha)e^{\gamma h_2}) - \delta C_{in}^h(\alpha)e^{-\delta h_2}) = -b_{in}\rho''J_{n-1}(\alpha\rho'') \\
 \alpha(A_{in}^e(\alpha)e^{-\gamma h_2} + B_{in}^e(\alpha)e^{\gamma h_2} - C_{in}^e(\alpha)e^{-\delta h_2}) + \\
 \frac{1}{j\omega\mu_0}n\alpha(\gamma(A_{in}^h(\alpha)e^{-\gamma h_2} - B_{in}^h(\alpha)e^{\gamma h_2}) - \delta C_{in}^h(\alpha)e^{-\delta h_2}) = b_{in}\rho''J_{n+1}(\alpha\rho'')
 \end{array} \right. \quad (3-46)$$

After solving the system of equations of (3-46) the unknown parts of the Green's functions are found as

$$\begin{aligned}
A_{in}^e(\alpha) &= a_{in} \left(\frac{-j\omega\epsilon_2\rho'}{\alpha\gamma} J'_n(\alpha\rho') \left[\frac{1}{1 - k^e e^{-2\gamma h_2}} \right] \right) - \\
&\quad b_{in} \left(\left(\frac{\delta/\epsilon_0}{\gamma/\epsilon_2 + \delta/\epsilon_0} \right) \frac{\rho''}{\alpha} J'_n(\alpha\rho'') \left[\frac{e^{-\gamma h_2}}{1 - k^e e^{-2\gamma h_2}} \right] \right) \\
B_{in}^e(\alpha) &= a_{in} \left(\frac{-j\omega\epsilon_2\rho'}{\alpha\gamma} J'_n(\alpha\rho') \left[\frac{k^e e^{-2\gamma h_2}}{1 - k^e e^{-2\gamma h_2}} \right] \right) - \\
&\quad b_{in} \left(\left(\frac{\delta/\epsilon_0}{\gamma/\epsilon_2 + \delta/\epsilon_0} \right) \frac{\rho''}{\alpha} J'_n(\alpha\rho'') \left[\frac{e^{-\gamma h_2}}{1 - k^e e^{-2\gamma h_2}} \right] \right) \\
C_{in}^e(\alpha) &= a_{in} \left(\frac{-j\omega\epsilon_0\rho'}{\alpha\delta} J'_n(\alpha\rho') \left[\frac{e^{\delta h_2} e^{-\gamma h_2} (1 - k^e)}{1 - k^e e^{-2\gamma h_2}} \right] \right) - \\
&\quad b_{in} \left(\left(\frac{\gamma/\epsilon_2}{\gamma/\epsilon_2 + \delta/\epsilon_0} \right) \frac{\rho''}{\alpha} J'_n(\alpha\rho'') \left[\frac{e^{\delta h_2} (e^{-2\gamma h_2} - 1)}{1 - k^e e^{-2\gamma h_2}} \right] \right) \\
A_{in}^h(\alpha) &= a_{in} \left(\frac{1}{\alpha^2} J_n(\alpha\rho') \left[\frac{1}{1 + k^h e^{-2\gamma h_2}} \right] \right) + \\
&\quad b_{in} \left(\frac{j\omega\mu_0}{\alpha^2} \left(\frac{1}{\gamma + \delta} \right) J_n(\alpha\rho'') \left[\frac{e^{-\gamma h_2}}{1 + k^h e^{-2\gamma h_2}} \right] \right) \\
B_{in}^h(\alpha) &= a_{in} \left(\frac{1}{\alpha^2} J_n(\alpha\rho') \left[\frac{k^h e^{-2\gamma h_2}}{1 + k^h e^{-2\gamma h_2}} \right] \right) - \\
&\quad b_{in} \left(\frac{j\omega\mu_0}{\alpha^2} \left(\frac{1}{\gamma + \delta} \right) J_n(\alpha\rho'') \left[\frac{e^{-\gamma h_2}}{1 + k^h e^{-2\gamma h_2}} \right] \right) \\
C_{in}^h(\alpha) &= a_{in} \left(\frac{1}{\alpha^2} J_n(\alpha\rho') \left[\frac{e^{\delta h_2} e^{-\gamma h_2} (1 + k^h)}{1 + k^h e^{-2\gamma h_2}} \right] \right) - \\
&\quad b_{in} \left(\frac{j\omega\mu_0}{\alpha^2} \left(\frac{1}{\gamma + \delta} \right) J_n(\alpha\rho'') \left[\frac{e^{\delta h_2} (1 - e^{-2\gamma h_2})}{1 + k^h e^{-2\gamma h_2}} \right] \right)
\end{aligned} \tag{3-47}$$

where k^e and k^h are given in (3-29). It is interesting to note that the Green's functions are a linear combination of the Green's functions due to each source.

3.7. TWO LAYERS OF DIELECTRIC

Now consider adding two layers of dielectric on top of a slotted ground plane (Fig.3.6). Similar to one layer of dielectric, the Green's functions can be found by the use of Hankel transform.

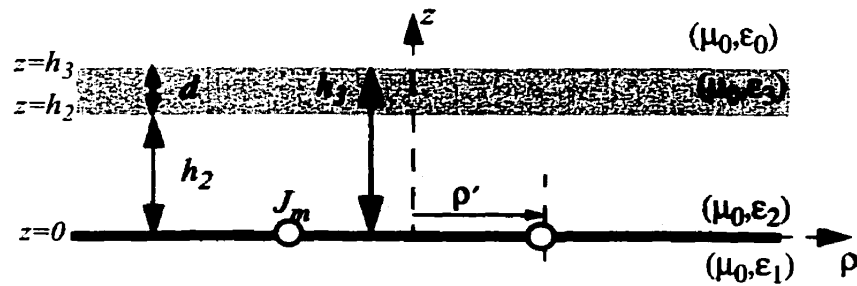


Fig.3.6. Magnetic current ring loaded with two layers of dielectric.

The Hankel transform of wave functions are

$$\begin{cases} \overline{\Psi}_{D2}^e(\alpha, \phi, z) = \sum_{n=0}^{\infty} (a_n \cos n\phi + b_n \sin n\phi) (Q_n^e(\alpha) e^{-\gamma z} + q_n^e(\alpha) e^{\gamma z}) \\ \overline{\Psi}_{D2}^h(\alpha, \phi, z) = \sum_{n=0}^{\infty} n (b_n \cos n\phi - a_n \sin n\phi) (Q_n^h(\alpha) e^{-\gamma z} + q_n^h(\alpha) e^{\gamma z}) \end{cases} \quad (3-48)$$

$$0 \leq z \leq h_2$$

$$\begin{cases} \overline{\Psi}_{D3}^e(\alpha, \phi, z) = \sum_{n=0}^{\infty} (a_n \cos n\phi + b_n \sin n\phi) (S_n^e(\alpha) e^{-\kappa z} + s_n^e(\alpha) e^{\kappa z}) \\ \overline{\Psi}_{D3}^h(\alpha, \phi, z) = \sum_{n=0}^{\infty} n (b_n \cos n\phi - a_n \sin n\phi) (S_n^h(\alpha) e^{-\kappa z} + s_n^h(\alpha) e^{\kappa z}) \end{cases} \quad (3-49)$$

$$h_2 \leq z \leq h_3$$

$$\begin{cases} \overline{\Psi}_{D0}^e(\alpha, \phi, z) = \sum_{n=0}^{\infty} (a_n \cos n\phi + b_n \sin n\phi) T_n^e(\alpha) e^{-\delta z} \\ \overline{\Psi}_{D0}^h(\alpha, \phi, z) = \sum_{n=0}^{\infty} n (b_n \cos n\phi - a_n \sin n\phi) T_n^h(\alpha) e^{-\delta z} \end{cases} \quad z > h_3 \quad (3-50)$$

where

$$\begin{aligned} \gamma^2 &= \alpha^2 - k_2^2 & k_2 &= \omega \sqrt{\mu_0 \epsilon_2} \\ \kappa^2 &= \alpha^2 - k_3^2 & k_3 &= \omega \sqrt{\mu_0 \epsilon_3} \\ \delta^2 &= \alpha^2 - k_0^2 & k_0 &= \omega \sqrt{\mu_0 \epsilon_0} \end{aligned} \quad (3-51)$$

and $Q_n^e, q_n^e, Q_n^h, q_n^h, S_n^e, s_n^e, S_n^h, s_n^h, T_n^e$, and T_n^h are unknown functions of α . To determine these ten unknown functions, ten boundary conditions are needed. Boundary conditions are applied at the boundaries of dielectric layers and on the slots.

$$\begin{cases} E_{\phi 2} = 0 \\ E_{\rho 2} = I_m(\phi) \delta(\rho - \rho') \end{cases} \quad z = 0 \quad (3-52)$$

$$\begin{cases} E_{\phi 2} = E_{\phi 3} \\ E_{\rho 2} = E_{\rho 3} \\ H_{\phi 2} = H_{\phi 3} \\ H_{\rho 2} = H_{\rho 3} \end{cases} \quad z = h_2 \quad (3-53)$$

$$\begin{cases} E_{\phi 3} = E_{\phi 0} \\ E_{\rho 3} = E_{\rho 0} \\ H_{\phi 3} = H_{\phi 0} \\ H_{\rho 3} = H_{\rho 0} \end{cases} \quad z = h_3 \quad (3-54)$$

where subscript 2 and 3 denote the dielectric layers and 0 refers to free space. Now using the three sets of boundary conditions given in (3-52)-(3-54) at $z = 0, h_2, h_3$, substituting (3-48)-(3-50) into (3-5), applying the orthogonality of sinusoidal functions, and using the method discussed in Appendix A, one obtains:

$$\begin{cases} \frac{-1}{j\omega\epsilon_2} \gamma \alpha [Q_n^e(\alpha) - q_n^e(\alpha)] + n \alpha [Q_n^h(\alpha) + q_n^h(\alpha)] = \rho' J_{n-1}(\alpha \rho') \\ \frac{1}{j\omega\epsilon_2} \gamma \alpha [Q_n^e(\alpha) - q_n^e(\alpha)] + n \alpha [Q_n^h(\alpha) + q_n^h(\alpha)] = \rho' J_{n+1}(\alpha \rho') \end{cases} \quad (3-55)$$

$$\begin{cases} \frac{\gamma}{\epsilon_2} [e^{-\gamma h_2} Q_n^e(\alpha) - e^{\gamma h_2} q_n^e(\alpha)] = \frac{\kappa}{\epsilon_3} [e^{-\kappa h_2} S_n^e(\alpha) - e^{\kappa h_2} s_n^e(\alpha)] \\ e^{-\gamma h_2} Q_n^h(\alpha) + e^{\gamma h_2} q_n^h(\alpha) = e^{-\kappa h_2} S_n^h(\alpha) + e^{\kappa h_2} s_n^h(\alpha) \\ e^{-\gamma h_2} Q_n^e(\alpha) + e^{\gamma h_2} q_n^e(\alpha) = e^{-\kappa h_2} S_n^e(\alpha) + e^{\kappa h_2} s_n^e(\alpha) \\ \gamma [e^{-\gamma h_2} Q_n^h(\alpha) - e^{\gamma h_2} q_n^h(\alpha)] = \kappa [e^{-\kappa h_2} S_n^h(\alpha) - e^{\kappa h_2} s_n^h(\alpha)] \end{cases} \quad (3-56)$$

$$\begin{cases} \frac{\kappa}{\epsilon_3} [e^{-\kappa h_3} S_n^e(\alpha) - e^{\kappa h_3} s_n^e(\alpha)] = \frac{\delta}{\epsilon_0} [e^{-\delta h_3} T_n^e(\alpha)] \\ e^{-\kappa h_3} S_n^h(\alpha) + e^{\kappa h_3} s_n^h(\alpha) = e^{-\delta h_3} T_n^h(\alpha) \\ e^{-\kappa h_3} S_n^e(\alpha) + e^{\kappa h_3} s_n^e(\alpha) = e^{-\delta h_3} T_n^e(\alpha) \\ \kappa [e^{-\kappa h_3} S_n^h(\alpha) - e^{\kappa h_3} s_n^h(\alpha)] = \delta [e^{-\delta h_3} T_n^h(\alpha)] \end{cases} \quad (3-57)$$

By solving these equations, the unknown functions are found as follows

$$\begin{aligned}
Q_n^e(\alpha) &= -j\omega\epsilon_2\rho' \frac{J_n'(\alpha\rho')}{\alpha\gamma} \left[\frac{X^e e^{\gamma h_2}}{X^e e^{\gamma h_2} - Y^e e^{-\gamma h_2}} \right] \\
q_n^e(\alpha) &= -j\omega\epsilon_2\rho' \frac{J_n'(\alpha\rho')}{\alpha\gamma} \left[\frac{Y^e e^{-\gamma h_2}}{X^e e^{\gamma h_2} - Y^e e^{-\gamma h_2}} \right] \\
S_n^e(\alpha) &= -j\omega\epsilon_3\rho' \frac{J_n'(\alpha\rho')}{\alpha\kappa} \left[\frac{2(k_2^e + 1)e^{\kappa h_3}}{X^e e^{\gamma h_2} - Y^e e^{-\gamma h_2}} \right] \\
s_n^e(\alpha) &= -j\omega\epsilon_3\rho' \frac{J_n'(\alpha\rho')}{\alpha\kappa} \left[\frac{2(k_2^e - 1)e^{-\kappa h_3}}{X^e e^{\gamma h_2} - Y^e e^{-\gamma h_2}} \right] \\
T_n^e(\alpha) &= -j\omega\epsilon_0 \frac{J_n'(\alpha\rho')}{\alpha\delta} \left[\frac{4e^{\delta h_3}}{X^e e^{\gamma h_2} - Y^e e^{-\gamma h_2}} \right] \\
Q_n^h(\alpha) &= \frac{J_n(\alpha\rho')}{\alpha^2} \left[\frac{X^h e^{\gamma h_2}}{X^h e^{\gamma h_2} + Y^h e^{-\gamma h_2}} \right] \\
q_n^h(\alpha) &= \frac{J_n(\alpha\rho')}{\alpha^2} \left[\frac{Y^h e^{-\gamma h_2}}{X^h e^{\gamma h_2} + Y^h e^{-\gamma h_2}} \right] \\
S_n^h(\alpha) &= \frac{J_n(\alpha\rho')}{\alpha^2} \left[\frac{2k_1^h(k_2^h + 1)e^{\kappa h_3}}{X^h e^{\gamma h_2} + Y^h e^{-\gamma h_2}} \right] \\
s_n^h(\alpha) &= \frac{J_n(\alpha\rho')}{\alpha^2} \left[\frac{2k_1^h(k_2^h - 1)e^{-\kappa h_3}}{X^h e^{\gamma h_2} + Y^h e^{-\gamma h_2}} \right] \\
T_n^h(\alpha) &= \frac{J_n(\alpha\rho')}{\alpha^2} \left[\frac{4k_1^h k_2^h e^{\delta h_3}}{X^h e^{\gamma h_2} + Y^h e^{-\gamma h_2}} \right]
\end{aligned} \tag{3-58}$$

where

$$\begin{aligned}
k_1^e &= \frac{\gamma/\epsilon_2}{\kappa/\epsilon_3} & k_2^e &= \frac{\kappa/\epsilon_3}{\delta/\epsilon_0} \\
X^e &= (k_2^e + 1)(k_1^e + 1)e^{\kappa d} + (k_2^e - 1)(k_1^e - 1)e^{-\kappa d} \\
Y^e &= (k_2^e + 1)(k_1^e - 1)e^{\kappa d} + (k_2^e - 1)(k_1^e + 1)e^{-\kappa d}
\end{aligned} \tag{3-59}$$

$$\begin{aligned}
 k_1^h &= \frac{\gamma}{\kappa} & k_2^h &= \frac{\kappa}{\delta} \\
 X^h &= (k_2^h + 1)(k_1^h + 1)e^{\kappa d} + (k_2^h - 1)(k_1^h - 1)e^{-\kappa d} \\
 Y^h &= (k_2^h + 1)(k_1^h - 1)e^{\kappa d} + (k_2^h - 1)(k_1^h + 1)e^{-\kappa d}
 \end{aligned} \tag{3-60}$$

and $d = h_3 - h_2$, as shown in Fig.3.6.

3.8. SINGULARITY AND BRANCH POINTS

As it was shown in (3-51), γ , κ and δ , are double-valued functions in the complex plane of α . To specify the branches of these functions which satisfy the finiteness of waves, one should note that the wave equations have the following forms:

$$\begin{aligned}
 \Psi^e &= \int_0^\infty C^e(\alpha, \phi, \rho') e^{-\gamma(\text{or } \kappa \text{ or } \delta)z} \frac{J_n(\alpha\rho)}{\gamma(\text{or } \kappa \text{ or } \delta)} d\alpha \\
 \Psi^h &= \int_0^\infty C^h(\alpha, \phi, \rho') e^{-\gamma(\text{or } \kappa \text{ or } \delta)z} \frac{J_n(\alpha\rho)}{\alpha} d\alpha
 \end{aligned} \tag{3-61}$$

For dielectric layers, we should take the cases where the dielectric layer is extended to infinity. To maintain the finiteness of waves, the term $e^{-\gamma(\text{or } \kappa \text{ or } \delta)z} J_n(\alpha\rho)$ must vanish for $r \rightarrow \infty$. This will be satisfied if this term vanishes for either $\rho \rightarrow \infty$ or $z \rightarrow \infty$. Taking the integral path where α is real or the imaginary part is small ensures this condition for $\rho \rightarrow \infty$. The convergence condition for $z \rightarrow \infty$ requires to choose the branch with positive real part for γ , κ and δ .

To discuss the singularities, let's take the case of one layer of dielectric. The wave equations for dielectric layer are

$$\Psi_2^e(\rho, \phi, z) = \sum_{n=0}^{\infty} (a_n \cos n\phi + b_n \sin n\phi)(-j\omega\epsilon_2) \int_0^{\infty} \left[\frac{e^{-\gamma z} + k^e e^{-2\gamma h_2} e^{\gamma z}}{1 - k^e e^{-2\gamma h_2}} \right] \rho' \frac{J_n'(\alpha\rho') J_n(\alpha\rho)}{\gamma} d\alpha \quad (3-62)$$

$$\Psi_2^h(\rho, \phi, z) = \sum_{n=0}^{\infty} n(b_n \cos n\phi - a_n \sin n\phi) \int_0^{\infty} \left[\frac{e^{-\gamma z} - k^h e^{-2\gamma h_2} e^{\gamma z}}{1 + k^h e^{-2\gamma h_2}} \right] \frac{J_n(\alpha\rho') J_n(\alpha\rho)}{\alpha} d\alpha$$

The integrands have a number of singular points. The singular points are due to the zeros of functions $1 - k^e e^{-2\gamma h_2}$ and $1 + k^h e^{-2\gamma h_2}$. For a lossless medium, the singular points are on the integrations path between k_0 and k_2 . The number of these singular points is

$$N = \lceil n \rceil + 1 \quad n = \frac{2h_2}{\lambda_0} \sqrt{\frac{\epsilon_2}{\epsilon_0} - 1} \quad (3-63)$$

where $\lceil n \rceil$ is the nearest integer smaller or equal to n , and λ_0 is the free space wavelength. The singular points are due to surface waves which propagate along the air-dielectric surface. To prevent the problem of singularity, we consider the dielectric layers are lossy. This makes k_0 complex and removes the singularities from the path of integration. For the lossless case the path of integration must be deformed and the branch cut must be kept outside the closed contour formed by the original and deformed path. This is discussed in more detail in [62].

3.9. SUMMARY

In this chapter the formulation for the Green's functions different structures were derived. The Green's function is the solution to the wave equation, when the source is assumed to be a magnetic or electric current ring, representing the slot and conducting ring, respectively. The antenna was divided into two parts. The interior part can be a radial waveguide with infinite extend in radial co-ordinate, or a cavity which is in fact a closed radial waveguide.

In this chapter the method of finding the Green's functions for the second part of the antenna which is the region containing the free space, were discussed in details. The novelty of the work was adding the dielectric layers and conducting rings of electric current as the second source to the structure. The Green's functions for this part were derived using the Hankel transform. Three different structures were investigated:

1. One layer of dielectric and free space
2. One layer of dielectric with an electric current ring on top and free space
3. Two layers of dielectric

To avoid singularity in the path of integration, the dielectric layer was assumed to be lossy. This assumptions removes the singular points from the path of integration.

Chapter 4

ANNULAR SLOT ARRAY ANTENNA FORMULATION

4.1. INTRODUCTION

In this chapter, the Green's functions derived in Chapter 3 are used to formulate the annular slot array antenna problem. In the antenna problem the slot fields are unknown. These unknown fields are expanded in terms of Fourier series in angular direction. The radial part of the field is expanded in terms of basis functions. This part is multiplied by the Green's functions and integrated over the radial co-ordinate. By applying the continuity of tangential magnetic field on the slot, a linear system of equation is obtained. This system of equation can be solved numerically to find the unknown coefficients of expansion of electric field. In the case of conducting ring loaded slots, the magnetic field on the conducting ring is also written in terms of basis functions and the boundary condition of zero electric field is imposed on the conducting ring in order to find the unknown coefficients of this expansion.

After finding the electric and magnetic fields, the induced magnetic current on the

top layer of dielectrics is written in terms of electric field. By using this magnetic current the far-field is determined.

At the end of chapter the higher order modes excitation is discussed.

4.2. ANTENNA WITH ONE LAYER OF DIELECTRIC

The magnetic surface current on the upper conducting plane of radial waveguide, which contains the slots, can be written as cross product of electromagnetic field and the unit vector normal to the surface. Assuming the narrow slots, the only component of electric field which contributes in the induced magnetic current is the radial component

$$\begin{aligned}\vec{J}_m &= \vec{E} \times \hat{n}|_{\text{aperture}} \\ J_m \hat{\phi} &= E_\rho (\hat{\rho} \times \hat{z})\end{aligned}\quad (4-1)$$

where \hat{n} is the normal unit vector and is equal to \hat{z} , and $\hat{\rho}$ is the radial unit vector. The radial component of electric field can be expanded in terms of Fourier series

$$E_\rho(\rho', \phi') = \sum_{n=0}^{\infty} R_n(\rho') (a_n \cos n\phi' + b_n \sin n\phi') \quad (4-2)$$

where $R_n(\rho')$ is the radial dependent part of the field. Now contribution from the slots to the total field can be obtained by integrating the product of $R_n(\rho')$ and the Green's functions obtained in the pervious sections over the aperture radial coordinate ρ' . The total field inside the waveguide region is the sum of the contribution from the slots and the sources inside this region. However, the total field in the upper region (dielectric and free

space) is entirely determined by the aperture field. The radial dependent part, $R_n(\rho')$, is generally an unknown function which can be expanded in terms of some basis functions. The simplest set of basis functions is a series of pulses of equal width and different strength, located side by side. The width of the pulses should be electrically small enough to suppress the radial variation of field. Each slot can be divided into a number of cells and the width of each cell is assumed to be the same as that for pulses. The expansion of radial dependent part is

$$R_n(\rho) = \sum_{i=1}^{IC} E_{in} P_i(\rho - \rho_i) \quad (4-3)$$

where ρ_i is the centre of the i th slot, IC is the total number of cells and

$$P_i(\rho - \rho_i) = \begin{cases} 1 & -\delta_{\rho_i}/2 \leq |\rho - \rho_i| < \delta_{\rho_i}/2 \\ 0 & \text{elsewhere} \end{cases} \quad (4-4)$$

where δ_{ρ_i} is the width of i th cell. In order to determine the complex unknowns, E_{in} , the continuity conditions of either H_ϕ or H_ρ must be performed. The extra boundary condition is the result of the assumption of narrow slots which makes the E_ϕ component negligible. In fact, one can construct another set of equations for the radial magnetic current, expand the angular dependent part in terms of basis functions and use the other continuity condition to determine the unknown coefficients for angular component of electric field. Now the wave functions inside the radial waveguide due to an array of slots on top of the radial waveguide and loaded with one layer of dielectric, as it is shown in Fig.4.1, can be written as follows

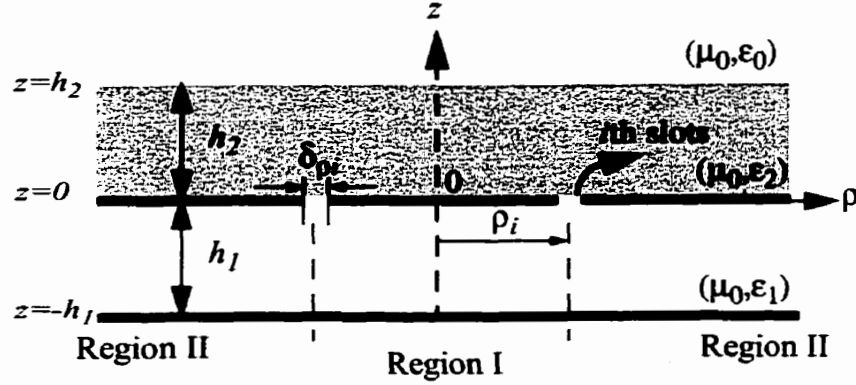


Fig.4.1. Slot array antenna on top of radial waveguide and loaded with one layer of dielectric.

$$\Psi_{1*}^{ae} = \frac{\pi\omega\epsilon_1}{2h_1} \sum_{i=1}^{IC} \sum_{n=0}^{\infty} \sum_{m=0}^{\infty} \frac{\epsilon_m}{k_{\rho m}} E_{in} (a_n \cos n\phi + b_n \sin n\phi) \cos\left(\frac{m\pi}{h_1} z\right) R_{1*inm}^{ae}(\rho, \rho_i) \quad (4-5)$$

$$\Psi_{1*}^{ah} = -j \frac{\pi^2}{2h_1^2} \sum_{i=1}^{IC} \sum_{n=0}^{\infty} \sum_{m=0}^{\infty} \frac{mn\epsilon_m}{k_{\rho m}^2} E_{in} n (b_n \cos n\phi - a_n \sin n\phi) \sin\left(\frac{m\pi}{h_1} z\right) R_{1*inm}^{ah}(\rho, \rho_i)$$

where $* \equiv R$ is for radial waveguide and $* \equiv C$ is for the cavity and:

$$R_{1Rinm}^{ae}(\rho, \rho_i) = \begin{cases} H_n^{(2)}(k_{\rho m}\rho) \rho_i J_n(k_{\rho m}\rho') \Big|_{\rho_i^-}^{\rho_i^+} & \rho \leq \rho_i \\ J_n(k_{\rho m}\rho) \rho_i H_n^{(2)}(k_{\rho m}\rho') \Big|_{\rho_i^-}^{\rho_i^+} & \rho > \rho_i \end{cases} \quad (4-6)$$

$$R_{1Rinm}^{ah}(\rho, \rho_i) = \begin{cases} H_n^{(2)}(k_{\rho m}\rho) L_n^J(k_{\rho m}\rho') \Big|_{\rho_i^-}^{\rho_i^+} & \rho \leq \rho_i \\ J_n(k_{\rho m}\rho) L_n^{H^{(2)}}(k_{\rho m}\rho') \Big|_{\rho_i^-}^{\rho_i^+} & \rho > \rho_i \end{cases}$$

where $\rho_i^{\pm} = \rho_i \pm (\delta_{\rho_i}/2)$ for replacing ρ' . The slot numbering starts from the cell with the smallest radius and ends with the cell on the last slot of largest radius. Because the

slots are assumed to be narrow the integral of product of ρ' and derivative of the Bessel function is approximated by

$$\int_{\rho_i^-}^{\rho_i^+} \rho' J_n'(k_{\rho m} \rho') d\rho' \approx \rho_i (J_n(k_{\rho m} \rho_i^+) - J_n(k_{\rho m} \rho_i^-)) = \rho_i J_n(k_{\rho m} \rho') \Big|_{\rho_i^-}^{\rho_i^+} \quad (4-7)$$

Operator $L_n^J(k_{\rho m} \rho')$ and $L_n^{H^{(2)}}(k_{\rho m} \rho')$ are defined as

$$L_n^Z(k_{\rho m} \rho') \Big|_{\rho_i^-}^{\rho_i^+} = \int_{\rho_i^-}^{\rho_i^+} Z_n(k_{\rho m} \rho') d\rho' \quad (4-8)$$

where $Z_n(x)$ denotes either the Bessel function of the first kind $J_n(x)$, Bessel function of the second kind $N_n(x)$, or the Hankel function of the first or second kind ($H_n^{(1)}(x)$ and $H_n^{(2)}(x)$). The integral in (4-8) can be calculated using the following equation[63]

$$\begin{cases} \int_0^z Z_{2n}(t) dt = \int_0^z Z_0(t) dt - 2 \sum_{k=0}^{n-1} Z_{2k+1}(z) \\ \int_0^z Z_{2n+1}(t) dt = 1 - Z_0(z) - 2 \sum_{k=0}^n Z_{2k}(z) \end{cases} \quad n = 1, 2, \dots \quad (4-9)$$

The corresponding functions for a cavity fed annular slot array antenna are

$$R_{1Cinm}^{ae}(\rho, \rho_i) = \begin{cases} J_n(k_{\rho m}\rho)\rho_i \left(N_n(k_{\rho m}\rho') \Big|_{\rho_i^-}^{\rho_i^+} - \frac{N_n(k_{\rho m}\rho_c)}{J_n(k_{\rho m}\rho_c)} J_n(k_{\rho m}\rho') \Big|_{\rho_i^-}^{\rho_i^+} \right) & \rho \leq \rho_i \\ \left(N_n(k_{\rho m}\rho) - \frac{N_n(k_{\rho m}\rho_c)}{J_n(k_{\rho m}\rho_c)} J_n(k_{\rho m}\rho) \right) \left(\rho_i J_n(k_{\rho m}\rho') \Big|_{\rho_i^-}^{\rho_i^+} \right) & \rho > \rho_i \end{cases} \quad (4-10)$$

$$R_{1Cinm}^{ah}(\rho, \rho_i) = \begin{cases} J_n(k_{\rho m}\rho) \left(L_n^N(k_{\rho m}\rho') \Big|_{\rho_i^-}^{\rho_i^+} - \frac{N_n'(k_{\rho m}\rho_c)}{J_n'(k_{\rho m}\rho_c)} L_n^J(k_{\rho m}\rho') \Big|_{\rho_i^-}^{\rho_i^+} \right) & \rho \leq \rho_i \\ \left(N_n(k_{\rho m}\rho) - \frac{N_n'(k_{\rho m}\rho_c)}{J_n'(k_{\rho m}\rho_c)} J_n(k_{\rho m}\rho) \right) \left(L_n^J(k_{\rho m}\rho') \Big|_{\rho_i^-}^{\rho_i^+} \right) & \rho > \rho_i \end{cases}$$

The wave functions for dielectric layer and free-space can be written as

$$\Psi_{**}^{ae} = \sum_{i=1}^{IC} \sum_{n=0}^{\infty} (-j\omega\epsilon_{**}) E_{in} (a_n \cos n\phi + b_n \sin n\phi) R_{**in}^{ae}(z, h_2, \rho, \rho_i) \quad (4-11)$$

$$\Psi_{**}^{ah} = \sum_{i=1}^{IC} \sum_{n=0}^{\infty} n E_{in} (b_n \cos n\phi - a_n \sin n\phi) R_{**in}^{ah}(z, h_2, \rho, \rho_i)$$

where $** \equiv 2$ is for dielectric layer and $** \equiv 0$ is for free space. The radial components for wave equations for each region are as follows

$$R_{2in}^{ae}(z, h_2, \rho, \rho_i) = \int_0^{\infty} \left[\frac{e^{-\gamma z} + k^e e^{-2\gamma h_2} e^{\gamma z}}{1 - k^e e^{-2\gamma h_2}} \right] \left(\rho_i J_n(\alpha \rho') \Big|_{\rho_i^-}^{\rho_i^+} \right) \frac{J_n(\alpha \rho) d\alpha}{\alpha \gamma} \quad (4-12)$$

$$R_{2in}^{ah}(z, h_2, \rho, \rho_i) = \int_0^{\infty} \left[\frac{e^{-\gamma z} + k^h e^{-2\gamma h_2} e^{\gamma z}}{1 + k^h e^{-2\gamma h_2}} \right] \left(L_n^J(\alpha \rho') \Big|_{\rho_i^-}^{\rho_i^+} \right) \frac{J_n(\alpha \rho) d\alpha}{\alpha}$$

$$R_{0in}^{ae}(z, h_2, \rho, \rho_i) = \int_0^{\infty} \left[\frac{(1 - k^e) e^{(\delta - \gamma) h_2} e^{-\delta z}}{1 - k^e e^{-2\gamma h_2}} \right] \left(\rho_i J_n(\alpha \rho') \Big|_{\rho_i^-}^{\rho_i^+} \right) \frac{J_n(\alpha \rho) d\alpha}{\alpha \delta} \quad (4-13)$$

$$R_{0in}^{ah}(z, h_2, \rho, \rho_i) = \int_0^{\infty} \left[\frac{(1 + k^h) e^{(\delta - \gamma) h_2} e^{-\delta z}}{1 + k^h e^{-2\gamma h_2}} \right] \left(L_n^J(\alpha \rho') \Big|_{\rho_i^-}^{\rho_i^+} \right) \frac{J_n(\alpha \rho) d\alpha}{\alpha}$$

where γ, δ are given by (3-24), and k^e, k^h are given by (3-29).

In order to determine unknown coefficients E_{in} , as it was mentioned earlier, the continuity of H_ϕ can be applied at $z = 0$

$$H_{\phi_1} - H_{\phi_2} = H_\phi^{inc} \quad (4-14)$$

where subscript 1 denotes waveguide or cavity region, and 2 denotes the dielectric region. Now, assuming a TM_{pq} mode of the radial waveguide to be incident in the waveguide or cavity region, its mode function is characterized by

$$\Psi_{1pq}^{inc} = \cos\left(\frac{p\pi}{h_1}z\right) \cos q\phi H_q^{(2)}(k_{\rho\rho}\rho) \quad \text{for radial waveguide}$$

$$\Psi_{1Cpq}^{inc} = \cos\left(\frac{p\pi}{h_1}z\right) \cos q\phi \left(N_q(k_{\rho\rho}\rho) - \frac{N_q(k_{\rho\rho}\rho_c)}{J_q(k_{\rho\rho}\rho_c)} J_n(k_{\rho\rho}\rho) \right) \quad \text{for cavity backed} \quad (4-15)$$

$$k_{\rho\rho} = \sqrt{k_1^2 - \left(\frac{p\pi}{h_1}\right)^2} \quad k_1 = \omega\sqrt{\mu_0\epsilon_1}$$

Utilizing the orthogonality property of sinusoidal functions, the coefficients of Fourier series must be

$$b_n = 0$$

$$a_n = \begin{cases} 0 & n \neq q \\ 1 & n = q \end{cases} \quad (4-16)$$

This eliminates the infinite summation on n . The summation on m is convergence and can be truncated for acceptable error margin. The boundary condition (4-17) is applied over the cells in an average sense

$$\bar{V}_{\phi 1j} = \bar{H}_{\phi 2j} \quad \begin{cases} z = 0 \\ |\rho - \rho_j| \leq \delta_{\rho j}/2 \\ 0 \leq \phi \leq 2\pi \end{cases} \quad (4-17)$$

where

$$\bar{H}_{\phi j} = \sum_{i=1}^{IC} \bar{h}(j, i) \quad (4-18)$$

$$\bar{h}(j, i) = \begin{cases} \frac{1}{\delta_{\rho j}} \int_{\rho_j^-}^{\rho_j^+} H_{i\phi} d\rho & i \neq j \\ \frac{1}{3} (H_{i\phi}(\rho_j^-) + H_{i\phi}(\rho_j) + H_{i\phi}(\rho_j^+)) & i = j \end{cases}$$

and $H_{i\phi}$ is the contribution of the i th slot to the magnetic field at the j th slot when $i \neq j$.

The average of $H_{i\phi}$ is taken for the sample points when $i = j$. The result of applying this boundary conditions is a set of linear equations in terms of aperture field coefficients in the form of

$$\left[\frac{a_{ji} + b_{ji^*}}{\delta_{\rho j}} \right] [E_{iq}] = \left[\frac{a_j^{inc}}{\delta_{\rho j}} \right] \quad (4-19)$$

Where * denotes either radial waveguide or cavity backed antenna. When the antenna is backed by a radial waveguide the result is (* \equiv R)

$$a_{jR}^{inc} = -H_q^{(2)}(k_{\rho\rho}\rho_j^+) + H_q^{(2)}(k_{\rho\rho}\rho_j^-) \quad (4-20)$$

and for antenna backed by a cavity (* \equiv C)

$$a_{jC}^{inc} = (-N_q(k_{\rho\rho}\rho_j^+) + N_q(k_{\rho\rho}\rho_j^-)) - \frac{N_q(k_{\rho\rho}c)}{J_q(k_{\rho\rho}c)} (-J_q(k_{\rho\rho}\rho_j^+) + J_q(k_{\rho\rho}\rho_j^-)) \quad (4-21)$$

and

$$a_{ji} = j\omega\epsilon_2\rho_i \int_0^\infty \left[\frac{1+k^e e^{-2\gamma h_2}}{1-k^e e^{-2\gamma h_2}} \right] \left[J_q(\alpha\rho) \Big|_{\rho_i}^{\rho_i^-} \right] \left[J_q(\alpha\rho) \Big|_{\rho_j}^{\rho_j^-} \right] \frac{d\alpha}{\alpha\gamma} +$$

$$\frac{q^2}{j\omega\mu_0\rho_j} \int_0^\infty \left[\frac{1-k^h e^{-2\gamma h_2}}{1+k^h e^{-2\gamma h_2}} \right] \left[L_q^J(\alpha\rho') \Big|_{\rho_i}^{\rho_i^-} \right] \left[L_q^J(\alpha\rho') \Big|_{\rho_j}^{\rho_j^-} \right] \frac{\gamma d\alpha}{\alpha}$$
(4-22)

$$b_{jiR} = \frac{\pi\omega\epsilon_1\rho_i}{2h_1} \sum_{m=0}^\infty \frac{\epsilon_m}{k_{\rho m}^2} \left[\begin{array}{c} J_q(k_{\rho m}\rho) \Big|_{\rho_i}^{\rho_i^-} \\ H_q^{(2)}(k_{\rho m}\rho) \Big|_{\rho_i}^{\rho_i^-} \end{array} \right] \left[\begin{array}{c} H_q^{(2)}(k_{\rho m}\rho) \Big|_{\rho_j}^{\rho_j^-} \\ J_q(k_{\rho m}\rho) \Big|_{\rho_j}^{\rho_j^-} \end{array} \right] -$$

$$\frac{\pi^3 q^2}{2\omega\mu_0 h_1^3 \rho_j} \sum_{m=0}^\infty \frac{m^2 \epsilon_m}{k_{\rho m}^2} \left[\begin{array}{c} L_q^J(k_{\rho m}\rho') \Big|_{\rho_i}^{\rho_i^-} \\ L_q^{H^{(2)}}(k_{\rho m}\rho') \Big|_{\rho_i}^{\rho_i^-} \end{array} \right] \left[\begin{array}{c} L_q^{H^{(2)}}(k_{\rho m}\rho') \Big|_{\rho_j}^{\rho_j^-} \\ L_q^J(k_{\rho m}\rho') \Big|_{\rho_j}^{\rho_j^-} \end{array} \right]$$
(4-23)

$$b_{jiC} = \frac{\pi\omega\epsilon_1\rho_i}{2h_1} \sum_{m=0}^\infty \frac{\epsilon_m}{k_{\rho m}^2} \left(\left[\begin{array}{c} N_q(k_{\rho m}\rho) \Big|_{\rho_j}^{\rho_j^-} - \left(\frac{N_q(k_{\rho m}c)}{J_q(k_{\rho m}c)} \right) J_q(k_{\rho m}\rho) \Big|_{\rho_j}^{\rho_j^-} \\ N_q(k_{\rho m}\rho) \Big|_{\rho_i}^{\rho_i^-} - \left(\frac{N_q(k_{\rho m}c)}{J_q(k_{\rho m}c)} \right) J_q(k_{\rho m}\rho) \Big|_{\rho_i}^{\rho_i^-} \end{array} \right] \left[\begin{array}{c} J_q(k_{\rho m}\rho) \Big|_{\rho_i}^{\rho_i^-} \\ J_q(k_{\rho m}\rho) \Big|_{\rho_j}^{\rho_j^-} \end{array} \right] - \right.$$

$$\left. \frac{\pi^3 q^2}{2\omega\mu_0 h_1^3 \rho_j} \sum_{m=0}^\infty \frac{m^2 \epsilon_m}{k_{\rho m}^2} \left(\left[\begin{array}{c} L_q^N(k_{\rho m}\rho') \Big|_{\rho_j}^{\rho_j^-} - \left(\frac{N_q'(k_{\rho m}c)}{J_q'(k_{\rho m}c)} \right) L_q^J(k_{\rho m}\rho') \Big|_{\rho_j}^{\rho_j^-} \\ L_q^N(k_{\rho m}\rho') \Big|_{\rho_i}^{\rho_i^-} - \left(\frac{N_q'(k_{\rho m}c)}{J_q'(k_{\rho m}c)} \right) L_q^J(k_{\rho m}\rho') \Big|_{\rho_i}^{\rho_i^-} \end{array} \right] \left[\begin{array}{c} L_q^J(k_{\rho m}\rho') \Big|_{\rho_i}^{\rho_i^-} \\ L_q^J(k_{\rho m}\rho') \Big|_{\rho_j}^{\rho_j^-} \end{array} \right] \right)$$
(4-24)

where, inside the brackets, the top row is for $j > i$ and the bottom row is for $j < i$. The diagonal elements for inside the waveguide are evaluated from the following equations

$$\begin{aligned}
b_{iiR} = & \delta_{\rho j} \frac{\pi \omega \epsilon_1 \rho_i}{6 h_1} \sum_{m=0}^{\infty} \frac{\epsilon_m}{k_{\rho m}} \left\{ \begin{aligned} & J_q'(k_{\rho m} \rho_i^-) H_q^{(2)}(k_{\rho m} \rho) \Big|_{\rho_i^-}^{\rho_i^+} + H_q^{(2)'}(k_{\rho m} \rho_i^+) J_q(k_{\rho m} \rho) \Big|_{\rho_i^-}^{\rho_i^+} + \\ & J_q'(k_{\rho m} \rho_i) H_q^{(2)}(k_{\rho m} \rho) \Big|_{\rho_i^-}^{\rho_i^-} + H_q^{(2)'}(k_{\rho m} \rho_i) J_q(k_{\rho m} \rho) \Big|_{\rho_i^-}^{\rho_i^-} \end{aligned} \right\} \\
& \delta_{\rho j} \frac{\pi^3 q^2}{6 \omega \mu_0 h_1^3 \rho_i} \sum_{m=0}^{\infty} \frac{m^2 \epsilon_m}{k_{\rho m}^2} \left\{ \begin{aligned} & J_q(k_{\rho m} \rho_i^-) \left(\int_{\rho_i^-}^{\rho_i^+} H_q^{(2)}(k_{\rho m} \rho) d\rho \right) + \\ & H_q^{(2)}(k_{\rho m} \rho_i^+) \left(\int_{\rho_i^-}^{\rho_i^+} J_q(k_{\rho m} \rho) d\rho \right) + \\ & J_q(k_{\rho m} \rho_i) \left(\int_{\rho_i^-}^{\rho_i^-} H_q^{(2)}(k_{\rho m} \rho) d\rho \right) + \\ & H_q^{(2)}(k_{\rho m} \rho_i) \left(\int_{\rho_i^-}^{\rho_i^-} J_q(k_{\rho m} \rho) d\rho \right) \end{aligned} \right\} \quad (4-25)
\end{aligned}$$

and

$$\begin{aligned}
b_{iiC} = & \frac{\delta_{\rho_j} \pi \omega \epsilon_1 \rho_i}{6h_1} \sum_{m=0}^{\infty} \frac{\epsilon_m}{k_{\rho m}} \left\{ \begin{aligned} & \left(N_q(k_{\rho m} \rho) \Big|_{\rho_i^-}^{\rho_i^-} - \left(\frac{N_q(k_{\rho m} c)}{J_q(k_{\rho m} c)} \right) J_q(k_{\rho m} \rho) \Big|_{\rho_i^-}^{\rho_i^-} \right) (J_q(k_{\rho m} \rho_i^-)) + \\ & \left(N_q'(k_{\rho m} \rho_i^+) - \left(\frac{N_q(k_{\rho m} c)}{J_q(k_{\rho m} c)} \right) J_q'(k_{\rho m} \rho_i^+) \right) (J_q(k_{\rho m} \rho) \Big|_{\rho_i^-}^{\rho_i^-}) + \\ & \left(N_q(k_{\rho m} \rho) \Big|_{\rho_i^-}^{\rho_i^-} - \left(\frac{N_q(k_{\rho m} c)}{J_q(k_{\rho m} c)} \right) J_q(k_{\rho m} \rho) \Big|_{\rho_i^-}^{\rho_i^-} \right) (J_q'(k_{\rho m} \rho_i)) + \\ & \left(N_q'(k_{\rho m} \rho_i) - \left(\frac{N_q(k_{\rho m} c)}{J_q(k_{\rho m} c)} \right) J_q'(k_{\rho m} \rho_i) \right) (J_q(k_{\rho m} \rho) \Big|_{\rho_i^-}^{\rho_i^-}) \end{aligned} \right\} \\
& \frac{\delta_{\rho_j} \pi^3 q^2}{6\omega \mu_0 h_1^3 \rho_i} \sum_{m=0}^{\infty} \frac{m^2 \epsilon_m}{k_{\rho m}^2} \left\{ \begin{aligned} & \left(L_q^N(k_{\rho m} \rho') \Big|_{\rho_i^-}^{\rho_i^-} - \left(\frac{N_q'(k_{\rho m} c)}{J_q'(k_{\rho m} c)} \right) L_q^J(k_{\rho m} \rho') \Big|_{\rho_i^-}^{\rho_i^-} \right) J_q(k_{\rho m} \rho_i^-) + \\ & \left(N_q(k_{\rho m} \rho_i^+) - \left(\frac{N_q'(k_{\rho m} c)}{J_q'(k_{\rho m} c)} \right) J_q(k_{\rho m} \rho_i^+) \right) (L_q^J(k_{\rho m} \rho') \Big|_{\rho_i^-}^{\rho_i^-}) + \\ & \left(L_q^N(k_{\rho m} \rho') \Big|_{\rho_i^-}^{\rho_i^-} - \left(\frac{N_q'(k_{\rho m} c)}{J_q'(k_{\rho m} c)} \right) L_q^J(k_{\rho m} \rho') \Big|_{\rho_i^-}^{\rho_i^-} \right) J_q(k_{\rho m} \rho_i) + \\ & \left(N_q(k_{\rho m} \rho_i) - \left(\frac{N_q'(k_{\rho m} c)}{J_q'(k_{\rho m} c)} \right) J_q(k_{\rho m} \rho_i) \right) (L_q^J(k_{\rho m} \rho') \Big|_{\rho_i^-}^{\rho_i^-}) \end{aligned} \right\} \quad (4-26)
\end{aligned}$$

4.3. CONDUCTING RING LOADED ANTENNA COVERED WITH ONE LAYER OF DIELECTRIC

In this section the structure under investigation consists of an array of annular slots on the ground plane covered with one layer of dielectric. On the top surface of dielectric an array of ring shaped conducting strips exists as shown in Fig.4.2. Each conducting ring is divided into a number of cells in radial co-ordinates. These conducting rings can be expressed as an array of electric sources (\vec{J}_e). Similarly, the array of slots can be

represented by an array of magnetic sources (\vec{J}_m).

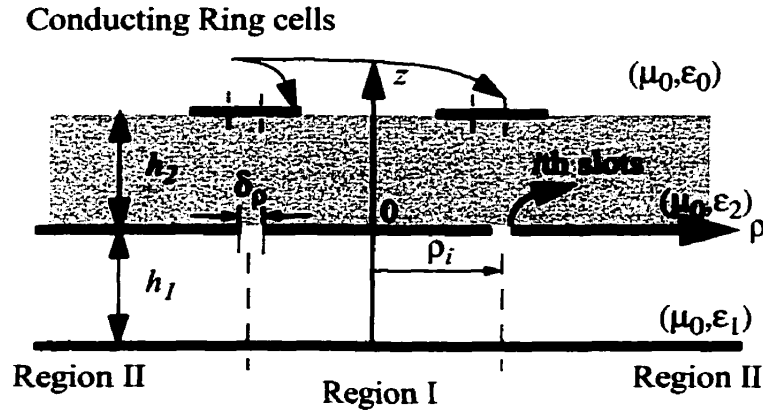


Fig.4.2. Annular slot array antenna loaded with conducting rings and covered with one layer of dielectric.

These electric and magnetic sources have unknown variation in radial co-ordinates, but their behavior in angular co-ordinates can be characterized by a Fourier series with unknown coefficients, as follows

$$\begin{aligned} \vec{J}_m &= \sum_{n=0}^{\infty} E_n(\rho') (a_{1n} \cos n\phi' + a_{2n} \sin n\phi') && \text{on the slots} \\ \vec{J}_e &= \sum_{n=0}^{\infty} H_n(\rho'') (b_{1n} \cos n\phi' + b_{2n} \sin n\phi') && \text{on the conductors} \end{aligned} \quad (4-27)$$

where the radial part of each of them can be expanded in terms of pulse basis functions. Each slot and conducting ring can be divided into a number of cells and the pulse width is the same as cell width. Total number of cells is called IS on the slots, and IC on the conducting rings. The cells on the slots are numbered from the slot with the smallest radial co-ordinate. Similarly the cells on the conducting rings are numbered from the cell with

the smallest radial co-ordinate, starting from $i = IS + 1$ to $i = IS + IC$.

$$\begin{aligned} E_n(\rho) &= \sum_{i=1}^{IS} E_{in} P_i(\rho - \rho_i) \\ H_n(\rho) &= \sum_{i=IS+1}^{IS+IC} H_{in} P_i(\rho - \rho_i) \end{aligned} \quad (4-28)$$

where $P_i(\rho - \rho_i)$ is given in (4-4).

Now the Green's functions for dielectric and free-space can be written in terms of these sources. It is worth mentioning that because the system is linear, the field at each point is the total field of contributions of slots plus the total field due to conducting rings.

The Green's functions for dielectric layer are

$$\begin{aligned} \Psi_{2L^{**}}^{ae} &= \sum_{i=1}^{IS} E_{in} (-j\omega\epsilon_{**}) \Phi_{en}(\phi) G_{in^{**}}^{ae}(\rho_i, \rho, h_2, z) + \\ &\quad \sum_{i=IS+1}^{IS+IC} H_{in} \Phi_{hn}(\phi) g_{in^{**}}^{ae}(\rho_i, \rho, h_2, z) \\ \Psi_{2L^{**}}^{ah} &= \sum_{i=1}^{IS} E_{in} n \Phi'_{en}(\phi) G_{in^{**}}^{ah}(\rho_i, \rho, h_2, z) + \\ &\quad \sum_{i=IS+1}^{IS+IC} H_{in} (j\omega\mu_0) n \Phi'_{hn}(\phi) g_{in^{**}}^{ah}(\rho_i, \rho, h_2, z) \end{aligned} \quad (4-29)$$

where:

$$\begin{aligned}
\Phi_{en}(\phi) &= a_{1n} \cos n\phi + a_{2n} \sin n\phi \\
\Phi_{hn}(\phi) &= b_{1n} \cos n\phi + b_{2n} \sin n\phi \\
\Phi'_{en}(\phi) &= a_{2n} \cos n\phi - a_{1n} \sin n\phi \\
\Phi'_{hn}(\phi) &= b_{2n} \cos n\phi - b_{1n} \sin n\phi
\end{aligned} \tag{4-30}$$

and for dielectric layer, where $** \equiv 2$, the radial components for wave functions are given by

$$\begin{aligned}
G_{in2}^{ae}(\rho_i, \rho, h_2, z) &= \int_0^\infty \left[\frac{e^{-\gamma z} + k^e e^{-2\gamma h_2} e^{\gamma z}}{1 - k^e e^{-2\gamma h_2}} \right] \left(\rho_i J_n(\alpha \rho') \Big|_{\rho_i^-}^{\rho_i^+} \right) \frac{J_n(\alpha \rho) d\alpha}{\alpha \gamma} \\
g_{in2}^{ae}(\rho_i, \rho, h_2, z) &= \int_0^\infty \left(\frac{\delta/\epsilon_0}{\gamma/\epsilon_2 + \delta/\epsilon_0} \right) \left[\frac{-e^{-\gamma h_2} (e^{-\gamma z} + e^{\gamma z})}{1 - k^e e^{-2\gamma h_2}} \right] \left(\rho_i J_n(\alpha \rho') \Big|_{\rho_i^-}^{\rho_i^+} \right) \frac{J_n(\alpha \rho) d\alpha}{\alpha}
\end{aligned} \tag{4-31}$$

$$\begin{aligned}
G_{in2}^{ah}(\rho_i, \rho, h_2, z) &= \int_0^\infty \left[\frac{e^{-\gamma z} + k^h e^{-2\gamma h_2} e^{\gamma z}}{1 + k^h e^{-2\gamma h_2}} \right] \left(L_n^J(\alpha \rho') \Big|_{\rho_i^-}^{\rho_i^+} \right) \frac{J_n(\alpha \rho) d\alpha}{\alpha} \\
g_{in2}^{ah}(\rho_i, \rho, h_2, z) &= \int_0^\infty \left(\frac{1}{\gamma + \delta} \right) \left[\frac{e^{-\gamma h_2} (e^{-\gamma z} - e^{\gamma z})}{1 + k^h e^{-2\gamma h_2}} \right] \left(L_n^J(\alpha \rho') \Big|_{\rho_i^-}^{\rho_i^+} \right) \frac{J_n(\alpha \rho) d\alpha}{\alpha}
\end{aligned}$$

where $L_n^J(\alpha \rho') \Big|_{\rho_i^-}^{\rho_i^+}$ is defined in (4-8). The Green's functions for free-space has the same form as (4-29), where $** \equiv 0$, when the radial parts are written as follows

$$\begin{aligned}
G_{in0}^{ae}(\rho_i, \rho, h_2, z) &= \int_0^\infty \left[\frac{(1 - k^e) e^{\delta h_2} e^{-\gamma h_2} e^{-\delta z}}{1 - k^e e^{-2\gamma h_2}} \right] \left(\rho_i J_n(\alpha \rho') \Big|_{\rho_i^-}^{\rho_i^+} \right) \frac{J_n(\alpha \rho) d\alpha}{\alpha \delta} \\
g_{in0}^{ae}(\rho_i, \rho, h_2, z) &= \int_0^\infty \left(\frac{\gamma/\epsilon_2}{\gamma/\epsilon_2 + \delta/\epsilon_0} \right) \left[\frac{(1 - e^{-2\gamma h_2}) e^{\delta h_2} e^{-\delta z}}{1 - k^e e^{-2\gamma h_2}} \right] \left(\rho_i J_n(\alpha \rho') \Big|_{\rho_i^-}^{\rho_i^+} \right) \frac{J_n(\alpha \rho) d\alpha}{\alpha} \\
G_{in0}^{ah}(\rho_i, \rho, h_2, z) &= \int_0^\infty \left[\frac{(1 + k^h) e^{\delta h_2} e^{-\gamma h_2} e^{-\delta z}}{1 + k^h e^{-2\gamma h_2}} \right] \left(L_n^J(\alpha \rho') \Big|_{\rho_i^-}^{\rho_i^+} \right) \frac{J_n(\alpha \rho) d\alpha}{\alpha} \\
g_{in0}^{ah}(\rho_i, \rho, h_2, z) &= \int_0^\infty \left(\frac{1}{\gamma + \delta} \right) \left[\frac{(1 - e^{-2\gamma h_2}) e^{\delta h_2} e^{-\delta z}}{1 + k^h e^{-2\gamma h_2}} \right] \left(L_n^J(\alpha \rho') \Big|_{\rho_i^-}^{\rho_i^+} \right) \frac{J_n(\alpha \rho) d\alpha}{\alpha}
\end{aligned} \tag{4-32}$$

Green's functions for the cavity and radial waveguide part is the same as those for antenna with one layer of dielectric, given in (4-10)-(4-13).

To find the unknown coefficients E_{in} and H_{in} , two sets of boundary conditions are required. The first set is the continuity of magnetic field on the slots and the second set is zero electric field on the conducting rings

$$\begin{aligned} H_{\phi_1} - H_{\phi_2} &= H_{\phi}^{inc} & z &= 0 \\ E_{\rho_2} &= E_{\rho_3} = 0 & z &= h_2 \end{aligned} \quad (4-33)$$

One should consider that in modeling the conducting ring, only the radial component of electric current was considered. If the angular component has considerable strength, both sources must be considered in deriving the Green's functions and in the antenna problem there will be an extra electric current source, which introduces extra set of unknown coefficients. Then imposing zero field on angular component of electric field can be used for forming the matrix equation.

Boundary conditions are applied in an average sense, the same way which was explained in previous section.

$$\begin{aligned} \bar{H}_{\phi j} &= \left(\sum_{i=1}^{IS+IC} \bar{h}(j, i) \right) \quad z = 0 \\ \bar{h}(j, i) &= \begin{cases} \frac{1}{\delta_{\rho_j}} \int_{\rho_j^-}^{\rho_j^+} H_{i\phi} d\rho & i \neq j \\ \frac{1}{3} (H_{i\phi}(\rho_j^-) + H_{i\phi}(\rho_j) + H_{i\phi}(\rho_j^+)) & i = j \end{cases} \\ \bar{E}_{\rho j} &= \left(\sum_{i=IS+1}^{IS+IC} \bar{e}(j, i) \right) \quad z = h_2 \\ \bar{e}(j, i) &= \frac{1}{\delta_{\rho_j}} \int_{\rho_j^-}^{\rho_j^+} E_{i\rho} d\rho \end{aligned} \quad (4-34)$$

The result of applying the mentioned boundary conditions is a set of linear system of equations. When only TM_{pq} mode is excited the matrix equation can be written in the following block matrix form

$$\begin{bmatrix} \left[\frac{a_{ji} + b_{ji}^*}{\delta_{\rho_j}} \right] & \left[\frac{c_{ji}}{\delta_{\rho_j}} \right] \\ \left[\frac{d_{ji}}{\delta_{\rho_j}} \right] & \left[\frac{e_{ji}}{\delta_{\rho_j}} \right] \end{bmatrix} \begin{bmatrix} [E_{iq}] \\ [H_{iq}] \end{bmatrix} = \begin{bmatrix} \left[\frac{a_{j^*}^{inc}}{\delta_{\rho_j}} \right] \\ [0] \end{bmatrix} \quad (4-35)$$

where the vectors $[E_{iq}]$ and $[H_{iq}]$ are unknown coefficients for the basis functions. The coefficient matrix consists of four blocks. The first block $[a_{ji} + b_{ji}^*]$ shows the contribution of the slots on the magnetic field of each slot. The second block $[c_{ji}]$ shows the contributions of each conducting ring cell on the field of each slot cell. Similarly, the third block $[d_{ji}]$ reflects the contribution of each slot on the electric field of the conducting ring cells. The last block $[e_{ji}]$ is the contribution of each conducting ring cell

on the other conducting ring cells. In (4-35), subscript * denotes either radial waveguide or cavity backed antenna. When the antenna is backed by a radial waveguide * $\equiv R$ and when it is backed by a cavity * $\equiv C$. The first block of the right hand side $[a_{j*}^{inc}]$ is given by either (4-20) or (4-21). Similarly the first block of the left hand side can be calculated from (4-22)-(4-26), where $i \leq IS$ and $j \leq IS$.

$$c_{ji} = \rho_i \int_0^\infty \left[\frac{2e^{-\gamma h_2}}{1 - k^e e^{-2\gamma h_2}} \right] \left(\frac{\delta/\epsilon_0}{\gamma/\epsilon_2 + \delta/\epsilon_0} \right) \left[J_q(\alpha\rho) \Big|_{\rho_i^-}^{\rho_i^+} \right] \left[J_q(\alpha\rho) \Big|_{\rho_j^-}^{\rho_j^+} \right] \frac{d\alpha}{\alpha} +$$

$$\frac{q^2}{\rho_j} \int_0^\infty \left[\frac{2e^{-\gamma h_2}}{1 + k^h e^{-2\gamma h_2}} \right] \left(\frac{\gamma}{\gamma + \delta} \right) \left(L_q^J(\alpha\rho') \Big|_{\rho_i^-}^{\rho_i^+} \right) \left(L_q^J(\alpha\rho') \Big|_{\rho_j^-}^{\rho_j^+} \right) \frac{d\alpha}{\alpha}$$
(4-36)

where $IS + 1 \leq i \leq IS + IC$ and $j \leq IS$.

$$d_{ji} = \rho_i \int_0^\infty \left[\frac{e^{-\gamma h_2}(1 - k^e)}{1 - k^e e^{-2\gamma h_2}} \right] \left[J_q(\alpha\rho) \Big|_{\rho_i^-}^{\rho_i^+} \right] \left[J_q(\alpha\rho) \Big|_{\rho_j^-}^{\rho_j^+} \right] \frac{d\alpha}{\alpha} +$$

$$\frac{q^2}{\rho_j} \int_0^\infty \left[\frac{e^{-\gamma h_2}(1 + k^h)}{1 + k^h e^{-2\gamma h_2}} \right] \left(L_q^J(\alpha\rho') \Big|_{\rho_i^-}^{\rho_i^+} \right) \left(L_q^J(\alpha\rho') \Big|_{\rho_j^-}^{\rho_j^+} \right) \frac{d\alpha}{\alpha}$$
(4-37)

where $i \leq IS$ and $IS + 1 \leq j \leq IS + IC$, and finally

$$e_{ji} = \frac{\rho_i}{j\omega\epsilon_0} \int_0^\infty \left[\frac{1 - e^{-2\gamma h_2}}{1 - k^e e^{-2\gamma h_2}} \right] \left[\frac{(-\delta)(\gamma/\epsilon_2)}{\gamma/\epsilon_2 + \delta/\epsilon_0} \right] \left[J_q(\alpha\rho) \Big|_{\rho_i^-}^{\rho_i^+} \right] \left[J_q(\alpha\rho) \Big|_{\rho_j^-}^{\rho_j^+} \right] \frac{d\alpha}{\alpha} +$$

$$\frac{j\omega\mu_0 q^2}{\rho_j} \int_0^\infty \left[\frac{1 - e^{-2\gamma h_2}}{1 + k^h e^{-2\gamma h_2}} \right] \left[\frac{-1}{\gamma + \delta} \right] \left(L_q^J(\alpha\rho') \Big|_{\rho_i^-}^{\rho_i^+} \right) \left(L_q^J(\alpha\rho') \Big|_{\rho_j^-}^{\rho_j^+} \right) \frac{d\alpha}{\alpha}$$
(4-38)

where $IS + 1 \leq i \leq IS + IC$ and $IS + 1 \leq j \leq IS + IC$.

4.4. ANTENNA COVERED WITH TWO LAYERS OF DIELECTRIC

For the antenna with two layers of dielectric, shown in Fig.4.3, utilizing similar routines, another set of linear equations can be found. To write these equations, first two new parameters are defined.

$$\begin{aligned} K^e &= Y^e / X^e \\ K^h &= Y^h / X^h \end{aligned} \quad (4-39)$$

where X^e, X^h, Y^e and Y^h are given by (3-59) and (3-60).

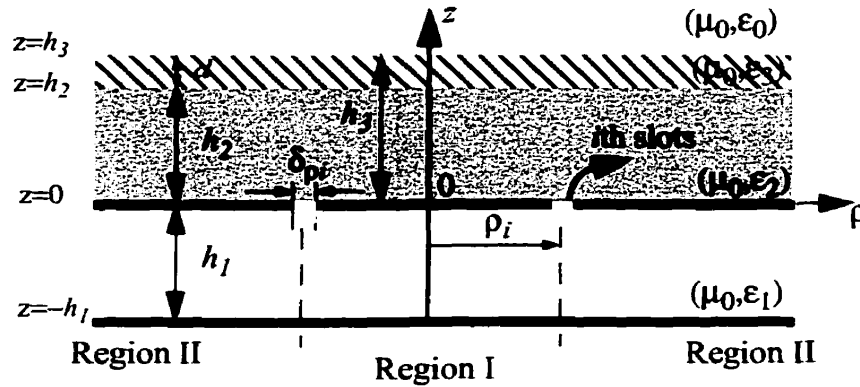


Fig.4.3. Annular slot array antenna covered with two layers of dielectric.

The Green's functions in the dielectric layer are rewritten as

$$\begin{aligned} \Psi_{D2}^e &= \sum_{n=0}^{\infty} (-j\omega\epsilon_2)(a_n \cos n\phi + b_n \sin n\phi) \int_0^{\infty} \left[\frac{e^{-\gamma z} + K^e e^{-2\gamma h_2} e^{\gamma z}}{1 - K^e e^{-2\gamma h_2}} \right] \frac{\rho' J_n'(\alpha\rho') J_n(\alpha\rho)}{\gamma} d\alpha \\ \Psi_{D2}^h &= \sum_{n=0}^{\infty} n(b_n \cos n\phi - a_n \sin n\phi) \int_0^{\infty} \left[\frac{e^{-\gamma z} + K^h e^{-2\gamma h_2} e^{\gamma z}}{1 + K^h e^{-2\gamma h_2}} \right] \frac{J_n(\alpha\rho') J_n(\alpha\rho)}{\alpha} d\alpha \end{aligned} \quad (4-40)$$

Now using this Green's functions the wave functions in the different layers can be written, using the same expansion of electric field on the slots given in (4-2)-(4-4)

$$\Psi_{D^*}^{ae} = \sum_{i=1}^{IC} \sum_{n=0}^{\infty} (-j\omega\epsilon_*) E_{in} (a_n \cos n\phi + b_n \sin n\phi) R_{D^*in}^{ae}(z, h_2, \rho, \rho_i) \quad (4-41)$$

$$\Psi_{D^*}^{ah} = \sum_{i=1}^{IC} \sum_{n=0}^{\infty} n E_{in} (b_n \cos n\phi - a_n \sin n\phi) R_{D^*in}^{ah}(z, h_2, \rho, \rho_i)$$

where subscript $*$ $\equiv 2$ represents the first dielectric layer on top of slots and for this layer the radial part is derived as:

$$R_{D2in}^{ae}(z, h_2, \rho, \rho_i) = \int_0^{\infty} \left[\frac{e^{-\gamma z} + K^e e^{-2\gamma h_2} e^{\gamma z}}{1 - K^e e^{-2\gamma h_2}} \right] \left(\rho_i J_n(k_{\rho m} \rho') \Big|_{\rho_i^-}^{\rho_i^+} \right) \frac{J_n(\alpha \rho) d\alpha}{\alpha \gamma} \quad (4-42)$$

$$R_{D2in}^{ah}(z, h_2, \rho, \rho_i) = \int_0^{\infty} \left[\frac{e^{-\gamma z} + K^h e^{-2\gamma h_2} e^{\gamma z}}{1 + K^h e^{-2\gamma h_2}} \right] \left(L_n^J(k_{\rho m} \rho') \Big|_{\rho_i^-}^{\rho_i^+} \right) \frac{J_n(\alpha \rho) d\alpha}{\alpha}$$

Comparing the result in (4-41) and (4-42) with (4-11) and (4-12), it can be seen that the Green's function for two layer case is exactly in the same form as those for one layer case when k^e, k^h are substituted by K^e, K^h , respectively. Similarly, the system of equation will be the same as (4-19)-(4-26), with the same substitution. After solving the system of equation the electric and magnetic field components can be found from the wave functions given in (4-41)-(4-42). For the second dielectric layer ($*$ $\equiv 3$) and free space ($*$ $\equiv 0$) wave functions are

$$\begin{aligned}
R_{D3in}^{ae}(z, h_2, \rho, \rho_i) &= \int_0^\infty \frac{2e^{-\gamma h_2}}{X^e} \left[\frac{(k_2^e + 1)e^{\kappa h_3} e^{-\kappa z} + (k_2^e - 1)e^{-\kappa h_3} e^{\kappa z}}{1 - K^e e^{-2\gamma h_2}} \right] \\
&\quad \left(\rho_i J_n(k_{\rho m} \rho') \Big|_{\rho_i^-}^{\rho_i^+} \right) \frac{J_n(\alpha \rho) d\alpha}{\alpha \kappa} \\
R_{D3in}^{ah}(z, h_2, \rho, \rho_i) &= \int_0^\infty \frac{2k_1^h e^{-\gamma h_2}}{X^h} \left[\frac{(k_2^h + 1)e^{\kappa h_3} e^{-\kappa z} + (k_2^h - 1)e^{-\kappa h_3} e^{\kappa z}}{1 + K^h e^{-2\gamma h_2}} \right] \\
&\quad \left(L_n^J(k_{\rho m} \rho') \Big|_{\rho_i^-}^{\rho_i^+} \right) \frac{J_n(\alpha \rho) d\alpha}{\alpha}
\end{aligned} \tag{4-43}$$

$$\begin{aligned}
R_{D0in}^{ae}(z, h_2, h_3, \rho, \rho_i) &= \int_0^\infty \left[\frac{(4e^{\delta h_3} e^{-\delta z} e^{-\gamma h_2})/X^e}{1 - K^e e^{-2\gamma h_2}} \right] \left(\rho_i J_n(k_{\rho m} \rho') \Big|_{\rho_i^-}^{\rho_i^+} \right) \frac{J_n(\alpha \rho) d\alpha}{\alpha \delta} \\
R_{D0in}^{ah}(z, h_2, h_3, \rho, \rho_i) &= \int_0^\infty \left[\frac{4(k_1^h k_2^h e^{\delta h_3} e^{-\delta z} e^{-\gamma h_2})/X^h}{1 + K^h e^{-2\gamma h_2}} \right] \left(L_n^J(k_{\rho m} \rho') \Big|_{\rho_i^-}^{\rho_i^+} \right) \frac{J_n(\alpha \rho) d\alpha}{\alpha}
\end{aligned} \tag{4-44}$$

where k_1^e, k_2^e, k_1^h and k_2^h are given by (3-59) and (3-60).

4.5. CALCULATION OF INFINITE INTEGRALS

Evaluation of matrix components in (4-19) and (4-35) involves calculation of infinite integrals of the following form

$$\begin{aligned}
I_1 &= \int_0^\infty \left[\frac{1 + k^e e^{-2\gamma h_2}}{1 - k^e e^{-2\gamma h_2}} \right] \left[J_q(\alpha \rho) \Big|_{\rho_i^-}^{\rho_i^+} \right] \left[J_q(\alpha \rho) \Big|_{\rho_j^-}^{\rho_j^+} \right] \frac{d\alpha}{\alpha \gamma} \\
I_2 &= \int_0^\infty \left[\frac{1 - k^h e^{-2\gamma h_2}}{1 + k^h e^{-2\gamma h_2}} \right] \left(\int_{\rho_i^-}^{\rho_i^+} J_q(\alpha \rho) d\rho \right) \left(\int_{\rho_j^-}^{\rho_j^+} J_q(\alpha \rho) d\rho \right) \frac{\gamma d\alpha}{\alpha}
\end{aligned} \tag{4-45}$$

To do the integration, integration path must be divided into two parts. These integrals can

be written in the form of $\int_0^\infty = \int_0^x + \int_x^\infty$, where x is an arbitrary point. For the first part the change of variable $\alpha = x \sin \tau$ and for the second part the change of variable $\alpha = \frac{x}{\sin \tau}$ are chosen. Then the integrals can be taken numerically using Gauss quadratures technique. To avoid the singularity points as it was mentioned in chapter 3, the dielectric layer is assumed to be lossy. By this assumption there are no singularity points on the path of integration.

4.6. FAR-FIELD CALCULATION FOR ANTENNA LOADED WITH ONE LAYER OF DIELECTRIC

In order to obtain the far field approximation, first the aperture field is replaced by the equivalent magnetic current distribution over the last dielectric layer, therefore the electric field at far point (r, θ, ϕ) can be expressed as [64]

$$\begin{aligned} \vec{E}(\vec{r}) &= -\frac{1}{4\pi} \nabla \times \int_{\text{aperture}} 2\vec{J}_m(\vec{r}') \frac{e^{-jk_0 R}}{R} ds' \\ \vec{J}_{ms} &= \vec{E}_{\text{aperture}} \times \hat{n} \end{aligned} \quad (4-46)$$

where $\vec{E}_{\text{aperture}}$ is the electric field over the dielectric layer, \hat{n} is the unit vector normal to the aperture, $R = |\vec{r} - \vec{r}'|$ and \vec{r}' is the vector to the source point (ρ', ϕ', z') . Using the approximation for the free space Green's function at large distances one obtains

$$\nabla \frac{e^{-jk_0 R}}{R} \approx -\frac{jk_0}{r} e^{-jk_0 r} e^{jk_0(\hat{r} \cdot \vec{r}')} \hat{r} \quad (4-47)$$

$$\vec{E}(\vec{r}) \approx \frac{jk_0}{2\pi r} e^{-jk_0 r} \int_{\text{aperture}} (J_{m\phi} \hat{\phi}' + J_{m\rho} \hat{\rho}') \times \hat{r} e^{jk_0(\hat{r} \cdot \vec{r}')} ds' \quad (4-48)$$

The cross product of unit vectors in cylindrical and spherical coordinates are

$$\begin{aligned}\hat{\phi}' \times \hat{r} &= -\sin(\phi - \phi') \cos\theta \hat{\phi} + \cos(\phi - \phi') \hat{\theta} \\ \hat{\rho}' \times \hat{r} &= -\cos(\phi - \phi') \cos\theta \hat{\phi} - \sin(\phi - \phi') \hat{\theta}\end{aligned}\quad (4-49)$$

Substituting (4-49) into (4-48) gives the following equation

$$\vec{E}(\vec{r}) \approx \frac{-jk_0}{2\pi r} e^{-jk_0 r} \{U_\phi \hat{\phi} + U_\theta \hat{\theta}\}$$

$$U_\phi = \int_0^{2\pi} \int_0^\infty (-J_{m\phi} \sin(\phi - \phi') - J_{m\rho} \cos(\phi - \phi')) \cos\theta e^{jk_0 \rho' \sin\theta \cos(\phi - \phi')} \rho' d\rho' d\phi' \quad (4-50)$$

$$U_\theta = \int_0^{2\pi} \int_0^\infty (J_{m\phi} \cos(\phi - \phi') - J_{m\rho} \sin(\phi - \phi')) e^{jk_0 \rho' \sin\theta \cos(\phi - \phi')} \rho' d\rho' d\phi'$$

$J_{m\phi}$ and $J_{m\rho}$ must be obtained from the aperture field, which can be calculated from the wave functions for free-space at $z = h_3$. After some algebraic manipulations explained in Appendix B the following results are obtained

$$\begin{aligned}U_\phi &= \sum_{i=1}^{IC} \sum_{n=0}^{\infty} -2\pi j^{n-1} E_{in} (b_n \cos n\phi - a_n \sin n\phi) \cos\theta (I_1 + I_2) \\ U_\theta &= \sum_{i=1}^{IC} \sum_{n=0}^{\infty} -2\pi j^{n-1} E_{in} (a_n \cos n\phi + b_n \sin n\phi) (I_3 + I_4)\end{aligned}\quad (4-51)$$

where

$$\begin{aligned}I_1 &= \frac{\rho_i}{k_0 \sin\theta} \int_0^\infty C_1(n, \alpha) \left(\int_0^\infty J_n'(\alpha \rho') J_n(k_0 \rho' \sin\theta) d\rho' \right) d\alpha \\ &+ \frac{n^2}{k_0 \sin\theta} \int_0^\infty \left(C_2(n, \alpha) \left(\int_0^\infty \frac{J_n(\alpha \rho') J_n(k_0 \rho' \sin\theta)}{\rho'} d\rho' \right) \right) \frac{d\alpha}{\alpha}\end{aligned}\quad (4-52)$$

$$\begin{aligned}
I_2 = & \rho_i \int_0^{\infty} C_1(n, \alpha) \left(\int_0^{\infty} J_n(\alpha \rho') J_n'(k_0 \rho' \sin \theta) d\rho' \right) \frac{d\alpha}{\alpha} \\
& + \int_0^{\infty} C_2(n, \alpha) \left(\int_0^{\infty} J_n'(\alpha \rho') J_n'(k_0 \rho' \sin \theta) \rho' d\rho' \right) d\alpha
\end{aligned} \tag{4-53}$$

$$\begin{aligned}
I_3 = & \rho_i \int_0^{\infty} C_1(n, \alpha) \left(\int_0^{\infty} J_n'(\alpha \rho') J_n'(k_0 \rho' \sin \theta) \rho' d\rho' \right) d\alpha \\
& + n^2 \int_0^{\infty} C_2(n, \alpha) \left(\int_0^{\infty} (J_n(\alpha \rho') J_n'(k_0 \rho' \sin \theta)) d\rho' \right) \frac{d\alpha}{\alpha}
\end{aligned} \tag{4-54}$$

$$\begin{aligned}
I_4 = & \frac{n^2 \rho_i}{k_0 \sin \theta} \int_0^{\infty} C_1(n, \alpha) \left(\int_0^{\infty} \frac{J_n(\alpha \rho') J_n(k_0 \rho' \sin \theta)}{\rho'} d\rho' \right) \frac{d\alpha}{\alpha} \\
& + \frac{n^2}{k_0 \sin \theta} \int_0^{\infty} C_2(n, \alpha) \left(\int_0^{\infty} (J_n'(\alpha \rho') J_n(k_0 \rho' \sin \theta)) d\rho' \right) d\alpha
\end{aligned} \tag{4-55}$$

and

$$\begin{aligned}
C_1(n, \alpha) &= \left[\frac{(1 - k^e) e^{-\gamma h_2}}{1 - k^e e^{-2\gamma h_2}} \right] (J_n(\alpha \rho_i^+) - J_n(\alpha \rho_i^-)) \\
C_2(n, \alpha) &= \left[\frac{(1 + k^h) e^{-\gamma h_2}}{1 + k^h e^{-2\gamma h_2}} \right] \int_{\rho_i^-}^{\rho_i^+} J_n(\alpha \rho) d\rho
\end{aligned} \tag{4-56}$$

These integrals can be solved analytically as explained in Appendix C. The results are

$$\begin{aligned}
U_\phi &= \sum_{i=1}^{IC} \sum_{n=0}^{\infty} -2\pi j^{n-1} E_{in} (b_n \cos n\phi - a_n \sin n\phi) \cos \theta \left(\frac{C_2(n, k_0 \sin \theta)}{k_0 \sin \theta} \right) \\
U_\theta &= \sum_{i=1}^{IC} \sum_{n=0}^{\infty} -2\pi j^{n-1} E_{in} (a_n \cos n\phi + b_n \sin n\phi) \left(\rho_i \frac{C_1(n, k_0 \sin \theta)}{k_0 \sin \theta} \right)
\end{aligned} \tag{4-57}$$

For TM_{pq} mode, $a_q = 1$ and $b_q = 0$. This simplifies the far-field patterns as follows.

$$\begin{aligned}
 U_\phi &= \sum_{i=1}^{IC} 2\pi j^{q-1} E_{iq} q \frac{\sin q\phi \cos\theta}{k_0 \sin\theta} C_2(q, k_0 \sin\theta) \\
 U_\theta &= \sum_{i=1}^{IC} -2\pi j^{q-1} E_{iq} \rho_i \frac{\cos q\phi}{k_0 \sin\theta} C_1(q, k_0 \sin\theta)
 \end{aligned} \tag{4-58}$$

where $C_1(n, \alpha)$ and $C_2(n, \alpha)$ are defined in (4-56).

4.7. FAR-FIELD CALCULATION FOR ANTENNA LOADED WITH ONE LAYER OF DIELECTRIC AND CONDUCTING RINGS

The procedure to derive far field for conducting ring loaded annular slot array antenna is very similar to that for dielectric covered one. In this case there are two sources of magnetic current on the top layer, as the electric field has two parts, one due to the slots and the other due to the conducting rings. The equation in (4-50) must be modified as

$$\vec{E}(\vec{r}) \approx \frac{-jk_0}{2\pi r} e^{-jk_0 r} \{ (U_\phi^S + U_\phi^C) \hat{\phi} + (U_\theta^S + U_\theta^C) \hat{\theta} \} \tag{4-59}$$

where superscript S refers to slot contribution and C refers to conducting ring contribution.

$$\begin{aligned}
U_{\phi}^S &= \sum_{i=1}^{IS} 2\pi j^{q-1} E_{iq} q \frac{\sin q\phi \cos \theta}{k_0 \sin \theta} C_2(q, k_0 \sin \theta) \\
U_{\theta}^S &= \sum_{i=1}^{IS} -2\pi j^{q-1} E_{iq} \rho_i \frac{\cos q\phi}{k_0 \sin \theta} C_1(q, k_0 \sin \theta) \\
U_{\phi}^C &= \sum_{i=IS+1}^{IS+IC} 2\pi j^{q-1} H_{iq} q \frac{\sin q\phi \cos \theta}{k_0 \sin \theta} C_4(q, k_0 \sin \theta) \\
U_{\theta}^C &= \sum_{i=IS+1}^{IS+IC} -2\pi j^{q-1} H_{iq} \rho_i \frac{\cos q\phi}{k_0 \sin \theta} C_3(q, k_0 \sin \theta)
\end{aligned} \tag{4-60}$$

where

$$\begin{aligned}
C_3(n, \alpha) &= \frac{1}{j\omega\epsilon_0} \left[\frac{(-\gamma)\delta/\epsilon_2}{\gamma/\epsilon_2 + \delta/\epsilon_0} \right] \left[\frac{1 - e^{-2\gamma h_2}}{1 - k^e e^{-2\gamma h_2}} \right] (J_n(\alpha\rho_i^+) - J_n(\alpha\rho_i^-)) \\
C_4(n, \alpha) &= j\omega\mu_0 \left[\frac{-1}{\gamma + \delta} \right] \left[\frac{1 - e^{-2\gamma h_2}}{1 + k^h e^{-2\gamma h_2}} \right] \int_{\rho_i^-}^{\rho_i^+} J_n(\alpha\rho) d\rho
\end{aligned} \tag{4-61}$$

4.8. FAR-FIELD CALCULATION FOR ANTENNA LOADED WITH TWO LAYERS OF DIELECTRIC

The wave functions for free-space in this case is very similar to that for the case of antenna covered with one layer of dielectric. By comparing (4-13) and (4-44), it can be seen that only coefficient dependent on the dielectric parameters are changed as follows

$$\begin{aligned}
\left[\frac{(1 - k^e) e^{\delta h_2} e^{-\delta z} e^{-\gamma h_2}}{1 - k^e e^{-2\gamma h_2}} \right] &\rightarrow \left[\frac{(4e^{\delta h_3} e^{-\delta z} e^{-\gamma h_2}) / X^e}{1 - K^e e^{-2\gamma h_2}} \right] \\
\left[\frac{(1 + k^h) e^{\delta h_2} e^{-\delta z} e^{-\gamma h_2}}{1 + k^h e^{-2\gamma h_2}} \right] &\rightarrow \left[\frac{4(k_1^h k_2^h e^{\delta h_3} e^{-\delta z} e^{-\gamma h_2}) / X^h}{1 + K^h e^{-2\gamma h_2}} \right]
\end{aligned} \tag{4-62}$$

Using the same approach mentioned for antenna with one layer of dielectric, the far field for TM_{pq} can be calculated and the results are:

$$\begin{aligned}
 U_{\phi} &= \sum_{i=1}^{IC} 2\pi j^{q-1} E_{iq} q \frac{\sin q\phi \cos\theta}{k_0 \sin\theta} D_2(q, k_0 \sin\theta) \\
 U_{\theta} &= \sum_{i=1}^{IC} -2\pi j^{q-1} E_{iq} \rho_i \frac{\cos q\phi}{k_0 \sin\theta} D_1(q, k_0 \sin\theta)
 \end{aligned}
 \tag{4-63}$$

where

$$\begin{aligned}
 D_1(n, \alpha) &= \left[\frac{(4k_1^h k_2^h e^{-\gamma h_2}) / X^e}{1 - K^e e^{-2\gamma h_2}} \right] \int_{\rho_i^-}^{\rho_i^+} J_n(\alpha\rho) d\rho \\
 D_2(n, \alpha) &= \left[\frac{(4e^{-\gamma h_2}) / X^h}{1 + K^h e^{-2\gamma h_2}} \right] (J_n(\alpha\rho_i^+) - J_n(\alpha\rho_i^-))
 \end{aligned}
 \tag{4-64}$$

4.9. EXCITATION OF HIGHER ORDER MODES

In order to cancel the even modes, it is assumed that the antenna is excited using two probes located at $\rho = \pm\rho_s$. The probes currents have equal amplitude and 180° phase difference. The outer conductor of the coaxial probe is assumed to be connected to the ground plane (Fig.4.4). In order to consider the effect of higher order modes, the power ratio of excited modes to the power of dominant mode must be calculated.

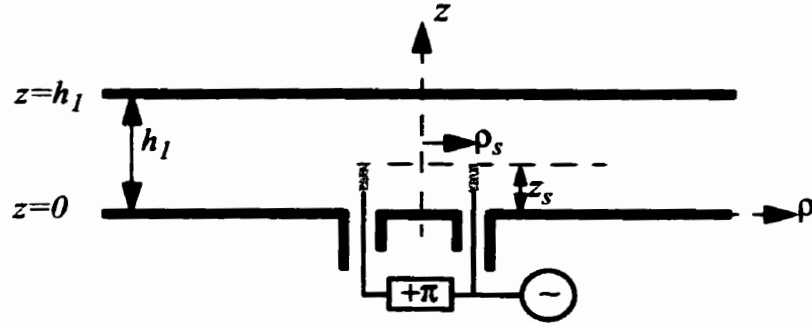


Fig.4.4. Probe configuration for radial waveguide excitation.

When the antenna is fed through infinite radial waveguide, the field inside the waveguide can be obtained from the following relation [59]

$$\begin{aligned}
 \Psi_{TM_{mn}}^{inc} &= \sum_{m=0}^{\infty} B_m \cos\left(\frac{m\pi}{h_1} z_s\right) \cos\left(\frac{m\pi}{h_1} z\right) (H_0^{(2)}(k_{\rho m} |\vec{\rho} - \vec{\rho}_s|) - H_0^{(2)}(k_{\rho m} |\vec{\rho} + \vec{\rho}_s|)) \\
 &= \sum_{m=0}^{\infty} \sum_{n=0}^{\infty} A_{mn} \cos\left(\frac{m\pi}{h_1} z\right) \begin{bmatrix} H_n^{(2)}(k_{\rho m} \rho_s) J_n(k_{\rho m} \rho) (e^{jn(\phi - \phi_s)} - e^{jn(\phi - \phi_s - \pi)}) \\ J_n(k_{\rho m} \rho_s) H_n^{(2)}(k_{\rho m} \rho) (e^{jn(\phi - \phi_s)} - e^{jn(\phi - \phi_s - \pi)}) \end{bmatrix} \quad (4-65) \\
 &= \sum_{m=0}^{\infty} \sum_{\substack{n=0 \\ n \text{ odd}}}^{\infty} 2A_{mn} \cos\left(\frac{m\pi}{h_1} z\right) \begin{bmatrix} H_n^{(2)}(k_{\rho m} \rho_s) J_n(k_{\rho m} \rho) \\ J_n(k_{\rho m} \rho_s) H_n^{(2)}(k_{\rho m} \rho) \end{bmatrix} \cos n(\phi - \phi_s)
 \end{aligned}$$

where the top row inside the bracket is for $\rho < \rho_s$, and the bottom row is for $\rho \geq \rho_s$. The addition theorem for Hankel function is used [59].

$$H_0^{(2)}(k_{\rho m} |\rho - \rho_s|) = \begin{cases} \sum_{n=0}^{\infty} H_n^{(2)}(k_{\rho m} \rho_s) J_n(k_{\rho m} \rho) e^{jn(\phi - \phi_s)} & \rho < \rho_s \\ \sum_{n=0}^{\infty} J_n(k_{\rho m} \rho_s) H_n^{(2)}(k_{\rho m} \rho) e^{jn(\phi - \phi_s)} & \rho \geq \rho_s \end{cases} \quad (4-66)$$

Using the incident wave function the magnetic field in the vicinity of the probe can be

calculated.

$$H_{\phi}^{in} = \sum_{m=0}^{\infty} \sum_{\substack{n=0 \\ n \text{ odd}}}^{\infty} -2k_{\rho m} A_{mn} \cos\left(\frac{m\pi}{h_1} z\right) H_n^{(2)}(k_{\rho m} \rho_s) J_n'(k_{\rho m} \rho) \cos n(\phi - \phi_s) \quad (4-67)$$

$$H_{\phi}^{out} = \sum_{m=0}^{\infty} \sum_{\substack{n=0 \\ n \text{ odd}}}^{\infty} -2k_{\rho m} A_{mn} \cos\left(\frac{m\pi}{h_1} z\right) J_n(k_{\rho m} \rho_s) H_n^{(2)'}(k_{\rho m} \rho) \cos n(\phi - \phi_s)$$

where H_{ϕ}^{in} refers to the region $\rho < \rho_s$ and H_{ϕ}^{out} refers to the region $\rho > \rho_s$. A_{mn} is the same for two regions to maintain the continuity of electric field. The discontinuity of H_{ϕ} caused by J_s , current on the probe, is expressed as

$$H_{\phi}^{in} \Big|_{\rho_s} - H_{\phi}^{out} \Big|_{\rho_s} = J_s \quad (4-68)$$

From this boundary condition the current on the probe can be written as

$$J_s = \sum_{m=0}^{\infty} \sum_{\substack{n=0 \\ n \text{ odd}}}^{\infty} A_{mn} \left(\frac{4j}{\pi \rho_s}\right) \cos\left(\frac{m\pi}{h_1} z\right) \cos n(\phi - \phi_s) \quad (4-69)$$

where the Wronskian of Hankel functions is used [63]

$$H_n^{(2)'}(k_{\rho m} \rho_s) J_n(k_{\rho m} \rho_s) - J_n'(k_{\rho m} \rho_s) H_n^{(2)}(k_{\rho m} \rho_s) = \frac{-2j}{\pi(k_{\rho m} \rho_s)} \quad (4-70)$$

Equation (4-69) is a Fourier cosine series in z and ϕ , where $A_{mn} \left(\frac{4j}{\pi \rho_s}\right)$ are the Fourier coefficients of J_s , that is

$$A_{mn} \left(\frac{4j}{\pi \rho_s}\right) = \frac{2\epsilon_m}{\pi h_1} \int_0^{2\pi} \int_0^{h_1} J_s \cos\left(\frac{m\pi}{h_1} z\right) \cos n(\phi - \phi_s) dz d\phi \quad (4-71)$$

where ϵ_m is defined in (3-3). For example let's assume the current on the probe can be expressed as sine function in z direction.

$$J_s = \begin{cases} \delta(\rho - \rho_s)[\delta(\phi - \phi_s) - \delta(\phi - \phi_s + \pi)] \cos k_1(z - z_s) & 0 < z < z_s \\ 0 & z_s < z < h_2 \end{cases} \quad (4-72)$$

Using (4-71)

$$A_{mn} \left(\frac{4j}{\pi \rho_s} \right) = \frac{2\epsilon_m}{\pi h_1} (1 + \cos n \phi_s) \left(\frac{\left(\frac{m\pi}{h_1} \right) \sin \left(\frac{m\pi}{h_1} z_s \right) - k_1 \sin k_1 z_s}{k^2 - \left(\frac{m\pi}{h_1} \right)^2} \right) \quad (4-73)$$

When the antenna is fed by a cavity, the incident wave function is changed as follows

$$\begin{aligned} \Psi_{TM_{mn}}^{inc} = & \sum_{m=0}^{\infty} A_m \cos \left(\frac{m\pi}{a} z \right) [N_0(k_{\rho m} |\vec{\rho} - \vec{\rho}_s|) - N_0(k_{\rho m} |\vec{\rho} + \vec{\rho}_s|)] \\ & \frac{N_0(k_{\rho m} c)}{J_0(k_{\rho m} c)} (J_0(k_{\rho m} |\rho - \rho_s|) - J_0(k_{\rho m} |\rho + \rho_s|)) (e^{jn(\phi - \phi_s)} - e^{jn(\phi - \phi_s - \pi)}) \end{aligned} \quad (4-74)$$

Using similar approach, by applying the addition theorem for Bessel functions, boundary condition at the probe, and using the Wronskian of Bessel functions, the following relation between probe current and unknown coefficients will be found

$$J_s = \sum_{m=0}^{\infty} \sum_{\substack{n=0 \\ n \text{ odd}}}^{\infty} A_{mn} \left(\frac{4}{\pi \rho_s} \right) \cos \left(\frac{m\pi}{h_1} z \right) \cos n(\phi - \phi_s) \quad (4-75)$$

4.10. SUMMARY

In this chapter it was described how to find field components for the annular slot array antennas, using the Green's functions derived in previous chapter. The solution is based on expanding the unknown electric field on the slot in terms of pulse basis function in radial co-ordinate and Fourier series in angular co-ordinate. The solution is found by integrating the product of Green's functions and the radial part of electric field over the radial co-ordinate. The unknown coefficient for pulse expansion of electric field is determined by applying the boundary conditions.

The method is expanded to the case of annular slot array antenna loaded with an array of conducting rings. The magnetic field on the conducting rings are also expanded in terms of pulse basis functions. The field components are found by adding the field components due to slots and those due to conducting rings.

The far-field is calculated using the magnetic currents on the surface of last dielectric layer. The excitation ratio for higher order modes also was found for the probe fed antenna.

In the next chapter the method described in this chapter is used to find the effects of different parameters on the antenna performance.

Chapter 5

RESULTS AND DISCUSSION

5.1. INTRODUCTION

In this chapter Boundary Value Method (BVM), described in the previous chapter for annular slot array antenna modeling, is used to show that dielectric and conducting ring loading improve the antenna performance. In the first section, to confirm the accuracy of boundary value method, its simulation results are compared with two commercial packages: Multi-Body Electromagnetic Scattering (MBES) and Zeland IE3D Software. MBES is based on the method of moments for bodies of revolution [66]. IE3D uses a general method of moments [67]. Both packages have limitations in the modeling of annular slot array antenna. MBES does not allow more than one dielectric in the structure and slots cannot be opened to a dielectric region. Also limited number of acceptable segments causes to have less accuracy for large antennas with more than three annular slots. However, MBES has the advantage of ability to simulate a finite dielectric layer. This advantage is later used to study the effects of finite radome for antennas with finite

ground plane. Also using MBES, further improvements are achieved by adding an open cavity to the structure. MBES is not able to model an infinite radial waveguide. In order to confirm the results for infinite radial waveguide and infinite dielectric layers, IE3D is used for comparison. The disadvantage of using IE3D is more computation time and required memory. The reason is that MBES and BVM use the angular symmetry to simplify the problem, while IE3D does not put any assumption on the structure. Adding the cavity wall also causes huge increase in the matrix dimension and increases the computation time further. Therefore this package is only used to confirm the results given by BVM for infinite radial waveguide fed antennas with one or two annular slots.

After confirming the BVM results, it is used to study the effect of various parameters on the antenna directivity and radiation characteristics.

5.2. CONFIRMATION OF BOUNDARY VALUE METHOD

5.2.1. Dielectric Covered Annular Slot Array Antenna

For the antenna fed by radial waveguide and covered with one layer of dielectric, simulation results were compared only with IE3D package. Structures in MBES can not have slots which open to a dielectric layer. In addition having infinite radial waveguide and ground plane is impossible in MBES. The feeding in IE3D was realized using two dipoles at the central region with 180 degrees phase difference. Table (5-1) shows the antennas dimensions and Fig.5.1 shows the configuration. Two groups of antennas were simulated. Antenna in group (a) were larger, because the first slots were located at $0.95\lambda_0$.

In group (b) the first slots were located at $0.45\lambda_0$. The radiation patterns in E and H- planes are shown for one and two slot antennas of group (a) in Fig.5.2 and Fig.5.3, respectively. Because of symmetry, only half of the radiation patterns are shown. The right side of the figure shows H-plane radiation patterns and left hand side shows E-plane radiation patterns. Good agreement was achieved. The difference could be because of higher order modes excitation. In BVM, it was assumed that only TM_{01} mode was excited inside the waveguide, while higher order modes were also excited in IE3D. This difference becomes more clear for antennas in group (b), where the first slot was moved toward the centre. Around the probes higher order modes were stronger and when the slots were closer to the probes their effects appeared in the radiation patterns. Fig.5.4-Fig.5.6 show the radiation patterns for antennas with one, two and three annular slots, respectively. The antennas were covered with one layer of dielectric of thickness $h_2=0.25\lambda_d$ as shown in Table (5-1). Although the higher order modes became more dominant in these cases, the side lobe levels in E-plane were much lower in comparison to the pervious cases, where the first slots were located at $\rho_1=0.95\lambda_0$.

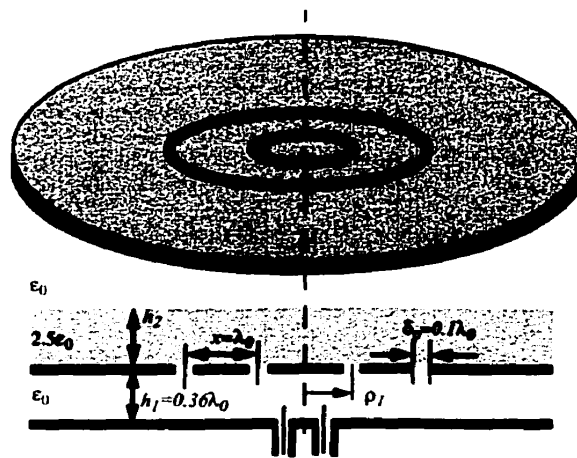


Fig.5.1. Configuration of dielectric covered antenna for comparison with IE3D.

Table (5-1) Dimensions for antenna covered with one layer of dielectric.

Parameter	Group (a) Value (Sizes in free-space wavelength (λ_0))	Group (b) Value (Sizes in free-space wavelength (λ_0))
δ_ρ	0.1	0.1
ρ_l	0.95	0.45
x	1	1
h_1	0.36	0.36
h_2	0.4	0.158
ϵ_{r1}	1.0	1.0
ϵ_{r2}	2.5	2.5

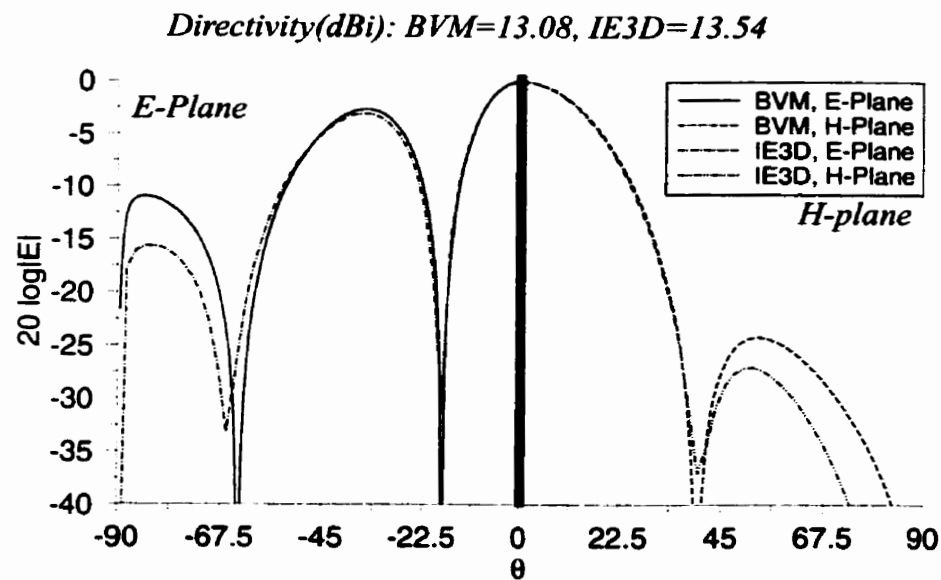


Fig.5.2. Radiation patterns for dielectric covered single slot antenna shown in Fig.5.1, comparison between BVM and IE3D, dimensions as group (a) in Table (5-1).

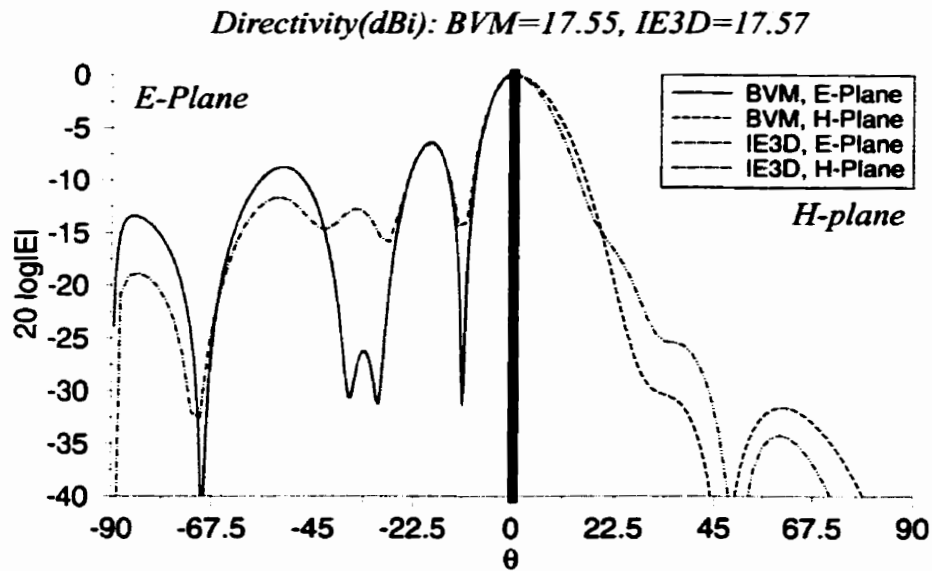


Fig.5.3. Radiation pattern for dielectric covered double slot antenna shown Fig.5.1, comparison between BVM and IE3D, dimensions as group (a) in Table (5-1).

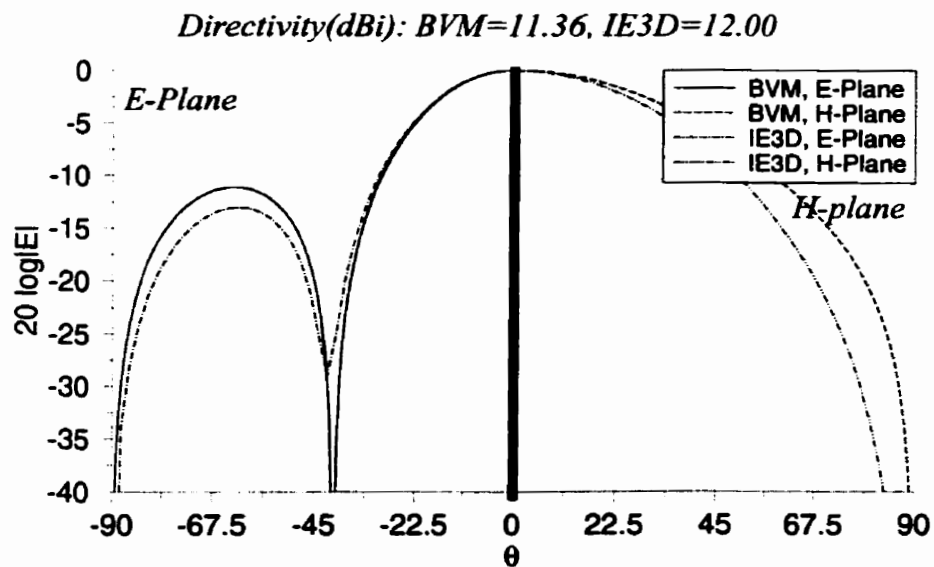


Fig.5.4. Radiation patterns for dielectric covered single slot antenna shown in Fig.5.1, when the first slot was moved toward the centre, dimensions as group (b) in Table (5-1).

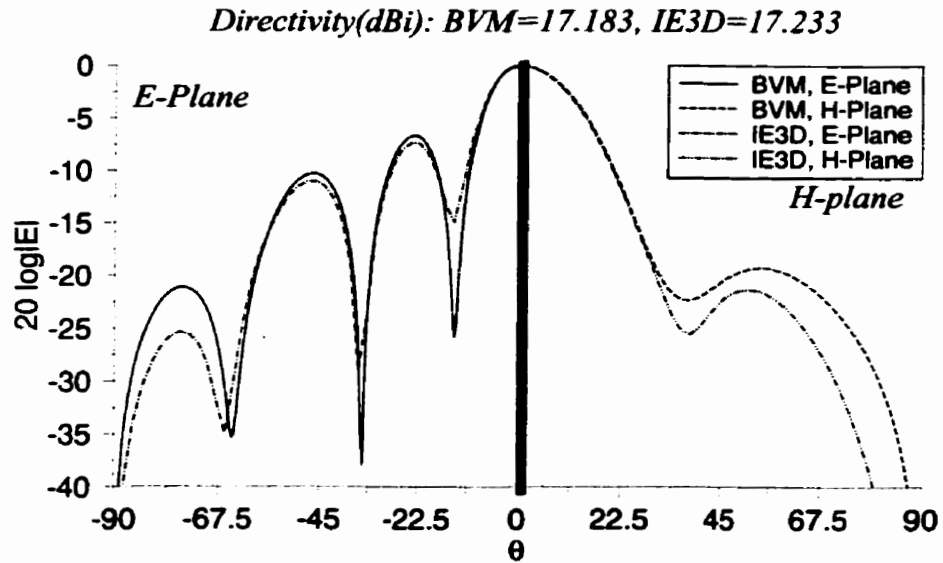


Fig.5.5. Radiation patterns for dielectric covered double slot antenna shown in Fig.5.1, when the first slot was moved toward the centre, dimensions as group (b) in Table (5-1).

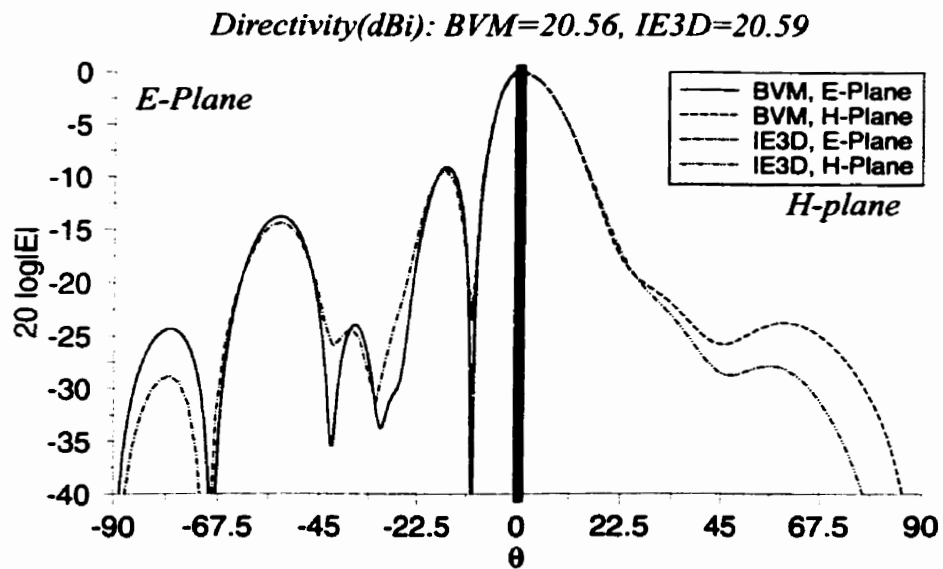


Fig.5.6. Radiation patterns for dielectric covered three slot antenna shown in Fig.5.1, when the first slot was moved toward the centre, dimensions as group (b) in Table (5-1).

For the antenna covered with two layers of dielectric, comparison was made among BVM, IE3D and MBES. The first layer was assumed to be air, so the configuration would be suitable for simulation by MBES. In MBES simulation slots were backed by a cavity, and ground plane was finite. This may provide better directivity. The waveguide fed antenna configuration is shown in Fig.5.7 and the dimensions are given in Table (5-2). Fig.5.8 shows the radiation patterns for three slot antenna without dielectric cover, and Fig.5.9 shows the radiation patterns of the same antenna when covered with a layer of dielectric at the distance of half a wavelength above the plane containing the slots.

Table (5-2) Dimensions for antenna covered with two layers of dielectric.

Parameter	Value (Sizes in free-space wavelength (λ_0))
δ_p	0.1
ρ_1	0.95
x	1
h_1	0.36
h_2	0.5
$d=h_3-h_2$	0.2
ϵ_{r1}	1.0
ϵ_{r2}	1.0
ϵ_{r3}	2.5

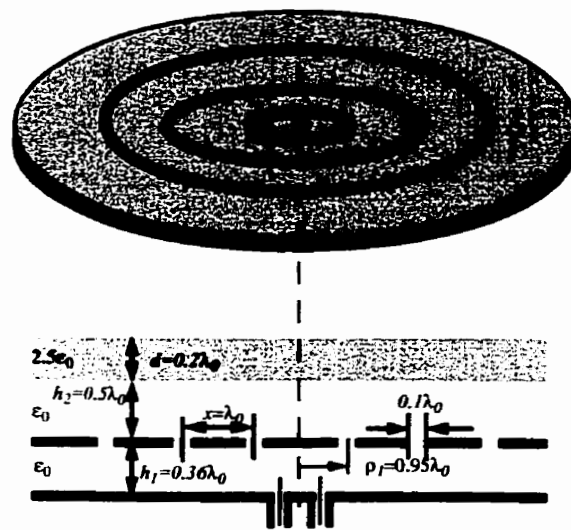


Fig.5.7. Radome covered three slot antenna configuration for comparison between BVM and IE3D.

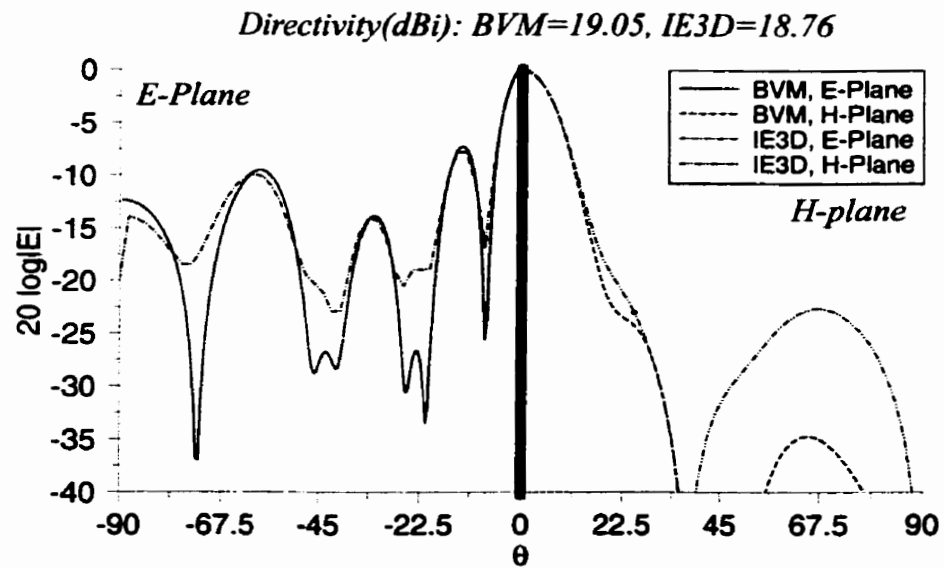


Fig.5.8. Radiation patterns for three slot antenna without dielectric radome, comparison between BVM and IE3D.

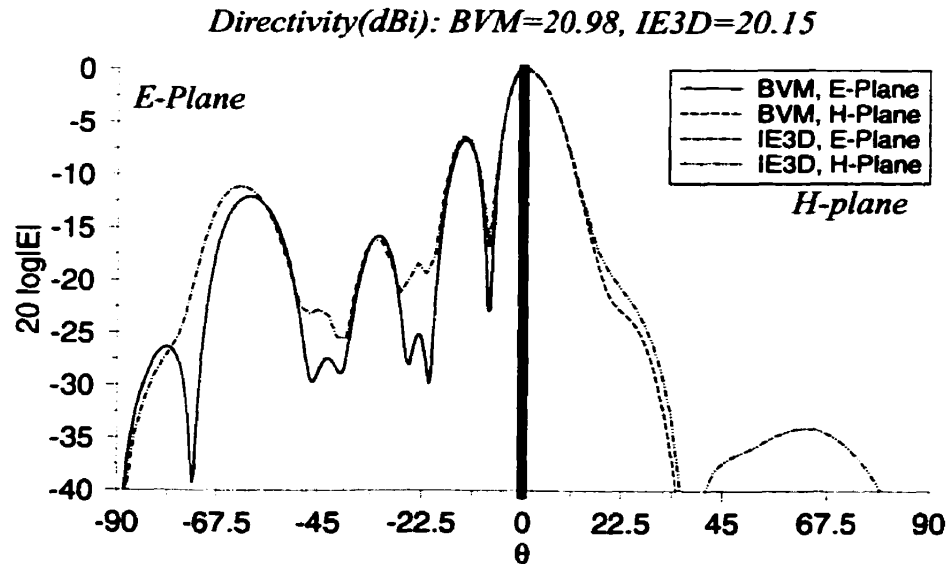


Fig.5.9. Radiation patterns for three slot antenna covered with dielectric radome as shown in Fig.5.7, comparison between BVM and IE3D.

The same antenna was simulated using BVM when it was fed through cavity and the result was compared with MBES simulation result. The cavity radius (ρ_c) was $3.3\lambda_0$ as shown in Fig.5.10. Radiation patterns shown in Fig.5.11 corresponds to the case when there was no dielectric cover on top. By adding the dielectric cover at the distance of half a wavelength above the slots, directivity is increased. Radiation patterns and directivities given by MBES and BVM are compared in Fig.5.12. It should be noted that although in both methods the antenna was backed by a cavity, the ground plane in BVM was assumed to be infinite, while in MBES its radius was the same as the cavity. This is a reason for the differences in the radiation patterns around the horizon.

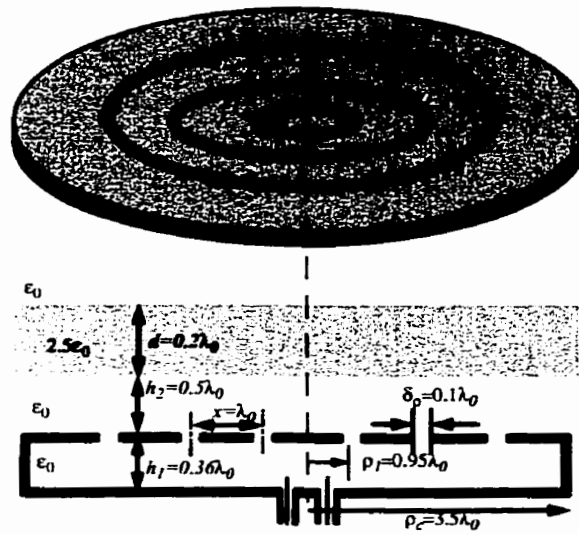


Fig.5.10. Cavity fed radome covered three slot antenna configuration for comparison between BVM and MBES.

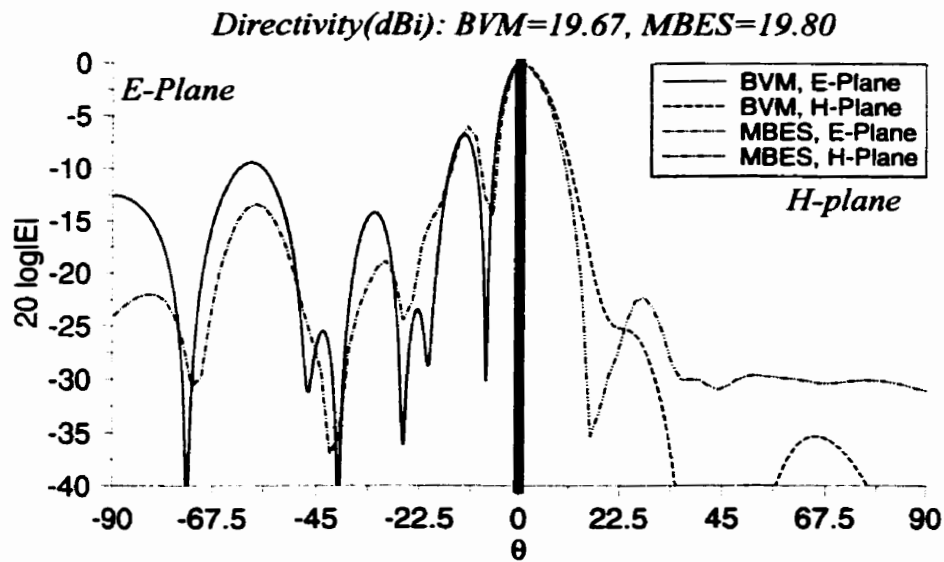


Fig.5.11. Radiation patterns for cavity fed three slot antenna without dielectric radome, comparison between BVM and MBES.

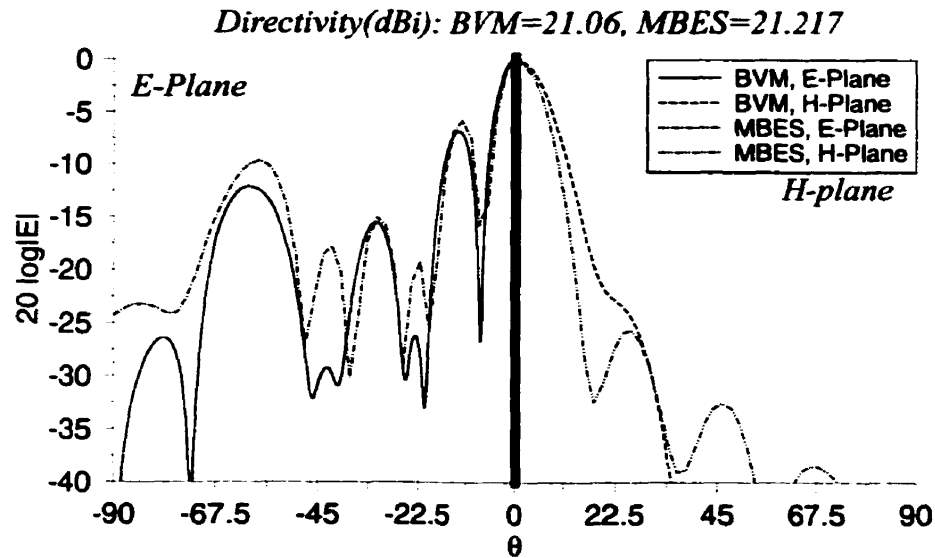


Fig.5.12. Radiation patterns for dielectric covered, cavity fed three slot antenna shown in Fig.5.10, comparison between BVM and MBES.

The simulation results for cavity fed antenna with smaller rings are also compared with MBES simulation results. Fig.5.13 shows the radiation patterns and directivity of a three slot cavity fed antenna covered with a radome with dielectric constant of $\epsilon_r=2.5$ and thickness of $d=0.158\lambda_0$, which is quarter wavelength in the dielectric. The distance between the dielectric and ground plane was half a wavelength. Cavity radius was λ_0 . Other cavity dimensions were the same as Fig.5.10.

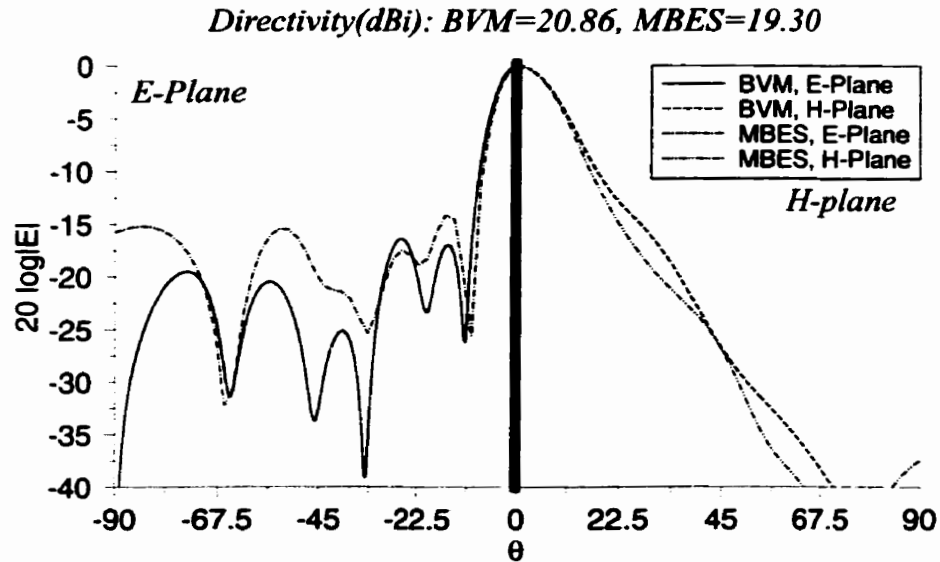


Fig.5.13. Radiation patterns for dielectric covered, cavity fed three slot antenna shown in Fig.5.10, when the first slot was moved toward the centre, $\rho_1=0.45\lambda_0$, $\rho_c=0.05\lambda_0$, $\epsilon_{r2}=2.5$, $h_2=0.158\lambda_0$.

5.2.2. Conducting Ring Loaded Annular Slot Array Antenna

For the conducting ring loaded annular slot array antenna, radiation pattern and directivity given by BVM method are compared with simulation results given by IE3D and MBES. The antenna structure is shown in Fig.5.14 and dimensions are given in Table (5-3). In IE3D and BVM simulations, antennas were fed through infinite radial waveguide. In MBES simulations, antennas were backed by a cavity with the radius of 1.5 and 2.5 wavelength for single and double slot antennas, respectively. Radiation pattern given by MBES shows differences around the horizon, due to finite ground plane. For both IE3D and BVM, ground planes were infinite.

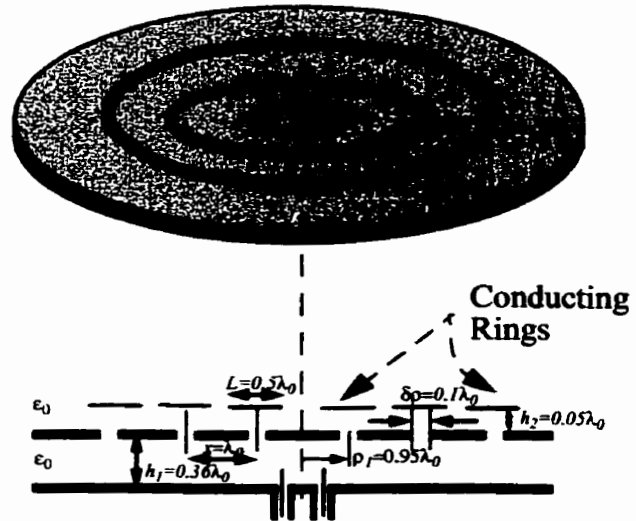


Fig.5.14. Conducting ring loaded annular slot array antenna fed through radial waveguide.

Table (5-3) Dimensions for conducting ring loaded antenna.

Parameter	Value (Sizes in free-space wavelength (λ_0))
δ_ρ	0.1
ρ_1	0.95
x	1
h_1	0.36
h_2	0.05
ϵ_{r1}	1.0
ϵ_{r2}	1.0
L	0.5

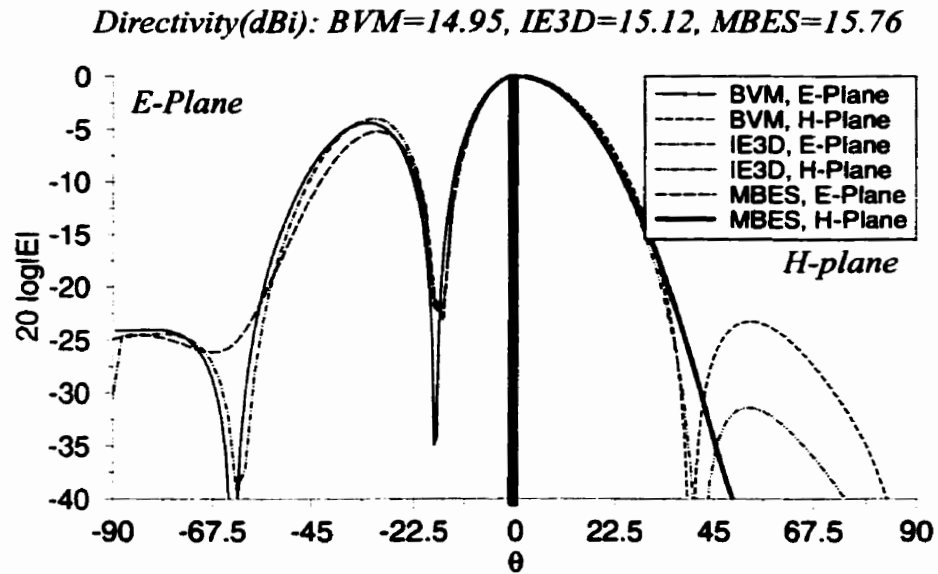


Fig.5.15. Radiation patterns for conducting ring loaded single slot antenna as shown in Fig.5.14, comparison among BVM, IE3D and MBES, dimensions as Table (5-3).

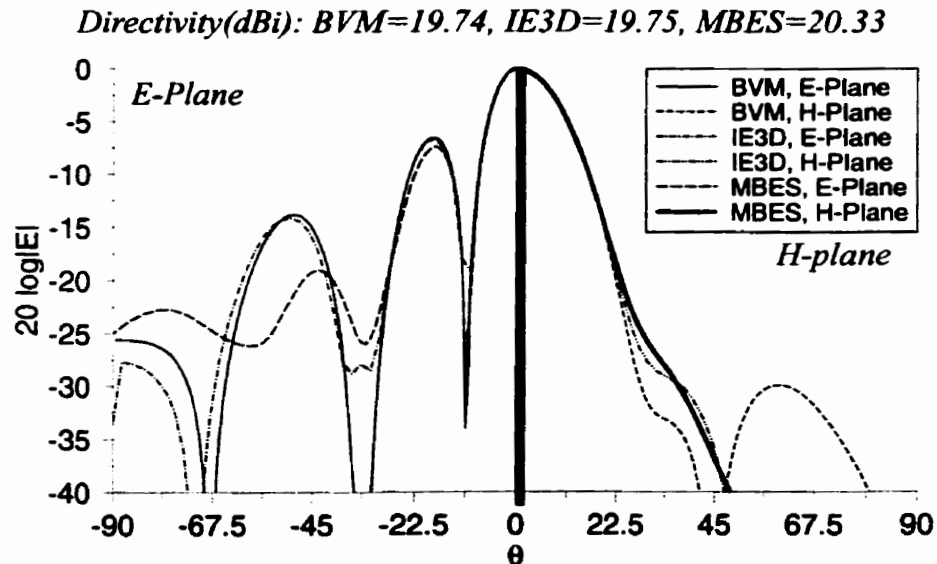


Fig.5.16. Radiation patterns for conducting ring loaded two slot antenna as shown in Fig.5.14, comparison among BVM, IE3D and MBES.

In [68], the conducting ring loaded annular slot array antenna was discussed as “*Double Layer High-Gain Microstrip Array Antenna*”. Experimental data given in this paper are compared with simulation results from BVM in Fig.5.17. Dimensions are given in Table (5-4). In this case, two first odd modes, TM_{01} and TM_{03} were excited and combined with the power ration of ‘ pr ’. It is not clear in the paper if the experiment was done by using two probes, canceling even modes or not, and the differences might be because of excitation of even modes and other higher order odd modes.

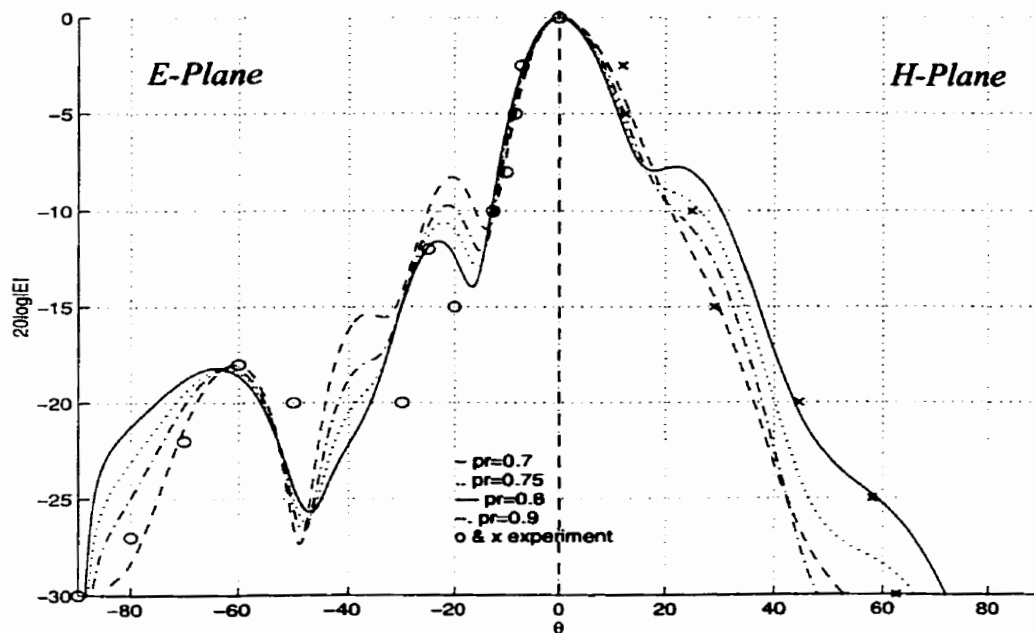


Fig.5.17. Radiation pattern comparison between BVM and experimental data taken from [68], ‘ pr ’ is the power ratio for the TM_{01}/TM_{03} modes.

Table (5-4) Dimensions for double layer microstrip array antenna.

Parameter	Value (Sizes in free-space wavelength (λ_0))
δ_p	0.0344
ρ_i	0.448, 1.138, 1.810
<i>number of slots</i>	3
h_2	0.0131
ϵ_{r1}	2.94
ϵ_{r2}	2.94
L	0.207

5.2.3. Input Impedance

For the antennas simulated by IE3D, the excitation was realized using two probes, with 180 degrees phase difference, to cancel the even modes. The probes were located close to the centre. All the antennas were designed for the frequency of 11.5GHz. For this frequency, it was found that the probes with the height of 5.9mm, located at 10mm from the centre of the antenna, provide good matching at the input. To investigate the effects of dielectric and conducting ring loading on the input impedance, S_{11} for antennas with one and two slots was compared with that for the same antennas covered with a layer of dielectric of dielectric constant 2.5 and thickness of $0.4\lambda_0$. The radiation patterns of these antennas are given in Fig.5.2 and Fig.5.3. Also for the same antennas, the conducting rings were added on the top. The radiation patterns of conducting ring loaded antenna are shown in Fig.5.15 and Fig.5.16. S_{11} for the single and double slot antennas, with and without

dielectric cover and conducting rings are shown in Fig.5.18 and Fig.5.19. The dimensions of the antennas were the same as Table (5-1) and Table (5-3). The results show that dielectric loading does not change the input impedance very much, but conducting ring loading decreases the return loss around the centre frequency.

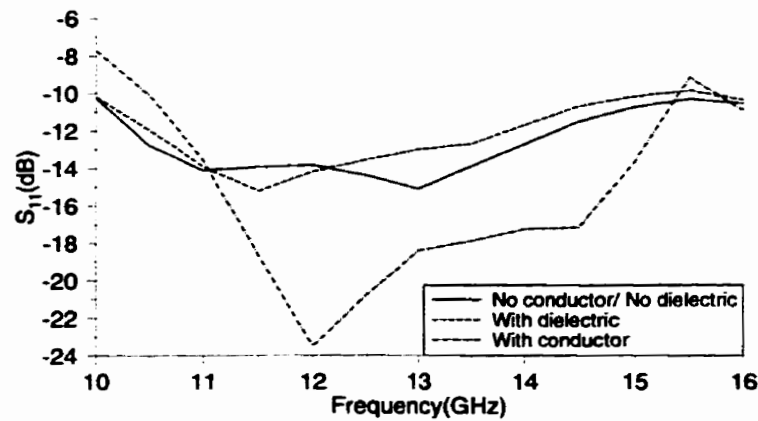


Fig.5.18. S_{11} for single slot antennas, with and without dielectric cover and conducting rings, dimensions as given in Table (5-1) and Table (5-3).

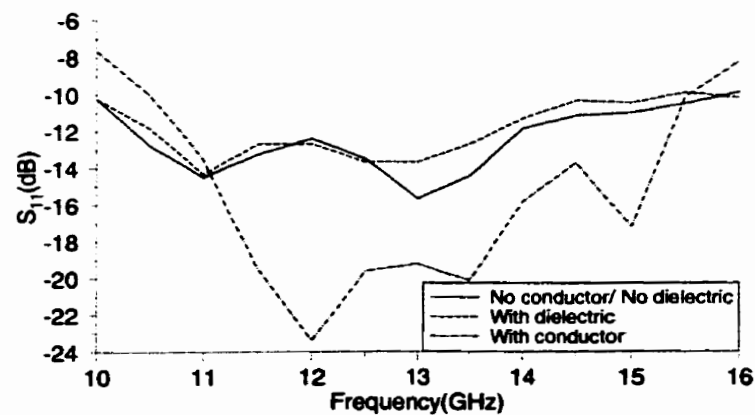


Fig.5.19. S_{11} for double slot antennas, with and without dielectric cover and conducting rings, dimensions as given in Table (5-1) and Table (5-3).

Fig.5.20 compares the return loss for three slot antennas, with and without dielectric radome, located at half a wavelength above the slots. The radiation patterns of the antenna are shown in Fig.5.6 and Fig.5.7. The dimensions are given in Table (5-2). Generally, the dielectric loading does not change the impedance bandwidth, while the conducting ring loading improves the input impedance around the centre frequency significantly.

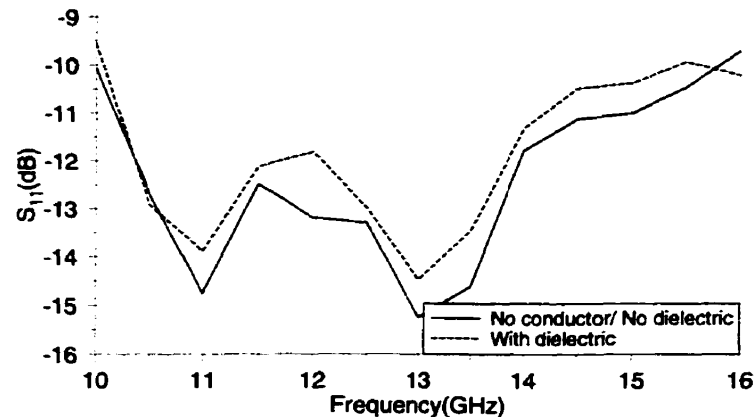


Fig.5.20. S_{11} for three slot antennas, with and without dielectric cover, dimensions as given in Table (5-2).

5.2.4. Computation Time

For two sets of simulation, memory requirement and CPU time are compared. Simulations for IE3D were done using a Personal Computer, Pentium 200MHz. BVM was implemented using MATLAB(Ver. 5) and ran on the same computer. In comparing the results, one should keep in mind that MATLAB run time is much higher than lower level programming languages, e.g. C or C++. It is expected that if the method was implemented

using such programming languages the run time would have been at least 50 to 200 times smaller. Table (5-5) shows the results for 6 different cases. The first two cases are dielectric covered annular slot antennas with one and two slot rings, using the same dimensions given in Table (5-1). Cases 4 and 5 are for three slot antennas with and without dielectric radome, respectively. Between the antenna slots and the radome there was an air gap, as shown in Fig.5.7, with dimension given in Table (5-2). The last two cases are conducting ring loaded annular slot antennas, as shown in Fig.5.14, with the dimensions given in Table (5-3). One can see that adding the conducting rings increases the run time for both BVM and IE3D. This increase in time for BVM was due to calculation of the infinite integrals, while for IE3D it was due to the increase of matrix size.

Table (5-5) Comparison of memory and CPU time requirement between IE3D and BVM.

Case #	No. of Slots	Dielectric Covered	No. of Conducting Rings	IE3D No. of Unknowns	BVM No. of Unknowns	IE3D CPU Time (sec-onds)	BVM CPU Time (sec-onds)
1	1	yes	0	330	1	104	6.2
2	2	yes	0	890	2	378	15.3
3	3	no	0	408	3	89	23.0
4	3	yes	0	1998	3	4063	28.9
5	1	no	1	924	6	398	76.6
6	2	no	2	2642	12	9665	351.0

MBES was run on Unix ULTRA-I workstation. BVM was run on MATLAB5 on the same machine. The first two cases are for antennas without any dielectric or conducting ring load, with one and two ring of slots. Antenna configuration is shown in Fig.5.10, when the dielectric covered is removed. Cases 3 and 4 are for three slot antennas with and without dielectric radome. The last two cases are conducting ring loaded antennas with one and two slots. In the case of conducting ring loaded antenna, MBES is faster than BVM. The reason is again the time required for computation of infinite integrals. This can be improved by using lower level programming languages and better and faster methods for integration. The method of integration in these simulations was Gauss-quadrature.

Table (5-6) Comparison of memory and CPU time requirement between MBES and BVM.

Case #	No. of Slots	Dielectric Covered	No. of Conducting Rings	MBES No. of Unknowns	BVM No. of Unknowns	MBES CPU Time (sec-onds)	BVM CPU Time (sec-onds)
1	1	no	0	188	1	7	5.3
2	2	no	0	216	2	22	12
3	3	no	0	304	3	40	20
4	3	yes	0	656	3	199	22
5	1	no	1	168	6	17	56.6
6	2	no	2	336	12	40	214

5.3. EFFECT OF VARIOUS PARAMETERS FOR INFINITE STRUCTURE

In this section BVM is used to investigate effects of various parameters and dimensions on the annular slot array antenna performance. In this method the dielectric layer and ground plane were assumed to be infinite. To consider the effect of finite ground plane and dielectric radome, a numerical method must be used. This is discussed in the next section. For all the simulations in this section, the antenna was fed through cavity, except when it is mentioned as fed by a radial waveguide.

5.3.1. Cavity Radius

In Fig.5.21-Fig.5.23 cavity radius effects on the antenna directivity, aperture efficiency and E-plane side lobe level are shown. The antennas with three and five slots without any dielectric cover were considered. When the distance between the last slot and conducting cavity wall becomes quarter wavelength in free space ($\rho_c - \rho_n = 0.25\lambda_0$), the directivity and aperture efficiency drop and E-plane side lobe level increases significantly.

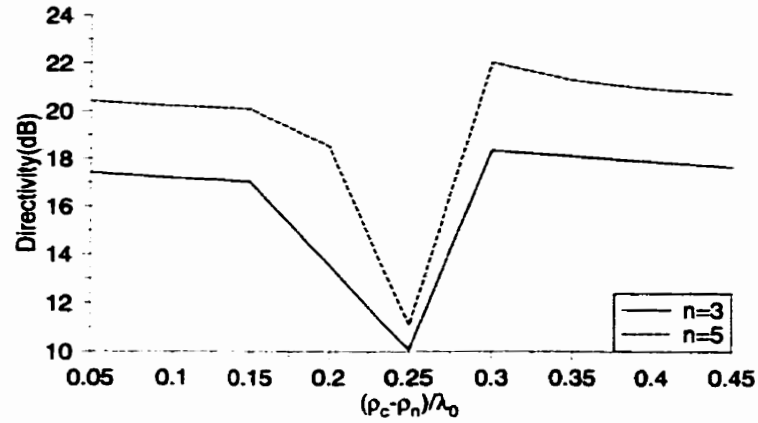


Fig.5.21. Cavity radius (ρ_c) effects on the directivity of unloaded annular slot array antennas, n =number of slots, $\rho_1=0.45\lambda_0$, $x=\lambda_0$, $\delta_p=0.1\lambda_0$, $\epsilon_{r1}=1$, $h_1=0.1\lambda_0$.

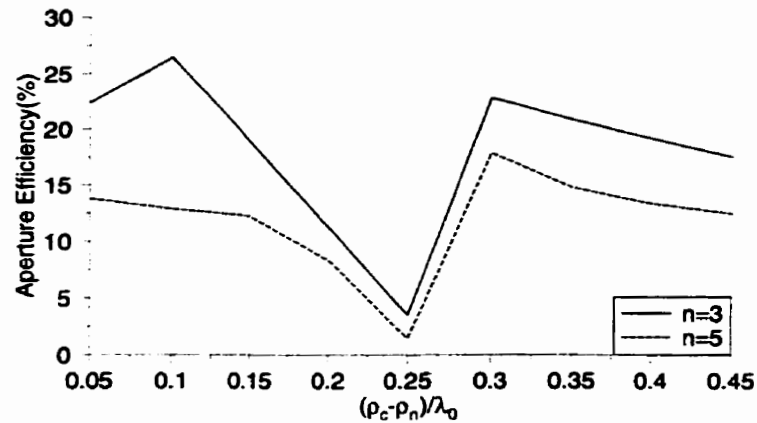


Fig.5.22. Cavity radius (ρ_c) effects on the aperture efficiency of unloaded annular slot array antennas, dimensions as Fig.5.21.

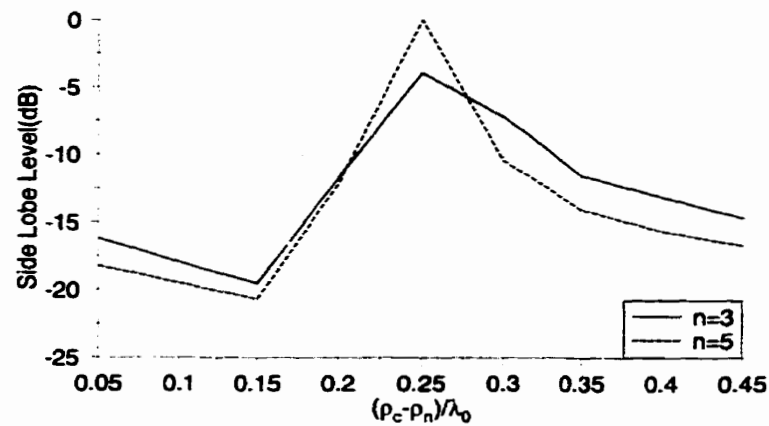


Fig.5.23. Cavity radius (ρ_c) effects on the E-plane side lobe level of unloaded annular slot array antennas, dimensions as Fig.5.21.

For dielectric loaded antennas, a three slot antenna was considered and covered with a dielectric layer with three different dielectric constants 2.5, 4.0 and 10. For dielectric thickness of $0.8\lambda_d$, where λ_d is the wavelength in the dielectric, directivity, aperture efficiency and E-plane side lobe level are shown in Fig.5.24-Fig.5.26. These figures show the drop in directivity when the distance from last slot to the cavity wall is the odd multiples of quarter wavelengths. But this is not the case when the dielectric thickness is changed from $0.8\lambda_d$ to $0.25\lambda_d$. Fig.5.27 and Fig.5.28 show that for dielectric constant of 4.0, the directivity remains almost constant and E-plane side lobe level is much lower than the other cases. Therefore, if it is desired to have insensitive directivity and low side lobe level, dielectric constant of 4.0 with quarter wavelength thickness is optimum. However, if the higher directivity is required, other dielectric constants must be chosen and the distance between the last slot and cavity wall must be kept around half a wavelength.

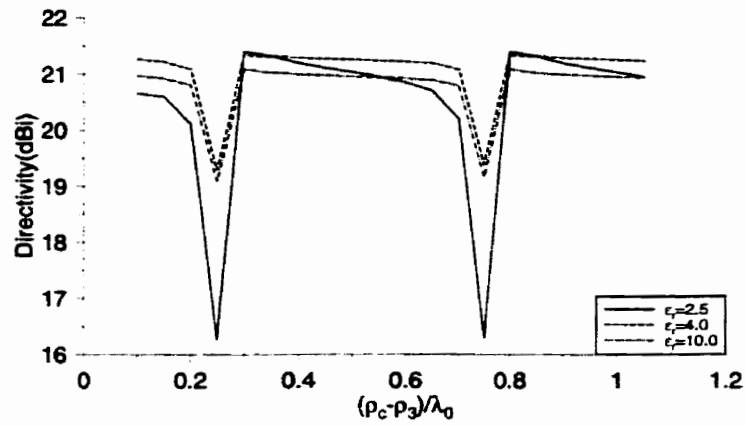


Fig.5.24. Cavity radius (ρ_c) effects on the directivity of dielectric covered three slot antennas, when dielectric thickness is ($h_2=0.8\lambda_d$), number of slots=3, $\rho_1=0.95\lambda_0$, $x=\lambda_0$, $\delta_p=0.1\lambda_0$, $\epsilon_{r1}=1, \epsilon_{r2}=\epsilon_r$, $h_1=0.36\lambda_0$.

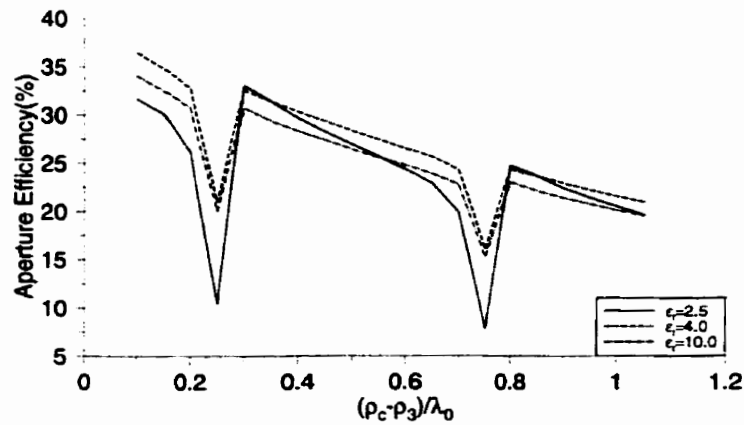


Fig.5.25. Cavity radius (ρ_c) effects on the aperture efficiency of dielectric covered three slot antennas, when dielectric thickness is ($h_2=0.8\lambda_d$), dimensions as Fig.5.24.

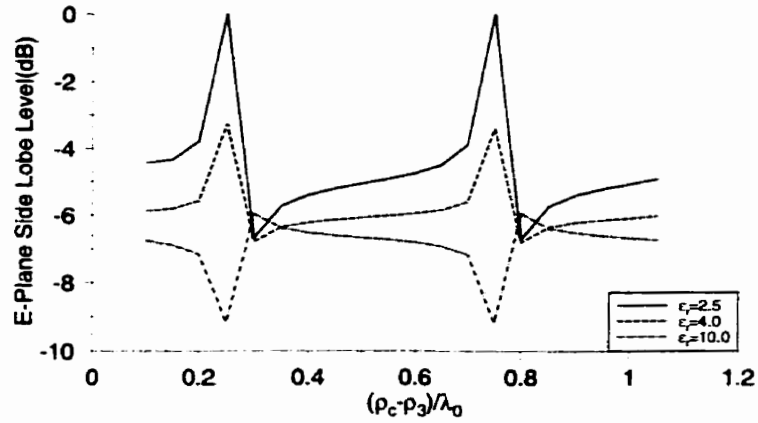


Fig.5.26. Cavity radius (ρ_c) effects on the E-plane side lobe level of dielectric covered three slot antennas, when dielectric thickness is ($h_2 = 0.8\lambda_d$), dimensions as Fig.5.24.

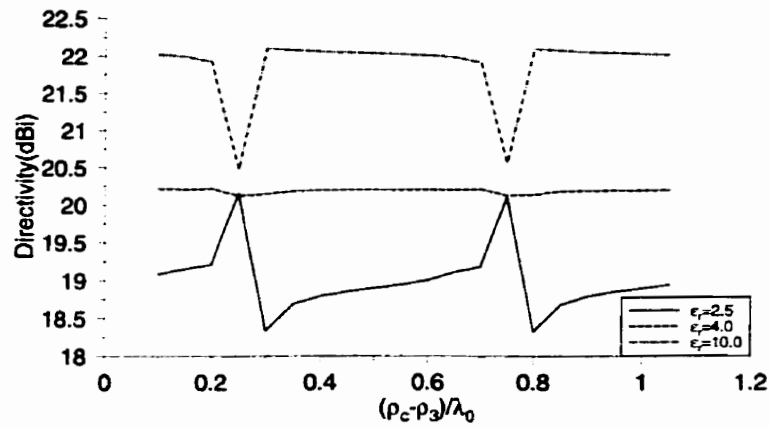


Fig.5.27. Cavity radius (ρ_c) effects on the directivity of dielectric covered three slot antennas, when dielectric thickness is ($h_2 = 0.25\lambda_d$), dimensions as Fig.5.24.

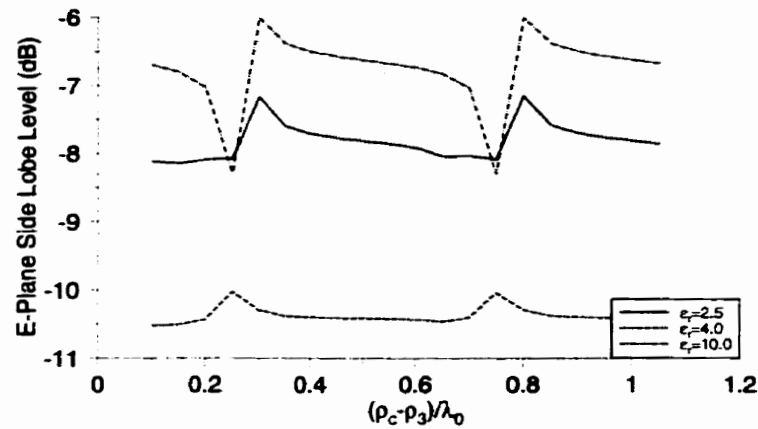


Fig.5.28. Cavity radius (ρ_c) effects on the E-plane side lobe level of dielectric covered three slot antennas, when dielectric thickness is ($h_2=0.25\lambda_d$), dimensions as Fig.5.24.

In the next set of simulations, antennas with one, two and three slots were considered and the effect of cavity radius on the directivity, aperture efficiency and E-plane side lobe level was investigated when the antenna was loaded with an array of conducting rings above the slots and they are compared with unloaded antennas. Similar to dielectric loaded antennas, when the distance between the cavity wall and the slot becomes quarter wave length, a significant drop in directivity happens. Also rapid changes in E-plane side lobe levels are observed when this distance is between $0.2\lambda_0$ and $0.3\lambda_0$.

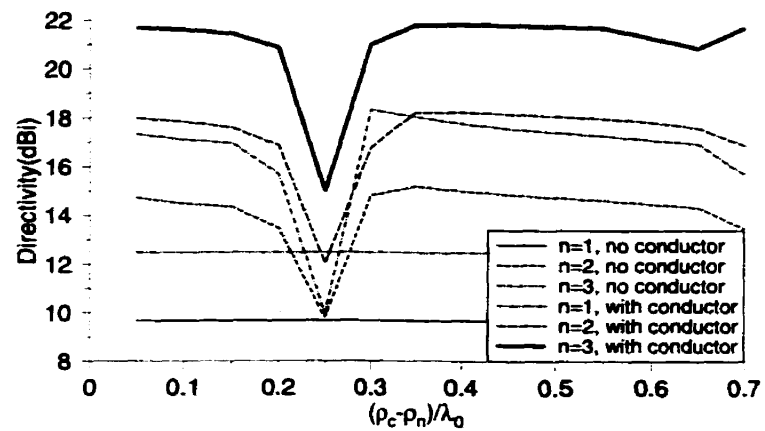


Fig. 5.29. Cavity radius (ρ_c) effects on the directivity slot antennas, with and without conducting rings, n =number of slots, $\rho_1=0.45\lambda_0$, $x=\lambda_0$, $\delta_\rho=0.1\lambda_0$, $\epsilon_{r1,2}=1$, $h_1=0.1\lambda_0$ and for the conducting ring $h_2=0.05\lambda_0$, $L=0.5\lambda_0$.

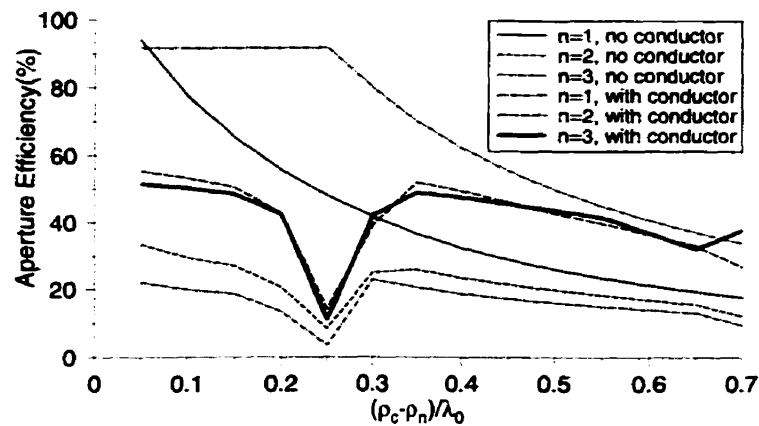


Fig. 5.30. Cavity radius (ρ_c) effects on the aperture efficiency of slot antennas, with and without conducting rings, n =number of slots, dimensions the same as Fig. 5.29.

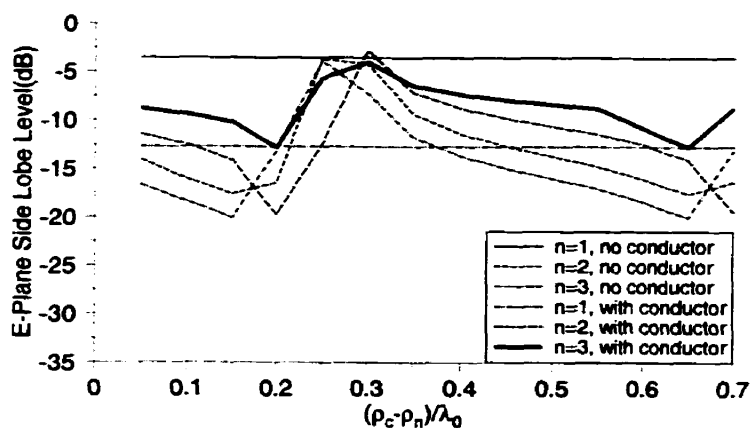


Fig. 5.31. Cavity radius (ρ_c) effects on the E-plane side lobe level of slot antennas, with and without conducting rings, n =number of slots, dimensions the same as Fig. 5.29.

5.3.2. Cavity Height

To investigate the effect of cavity height, two antennas with three and five slots were selected and the directivity, aperture efficiency and E-plane side lobe level for different cavity heights were recorded. The same was done for the same antennas when a dielectric radome of permittivity of 2.5 and thickness of quarter wavelength in dielectric were added at the distance of half a wavelength on the top of plane containing the slots. Fig. 5.32-Fig. 5.34 show the result. From these figures one can conclude that regardless of having a dielectric or not, height of $0.1\lambda_0$ is a critical height, and after that the directivity remains almost constant up to the height of $0.35\lambda_0$. However, the side lobe level in E-plane decreases rapidly for cavity heights less than $0.1\lambda_0$. If it is required to have lower side lobe level shallow cavity is recommended, otherwise $0.1\lambda_0$ is the ideal height for maintaining a better directivity.

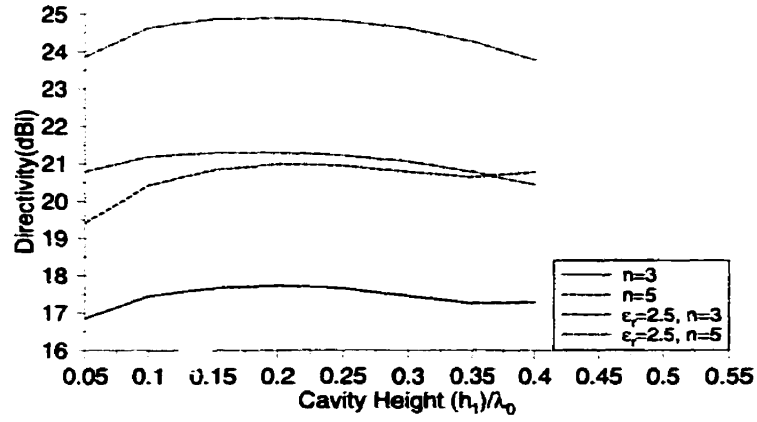


Fig.5.32. Cavity height (h_1) effects on the directivity, n =number of slots, $\rho_1=0.45\lambda_0$, $x=\lambda_0$, $(\rho_c-\rho_n)=0.05\lambda_0$, $\delta_\rho=0.1\lambda_0$, $\epsilon_{r1,2}=1$, $h_2=0.5\lambda_0$, for dielectric layer $d=0.25\lambda_d$, $\epsilon_{r3}=2.5$.

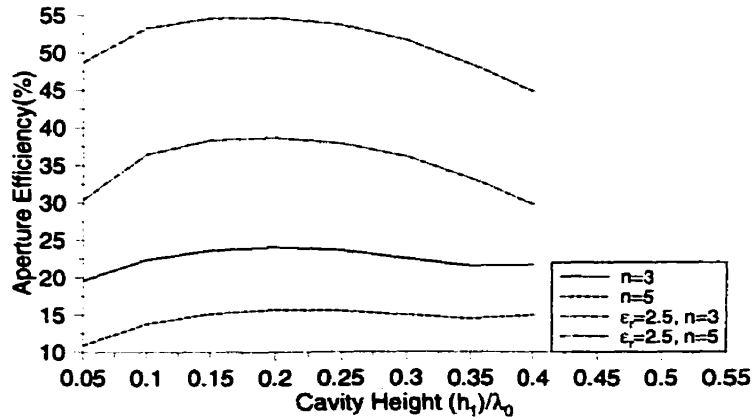


Fig.5.33. Cavity height (h_1) effects on the aperture efficiency, n =number of slots, dimensions the same as Fig.5.32.

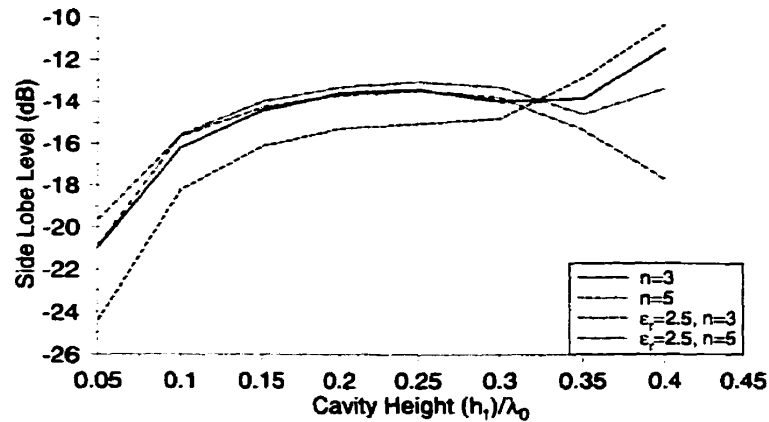


Fig.5.34. Cavity height (h_1) effects on the E-plane side lobe level, n =number of slots, dimensions the same as Fig.5.32.

5.3.3. Slots Locations

To study the effect of slots location, three and five slot antennas were selected and the cavity height was kept $0.1\lambda_0$. Slots were one wavelength apart, but the first slot location was changed and the distance between the last slot and cavity wall was $0.05\lambda_0$. For antennas with no dielectric cover, directivity is maximum when $\rho_1=0.4\lambda_0$ and $0.95\lambda_0$ (Fig.5.35). Both locations give around the same amount of aperture efficiency as shown in Fig.5.36. For dielectric covered antennas, the optimum slot locations shifts toward $0.5\lambda_0$ for antennas with radome of dielectric constant of 2.5 and moves back toward $0.45\lambda_0$ as the dielectric constant increases. The reason could be the reflections from the dielectric layer which can be added or subtracted from the radiated field from the slot, depending on the phase of reflected waves.

Fig.5.37 shows the E-plane side lobe level in terms of first slot location. For

antennas without dielectric cover, the minimum is located at $0.4\lambda_0$, while the minimum for dielectric covered antennas moves toward $0.3\lambda_0$, as the dielectric constant and number of slots increases.

The effect of first slot location is very different when the conducting rings are above the slots. Antennas with one and two slots were selected and above the slots conducting rings with the width of $0.5\lambda_0$ where placed at the height of $0.05\lambda_0$. Fig.5.38- Fig.5.40 show the changes in the directivity, aperture efficiency and E-plane side lobe level, for these antennas. The aperture efficiency was calculated based on the cavity size or the outer radius of the outermost conducting ring, which ever was larger. However, in reality a part of ground plane will contribute to the radiation due to the fringing fields. One can see that for the antennas loaded with conducting rings, smaller antennas provide better aperture efficiency and lower E-plane side lobe level.

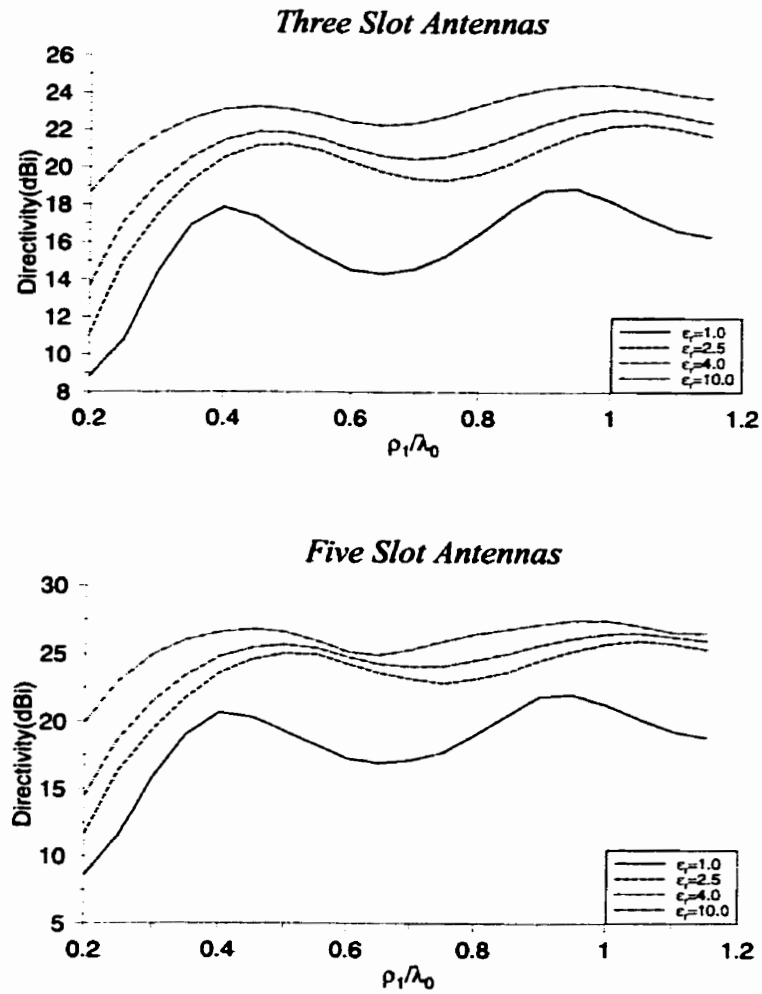


Fig.5.35. Effect of first slot location (ρ_1) on the directivity of dielectric covered three and five slot antennas, $x=\lambda_0$, $(\rho_c-\rho_n)=0.05\lambda_0$, $\delta_p=0.1\lambda_0$, $\epsilon_{r1,2}=1$, $h_1=0.1\lambda_0$, $h_2=0.5\lambda_0$, for dielectric layer $d=0.25\lambda_d$.

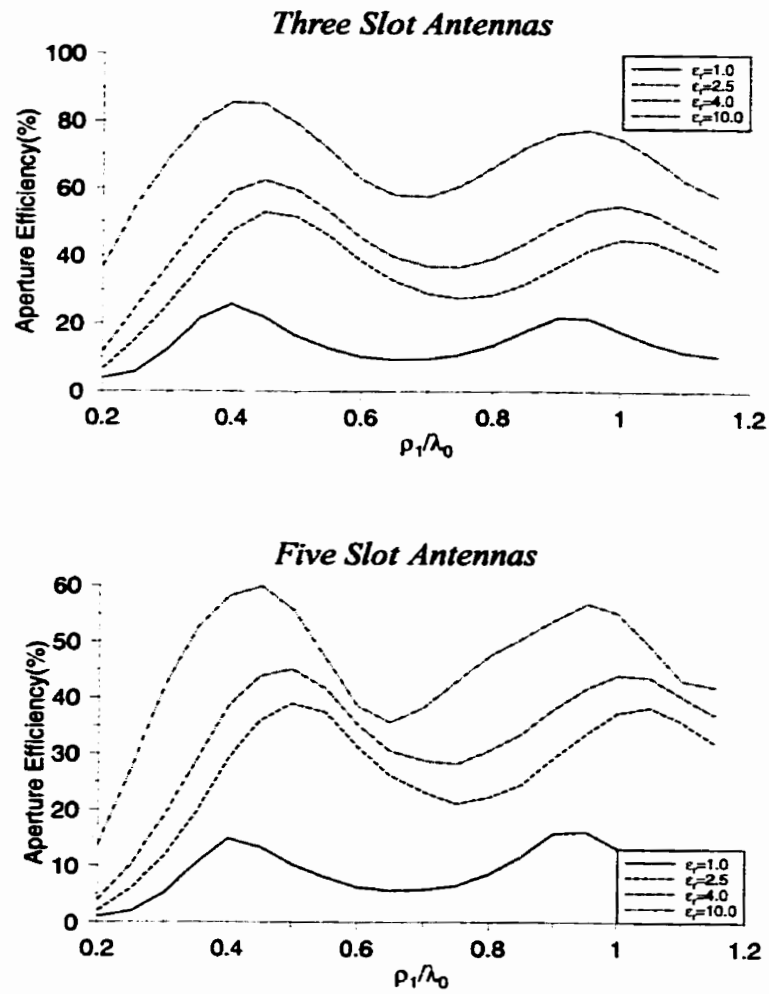


Fig.5.36. Effect of first slot location (ρ_1) on the aperture efficiency of dielectric covered three and five slot antennas, parameters were the same as Fig.5.35.

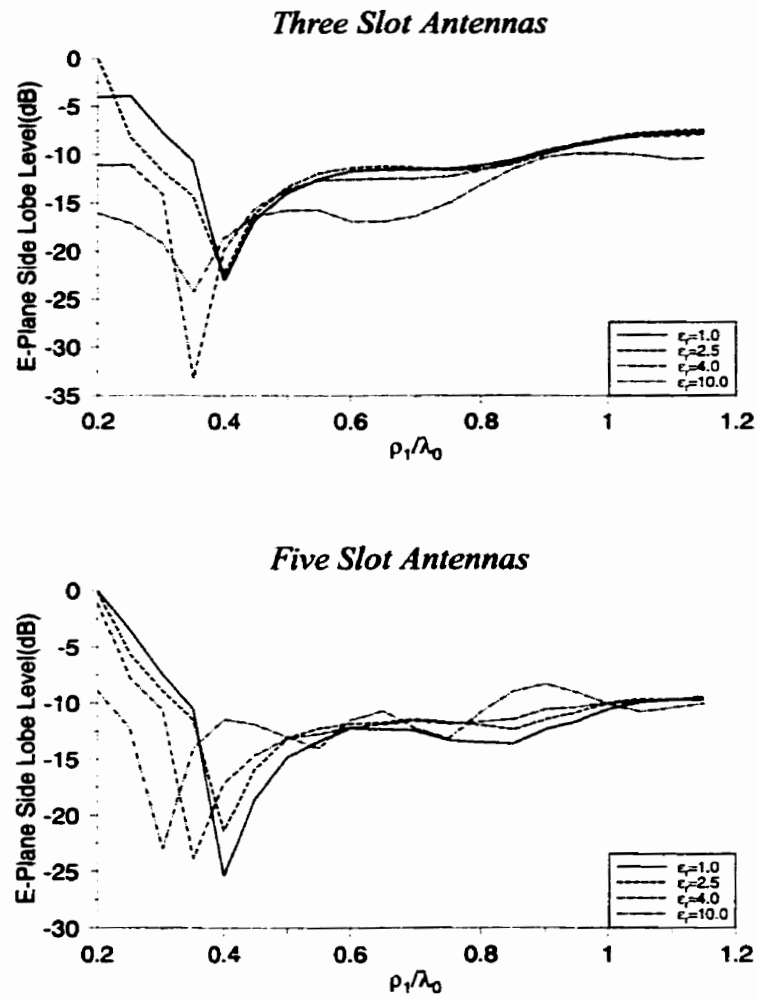


Fig.5.37. Effect of first slot location (ρ_1) on the E-plane side lobe level of dielectric covered three and five slot antennas, parameters were the same as Fig.5.35.

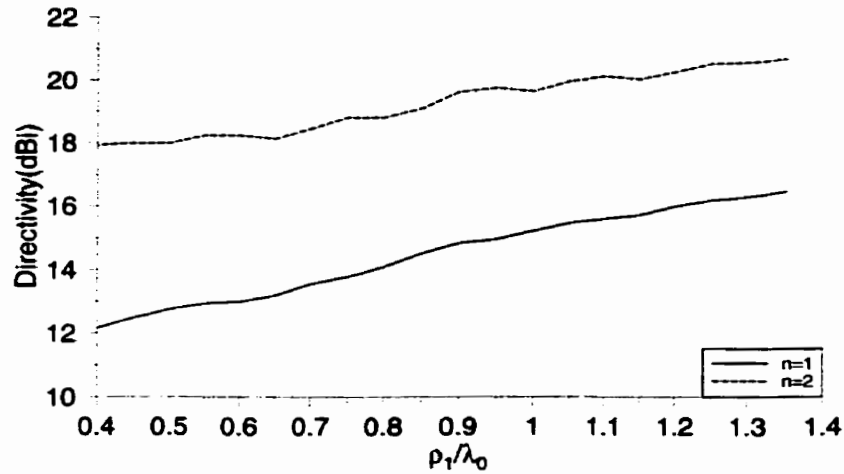


Fig.5.38. Effect of first slot location (ρ_1) on the directivity of conducting ring loaded antennas, n =number of slots, $x=\lambda_0$, $(\rho_c-\rho_n)=0.05\lambda_0$, $\delta_\rho=0.1\lambda_0$, $\epsilon_{r1,2}=1$, $h_1=0.1\lambda_0$, $h_2=0.05\lambda_0$, conducting ring width $L=0.5\lambda_0$

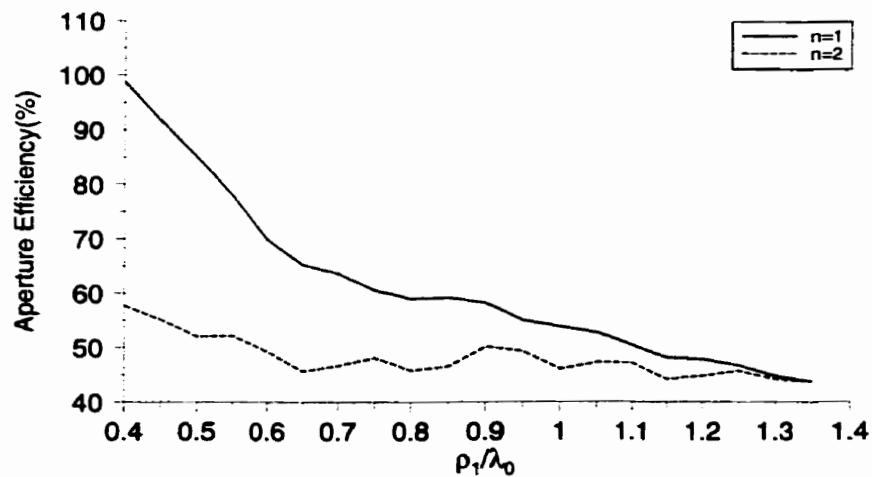


Fig.5.39. Effect of first slot location (ρ_1) on the aperture efficiency of conducting ring loaded antennas, n =number of slots, parameters the same as Fig.5.38.

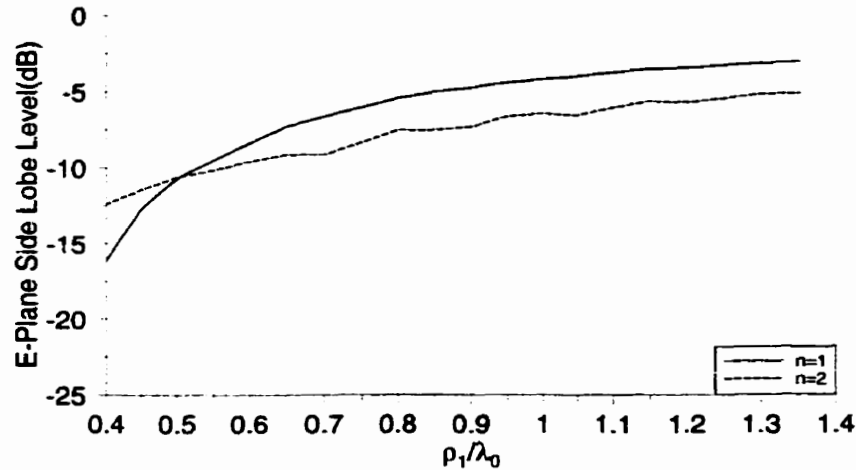


Fig.5.40. Effect of first slot location (ρ_1) on the E-plane side lobe level of conducting ring loaded antennas, n =number of slots, parameters the same as Fig.5.38.

5.3.4. Slots Separation

In order to improve the aperture illumination, the slots must be located at a certain distance from each other to maintain all the slots in phase. The initial guess was that this distance must be around one wavelength. To prove this, three and five slot antennas were selected and for both with and without dielectric cover cases, the directivity, aperture efficiency and E-plane side lobe level were calculated. Dielectric layer had the permittivity of 2.5, and was located at the distance of half a wavelength above the antenna. Fig.5.41- Fig.5.43 show the results. In terms of directivity, one wavelength spacing between the slots shows good improvement in directivity, but in the case of three slot antenna with no dielectric aperture efficiency is maximum when the separation is around $0.8\lambda_0$. This is because the directivity for this antenna remains almost constant after $x=0.8\lambda_0$, while the

aperture size increases when x is increased. For the selected antennas, the E-plane side lobe level is minimum for the separation between $0.8\lambda_0$ and $0.9\lambda_0$.

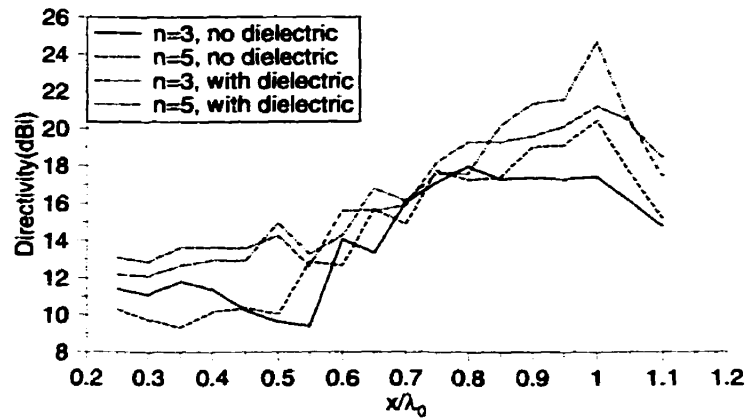


Fig. 5.41. Slot separation (x) effects on the directivity of three and five slot antennas with and without dielectric radome, n =number of slots, $\rho_1=0.45$, $(\rho_c-\rho_n)=0.05\lambda_0$, $\delta_p=0.1\lambda_0$, $x=\lambda_0$, $\epsilon_{r1,2}=1$, $h_1=0.1\lambda_0$, $h_2=0.5\lambda_0$, for dielectric layer $d=0.25\lambda_d$, $\epsilon_{r3}=2.5$.

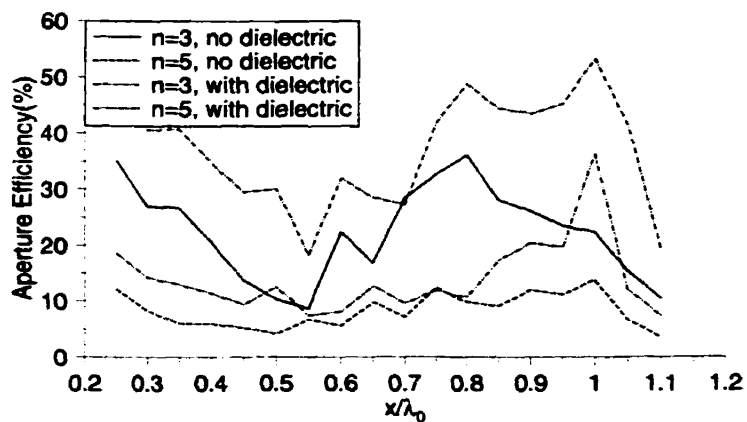


Fig. 5.42. Slot separation (x) effects on the aperture efficiency of three and five slot antennas with and without dielectric radome, n =number of slots, parameters as given in Fig. 5.41.

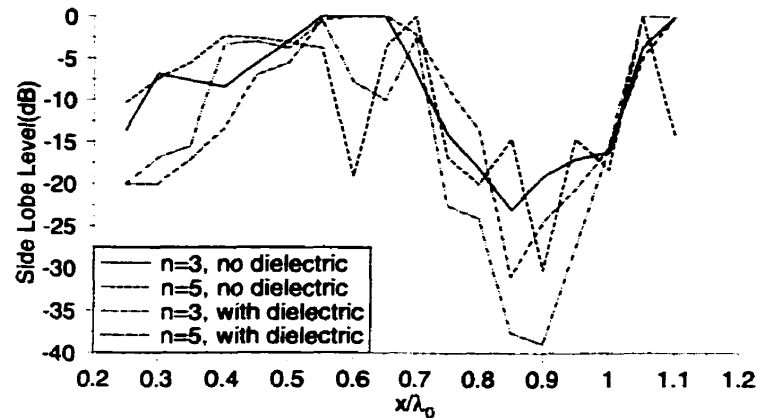


Fig.5.43. Slot separation (x) effects on the E-plane side lobe level of three and five slot antennas with and without dielectric radome, n =number of slots, parameters as given in Fig.5.41.

5.3.5. Dielectric Thickness

To see the effect of dielectric loading, one and two slot antennas fed through radial waveguide and covered with a layer of dielectric on top of slots without any air gap were considered. Fig.5.44 shows the dielectric thickness effects on the directivity for three different dielectric constants: 2.5, 4.0 and 10. It can be observed that the dependency of directivity on the thickness of dielectric has a periodical behavior and the period is half a wavelength in dielectric. The first maximum is located around $0.25\lambda_d$. The improvements of more than 3.5dB in the directivity are achieved. The improvements do not strongly depend on the dielectric permittivity. Thus, by using higher permittivity dielectric, similar degree of improvements can be obtained with thinner layers ($\lambda_d = \lambda_0/\sqrt{\epsilon_r}$). Fig.5.45 shows the aperture efficiency for these antennas. The improvements in aperture efficiency are more than 45% and 30% for one and two slot antennas, respectively.

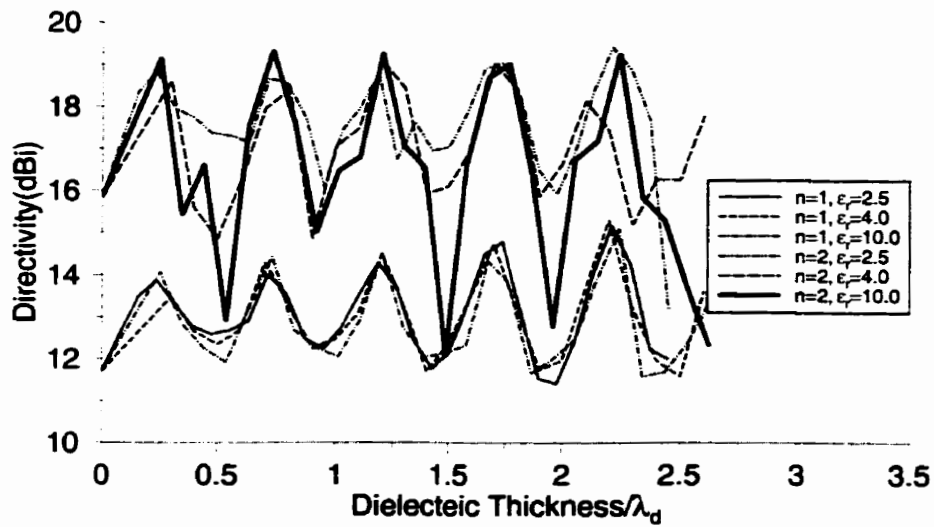


Fig.5.44. Dielectric thickness (h_2) effects for different dielectric constants ($\epsilon_r=\epsilon_{r2}$) on the directivity of dielectric covered single and double slot antennas, $\rho_1=0.95$, $\delta_p=0.1\lambda_0$, $x=\lambda_0$, $\epsilon_{r1}=1$, $h_1=0.36\lambda_0$.

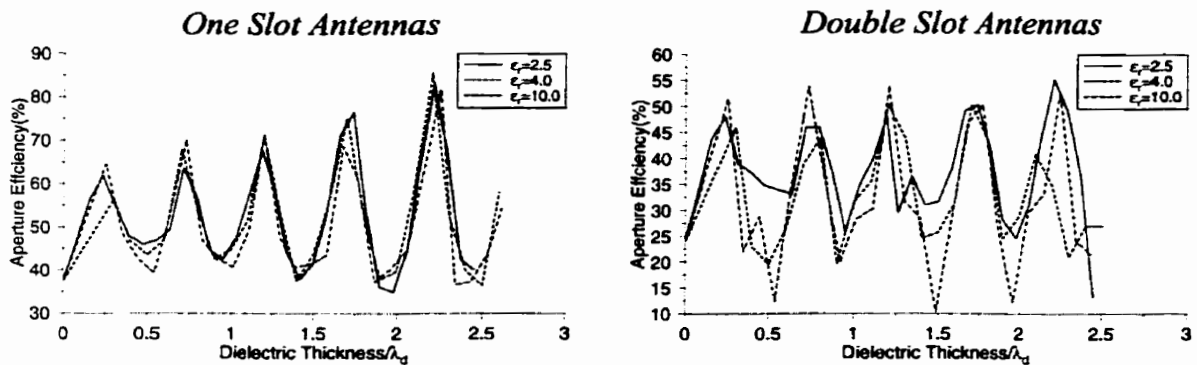


Fig.5.45. Dielectric thickness (h_2) effects for different dielectric constants ($\epsilon_r=\epsilon_{r2}$) on the aperture efficiency of dielectric covered single and double slot antennas, parameters as given in Fig.5.44.

For cavity backed annular slot array antenna, single and double slot antennas with a layer of dielectric located half a wavelength from the plane of slots and with three different dielectric constants: 2.5, 4.0, 10.0 were selected. Two sets of simulation were performed. For the first group, the first slot location was at $0.95\lambda_0$ and for the second set was at $0.45\lambda_0$. The cavity radius was equal to $\rho_c = \rho_n + 0.05\lambda_0$ (The distance between the last slot and the cavity conducting wall was $0.05\lambda_0$). All the other parameters were chosen the same as the radial waveguide fed antenna. Results are shown in Fig.5.46-Fig.5.51. The periodical behavior as before is observed. Also, the optimum thickness of odd multiples of quarter wavelength in dielectric, is the same as dielectric layer with no air gap. However the improvement in directivity for cavity backed antennas is also dependent on the dielectric constant. Higher dielectric constants give better directivities and smaller E-plane side lobe levels. The aperture efficiencies of more than 100% are due to the fact that the aperture efficiency was obtained using the cavity surface as radiating aperture, while the actual radiating aperture is on the dielectric layer.

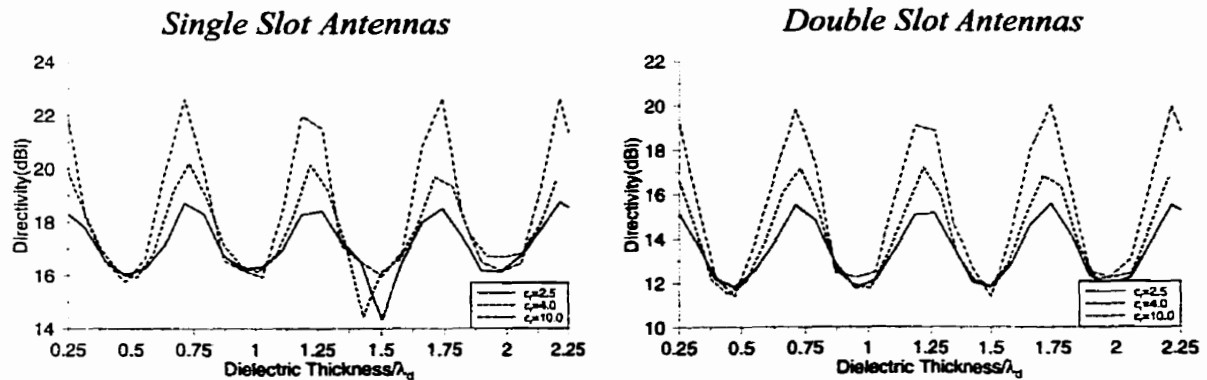


Fig.5.46. Dielectric thickness (d) effects for different dielectric constants ($\epsilon_r = \epsilon_{r3}$) on the directivity of single and double slot cavity backed antennas, $\rho_1 = 0.95$, $(\rho_c - \rho_n) = 0.05\lambda_0$, $\delta_p = 0.1\lambda_0$, $x = \lambda_0$, $\epsilon_{r1,2} = 1$, $h_1 = 0.36\lambda_0$, $\epsilon_{r1,2} = 1$.

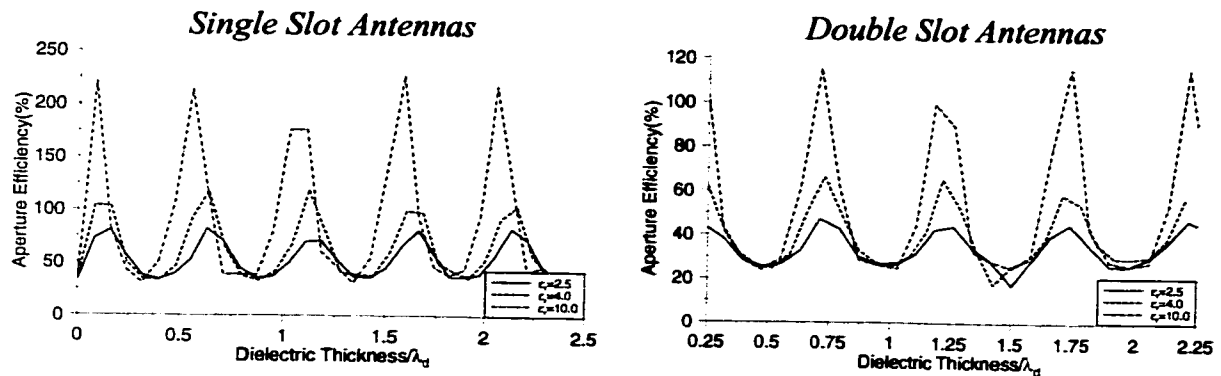


Fig.5.47. Dielectric thickness (d) effects for different dielectric constants ($\epsilon_r = \epsilon_{r3}$) on the aperture efficiency of single and double slot cavity backed antennas, parameters as given in Fig.5.46.

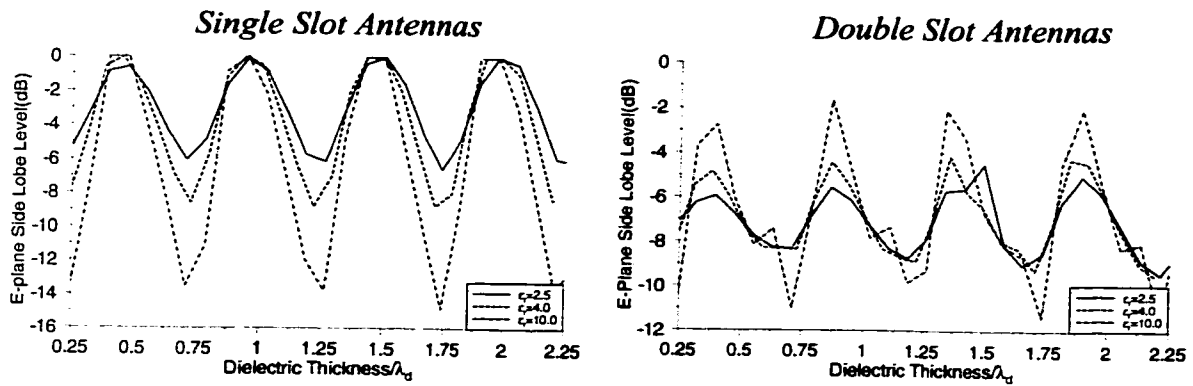


Fig.5.48. Dielectric thickness (d) effects for different dielectric constants ($\epsilon_r = \epsilon_{r3}$) on the E-plane side lobe level of single and double slot cavity backed antennas, parameters as given in Fig.5.46.

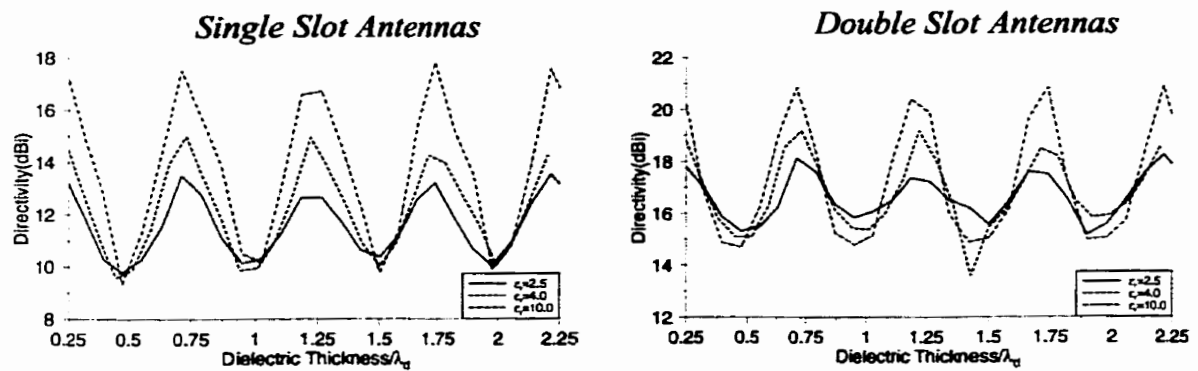


Fig.5.49. Dielectric thickness (d) effects for different dielectric constants ($\epsilon_r = \epsilon_{r,3}$) on the directivity of single and double slot cavity backed antennas, $\rho_l = 0.45$, $(\rho_c - \rho_n) = 0.05\lambda_0$, $\delta_p = 0.1\lambda_0$, $x = \lambda_0$, $\epsilon_{r,1,2} = 1$, $h_l = 0.36\lambda_0$.

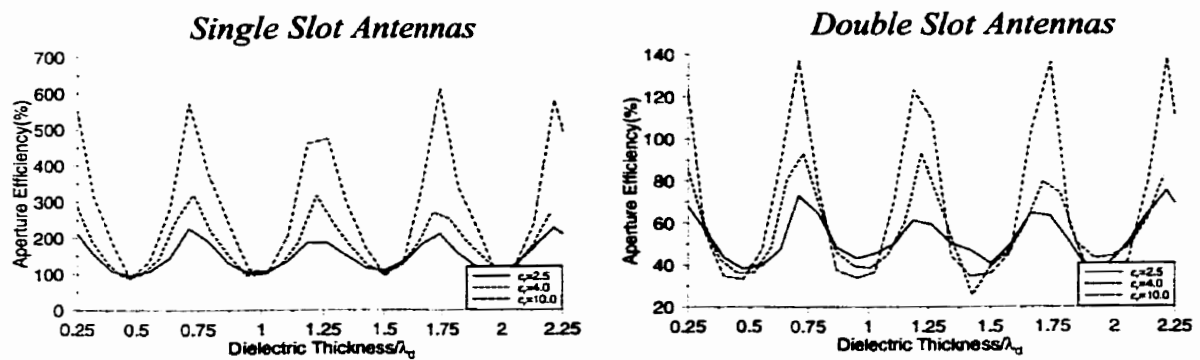


Fig.5.50. Dielectric thickness (d) effects for different dielectric constants ($\epsilon_r = \epsilon_{r,3}$) on the aperture efficiency of single and double slot cavity backed antennas, parameters are given in Fig.5.49.

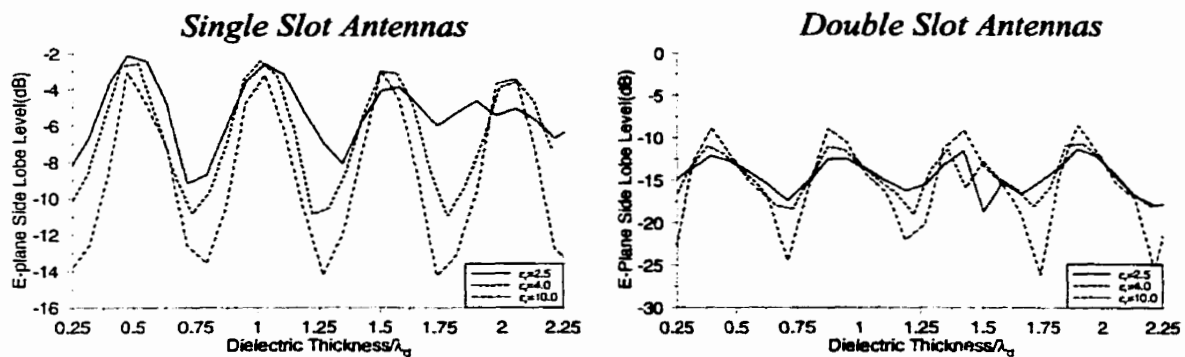


Fig.5.51. Dielectric thickness (d) effects for different dielectric constants ($\epsilon_r = \epsilon_{r3}$) on the E-plane side lobe level of single and double cavity backed antennas, parameters are given in Fig.5.49.

5.3.6. Dielectric Spacing

The air gap between the radome and the plane of slots must be chosen to optimize the aperture distribution. To find out the best spacing, cavity fed antennas with three and five slots were chosen. A layer of dielectric with dielectric constant of 2.5 was added on the top of the antennas and the spacing between this dielectric layer and antennas surfaces were increased from $0.05\lambda_0$ to $0.6\lambda_0$. Fig.5.52-Fig.5.54 show the results. For both antennas when the spacing is a quarter of free-space wavelength, directivity drops and E-plane side lobe level increases. The optimum spacing is at the half a wavelength for the best directivity and aperture efficiency. However E-plane side lobe level is not minimum for this size.

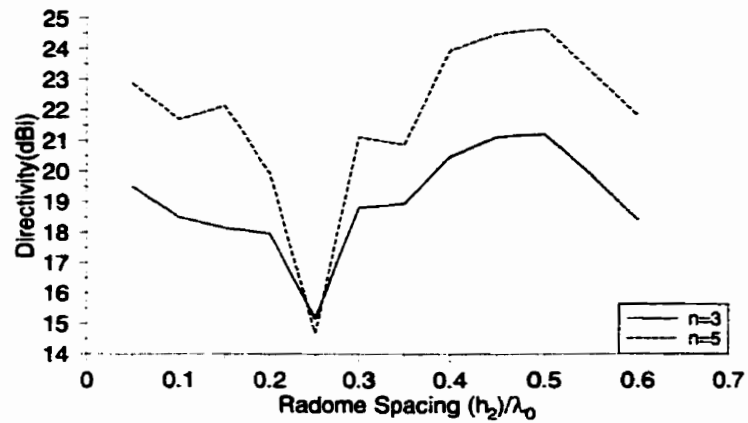


Fig.5.52. Effect of spacing between radome and slot plane (h_2) on the directivity, n =number of slots, $\rho_1=0.45$, $(\rho_c-\rho_n)=0.05\lambda_0$, $\delta_p=0.1\lambda_0$, $x=\lambda_0$, $\epsilon_{r1,2}=1$, $h_1=0.1\lambda_0$, $h_2=0.5\lambda_0$, for dielectric layer $d=0.25\lambda_d$, $\epsilon_{r3}=2.5$.

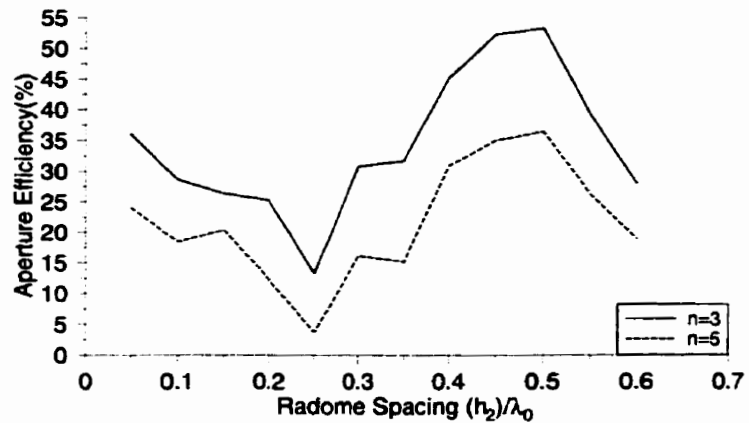


Fig.5.53. Effect of spacing between radome and slot plane (h_2) on the aperture efficiency, n =number of slots, other parameters as given in Fig.5.52.

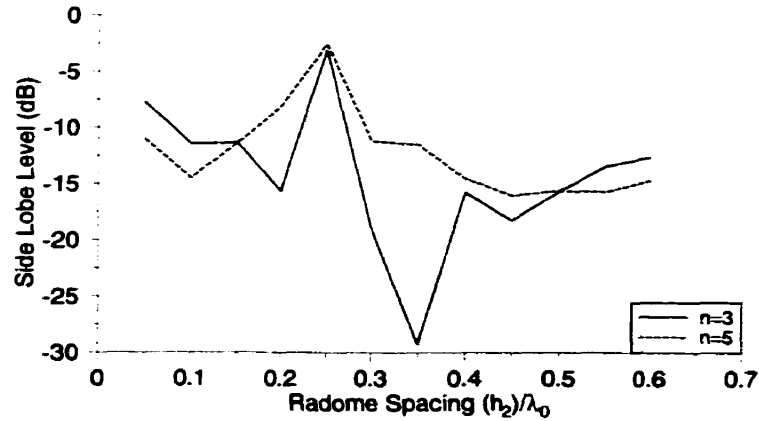


Fig. 5.54. Effect of spacing between radome and slot plane (h_2) on the E-plane side lobe level, n =number of slots, parameters are given in Fig. 5.49.

5.3.7. Dielectric Constant

As it was discussed in section 5.3.5., the dielectric constant has pronounce effects on the performance of cavity backed dielectric loaded antennas. Here, this fact is studied more in details. Antennas with three and five slots were selected and covered with a layer of dielectric, at the distance of half a wavelength above the antenna surface. The thickness of dielectric was kept as a quarter wavelength in dielectric ($d/\lambda_d=0.25$). Other dimensions are given in Table (5-7). Antennas directivity, aperture efficiency and E-plane side lobe level are summarized in Table (5-8) and Table (5-9) for three and five slot antennas, respectively.

Table (5-7) Antenna dimensions for the study of dielectric constant effects, structure the same as shown in Fig.5.10.

Parameter	Value (Sizes in free-space wavelength (λ_0))
δ_p	0.1
ρ_l	0.45
$\rho_c - \rho_n$	0.05
h_1	0.1
h_2	0.5
x	1
ϵ_{r1}	1.0
ϵ_{r2}	1.0
d	$0.25 / \sqrt{\epsilon_{r3}}$
<i>number of slots</i>	3 and 5

The radiation patterns are shown in Fig.5.55 and Fig.5.56. From these results, one can conclude that dielectric radome with higher permittivity gives better directivity and aperture efficiency, while the optimum dielectric thickness is smaller. The increase in directivity for higher permittivities is mainly due to lower beam width in H-plane radiation patterns. In fact, having dielectric radome with higher permittivity does not necessarily mean lower E-plane side lobe. Also E-plane beam width is almost constant and does not change very much with changing the dielectric radome permittivity.

Table (5-8) Dielectric constant effects on the directivity, aperture efficiency and E-plane side lobe level of three slot antennas, dimensions are given in Table (5-7).

ϵ_{r3}	d/λ_0	Directivity(dBi)	Aperture Efficiency(%)	E-Plane Side Lobe Level(dB)
2.5	0.1581	21.14	52.72	-16.12
4.0	0.1250	21.87	62.39	-15.53
6.0	0.1021	22.34	69.53	-16.76
8.0	0.0884	22.75	76.34	-17.41
10.0	0.0791	23.09	82.59	-17.93
20.0	0.056	23.83	97.92	-26.78

Table (5-9) Dielectric constant effects on the directivity, aperture efficiency and E-plane side lobe level of five slot antennas, dimensions are given in Table (5-7).

ϵ_{r3}	d/λ_0	Directivity(dBi)	Aperture Efficiency(%)	E-Plane Side Lobe Level(dB)
2.5	0.1581	24.58	35.95	-15.89
4.0	0.1250	25.45	43.89	-14.60
6.0	0.1021	26.02	50.07	-14.24
8.0	0.0884	26.41	54.70	-13.98
10.0	0.0791	26.71	58.61	-13.59
20.0	0.056	27.20	65.58	-18.21

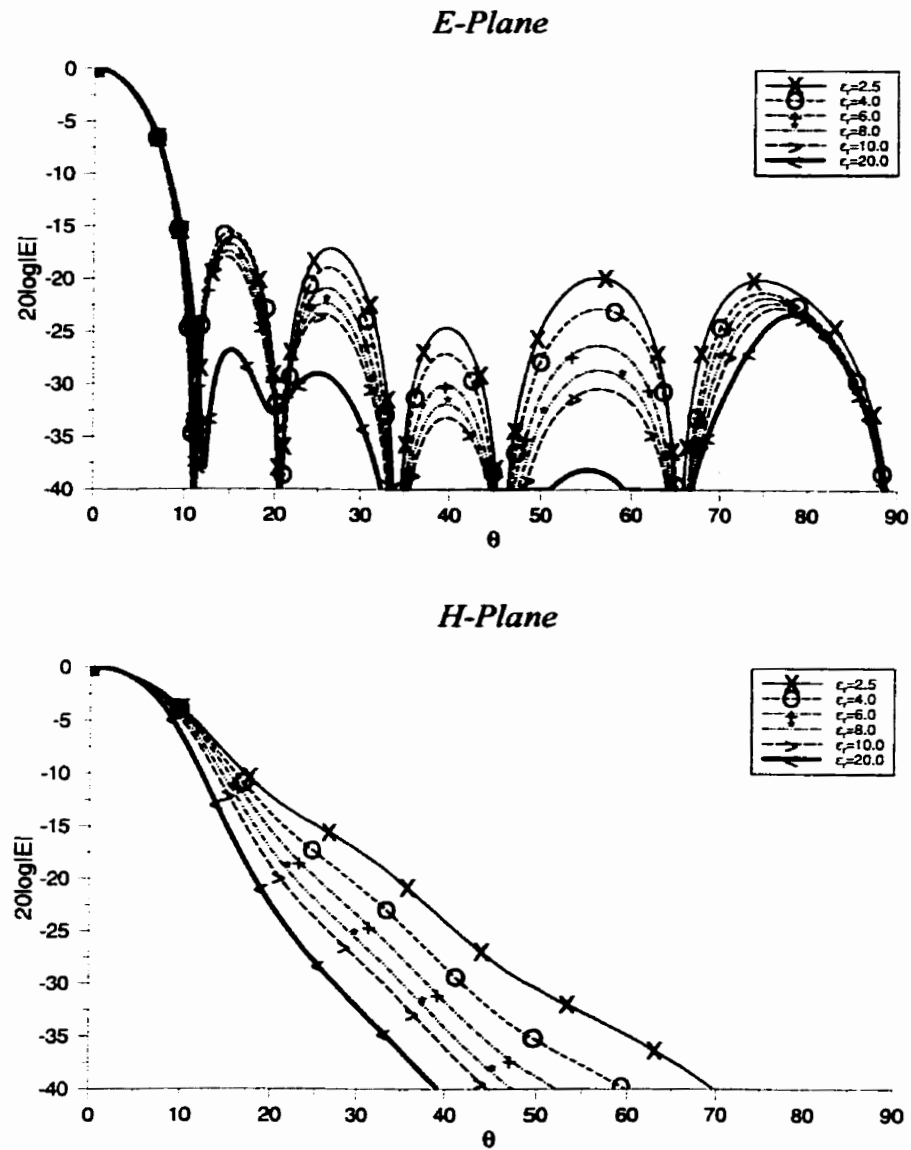


Fig.5.55. Radiation patterns for three slot antennas covered with different dielectric materials, dimensions are given in Table (5-7).

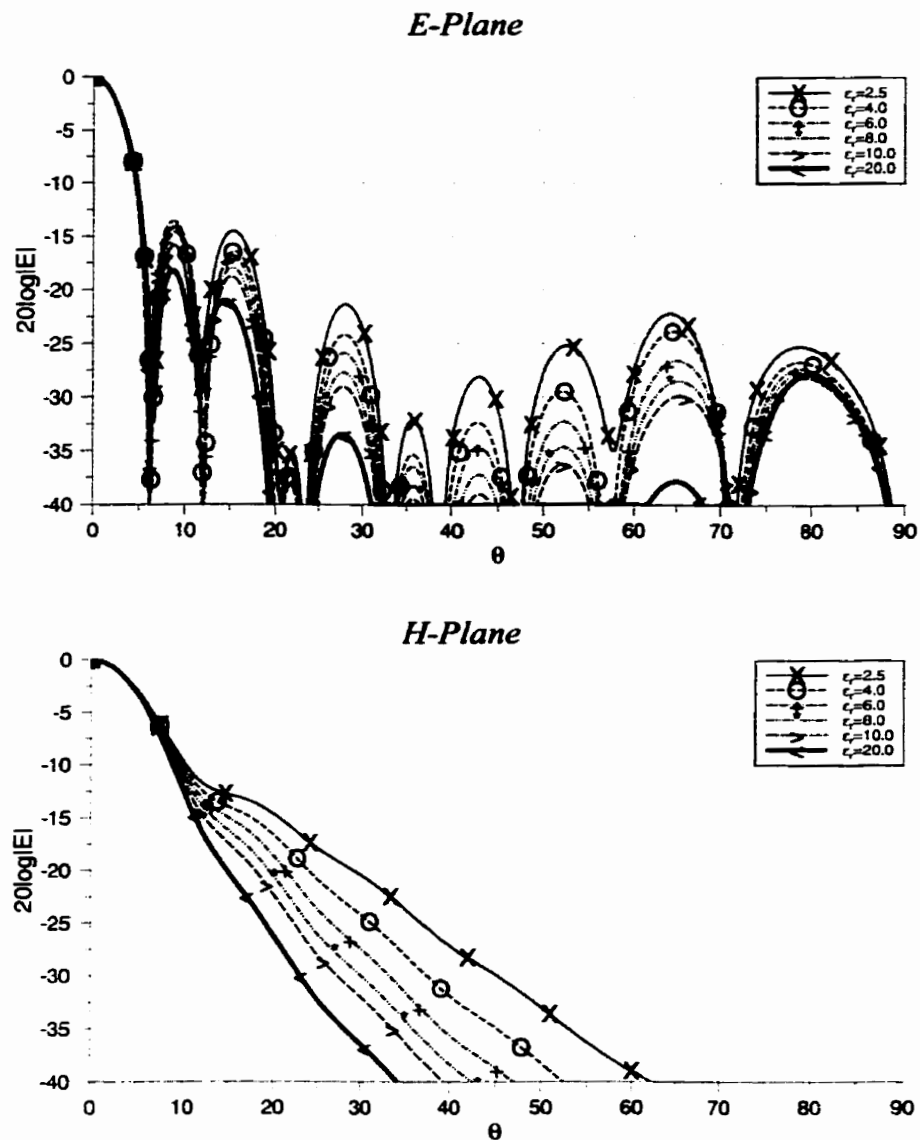


Fig.5.56. Radiation patterns for five slot antennas covered with different dielectric materials, dimensions are given in Table (5-7).

Because the same study is performed and discussed later in this chapter for single slot antennas with finite dielectric radome and larger slot radius, similar antenna with infinite ground plane and dielectric is simulated. The dimensions of the antenna are given

in Table (5-10), and the radiation patterns are shown in Fig.5.57. The radiation pattern characteristics are summarized in Table (5-11).

Table (5-10) Single slot antenna dimensions for the study of dielectric constant effects, structure the same as shown in Fig.5.10.

Parameter	Value (Sizes in free-space wavelength (λ_0))
δ_p	0.1
ρ_l	0.95
$\rho_c - \rho_n$	0.55
h_1	0.36
h_2	0.5
x	1
ϵ_{r1}	1.0
ϵ_{r2}	1.0
d	$0.25/\sqrt{\epsilon_{r3}}$
number of slots	1

Table (5-11) Dielectric constant effects on the directivity, aperture efficiency and E-plane side lobe level of single slot antennas, dimensions are given in Table (5-10).

ϵ_{r3}	d/λ_0	Directivity(dBi)	Aperture Efficiency(%)	E-Plane Side Lobe Level(dB)
2.5	0.1581	15.27	37.91	-5.40
4.0	0.1250	16.74	53.15	-7.86
6.0	0.1021	17.99	70.92	-10.43
8.0	0.0884	18.85	86.49	-12.48
10.0	0.0791	19.50	100.36	-14.17
20.0	0.056	21.47	158.13	-19.78

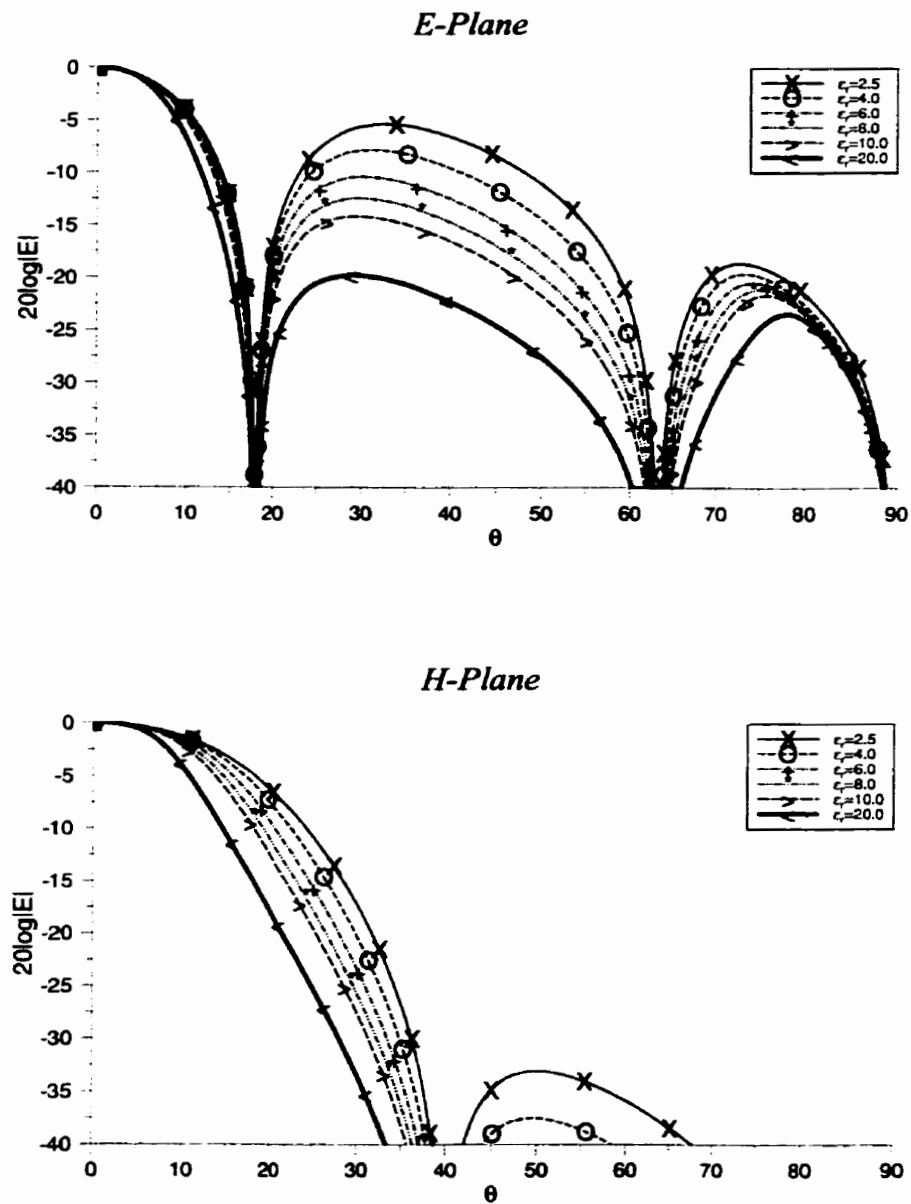


Fig.5.57. Radiation patterns for single slot antennas covered with different dielectric materials, dimensions are given in Table (5-10)

5.3.8. Conducting Ring Width

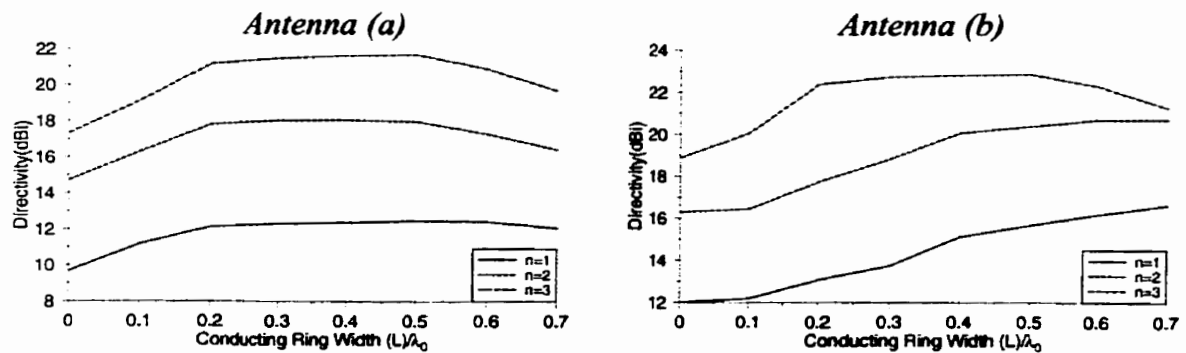
The BVM was also applied to the conducting ring loaded annular slot array antennas. The antenna configuration is shown in Fig.5.14, but instead of infinite radial waveguide, antenna was fed through a cavity. Antennas with one, two and three slots were considered. Above each slot a conducting ring with the height of $0.05\lambda_0$ was located. The conducting ring width was increased from $0.1\lambda_0$ to $0.7\lambda_0$. Zero width represents the antennas without conducting rings.

Two sets of antennas were considered. For the first set, the first slot radii were small and the cavity radii could be smaller than the aperture size. This happens when $\rho_n + (L/2) > \rho_c$. All the dimensions are given in Table (5-12).

Fig.5.58 shows that for all the antennas except for the single and double slot ones with the cavity radius of $\rho_c = \rho_n + 0.55\lambda_0$, directivity starts to decrease after ring width of half a wavelength. In calculating the aperture efficiency, radius of cavity or outer radius of the outermost conducting ring, whichever was larger was chosen as the aperture radius. Fig.5.59 shows the aperture efficiency. For the second set of the antennas aperture radius was always the same as cavity radius. As shown in Fig.5.60, for single slot antennas, E-plane side lobe level decreases, but for two and three slot antennas, it reaches to a level and does not change much further. These results show that for smaller antennas, the uniform ring width of half a wavelength works well, but for more number of slots, the ring width must be optimized based on its radius.

Table (5-12) Dimensions of conducting ring loaded annular slot array antennas.

Parameter	Antenna (a) (Sizes in free-space wavelength (λ_0))	Antenna (b) (Sizes in free-space wavelength (λ_0))
δ_p	0.1	0.1
ρ_l	0.45	0.95
$\rho_c - \rho_n$	0.05	0.55
h_1	0.1	0.36
h_2	0.05	0.05
x	1	1
ϵ_{r1}	1.0	1.0
ϵ_{r2}	1.0	1.0

Fig. 5.58. Conducting ring width (L) effects on the directivity of cavity backed antennas, dimensions were as given in Table (5-12), n = number of slots and conducting rings.

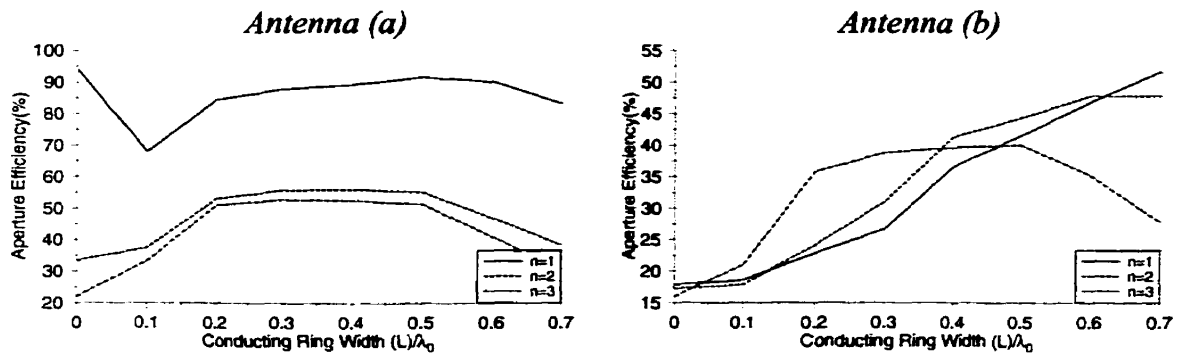


Fig. 5.59. Conducting ring width (L) effects on the aperture efficiency of cavity backed antenna, dimensions were as given in Table (5-12), n =number of slots and conducting rings.

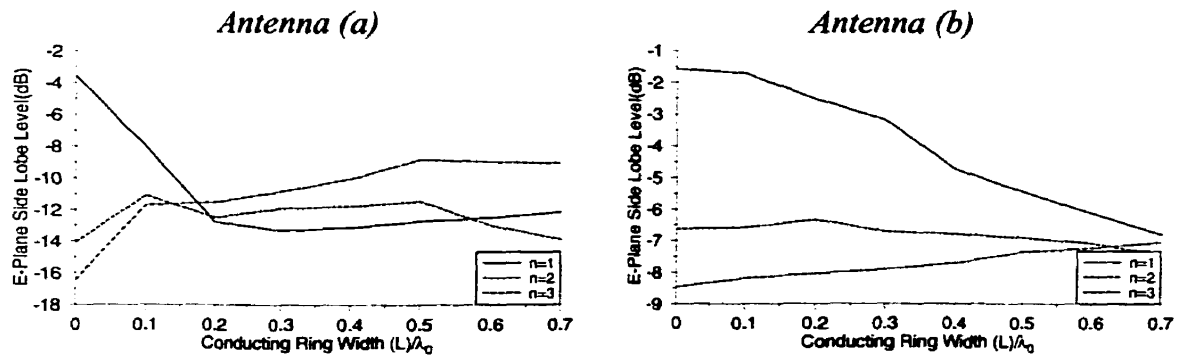


Fig. 5.60. Conducting ring width (L) effects on the E-plane side lobe level of cavity backed antennas, dimensions were as given in Table (5-12), n =number of slots and conducting rings.

5.3.9. Conducting Ring Height

For the same antennas as previous section, the effect of spacing between the conducting ring and the plane of slots was studied. For this purpose, the conducting ring width was kept at half a wavelength and the height was changed. As it is shown in

Fig.5.61-Fig.5.63, the conducting ring height does not show significant effects on the antenna performance. The directivity and aperture efficiency remain almost constant. E-plane side lobe also reaches to a level and remains at about the same level.

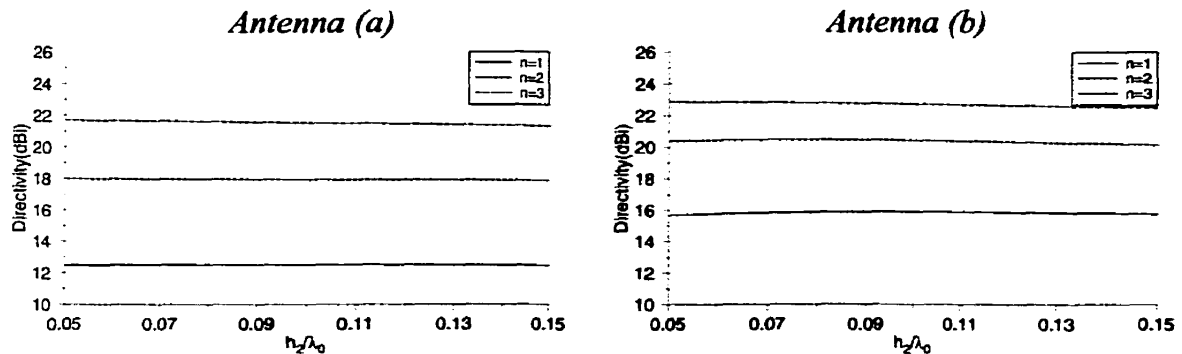


Fig.5.61. Conducting ring height (h_2) effect on the directivity of cavity backed antennas, $L=0.5\lambda_0$, other antenna dimensions were as given in Table (5-12), n =number of slots and conducting rings.

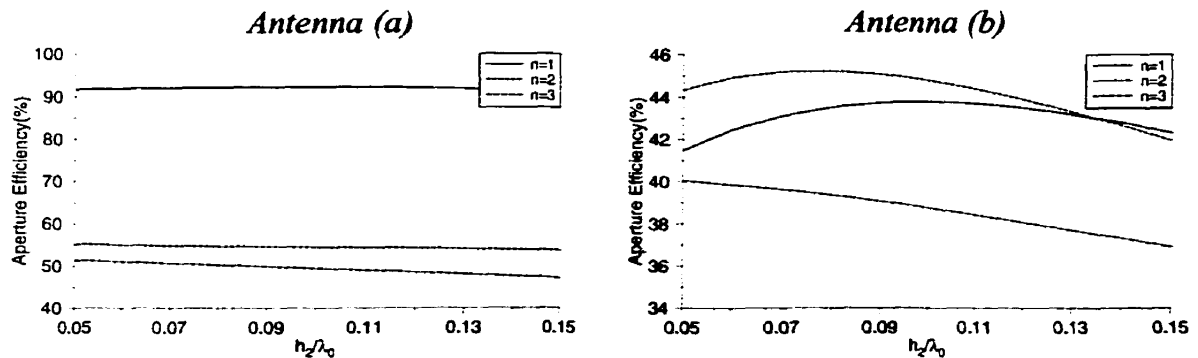


Fig.5.62. Conducting ring height (h_2) effect on the aperture efficiency of cavity backed antennas, $L=0.5\lambda_0$, other antenna dimensions were as given in Table (5-12), n =number of slots and conducting rings.

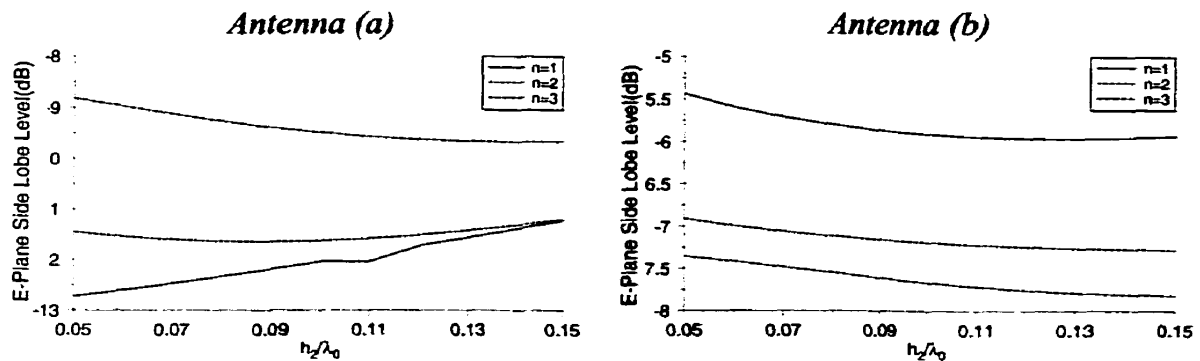


Fig. 5.63. Conducting ring height (h_2) effect on the E-plane side lobe level of cavity backed antennas, $L=0.5\lambda_0$, other antenna dimensions were as given in Table (5-12), n =number of slots and conducting rings.

5.4. COMPARISON BETWEEN DIELECTRIC AND CONDUCTING RING LOADING

Pervious results showed that both dielectric and conducting ring loading improve the antenna performance. Each of these methods has some advantages and disadvantages. The summary of comparison between these two methods are given in Table (5-13). In comparing the E-plane side lobe level, one should note that for single slot antennas, ring loading gives better improvement than dielectric loading. This is also true for antenna with finite dielectric and finite ground plane as it is discussed later in this chapter (Table (5-17)). However adding the conducting rings for larger antennas with more slots must be done more carefully, as it may increase the E-plane side lobe level. It is expected that optimizing the ring width based on its radius would improve the E-plane side lobe level for larger antennas as well. It is expected that combination of two methods along with optimization of ring widths will provide good aperture efficiencies in excess of 50% and

low side lobe level in the E-plane.

Table (5-13) Summary of comparison between dielectric and conducting ring loading effects on the annular slot array antenna performance.

	Dielectric loading	Ring loading
Physical	Heavy and lossy	Light and lossless
Impedance bandwidth	Not much change	Better S_{11} around the centre frequency
Simulation run time	Fast, same matrix size as unloaded antenna	Slow, larger matrix size
Cavity radius	Very sensitive around $\rho_c - \rho_n = 0.25\lambda_0$	The same as dielectric loading
First slot radius	Optimum size of $0.45\lambda_0$ and $0.95\lambda_0$, with less E-plane side lobe level for $0.45\lambda_0$. Radius of $0.45\lambda_0$ is harder to realize because of sensitivity of radiation pattern to probe location, due to the stronger higher order modes around the first slot.	The smaller radius provides better aperture efficiency.
Directivity	Directivity improves with higher dielectric permittivity is higher. The optimum thickness is around $0.25\lambda_d$. Best spacing is half a wave length. Aperture efficiency of 100% is achievable. Improves the directivity by increasing the physical radiating aperture size.	Improvement up to 50% in aperture efficiency is achievable. The directivity is almost the same as dielectric layer with smaller permittivity ($\epsilon_r = 2.5$).
E-plane side lobe level	Lower side lobe level for higher permittivity dielectric layers.	For small antennas E-plane side lobe level improves by more than 4dB, but there is no improvement for more slots with uniform ring width. Generally it is higher than antennas with dielectric load.

To visualize the effects on the radiation patterns, a sample antenna with three slots was chosen and the original radiation patterns are compared with dielectric and conducting ring loaded antennas in Fig.5.64. Table (5-14) summarizes the results.

Table (5-14) Radiation characteristics for three slot sample antennas loaded with dielectric or ring shown in Fig.5.64.

ρ_1	Antenna	Directivity (dBi)	Aperture Efficiency(%)	E-Plane Side Lobe Level
$0.45\lambda_0$	Original	17.34	21.98	-16.64
	Dielectric loaded ($\epsilon_r=2.5$)	21.15	52.83	-16.05
	Dielectric loaded ($\epsilon_r=10.0$)	23.09	82.88	-17.93
	Ring loaded $h_2=0.05\lambda_0$ $L=0.5\lambda_0$.	21.70	53.33	-8.82
$0.95\lambda_0$	Original	18.84	21.55	-9.04
	Dielectric loaded ($\epsilon_r=2.5$)	21.73	41.96	-9.00
	Dielectric loaded ($\epsilon_r=10.0$)	24.36	76.79	-10.51
	Ring loaded $h_2=0.05\lambda_0$ $L=0.5\lambda_0$.	22.88	49.51	-7.30

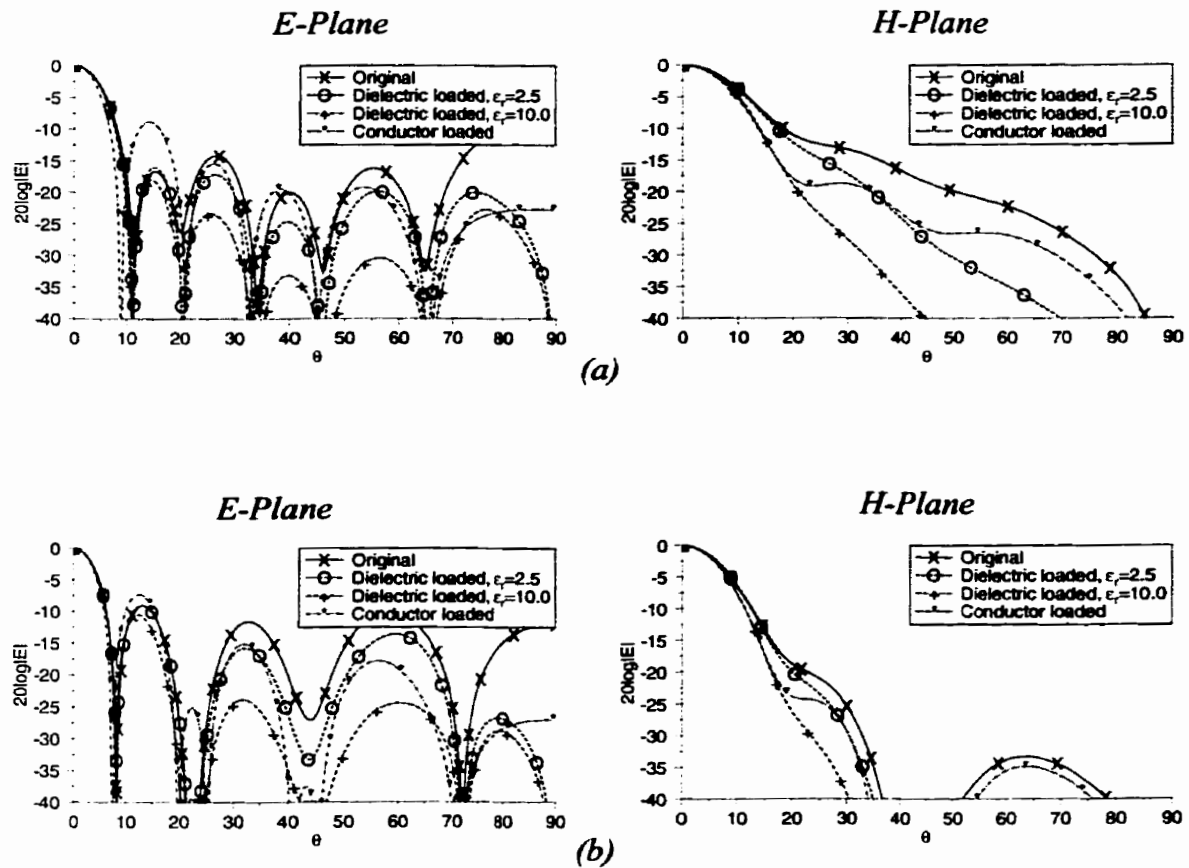


Fig.5.64. Radiation patterns comparison for the original and improved three slot antennas, (a) $\rho_I=0.45\lambda_0$, (b) $\rho_I=0.95\lambda_0$, other parameters: $(\rho_c-\rho_n)=0.05\lambda_0$, $\delta_p=0.1\lambda_0$, $x=\lambda_0$, $\epsilon_{r1,2}=1$, $h_1=0.1\lambda_0$, for dielectric: $h_2=0.5\lambda_0$, $d=0.25\lambda_0$, $\epsilon_{r3}=\epsilon_r$ for conducting ring: $h_2=0.05\lambda_0$, $L=0.5\lambda_0$

5.5. FINITE STRUCTURES PARAMETRIC STUDY

In this section small annular slot antennas fed by a cavity are studied numerically, using MBES. Two methods proposed earlier for performance improvement, dielectric and conducting ring loading, were investigated for finite dielectric radii and finite ground planes. The effects of different parameters were studied and the results are compared with those given by BVM which assumes infinite ground plane and dielectric. At the end some modifications are proposed to improve the antenna directivity. An open cavity with additional chokes was used to decrease the back lobe level and increase the directivity. Because in MBES the maximum number of unknowns is fixed, only antennas with a single annular slot were considered.

5.5.1. Antenna Structure

For maintaining the single dominant mode, to radiate a directive gain along the ring axis, a cavity excitation was used. The cavity itself was excited using two probes which, in the numerical analysis, were simulated with two dipoles located at $(\pm x_f, z_f)$, as shown in Fig.5.65. The two dipoles were 180° out of phase in order to cancel even modes.

Dimensions of the selected antenna for study are given in Table (5-15). Its radiation patterns in the E and H-planes, and without loading, are shown in Fig.5.66. For this antenna the aperture efficiency was 24.63% and its directivity was 13.4dBi. The side lobe level in the E-plane was -2.77dB. Its radiation characteristics are therefore very poor. In the following sections the geometrical modifications and dielectric and conducting ring

loading are used to improve its performance.

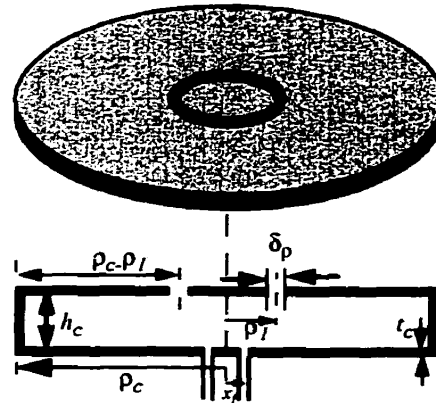


Fig. 5.65. Structure of annular slot antenna with finite ground plane.

Table (5-15) Antenna dimensions with finite ground plane.

Parameter	Sizes in free-space wavelength (λ_0)
δ_p	0.1
ρ_l	0.95
ρ_c	1.5
t_c	0.02
h_c	0.36
$\rho_c - \rho_l$	0.55

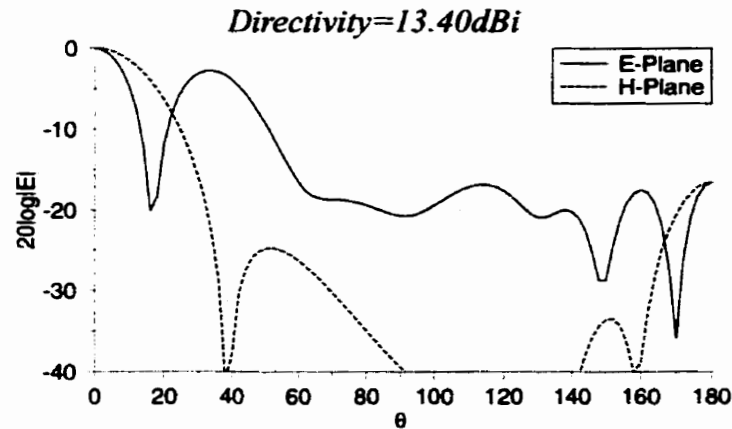


Fig.5.66. Radiation patterns for annular slot antenna of Table (5-15).

5.5.2. Cavity Size and Slot Location

To excite the TM_{01} mode, dipoles must be located close to the centre. As the distance from the centre increases, higher order modes become excited and the directivity decreases. Referring to , Table (5-16) shows the directivity of the antennas with different slot locations and aperture sizes. Feed locations were $(x_f = \pm 0.2, z_f = 0.2)$. It can be seen that when first slot was located at around $0.95\lambda_0$ the directivity was maximum. This is in agreement with the results for infinite ground plane structure simulated by BVM. The cavity radius (ρ_c/λ_0) also has a pronounced effect on the directivity. The slot location $\rho_l/\lambda_0=0.95$ and $\rho_c/\lambda_0=1.5$ were chosen for the rest of simulations.

Table (5-16) Effect of slot location on the directivity.

ρ_l/λ_0	ρ_c/λ_0	Directivity(dBi)
0.75	1.3	9.36
0.75	1.5	8.07
0.85	1.4	11.62
0.85	1.5	11.32
0.95	1.2	10.94
0.95	1.5	13.40
0.95	1.6	13.09
0.95	1.7	11.36

5.5.3. Conducting Ring and Dielectric Loading

Two methods proposed earlier to increase the directivity were investigated for finite structure. In the first method, a conducting ring was added to the structure above the slot, at a distance h , and with the width of L . In the second method, a layer of dielectric sheet with dielectric constant ϵ_r and thickness of d was added to the structure, at the distance of $h_2=0.5\lambda_0$ from the slot surface. The dielectric sheet had a finite diameter (R). The combination of these two methods was also studied. Fig.5.67 shows the structure of the antenna. The ring parameters were the height (h) and width (L). Their effects on the antenna directivity and E-plane side lobe level were investigated, for both cases of without and with a dielectric radome. The antenna parameters were $R=1.7\lambda_0$, $d=0.15\lambda_0$, and $\epsilon_r=2.5$.

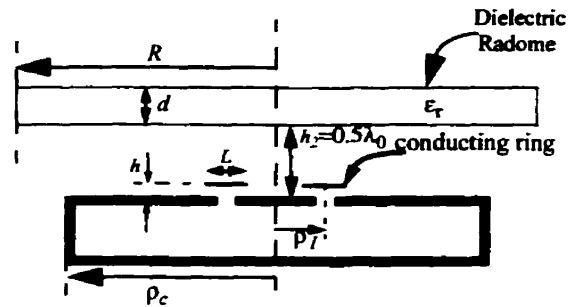


Fig.5.67. Radome covered annular slot antenna with conducting ring added.

The comparison of the results is shown in Fig.5.68 and Fig.5.69. These figures show that there is an optimum size for ring height and width in terms of directivity. But, the E-plane side lobe level, generally, decreases by increasing the parameters. This is in agreement with results for infinite structure, shown in Fig.5.60 and Fig.5.63. However the side lobe level is generally smaller for antenna with finite ground plane.

When $L=0.65\lambda_0$ and $h_r=0.05\lambda_0$, without any dielectric radome, the improvement in directivity is 2.92dB, and the E-plane side lobe level is decreased from -2.77dB to -7.12dB. The cases of $L=0$ correspond to antennas without a conducting ring. The introduction of the dielectric radome increases the directivity from 13.40dBi to 15.57dBi, an increase of 2.17dB. With the conducting ring the directivity further increases to 17.47dBi, an additional 1.9dB. Thus, in comparison with the original antenna, the directivity enhancement is 4.07dB. At the same time, the E-plane side lobe level has decreased by 7.01dB, to -9.78dB. The results are summarized in Table (5-17) and the radiation patterns for two different ring sizes, with and without dielectric cover are shown in Fig.5.70 and Fig.5.71.

Table (5-17) Directivity and side lobe level improvement for antennas in Fig.5.70 and Fig.5.71.

Antenna type	Directivity improvement(dB)	E plane side lobe level improvement(dB)
Antenna with conducting ring only ($L=0.65\lambda_0$ and $h=0.05\lambda_0$)	2.92	4.35
Antenna with dielectric radome only ($R=1.7\lambda_0$, $d=0.15\lambda_0$, and $\epsilon_r=2.5$)	2.17	2.07
Antenna with both conducting ring and dielectric radome ($L=0.65\lambda_0$, $h=0.05\lambda_0$, $R=1.7\lambda_0$, $d=0.15\lambda_0$, and $\epsilon_r=2.5$)	4.07	7.01

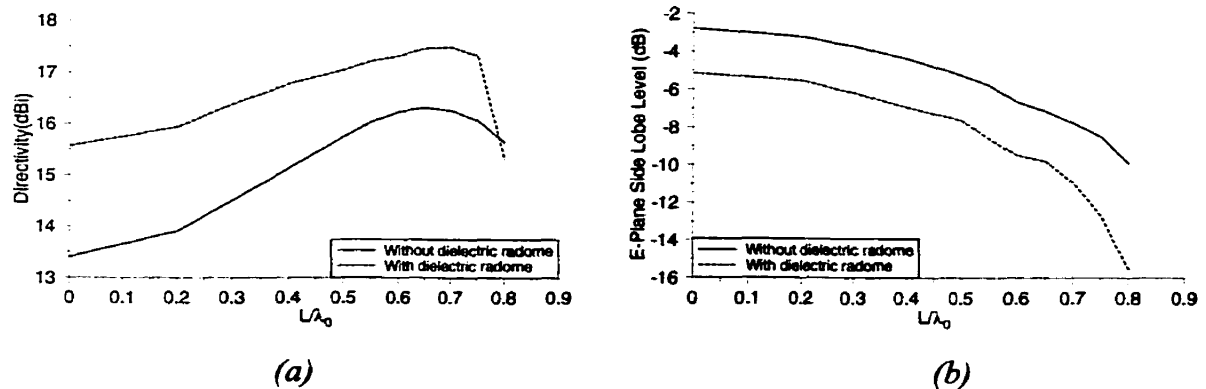


Fig.5.68. Effect of conducting ring width (L) on the (a) directivity and (b) E-plane side lobe level of the antenna without and with dielectric radome ($R=1.7\lambda_0$, $d=0.15\lambda_0$, $\epsilon_r=2.5$, $h=0.05\lambda_0$).

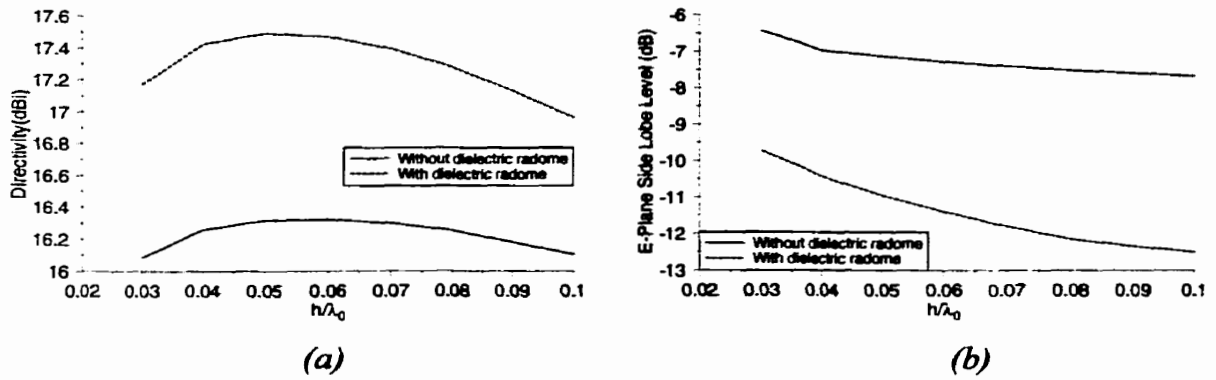


Fig.5.69. Effect of conducting ring height (h_1) on the (a) directivity and (b) E-plane side lobe level of the antenna without and with dielectric radome ($R=1.7\lambda_0$, $d=0.15\lambda_0$, $\epsilon_r=2.5$, $L=0.7\lambda_0$).

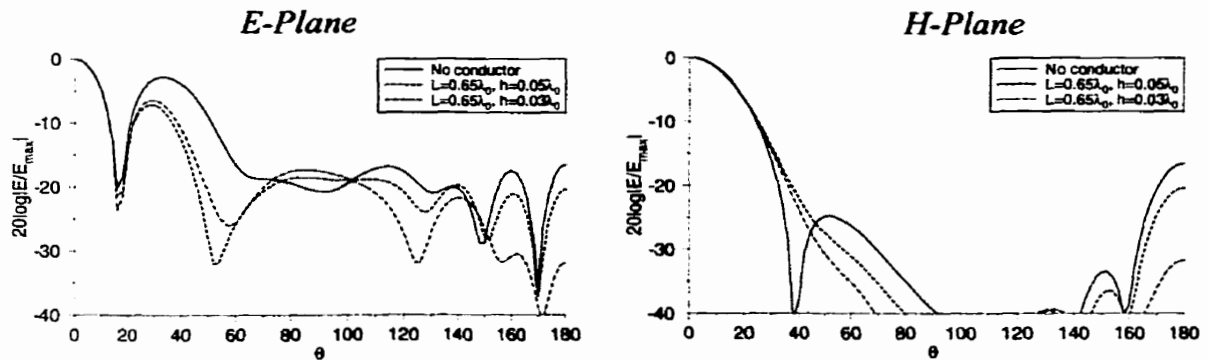


Fig.5.70. Radiation patterns for three antennas with and without a conducting ring, Directivity: without conducting ring = 13.40dBi, with conducting ring with ($h=0.05\lambda_0$) = 16.318, and with ($h=0.03\lambda_0$) = 16.085dBi.

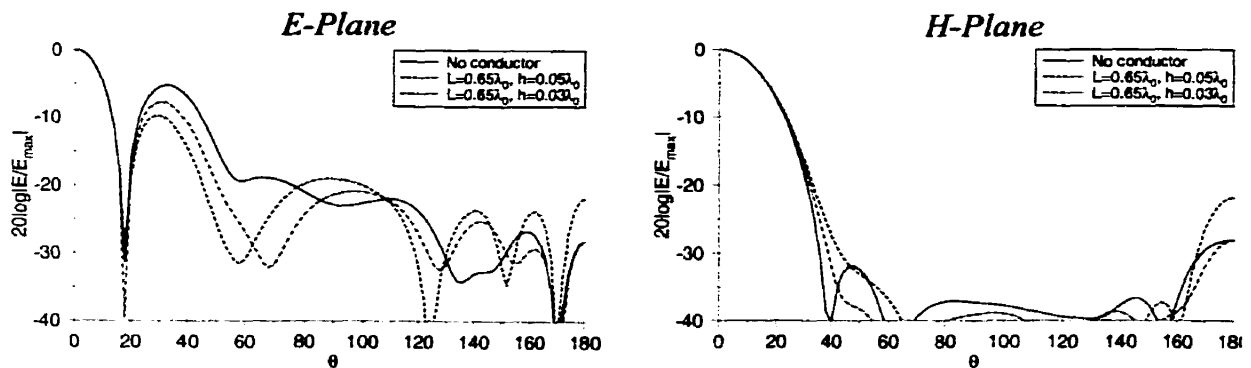


Fig.5.71. Radiation patterns for three antennas with and without a conducting ring and covered with dielectric ($R=1.7\lambda_0$, $d=0.15\lambda_0$, $\epsilon_r=2.5$) Directivity: without conducting ring = 15.566dBi, with conducting ring with ($h=0.05\lambda_0$) = 17.471, and with ($h=0.03\lambda_0$) = 16.996dBi.

The effect of dielectric thickness (d) on the directivity of antenna with two different dielectric primitivities (2.5 and 4) and two different dielectric radii ($1.15\lambda_0$ and $1.7\lambda_0$), with and without a conducting ring are shown in Fig.5.72. These graphs have a periodic behavior. The period is $0.5\lambda_d$, where λ_d is the wavelength in dielectric ($\lambda_d = \lambda_0 / \sqrt{\epsilon_r}$). The first maximum is for the thickness slightly less than $0.25\lambda_d$, which is the same size obtained for infinite dielectric. One should note, however, that the increase in directivity, by increasing the dielectric thickness, occurs only when the dielectric radius is larger than the cavity radius.

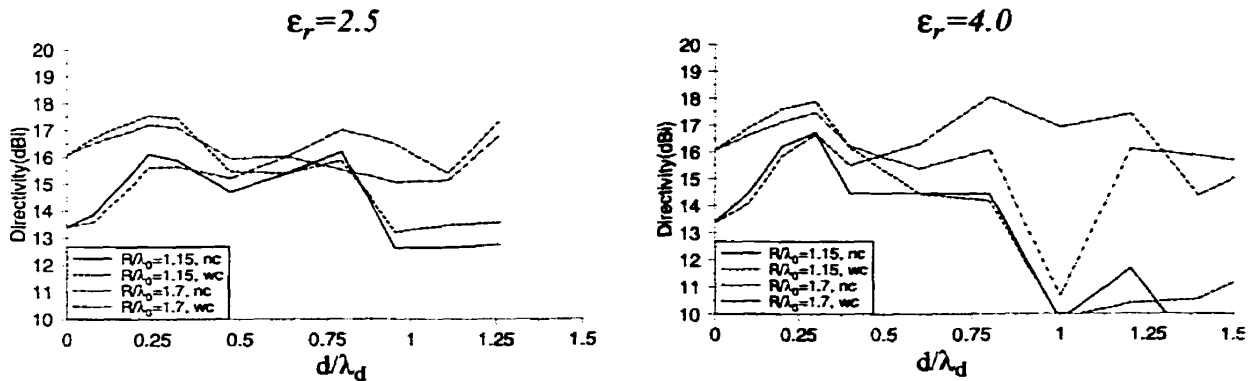


Fig.5.72. Effect of dielectric thickness (d) on the antenna directivity *nc*: No conducting ring is added, *wc*: with conducting ring ($L=0.75\lambda_0$, $h=0.05\lambda_0$).

Fig.5.73 shows the effect of dielectric radius on the directivity. It shows that regardless of the dielectric constant and presence of the conducting ring, the optimum radii are the same for both dielectrics. The first maximum occurs for $R=1.15\lambda_0$ and the second one is at $1.7\lambda_0$, nearly half wavelength larger.

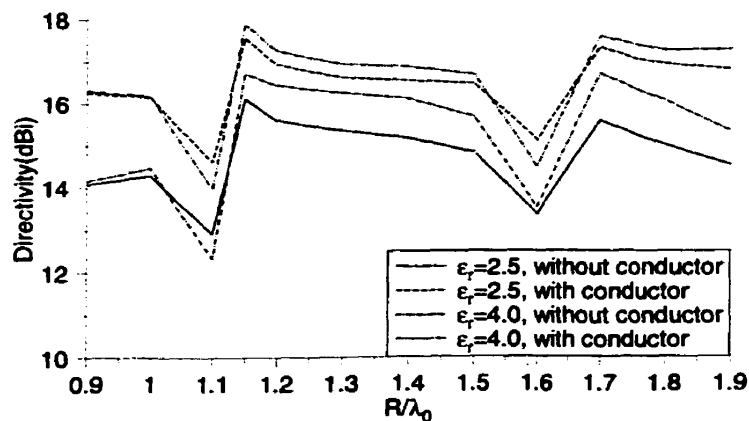


Fig.5.73. Effect of dielectric radius (R) on the directivity of the antenna without and with a conducting ring ($L=0.75\lambda_0$, $h=0.05\lambda_0$, $d=0.15\lambda_0$).

To study the effect of dielectric layer permittivity, the single slot antenna was covered with different dielectric layers. Table (5-18) shows the directivity, E-plane side lobe level and back lobe level for the dielectric covered antennas for two cases. In the first case the antenna was only covered with a dielectric layer. In the second case, a conducting ring was added above the slot, in addition to the dielectric radome. For both groups, the dielectric physical thickness varies for each dielectric layer, but it was always quarter wavelength in the dielectric ($d=0.25\lambda_d$). In MBES the segmentations inside the dielectric and in free-space are done with the same segment size. This reduces the accuracy for high permittivity dielectrics. Considering this fact, the permittivity (ϵ_r) up to 6 was used for the study. The radiation patterns in the E and H-planes, for these two groups of antennas are shown in Fig.5.74 and Fig.5.75. By increasing the dielectric constant the directivity increases and E-plane side lobe level decreases, but back lobe level increases. The increase in directivity and decrease in E-plane side lobe level were also observed for infinite dielectric with BVM, when the dielectric permittivity was increased. However, the E-plane side lobe level does not decrease as much as it was observed for infinite dielectric layer (Fig.5.57 and Table (5-11)). In the H-plane, beamwidth decreases, which was also observed for infinite structures.

Table (5-18) Directivity, E-plane side lobe and back lobe levels for antennas with different dielectric covers ($R=1.15\lambda_0$, $d=0.25\lambda_0$, $L=0.7\lambda_0$, $h_1=0.05\lambda_0$).

ϵ_r	Without Conducting Ring			With Conducting Ring		
	Directivity (dBi)	Side lobe level (dB)	Back lobe level (dB)	Directivity (dBi)	Side lobe level (dB)	Back lobe level (dB)
2.5	16.111	-5.17	-22.89	17.55	-11.53	-20.42
4.0	16.817	-6.22	-23.27	17.83	-12.31	-20.15
6.0	17.331	-7.12	-22.73	17.89	-13.04	-19.11

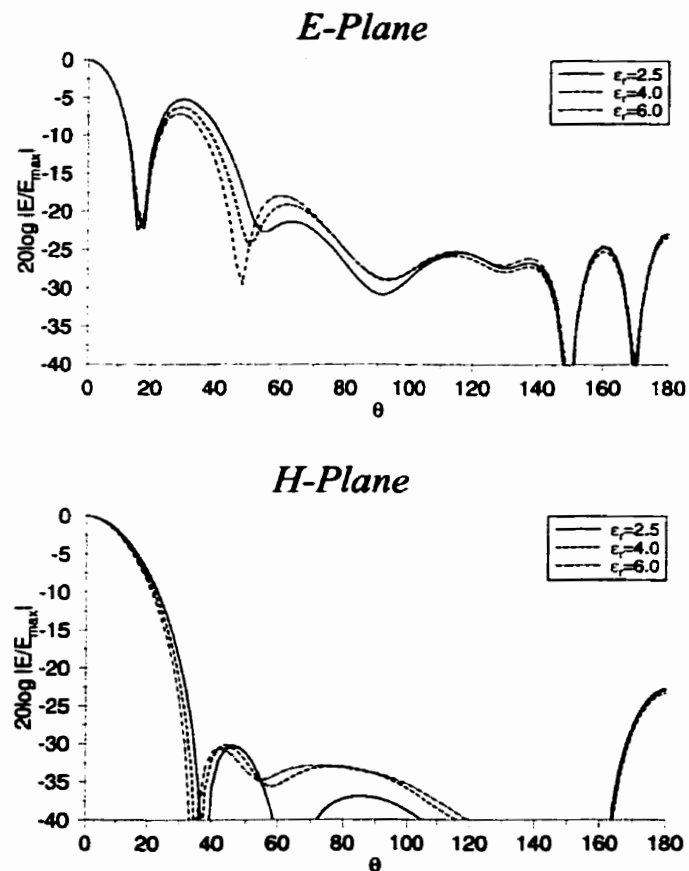


Fig.5.74. Effects of dielectric constant on the radiation when there was no conducting ring above the slot.

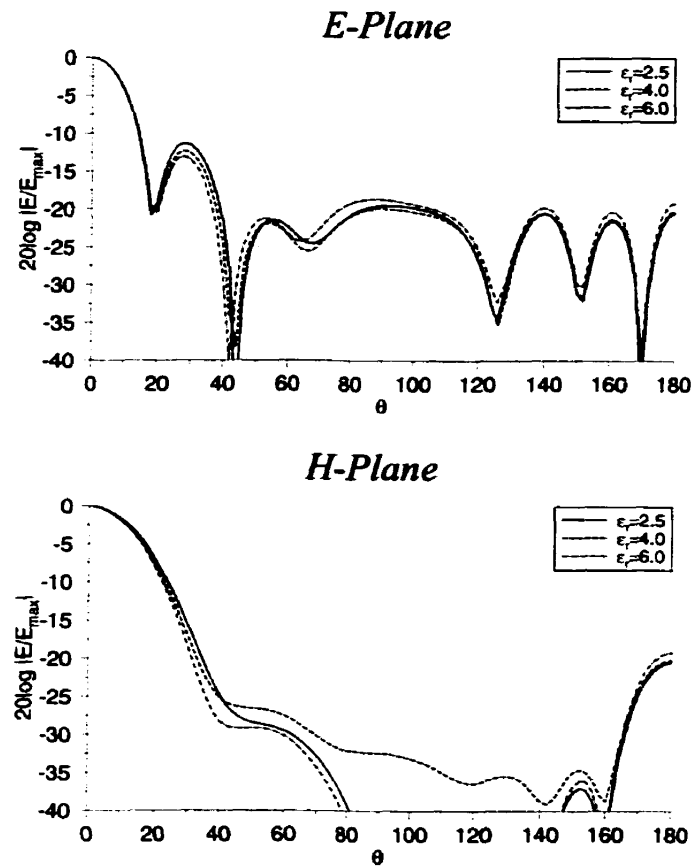


Fig. 5.75. Effects of dielectric constant when a conducting ring with the width of $L=0.7\lambda_0$ was located at the height of $h_2=0.05\lambda_0$ above the slot.

5.5.4. Extra Central Slot

Because the slot radius was large, $\rho_1=0.95\lambda_0$, it was felt that the central region of the antenna may not be excited adequately, resulting in poor performance. To remedy, a narrow central slot was also added, just above the exciting dipoles, ($\rho_e \equiv |x_f|$). Investigation showed that, if the slot is narrow, the directivity will increase and the side lobe level will decrease. But, if the slot is wide, both directivity and side lobe level will deteriorate. The back lobe level decreases as the slot width increases. The slot width must

be kept around $0.04\lambda_0$ to achieve the best directivity and side lobe level. Directivity, and E-plane side and back lobe level for different slot widths are shown in Table (5-19).

Table (5-19) Effect of narrow central slot on radiation characteristics of the original annular slot antenna, slot location $\rho_e=0.18\lambda_0$.

w/λ_0	Directivity (dBi)	Side lobe level (dB)	Back lobe level (dB)
no slot	13.40	-2.77	-16.56
0.02	14.86	-5.65	-16.93
0.04	15.18	-7.91	-17.51
0.06	14.54	-7.71	-17.91
0.08	13.64	-6.27	-18.30
0.10	13.32	-5.38	-18.52

This method can also be combined with the pervious methods to increase the aperture efficiency. For example, the radiation patterns for the antenna with an extra slot of $0.04\lambda_0$ width and located at $\rho_e=0.2\lambda_0$, loaded with a layer of dielectric ($R=1.7\lambda_0$, $d=0.15\lambda_0$, $\epsilon_r=2.5$) and a ring conducting ring ($L=0.7\lambda_0$, $h=0.05\lambda_0$) are shown in Fig.5.76-(a). Its directivity is 17.41dBi, which gives more than 4dB improvement over the original antenna. The side and back lobe levels are -20.69dB, and -20.11dB, respectively. If the conducting ring conducting ring width is decreased from $0.7\lambda_0$ to $0.5\lambda_0$, the directivity increases further to 17.90dBi, and the back lobe level decreases from -20.11dB to -27.48dB. But the side lobe level is higher than the case with $L=0.7\lambda_0$, increasing from -20.96dB to -14.41dB, as shown in Fig.5.76-b. The side lobe level improvement is still about 11.64dB in comparison to the original antenna.

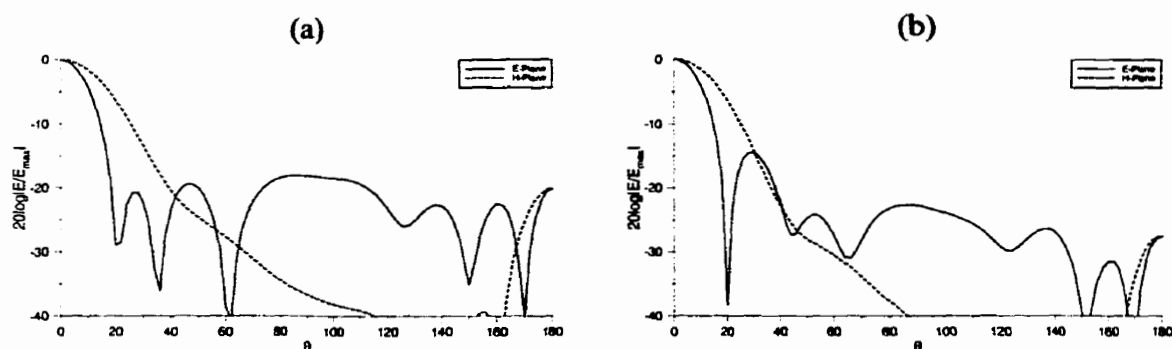


Fig.5.76. Radiation patterns for annular slot antenna loaded with dielectric and conducting ring and with one extra slot above the probes, $R=1.7\lambda_0$, $d=0.15\lambda_0$, $\epsilon_r=2.5$, $w=0.04\lambda_0$, $\rho_e=0.20\lambda_0$, $h=0.05\lambda_0$, (a) $L=0.7\lambda_0$, Directivity = 17.409dBi, (b) $L=0.5\lambda_0$, Directivity = 17.897dBi.

5.5.5. Open Cavity

To this extent the effort was to increase the directivity and decrease the side lobe level in the E-plane. To decrease the back lobe level, the structure with an open cavity and chokes is suggested, as shown in Fig.5.77. The effects of cavity wall size (h_{oc}) on the directivity, side and back lobe levels of the antenna loaded with dielectric, and without a choke, are shown in Fig.5.78 and Fig.5.79. They show that for $h_{oc}=0.2\lambda_0$ directivity and back lobe levels are good. When the wall extension (h_{oc}) is increased to $1.1\lambda_0$ the second maximum for directivity occurs. Adding the open cavity generally increases the side lobe level. The radiation patterns for the antenna without and with an open cavity with wall size of one free-space wavelength are shown in Fig.5.80. The directivity is increased from 16.92dBi to 17.63dBi, and back lobe level is decreased from -17.85dB to -28.30dB, but the side lobe level is increased from -19.24dB to -15.30dB.

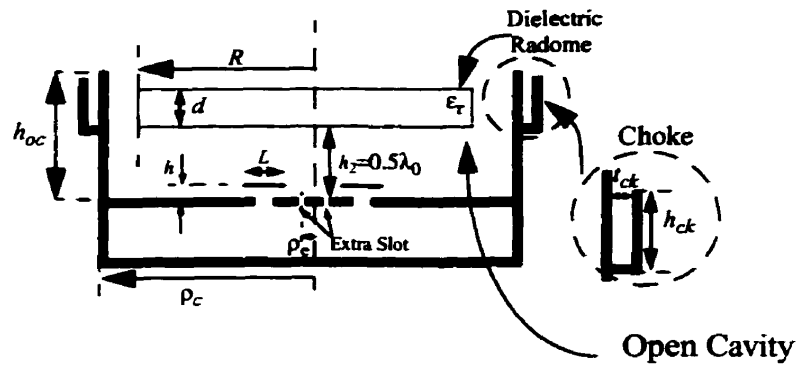


Fig.5.77. Structure of annular slot antenna covered with dielectric and with open cavity and choke.

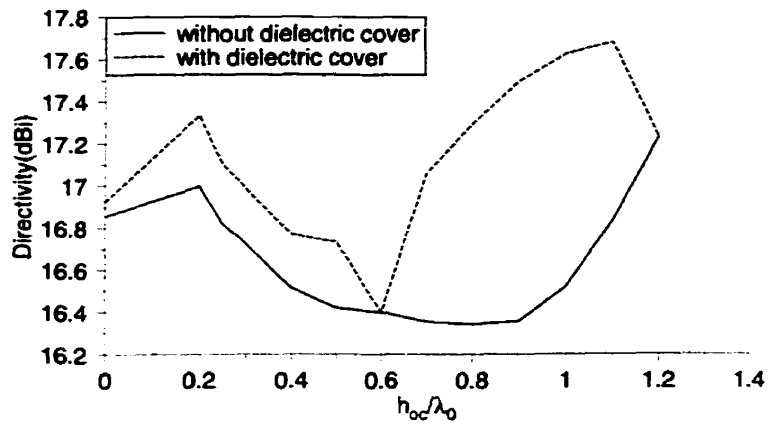


Fig.5.78. Effect of open cavity wall size on the directivity of the antenna without dielectric and with dielectric layer ($R=1.15\lambda_0$, $d=0.15\lambda_0$, $\epsilon_r=2.5$), antenna had a conducting ring ($L=0.5\lambda_0$, $h=0.05\lambda_0$) and extra central slot ($w=0.04\lambda_0$, $\rho_e=0.2\lambda_0$), cavity radius (ρ_c)= $1.5\lambda_0$.

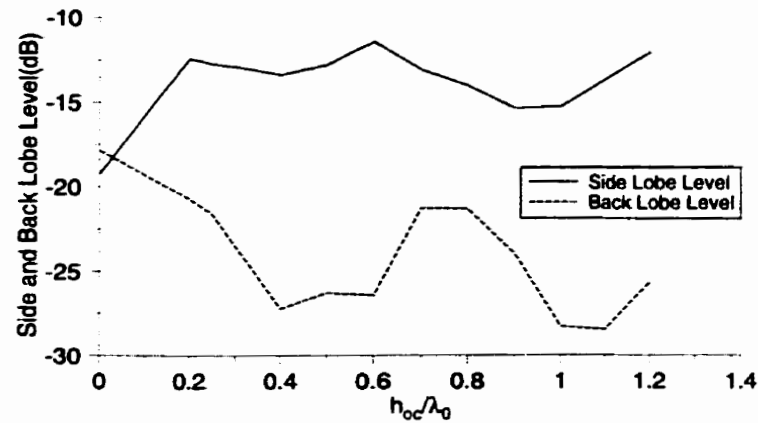


Fig. 5.79. Effect of open cavity wall size on the side and back lobe level of the antenna with configuration given in Fig. 5.78.

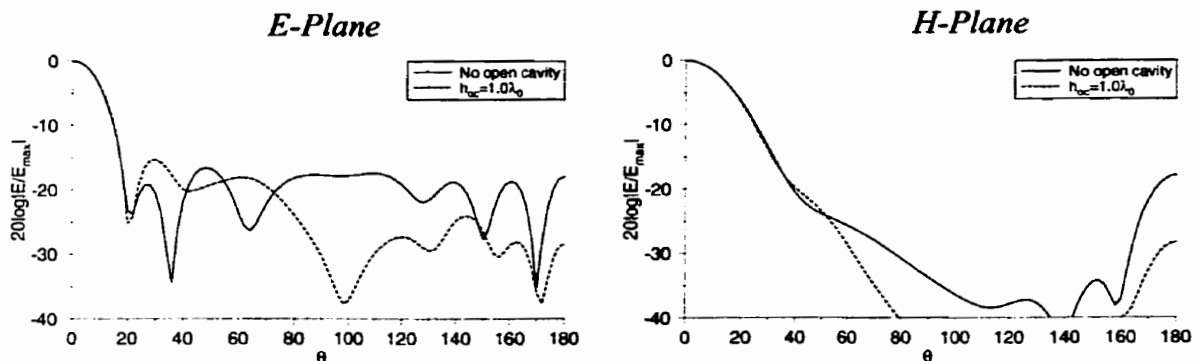


Fig. 5.80. Radiation patterns for the antenna with and without open cavity and covered with dielectric ($R=1.15\lambda_0$, $d=0.15\lambda_0$, $\epsilon_r=2.5$) and with conducting ring ($L=0.5\lambda_0$, $h=0.05\lambda_0$) Directivity: without cavity= 16.924dBi , with open cavity= 17.628dBi .

To further decrease the back lobe level and increase the directivity, one or two quarter wavelength chokes ($h_{ck}=0.25\lambda_0$) can be added to the structure. Fig. 5.81 shows the radiation patterns for the antenna with two chokes and cavity wall size of $h_{oc}=0.9\lambda_0$. In

comparison to the antenna without chokes, the directivity is increased from 17.50dB to 18.12dBi, which has more than 72% aperture efficiency. Side and back lobe levels for antennas with chokes are -14.03dB and -46.50dB, respectively, while for the antenna without chokes are -15.38dB and -23.98dB, respectively. This shows significant improvement in the back lobe level.

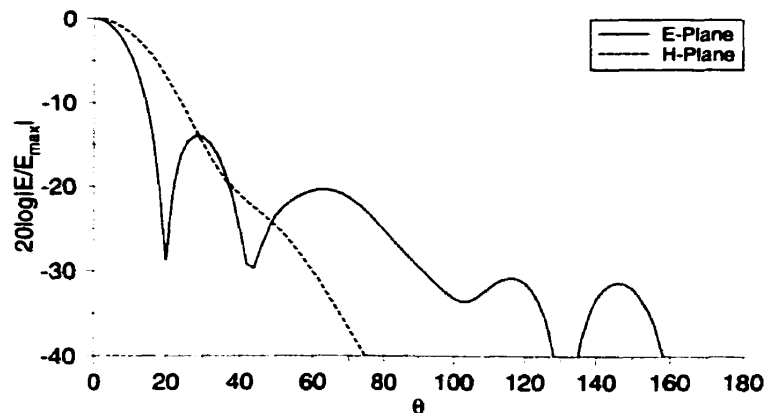


Fig.5.81. Radiation patterns for the antenna with double choke, Directivity=18.117dBi, $R=1.15\lambda_0$, $d=0.15\lambda_0$, $\epsilon_r=2.5$, $h_{ck}=0.25\lambda_0$, $t_{ck}=0.06\lambda_0$, $h_{oc}=0.9\lambda_0$.

To achieve better side lobe level for this antenna, dielectric thickness is increased to $0.55\lambda_0$ and a circular disk patch and a ring patch are added on the top surface of dielectric as shown in Fig.5.82. By changing their dimensions, one can achieve better equality between E and H-plane patterns. Two samples are given in Fig.5.83 and Fig.5.84. The antenna directivity decreases, as the pattern symmetry is increased, as shown in Fig.5.84.

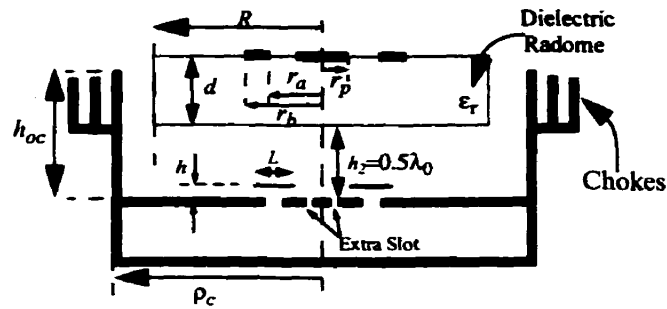


Fig.5.82. Configuration of the antenna with microstrip patch.

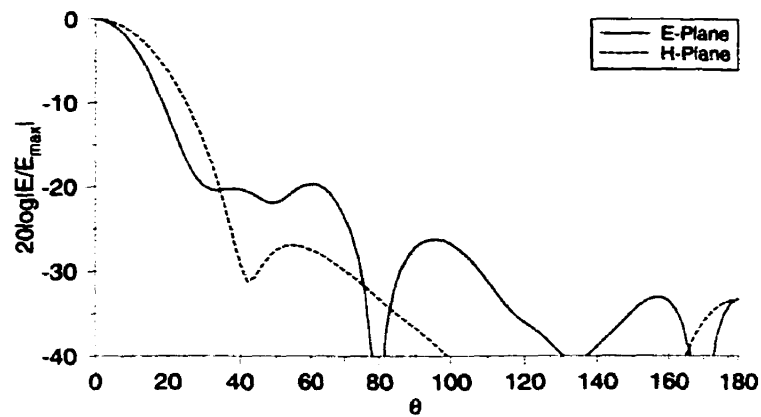


Fig.5.83. Radiation patterns for the antenna with circular and ring patch added to the dielectric radome, Directivity=17.531dBi, $d=0.55\lambda_0$, $r_p=0.136\lambda_0$, $r_a=0.9\lambda_0$, $r_b=\lambda_0$, other dimension the same as Fig.5.81.

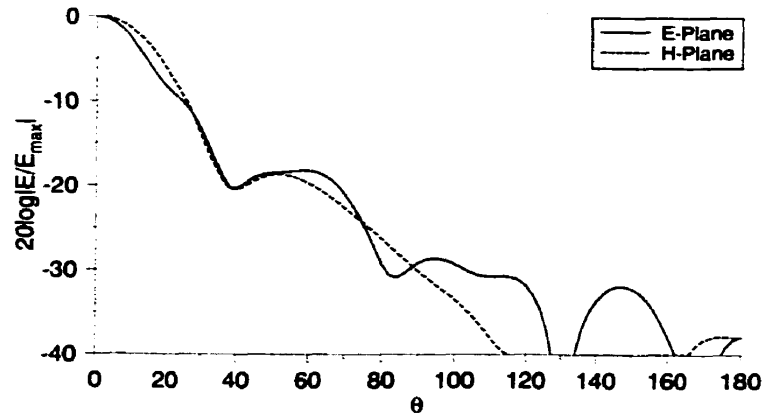


Fig.5.84. Radiation patterns for the antenna with circular and ring path added to the dielectric radome, Directivity=16.564dBi, $d=0.55\lambda_0$, $r_p=0.136\lambda_0$, $r_a=0.35\lambda_0$, $r_b=0.45\lambda_0$, other dimensions the same as Fig.5.81.

5.5.6. Frequency Bandwidth

To see the effect of the mentioned methods on the frequency bandwidth, three antennas were selected and their directivity frequency bandwidth are compared in Fig.5.85. Antenna (a) is the original annular slot antenna with no conducting ring or dielectric cover as shown in Fig.5.65. Antenna (b) is the same as Fig.5.67, with conducting ring ($L=0.5\lambda_0$, $h=0.05\lambda_0$) and dielectric layer ($R=1.7\lambda_0$, $d=0.15\lambda_0$, $\epsilon_r=2.5$). Antenna (c) is the same as Fig.5.82, with dielectric ($R=1.15\lambda_0$, $d=0.55\lambda_0$, $\epsilon_r=2.5$), conducting ring ($L=0.5\lambda_0$, $h=0.05\lambda_0$) and central slot ($w=0.04\lambda_0$, $\rho_e=0.18\lambda_0$). Dimensions of two patches (disk and ring) that are added to the dielectric are ($r_p=0.136\lambda_0$, $r_a=0.35\lambda_0$, $r_b=0.45\lambda_0$), and open cavity dimensions are ($h_{oc}=0.9\lambda_0$, $h_{ck}=0.25\lambda_0$, $t_{ck}=0.06\lambda_0$). The bandwidths of the antennas (b) and (c) are similar. They show less sensitivity at the lower frequency end.

Their overall bandwidths seem similar.

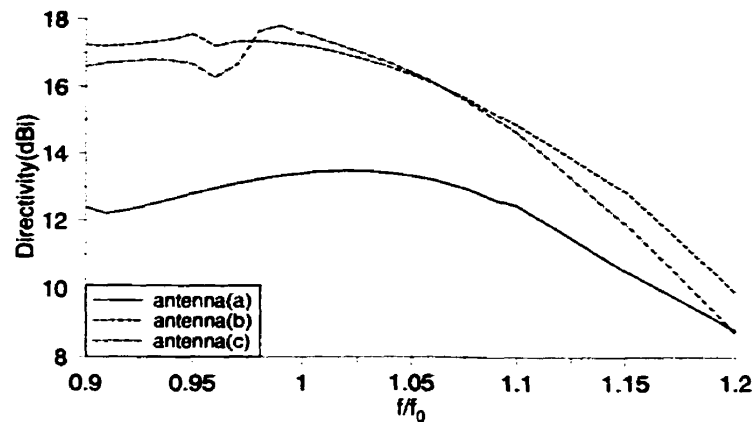


Fig.5.85. Frequency bandwidth of three antennas, antenna (a) is shown in Fig.5.65, antenna (b) is shown in Fig.5.67, and antenna (c) is shown in Fig.5.82.

5.6. SUMMARY

In the beginning of this chapter, the results given by field solution for dielectric and conducting ring loaded annular slot array antennas using the BVM, which was developed in Chapter 3 and 4, were compared with two commercial numerical tools: IE3D and MBES. Good agreement in all cases were achieved. BVM has the advantage of requiring less computation time and computing facilities. On the other hand, it has limitations because of the assumption of infinite ground plane and narrow slots. It can provide a good tool for optimization problems where the time is a concern. After finding the optimum dimensions fine tuning can be done numerically for the finite dielectric and ground plane.

In the second part of this chapter, BVM was used to study the effect of various

parameters on the annular slot array antenna performance. It can be concluded that both dielectric and conducting ring loading improve the antenna performance. The dielectric loading causes reflections which can be used to improve the aperture illumination. Conducting rings, in fact, are microstrip patches fed by slots.

The optimum thickness for dielectric was found to be a quarter wavelength in dielectric. The higher permittivity provides more directivity, while the optimum physical thickness is smaller. First slot location of around $0.45\lambda_0$ and slot separation of around one wavelength were found to be the best choices. When there is an air gap between the dielectric layer and antenna surface, the distance of half a wavelength will provide the best performance. The distance between the last slot and conductor cavity wall must not be odd multiples $0.25\lambda_0$, where the directivity drops significantly.

The conducting ring loading can improve the aperture efficiency up to around 50%. The directivity is similar to antennas covered with low permittivity dielectrics, but the side lobe level for antennas with more than two slots is generally higher in comparison to dielectric loaded antennas. It is expected that by using optimized non uniform ring widths better side lobe level can be achieved.

In the last section of this chapter small annular slot antennas were studied numerically using MBES, to investigate the effect of various parameters of the finite structure on the antenna performance. Similar results for the BVM (infinite structure) having dielectric thickness, slot location, and conducting ring height and width were obtained. Effects of the dielectric radius on the directivity were also studied. It was shown that the dielectric permittivity does not have pronounce effects on the optimum dielectric

radius. By adding a conducting ring above the slots, directivity increases and the side lobe level in the E-plane decreases. The dielectric loading was also combined with conducting ring loading and it was concluded that when two methods are combined, the conducting ring width must be decreased to achieve better performance.

To improve the antenna performance further, modifications in the structure were suggested. First by adding a narrow annular slot, in central region and above the exciting probes, the antenna performance was improved. This was combined with two other methods; dielectric and conducting ring loadings. By having an extra slot and larger conducting ring, side lobe level decreased to less than -20dB. However, a smaller conducting ring provides better back lobe level and directivity.

To decrease the side and back lobe levels together and keep the directivity reasonable, an open cavity with chokes was added to the structure. Adding additional patches over the dielectric was shown to improve the equality of E and H-plane patterns. This property can be used to reduce the cross polarization and the axial ratio in circular polarized antenna applications.

Chapter 6

CONCLUSION AND RECOMMENDATION

6.1. CONCLUSION

This thesis addresses the problem of dielectric loaded annular slot array antennas. The formulations are based on the boundary value method. The solution was developed by defining two appropriate types of Green's functions for dielectric layers and free-space. Green's functions represent the magnetic current ring that are expanded in terms of Fourier series in angular direction. The Green's functions for the magnetic current ring covered with one or two layers of dielectric are developed.

For the final formulation for annular slot array antennas, the Green's functions were utilized. The electric field on the slots were expanded in terms of basis functions with unknown coefficients in radial direction, and Fourier series in angular direction. The equivalent magnetic current was found using the electric field. The wave functions for each region were found by integrating the radial expansion of magnetic current on the slots and proper Green's function in radial direction. Then, by applying the boundary

conditions, the unknown coefficients for electric field expansion were found. The far-field formulation was carried out using the electric field just above the last layer of dielectric. A closed form formulation was found for the far-field. The far-field in E-plane is in the form of differences of Bessel functions at the edges of the slots, and in H-plane is in the form of integral of Bessel functions over each slot. This creates very high side lobe level in E-plane and very small side lobe in H-plane.

Effect of dielectric layers is on how the patterns of each slot are combined with the other ones. By choosing the appropriate dielectric thickness and material, one can reduce the E-plane side lobe level. Through the simulations, it was found that the higher permittivity for dielectric layer provides lower E-plane side lobe level and better directivity by reducing the H-plane beamwidth. The optimum thickness for dielectric layer is near quarter wavelength in the dielectric. If there is an air gap between the dielectric and antenna, the best distance between them is half a wavelength.

Another way of improving the antenna performance is placing the conductor rings above the slots. This forms microstrip ring arrays fed by slots. To analyze this structure, using boundary value method, the Green's functions for a problem containing one magnetic current ring and one electric current ring locating at two different heights were found. The formulation for array of slots and conductors was performed using these Green's functions. Each Green's function contains two parts; one due to the magnetic ring current and one due to the electric ring current. The wave functions for antenna problem also have two parts. For antenna problem, electric current on the slot and magnetic current on the conductor were expanded in terms of Fourier series in the angular direction and

pulses basis functions in the radial directions. These indicate the need of two sets of boundary conditions to define the unknown coefficients for these expansions. The first boundary condition was the continuity of magnetic field imposed on the slots, and the second boundary condition was the zero electric field on the conductor rings. After defining the field for each region, the far-field formulation was carried out. The effect of rings on the far field is reducing the E-plane side lobe level and reducing the radiation around the horizon. This enhances the directivity.

The boundary value method has the advantage of requiring much less memory and time, in comparison to the numerical methods. The matrix size is of the order of number of slots. On the other hand assumption of infinite ground plane and infinite dielectric layer is unrealistic. However, simulation results showed good agreement between this method and numerical methods. By implementing this method in a computer program and performing some simulations, the effect of various antennas parameters on their radiation characteristics were investigated. To include the effect of finiteness of dielectric and the ground plane, method of moments for bodies of revolution was used and new structures were proposed for further improvements. It was shown that adding an open cavity wall, with quarter wavelength chokes, in front of the antenna reduces the back radiation. Adding microstrip circular and ring patches on top of the dielectric layer improves the equality of E and H-plane radiation patterns, which can reduce the cross polarization for the circular polarized applications.

6.2. RECOMMENDATIONS FOR FUTURE RESEARCH

There are a few topics which can be considered for more investigations. The closed formed formulations can be easily used in an optimization program. Using the optimization program, the non uniform spacing between the slots and conductor rings can be studied in detail. It is expected that non uniform spacing can provide better aperture distribution. Also the non uniform conducting ring width can reduce the side lobe level in E-plane. To reduce the run time, it is strongly recommended to implement the program in a low level programming language such as C++. Also, the calculation of infinite integrals can be done in a faster and more efficient way.

Using Geometrical Theory of Diffraction (GTD) the effect of finite ground plane can be considered. Also the numerical results can be verified by experiments.

In the calculation of conductor loaded antenna, only the radial component of the induced electric current was taken into account, as it is the dominant current. The angular component can be considered using the same approach. This component is expected to have more effects on the radiation around horizon. Also the conducting ring ohmic losses must be included.

More detailed studies can be performed on the input impedance and frequency bandwidth of the antenna and effects of dielectric and conductor loading on them. Other feeding systems, rather than probe feeding may be investigated and performance of different feeding method can be compared and discussed.

Appendix A

BOUNDARY CONDITIONS IMPLEMENTATION

Using the first set of boundary conditions at $z = 0$ given in (3-25), substituting inverse Hankel transform of (3-22) and (3-23) into (3-5), and applying the orthogonality property of sinusoidal functions, one obtains

$$\frac{1}{j\omega\epsilon_2} \int_0^\infty \gamma \alpha^2 [F_n^e - f_n^e] J_n'(\alpha\rho) d\alpha + \frac{n^2}{\rho} \int_0^\infty \alpha [F_n^h + f_n^h] J_n(\alpha\rho) d\alpha = \delta(\rho - \rho') \quad (\text{A-1})$$

$$-\frac{n}{j\omega\epsilon_2\rho} \int_0^\infty \gamma \alpha [F_n^e - f_n^e] J_n(\alpha\rho) d\alpha + n \int_0^\infty \alpha^2 [F_n^h + f_n^h] J_n'(\alpha\rho) d\alpha = \delta(\rho - \rho') \quad (\text{A-2})$$

By adding these two equations, one finds

$$\frac{1}{j\omega\epsilon_2} \int_0^\infty \gamma \alpha^2 [F_n^e - f_n^e] J_{n-1}(\alpha\rho) d\alpha + n \int_0^\infty \alpha^2 [F_n^h + f_n^h] J_{n-1}(\alpha\rho) d\alpha = \delta(\rho - \rho') \quad (\text{A-3})$$

where a use has been made of the following relation for derivative of Bessel functions [63]

$$J_{n-1}(\alpha\rho) = J_n'(\alpha\rho) + \frac{n}{\alpha\rho} J_n(\alpha\rho) \quad (\text{A-4})$$

Subtraction (A-2) from (A-1) gives the following equation

$$\frac{1}{\omega\epsilon_2} \int_0^\infty \gamma \alpha^2 [F_n^e - f_n^e] J_{n+1}(\alpha\rho) d\alpha + n \int_0^\infty \alpha^2 [F_n^h + f_n^h] J_{n+1}(\alpha\rho) d\alpha = \delta(\rho - \rho') \quad (\text{A-5})$$

where the following relation for derivative of Bessel functions has been used [63]

$$J_{n+1}(\alpha\rho) = -J_n'(\alpha\rho) + \frac{n}{\alpha\rho} J_n(\alpha\rho) \quad (\text{A-6})$$

Now taking the Hankel transform of order (n-1) and (n+1) of equations (A-3) and (A-5), respectively, one obtains

$$\begin{aligned} & -\frac{1}{j\omega\epsilon_2} \int_0^\infty \gamma \alpha [F_n^e - f_n^e] \left[\alpha \int_0^\infty J_{n-1}(\alpha\rho) J_{n-1}(\alpha\rho) \rho d\rho \right] d\alpha + \\ & \gamma \int_0^\infty \alpha [F_n^h + f_n^h] \left[\alpha \int_0^\infty J_{n-1}(\alpha\rho) J_{n-1}(\alpha\rho) \rho d\rho \right] d\alpha = \int_0^\infty \delta(\rho - \rho') J_{n-1}(\alpha\rho) \rho d\rho \end{aligned} \quad (\text{A-7})$$

$$\begin{aligned} & \frac{1}{j\omega\epsilon_2} \int_0^\infty \gamma \alpha [F_n^e - f_n^e] \left[\alpha \int_0^\infty J_{n+1}(\alpha\rho) J_{n+1}(\alpha\rho) \rho d\rho \right] d\alpha + \\ & \gamma \int_0^\infty \alpha [F_n^h + f_n^h] \left[\alpha \int_0^\infty J_{n+1}(\alpha\rho) J_{n+1}(\alpha\rho) \rho d\rho \right] d\alpha = \int_0^\infty \delta(\rho - \rho') J_{n+1}(\alpha\rho) \rho d\rho \end{aligned} \quad (\text{A-8})$$

which can be simplified as

$$\begin{aligned} & -\frac{1}{j\omega\epsilon_2} \gamma \alpha [F_n^e - f_n^e] + n \alpha [F_n^h + f_n^h] = \rho' J_{n-1}(\alpha\rho') \\ & \frac{1}{\omega\epsilon_2} \gamma \alpha [F_n^e - f_n^e] + n \alpha [F_n^h + f_n^h] = \rho' J_{n+1}(\alpha\rho') \end{aligned} \quad (\text{A-9})$$

where a use has been made of the following property of delta function [61]

$$\beta \int_0^\infty J_\nu(\alpha x) J_\nu(\beta x) x dx = \delta(\alpha - \beta) \quad (\text{A-10})$$

Now let's assume that variables for Hankel transform for dielectric region and free-space are different, i.e. α_1 for dielectric and α_2 for free-space. By the first two boundary

conditions in (3-26) the following equation is concluded

$$\frac{1}{j\omega\epsilon_2} \int_0^\infty \gamma \alpha_1^2 [F_n^e e^{-\gamma h_2} - f_n^e e^{\gamma h_2}] J_n'(\alpha_1 \rho) d\alpha_1 + \frac{n^2}{\rho} \int_0^\infty \alpha_1 [F_n^h e^{-\gamma h_2} + f_n^h e^{\gamma h_2}] J_n(\alpha_1 \rho) d\alpha_1 = \quad (A-11)$$

$$\frac{1}{j\omega\epsilon_0} \int_0^\infty \delta \alpha_2^2 G_n^e e^{-\delta h_2} J_n'(\alpha_2 \rho) d\alpha_2 + \frac{n^2}{\rho} \int_0^\infty \alpha_2 G_n^h e^{-\delta h_2} J_n(\alpha_2 \rho) d\alpha_2$$

$$\frac{n}{j\omega\epsilon_2 \rho} \int_0^\infty \gamma \alpha_1 [F_n^e e^{-\gamma h_2} - f_n^e e^{\gamma h_2}] J_n(\alpha_1 \rho) d\alpha_1 + n \int_0^\infty \alpha_1^2 [F_n^h e^{-\gamma h_2} + f_n^h e^{\gamma h_2}] J_n'(\alpha_1 \rho) d\alpha_1 = \quad (A-12)$$

$$\frac{n}{j\omega\epsilon_0 \rho} \int_0^\infty \gamma \alpha_2 G_n^e e^{-\delta h_2} J_n(\alpha_2 \rho) d\alpha_2 + n \int_0^\infty \alpha_2^2 G_n^h e^{-\delta h_2} J_n'(\alpha_2 \rho) d\alpha_2$$

By addition and subtraction of these equations the following equations are obtained

$$\frac{-1}{\omega\epsilon_2} \int_0^\infty \gamma \alpha_1^2 [F_n^e e^{-\gamma h_2} - f_n^e e^{\gamma h_2}] J_{n-1}(\alpha_1 \rho) d\alpha_1 + n \int_0^\infty \alpha_1^2 [F_n^h e^{-\gamma h_2} + f_n^h e^{\gamma h_2}] J_{n-1}(\alpha_1 \rho) d\alpha_1 = \quad (A-13)$$

$$\frac{-1}{\omega\epsilon_0} \int_0^\infty \delta \alpha_2^2 G_n^e e^{-\delta h_2} J_{n-1}(\alpha_2 \rho) d\alpha_2 + n \int_0^\infty \alpha_2^2 G_n^h e^{-\delta h_2} J_{n-1}(\alpha_2 \rho) d\alpha_2$$

$$\frac{1}{\omega\epsilon_2} \int_0^\infty \gamma \alpha_1^2 [F_n^e e^{-\gamma h_2} - f_n^e e^{\gamma h_2}] J_{n+1}(\alpha_1 \rho) d\alpha_1 + n \int_0^\infty \alpha_1^2 [F_n^h e^{-\gamma h_2} + f_n^h e^{\gamma h_2}] J_{n+1}(\alpha_1 \rho) d\alpha_1 = \quad (A-14)$$

$$\frac{1}{\omega\epsilon_0} \int_0^\infty \delta \alpha_2^2 G_n^e e^{-\delta h_2} J_{n+1}(\alpha_2 \rho) d\alpha_2 + n \int_0^\infty \alpha_2^2 G_n^h e^{-\delta h_2} J_{n+1}(\alpha_2 \rho) d\alpha_2$$

Now we must multiply equation (A-13) by $\rho J_{n-1}(\alpha \rho)$ and equation (A-14) by

$\rho J_{n+1}(\alpha \rho)$ and integrate on ρ from zero to infinity. Using (A-10) the result will be

$$\frac{-1}{\omega\epsilon_2} \gamma \alpha [F_n^e e^{-\gamma h_2} - f_n^e e^{\gamma h_2}] + n \alpha [F_n^h e^{-\gamma h_2} + f_n^h e^{\gamma h_2}] = \frac{-1}{j\omega\epsilon_0} \delta \alpha G_n^e e^{-\gamma h_2} + n \alpha G_n^h e^{-\gamma h_2} \quad (A-15)$$

$$\frac{1}{\omega\epsilon_2} \gamma \alpha [F_n^e e^{-\gamma h_2} - f_n^e e^{\gamma h_2}] + n \alpha [F_n^h e^{-\gamma h_2} + f_n^h e^{\gamma h_2}] = \frac{1}{j\omega\epsilon_0} \delta \alpha G_n^e e^{-\gamma h_2} + n \alpha G_n^h e^{-\gamma h_2}$$

Where a use has been made of the following property of delta function

$$\int_0^\infty R(\beta x) \delta(\alpha - \beta) d\beta = R(\alpha) \quad (A-16)$$

Appendix B

DERIVATION OF MAGNETIC SURFACE CURRENTS

The magnetic current on the dielectric layer at $z = h_3$ can be written in terms of electric field

$$\begin{aligned}\vec{J}_{ms} &= \vec{E} \times \hat{n} \\ J_{m\phi} &= -E_\rho \\ J_{m\rho} &= E_\phi\end{aligned}\tag{B-1}$$

The electric field can be calculated using (3-5). The result of substitution of wave functions for free space given by (4-11) and (4-13) into (3-5) is

$$\begin{aligned}E_\rho(\rho', \phi', z' = h_2) &= -J_{m\phi} = \sum_{i=1}^{IC} \sum_{n=0}^{\infty} E_{in}(a_n \cos n\phi' + b_n \sin n\phi') \cdot F_\phi(\rho', \rho_i) \\ F_\phi(\rho', \rho_i) &= \left\{ \rho_i \int_0^\infty \left[\frac{(1 - k^e) e^{-\gamma h_2}}{1 - k^e e^{-2\gamma h_2}} \right] \left(J_n(\alpha \rho) \Big|_{\rho_i}^{\rho_i'} \right) J_n'(\alpha \rho') d\alpha + \right. \\ &\quad \left. \frac{n^2}{\rho'} \int_0^\infty \left[\frac{(1 + k^h) e^{-\gamma h_2}}{1 + k^h e^{-2\gamma h_2}} \right] \left(L_n^J(\alpha \rho) \Big|_{\rho_i}^{\rho_i'} \right) J_n(\alpha \rho') \frac{d\alpha}{\alpha} \right\}\end{aligned}\tag{B-2}$$

$$\begin{aligned}
E_{\phi}(\rho', \phi', z' = h_2) &= J_{m\rho} = \sum_{i=1}^{IC} \sum_{n=0}^{\infty} E_{in} n (b_n \cos n\phi' - a_n \sin n\phi') \cdot F_{\rho}(\rho', \rho_i) \\
F_{\rho}(\rho', \rho_i) &= \left\{ \frac{\rho_i}{\rho'} \int_0^{\infty} \left[\frac{(1-k^e)e^{-\gamma h_2}}{1-k^e e^{-2\gamma h_2}} \right] \left(J_n(\alpha\rho) \Big|_{\rho_i}^{\rho_i^+} \right) J_n(\alpha\rho') \frac{d\alpha}{\alpha} + \right. \\
&\quad \left. \int_0^{\infty} \left[\frac{(1+k^h)e^{-\gamma h_2}}{1+k^h e^{-2\gamma h_2}} \right] \left(L_n^J(\alpha\rho) \Big|_{\rho_i}^{\rho_i^+} \right) J_n'(\alpha\rho') d\alpha \right\}
\end{aligned} \tag{B-3}$$

Now substituting (B-2) and (B-3) into (4-50), the following equations are found

$$\begin{aligned}
U_{\phi 1} &= \int_0^{2\pi} \int_0^{\infty} -J_{m\phi} \sin(\phi - \phi') \cos\theta e^{jk_0\rho' \sin\theta \cos(\phi - \phi')} \rho' d\rho' d\phi' \\
&= -\cos\theta \sum_{i=1}^{IC} \sum_{n=0}^{\infty} E_{in} \int_0^{\infty} -F_{\phi}(\rho', \rho_i) T_{1n}(\rho') \rho' d\rho'
\end{aligned} \tag{B-4}$$

$$T_{1n}(\rho') = \int_0^{2\pi} (a_n \cos n\phi' + b_n \sin n\phi') \sin(\phi - \phi') e^{jk_0\rho' \sin\theta \cos(\phi - \phi')} d\phi'$$

$$\begin{aligned}
U_{\phi 2} &= \int_0^{2\pi} \int_0^{\infty} -J_{m\rho} \cos(\phi - \phi') \cos\theta e^{jk_0\rho' \sin\theta \cos(\phi - \phi')} \rho' d\rho' d\phi' \\
&= -\cos\theta \sum_{i=1}^{IC} \sum_{n=0}^{\infty} E_{in} \int_0^{\infty} F_{\rho}(\rho', \rho_i) T_{2n}(\rho') \rho' d\rho'
\end{aligned} \tag{B-5}$$

$$T_{2n}(\rho') = \int_0^{2\pi} n(b_n \cos n\phi - a_n \sin n\phi) \cos(\phi - \phi') e^{jk_0\rho' \sin\theta \cos(\phi - \phi')} d\phi'$$

where $U_{\phi} = U_{\phi 1} + U_{\phi 2}$. Similarly

$$\begin{aligned}
U_{\theta 1} &= \int_0^{2\pi} \int_0^{\infty} J_{m\phi} \cos(\phi - \phi') e^{jk_0\rho' \sin\theta \cos(\phi - \phi')} \rho' d\rho' d\phi' \\
&= -\sum_{i=1}^{IC} \sum_{n=0}^{\infty} E_{in} \int_0^{\infty} F_{\phi}(\rho', \rho_i) T_{3n}(\rho') \rho' d\rho'
\end{aligned} \tag{B-6}$$

$$T_{3n}(\rho') = \int_0^{2\pi} (a_n \cos n\phi' + b_n \sin n\phi') \cos(\phi - \phi') e^{jk_0\rho' \sin\theta \cos(\phi - \phi')} d\phi'$$

$$\begin{aligned}
U_{\theta 2} &= \int_0^{2\pi} \int_0^{\infty} -J_{m\rho} \sin(\phi - \phi') e^{jk_0\rho' \sin\theta \cos(\phi - \phi')} \rho' d\rho' d\phi' \\
&= - \sum_{i=1}^{IC} \sum_{n=0}^{\infty} E_{in} \int_0^{\infty} F_{\rho}(\rho', \rho_i) T_{4n}(\rho') \rho' d\rho' \\
T_{4n}(\rho') &= \int_0^{2\pi} n(b_n \cos n\phi' - a_n \sin n\phi') \sin(\phi - \phi') e^{jk_0\rho' \sin\theta \cos(\phi - \phi')} d\phi'
\end{aligned} \tag{B-7}$$

where $U_{\theta} = U_{\theta 1} + U_{\theta 2}$. To carry out the integration for T_{1n} , T_{2n} , T_{3n} and T_{4n} , one can use the following properties of sinusoidal functions

$$\begin{aligned}
2 \cos n u \cos u &= \cos(n-1)u + \cos(n+1)u \\
2 \sin n u \sin u &= \cos(n-1)u - \cos(n+1)u
\end{aligned} \tag{B-8}$$

and the following property of Bessel function [63]

$$\int_0^{\pi} e^{j\tau \cos t} \cos n t dt = j^n \pi J_n(\tau) \tag{B-9}$$

One can rewrite the integral in T_{1n} by changing the variable $\phi' = \phi + u$. Since the integration on ϕ' represents the contribution of all points over an angular range equal to 2π , we are free to select the starting point in the integration.

$$\begin{aligned}
T_{1n}(\rho') &= \int_{-\pi}^{\pi} (a_n \cos n(\phi + u) + b_n \sin n(\phi + u)) (-\sin u) e^{j\tau \cos u} du \\
\phi' &= \phi + u \\
\tau &= k_0 \rho' \sin \theta
\end{aligned} \tag{B-10}$$

This integral can be simplified by re-arranging the sinusoidal terms in the integrand as follows

$$\begin{aligned}
&(a_n \cos n(\phi + u) + b_n \sin n(\phi + u)) (-\sin u) \\
&= -(a_n \cos n\phi + b_n \sin n\phi) \cos n u \sin u - (-a_n \sin n\phi + b_n \cos n\phi) \sin n u \sin u
\end{aligned} \tag{B-11}$$

The first term in (B-11) is an odd function of u and the integration over the angular range will be zero. The second term is an even function of u . Therefore, using (B-8) and (B-9),

T_{1n} is equal to

$$\begin{aligned}
 T_{1n}(\rho') &= 2 \int_0^\pi (a_n \sin n\phi - b_n \cos n\phi) (\sin u \sin u) e^{j\tau \cos u} du \\
 &= (a_n \sin n\phi - b_n \cos n\phi) \int_0^\pi (\cos(n-1)u - \cos(n+1)u) e^{j\tau \cos u} du \\
 &= (a_n \sin n\phi - b_n \cos n\phi) [j^{n-1} \pi J_{n-1}(\tau) - j^{n+1} \pi J_{n+1}(\tau)] \quad (\text{B-12}) \\
 &= (a_n \sin n\phi - b_n \cos n\phi) \pi j^{n-1} [J_{n-1}(\tau) + J_{n+1}(\tau)] \\
 &= n(a_n \sin n\phi - b_n \cos n\phi) \frac{2\pi j^{n-1}}{\tau} J_n(\tau)
 \end{aligned}$$

where a use has been made of

$$\frac{2n}{x} J_n(x) = J_{n-1}(x) + J_{n+1}(x) \quad (\text{B-13})$$

Similarly for T_{2n}

$$\begin{aligned}
 &(b_n \cos n(\phi + u) - a_n \sin n(\phi + u)) \cos u \\
 &= (b_n \cos n\phi - a_n \sin n\phi) \cos n u \cos u + (-b_n \sin n\phi - a_n \cos n\phi) \sin n u \cos u \quad (\text{B-14})
 \end{aligned}$$

and

$$\begin{aligned}
T_{2n}(\rho') &= \int_{-\pi}^{\pi} n(b_n \cos n(\phi + u) - a_n \sin n(\phi + u)) \cos u e^{j\tau \cos u} du \\
&= 2 \int_0^{\pi} n(b_n \cos n\phi - a_n \sin n\phi) (\cos nu \cos u) e^{j\tau \cos u} du \\
&= n(b_n \cos n\phi - a_n \sin n\phi) \int_0^{\pi} (\cos(n-1)u + \cos(n+1)u) e^{j\tau \cos u} du \quad (\text{B-15}) \\
&= n(b_n \cos n\phi - a_n \sin n\phi) [j^{n-1} \pi J_{n-1}(\tau) + j^{n+1} \pi J_{n+1}(\tau)] \\
&= n(b_n \cos n\phi - a_n \sin n\phi) \pi j^{n-1} [J_{n-1}(\tau) - J_{n+1}(\tau)] \\
&= n(b_n \cos n\phi - a_n \sin n\phi) (2\pi j^{n-1}) J_n'(\tau)
\end{aligned}$$

where the following property of Bessel functions has been used

$$2J_n'(x) = 2 \frac{d}{dx} J_n(x) = J_{n-1}(x) - J_{n+1}(x) \quad (\text{B-16})$$

Similarly for U_{θ}

$$\begin{aligned}
T_{3n}(\rho') &= \int_{-\pi}^{\pi} (a_n \cos n(\phi + u) + b_n \sin n(\phi + u)) \cos u e^{j\tau \cos u} du \\
&= 2 \int_0^{\pi} (a_n \cos n\phi + b_n \sin n\phi) (\cos nu \cos u) e^{j\tau \cos u} du \quad (\text{B-17}) \\
&= (a_n \cos n\phi + b_n \sin n\phi) \pi j^{n-1} [J_{n-1}(\tau) - J_{n+1}(\tau)] \\
&= (a_n \cos n\phi + b_n \sin n\phi) (2\pi j^{n-1}) J_n'(\tau)
\end{aligned}$$

using

$$\begin{aligned}
&(a_n \cos n(\phi + u) + b_n \sin n(\phi + u)) \cos u \\
&= (a_n \cos n\phi + b_n \sin n\phi) \cos nu \cos u + (-a_n \sin n\phi + b_n \cos n\phi) \sin nu \cos u \quad (\text{B-18})
\end{aligned}$$

and

$$\begin{aligned}
T_{4n}(\rho') &= \int_{-\pi}^{\pi} n(b_n \cos n(\phi + u) - a_n \sin n(\phi + u))(-\sin u) e^{j\tau \cos u} du \\
&= 2n(a_n \cos n\phi + b_n \sin n\phi) \int_0^{\pi} \sin u \sin u e^{j\tau \cos u} du \\
&= n(a_n \cos n\phi + b_n \sin n\phi) [j^{n-1} \pi J_{n-1}(\tau) - j^{n+1} \pi J_{n+1}(\tau)] \\
&= (a_n \cos n\phi + b_n \sin n\phi) \left(\frac{2n^2 \pi j^{n-1}}{\tau} J_n(\tau) \right)
\end{aligned} \tag{B-19}$$

using

$$\begin{aligned}
&(b_n \cos n(\phi + u) - a_n \sin n(\phi + u))(-\sin u) \\
&= -(b_n \cos n\phi - a_n \sin n\phi) \cos n u \sin u - (-b_n \sin n\phi - a_n \cos n\phi) \sin n u \sin u
\end{aligned} \tag{B-20}$$

Appendix C

DERIVATION OF INFINITE INTEGRALS FOR FAR-FIELD CALCULATION

To calculate far-field, first the integrations on ρ' is carried out, as they have closed form solutions. The first integral is calculated using by writing the derivative of Bessel function of order n in terms of Bessel function of order $n+1$ and $n-1$

$$\begin{aligned} \int_0^{\infty} J_n'(\alpha\rho')J_n(\beta\rho')d\rho' &= \frac{1}{2}\left(\int_0^{\infty} (J_{n-1}(\alpha\rho')J_n(\beta\rho')d\rho') - \int_0^{\infty} J_{n+1}(\alpha\rho')J_n(\beta\rho')d\rho'\right) \\ &= \begin{cases} \frac{1}{2\alpha}\left(\frac{\alpha}{\beta}\right)^n & \alpha < \beta \\ 0 & \alpha = \beta \\ \frac{1}{2\alpha}\left(\frac{\beta}{\alpha}\right)^n & \alpha > \beta \end{cases} \end{aligned} \quad (C-1)$$

where $\beta = k_0 \sin\theta$. and the following integral is used [65]

$$\int_0^{\infty} J_{n+1}(\alpha\rho')J_n(\beta\rho')d\rho' = \begin{cases} 0 & \alpha < \beta \\ \frac{1}{2\alpha} & \alpha = \beta \\ \frac{1}{\alpha}\left(\frac{\beta}{\alpha}\right)^n & \alpha > \beta \end{cases} \quad (C-2)$$

The next integral is taken from [65].

$$\int_0^{\infty} \frac{J_n(\alpha\rho')J_n(\beta\rho')}{\rho'} d\rho' = \begin{cases} \frac{1}{2n} \left(\frac{\alpha}{\beta}\right)^n & \alpha < \beta \\ 0 & \alpha = \beta \\ \frac{1}{2n} \left(\frac{\beta}{\alpha}\right)^n & \alpha > \beta \end{cases} \quad (\text{C-3})$$

The last integral is calculated by writing the expansion of derivative of Bessel functions in terms of Bessel functions of lower and higher orders.

$$\begin{aligned} \int_0^{\infty} J_n'(\alpha\rho')J_n'(k_0\rho'\sin\theta)\rho' d\rho' &= \frac{1}{4} \left(\int_0^{\infty} J_{n-1}(\alpha\rho')J_{n-1}(\beta\rho')\rho' d\rho' - \right. \\ &= \int_0^{\infty} J_{n+1}(\alpha\rho')J_{n-1}(\beta\rho')\rho' d\rho' - \\ &\quad \int_0^{\infty} J_{n-1}(\alpha\rho')J_{n+1}(\beta\rho')\rho' d\rho' + \\ &\quad \left. \int_0^{\infty} J_{n+1}(\alpha\rho')J_{n+1}(\beta\rho')\rho' d\rho' \right) \end{aligned} \quad (\text{C-4})$$

Using the following properties of Bessel functions,

$$\int_0^{\infty} J_\nu(\alpha\rho')J_\nu(\beta\rho')\rho' d\rho' = \frac{\delta(\alpha-\beta)}{\alpha} \quad (\text{C-5})$$

$$\begin{aligned} \int_0^{\infty} J_{n+1}(\alpha\rho')J_{n-1}(\beta\rho')\rho' d\rho' &= \int_0^{\infty} J_{n+1}(\alpha\rho') \left(-J_{n+1}(\beta\rho') + \frac{2n}{\beta\rho'} J_n(\beta\rho') \right) \rho' d\rho' \\ &= -\frac{\delta(\alpha-\beta)}{\alpha} + \frac{2n}{\beta} \begin{cases} 0 & \alpha < \beta \\ \frac{1}{2\alpha} & \alpha = \beta \\ \frac{1}{\alpha} \left(\frac{\beta}{\alpha}\right)^n & \alpha > \beta \end{cases} \end{aligned} \quad (\text{C-6})$$

the result of integration is

$$\int_0^{\infty} J_n'(\alpha\rho') J_n'(k_0\rho' \sin\theta) \rho' d\rho' = \frac{\delta(\alpha - \beta)}{\alpha} - \frac{n}{2\alpha\beta} \begin{cases} \left(\frac{\alpha}{\beta}\right)^n & \alpha \leq \beta \\ \left(\frac{\beta}{\alpha}\right)^n & \alpha \geq \beta \end{cases} \quad (\text{C-7})$$

Now the integrals in (4-52)-(4-55) can be simplified as integrals of α .

$$\begin{aligned} I_1 &= \frac{\rho_i}{2\beta}(P_1 - P_2) + \frac{n}{2\beta}(P_3 + P_4) \\ I_2 &= \frac{\rho_i}{2\beta}(-P_1 + P_2) - \frac{n}{2\beta}(P_3 + P_4) + \frac{C_2(n, \beta)}{\beta} \\ I_3 &= \frac{n\rho_i}{2\beta}(-P_1 - P_2) - \frac{n^2}{2\beta}(-P_3 + P_4) + \rho_i \frac{C_1(n, \beta)}{\beta} \\ I_4 &= \frac{n\rho_i}{2\beta}(P_1 + P_2) + \frac{n^2}{2\beta}(P_3 - P_4) \end{aligned} \quad (\text{C-8})$$

where:

$$\begin{aligned} P_1 &= \int_0^{\beta} C_1(n, \alpha) \left(\frac{\alpha}{\beta}\right)^n \frac{d\alpha}{\alpha} \\ P_2 &= \int_{\beta}^{\infty} C_1(n, \alpha) \left(\frac{\beta}{\alpha}\right)^n \frac{d\alpha}{\alpha} \\ P_3 &= \int_0^{\beta} C_2(n, \alpha) \left(\frac{\alpha}{\beta}\right)^n \frac{d\alpha}{\alpha} \\ P_4 &= \int_{\beta}^{\infty} C_2(n, \alpha) \left(\frac{\beta}{\alpha}\right)^n \frac{d\alpha}{\alpha} \end{aligned} \quad (\text{C-9})$$

The integrals of α cancel each other, and the result of integration is

$$\begin{aligned} I_1 + I_2 &= \frac{C_2(n, \beta)}{\beta} \\ I_3 + I_4 &= \frac{\rho_i C_1(n, \beta)}{\beta} \end{aligned} \quad (\text{C-10})$$

REFERENCES

- [1] B. Azarbar, "Filtering and Radiation Characteristics of Annular Slot Array Structures," Ph. D. Thesis, Department of Electrical and Computer Engineering, University of Manitoba, October 1978.
- [2] B. Azarbar, and L. Shafai, "Field Solution for Radial Waveguides with Annular Discontinuities," *IEEE Transactions on Microwave Theory and Techniques*, MTT-27, November 1979, pp. 883-890.
- [3] B. Azarbar, and L. Shafai, "Radiation Characteristics of Annular-Slot Arrays Fed by Radial Waveguides," *Canadian Electrical Engineering Journal*, Vol. 5, No. 2, 1980, pp.29-35.
- [4] B. Azarbar, and L. Shafai, "Field Solution of an Annular Slot Array Over a Radial Waveguide Cavity," *Canadian Journal of Physics*, Vol. 61, 1983, pp. 1549-1557.
- [5] H. Levine, and C. H. Papas, "Theory of Circular Diffraction Antenna," *Journal of Applied Physics*, Vol. 22, No. 1, January, 1951, pp. 29-43.
- [6] K. C. Kelly, "Recent Annular Slot Array Experiments," *IRE National Convention*

- Record*, Vol. 5, No. 1, March 1957, pp. 144-151.
- [7] F. J. Goebels, Jr. and, K. C. Kelly, "Arbitrary Polarization from Annular Slot Planar Antennas," *IRE Transactions on Antennas and Propagation*, AP-9, July 1961, pp. 342-349.
- [8] K. C. Kelly, and F. J. Goebels, Jr., "Annular Slot Monopulse Antenna Arrays," *IEEE Transactions on Antennas and Propagation*, AP-12, July 1964, pp. 391-403.
- [9] J. Galejs, and T. W. Thompson, "Admittance of a Cavity-Backed Annular Slot Antenna," *IRE Transactions on Antennas and Propagation*, AP-10, November 1962, pp. 671-678.
- [10] D. C. Chang, "Input Admittance and Complete Near-Field Distribution on an Annular Aperture Antenna Driven by a Coaxial Line," *IEEE Transactions on Antennas and Propagation*, AP-18, September 1970, pp. 610-616.
- [11] C. W. Harrison, Jr., and D. C. Chang, "Theory of the Annular Slot Antenna Based on Duality," *IEEE Transactions on Electromagnetic Compatibility*, EMC-13, February 1971, pp. 8-14.
- [12] D. W. Holst, "Radiation Patterns of Radial Waveguides with TM Mode Excitation," *IEEE Transactions on Antennas and Propagation*, AP-21, March 1973, pp. 238-241.
- [13] E. P. Irzinski, "The Input Impedance of a TEM Excited Annular Slot Antenna," *IEEE Transactions on Antennas and Propagation*, AP-23, November 1975, pp. 829-834.

REFERENCES

- [14] C. M. Butler, and T. L. Keshavamurthy, "Investigation of Radial, Parallel-Plate Waveguide with an Annular Slot," *Radio Science*, Vol. 16, No. 2, March-April 1981, pp. 159-168.
- [15] R. D. Nevels, C. M. Butler, and W. Yablon, "The Annular Slot Antenna in a Lossy Biological Medium," *IEEE Transactions on Microwave Theory and Techniques*, MTT-33, April 1985, pp. 314-319.
- [16] A. Luedtke, and W. F. Bentley, "Directional Annular Slot Antenna," US Patent 4,229,744, October 21, 1980.
- [17] H. Morishita, K. Hirasawa, and K. Fujimoto, "Analysis of a Cavity-Backed Annular Slot Antenna with one Point Shorted," *IEEE Transactions on Antennas and Propagation*, AP-39, October 1991, pp. 1472-1478.
- [18] R. E. Munson, and M. W. Schnetzer, "Annular Slot Antenna," US Patent 4,994,817, February 19, 1991.
- [19] C. Chen, E. McKinzie, and N. G. Alexopoulos, "Stripline-Fed Arbitrary-Shaped Printed-Aperture Antennas," *IEEE Transactions on Antennas and Propagation*, AP-45, July 1997, pp. 1186-1198.
- [20] N. Nikolic, "Empirical Model of the Ring-Slot Antenna Including Ground-Plane Effects," *Journal of Electrical and Engineering, Australia, IE - Aust & The IREE Society*, Vol. 15, No. 1, March 1995, pp. 71-76.
- [21] N. Nikolic, J. S. Kot, and T. S. Bird, "Theoretical and Experimental Study of a Cavity Backed Annular-Slot Antenna," *IEE Proceedings - Microwave, Antennas and Propagation*, Vol. 144, No. 5, October 1997, pp. 337-340.

- [22] J. S. Kot, N. Nikolic, and T. S. Bird, "Integrated-Circuit Antenna for High-Permittivity Substrates," *IEE Proceedings - Microwave, Antennas and Propagation*, Vol. 144, No. 1, February 1997, pp. 47-51.
- [23] N. Nikolic, and J. S. Kot, "Analysis of a Cavity-Backed Coaxial Array of Ring-Slot Antennas," *IEEE Antennas and Propagation Society International Symposium Digests*, 1995, pp. 2078-2081.
- [24] N. Nikolic, and J. S. Kot, "Analysis of Mutual Coupling in a Cavity-Backed Coaxial Array of Annular-Slot Antennas," *IEE Proceedings - Microwave, Antennas and Propagation*, Vol. 145, No. 5, October 1998, pp. 427-429.
- [25] S. Zeilinger, and D. L. Sengupta, "Magnetic Current Distribution and Far-Field Radiation Characteristics of a Dual-Fed Annular Slot," *IEEE Antennas and Propagation Society International Symposium Digests*, 2000, pp. 1624-1627.
- [26] H. Tehrani and K. Chang, "A Multi-Frequency Microstrip-Fed Annular Slot Antenna," *IEEE Antennas and Propagation Society International Symposium Digests*, 1995, pp. 632-635.
- [27] J. E. Jones, "The Influence of Air-Gap Tolerances on the Admittance of a Dielectric-Coated Slot Antenna," *IEEE Transactions on Antennas and Propagation*, AP-17, January 1969, pp. 63-68.
- [28] M. C. Baily, and C. T. Swift, "Input Admittance of a Circular Waveguide Aperture Covered by a Dielectric Slab," *IEEE Transactions on Antennas and Propagation*, AP-16, July 1968, pp. 386-391.
- [29] M. C. Baily, "The Impedance Properties of Dielectric-Covered Narrow Radiating

- Slots in the Broad Face of Rectangular Waveguide," *IEEE Transactions on Antennas and Propagation*, AP-18, September 1970, pp. 596-603.
- [30] R. D. Nevels, and C. M. Butler, "Electromagnetic Diffraction by a Slot in a Ground Screen Covered by a Dielectric Slab," *IEEE Transactions on Antennas and Propagation*, AP-30, March 1982, pp. 390-394.
- [31] C. M. Butler, and R. D. Nevels, "Coupling Through a Slot in a Parallel-Plate Waveguide Covered by a Dielectric Slab," *Archiv fuer Elektronik und Uebertragungstechnik, AEU*, Vol. 42, No. 1, January-February 1988, pp. 42-53.
- [32] C. M. Butler, "General Analysis of a Narrow Slot in a Conducting Screen Between Half-Spaces of Different Electromagnetic Properties," *Radio Science*, Vol. 22, No. 7, December 1987, pp. 1149-1154.
- [33] A.A. Kishk, and L. Shafai, "Gain Enhancement of Antennas over Finite Ground Plane Covered by a Dielectric Sheet," *IEE Proceedings - Microwave, Antennas and Propagation*, Vol. 134, No. 1, February 1987.
- [34] Y. Sugio, T. Makimoto, and T. Tsugawa, "Variational Analysis for Gain Enhancement and Input Characteristics of Dielectric Loaded Antennas," *IEEE Antennas and Propagation Society International Symposium Digests*, 1989, pp. 1364-1367.
- [35] T. Tsugawa, Y. Sugio, and T. Makimoto, "Experimental Study of Gain Enhancement of Dielectric Loaded Antennas with a Ground Plane," *IEEE Antennas and Propagation Society International Symposium Digests*, 1989, pp. 1368-1371.

REFERENCES

- [36] T. Tsugawa, M. Kawahara, Y. Sugio, and Y. Yamada, "Experimental Study of Dielectric Loaded Planar Antenna Fed by Waveguide Network," *IEEE Antennas and Propagation Society International Symposium Digests*, 1994, pp. 480-483.
- [37] Y. Sugio, U. Banyatsupasil, T. Tsugawa, and Y. Yamada, "Triplate-Type Dielectric Loaded Patch Antennas," *IEEE Antennas and Propagation Society International Symposium Digests*, 1994, pp. 484-487.
- [38] C. E. Tong, and R. Blundell, "An Annular Slot Antenna on a Dielectric Half-Space," *IEEE Transactions on Antennas and Propagation*, AP-42, July 1994, pp. 967-974.
- [39] D. I. Kaklamani, C. N. Capsalis, and N. K. Uzungolu, "Radiation from an Annular Slot Antenna Symmetrically Covered by a Dielectric Cylinder of Finite Height," *Journal of Electromagnetic Waves and Applications*, Vol. 8, No 1, 1994, pp. 19-41.
- [40] D. I. Kaklamani, and N. K. Uzungolu, "Analysis of Dielectrically Loaded Radiators Using Entire-Domain Galerkin Technique," *IEEE Antennas and Propagation Magazine*, Vol. 39, No. 5, October 1997, pp. 30-53.
- [41] J. E. Wheeler, and R. D. Nevels, "Reflection and Transmission Properties of Annular Slot Covered by Dielectric Hemisphere," *IEE Proceedings - Microwave, Antennas and Propagation*, Vol. 136, No. 1, February 1989, pp. 59-63.
- [42] F. Colomb, K. Hur, W. Stacey and M Grigas, "Annular Slot Antennas on Extended Hemispherical Dielectric Lens," *IEEE Antennas and Propagation Society International Symposium Digests*, 1996, pp. 2192-2195.
- [43] K. A. Michalski, X. Di, and A. W. Glisson, "Rigorous Analysis of the TM_{0n}

- Modes in a Dielectric Post Resonator with an Annular Slot in Upper Plate," *IEE Proceedings - Microwave, Antennas and Propagation*, Vol. 138, No. 5, October 1991, pp. 429-434.
- [44] K. W. Leung, W. C. Wong, K. M. Luk and E. K. N. Yung, "Annular Slot-Coupled Dielectric Resonator Antenna," *Electronic Letters*, Vol. 34, No. 13, June 1998, pp. 1275-1277.
- [45] M. Ando, K. Sakurai, N. Goto, K. Arimura, and Y. Ito, "A Radial Line Slot Antenna for 12GHz Satellite TV Reception," *IEEE Transactions on Antennas and Propagation*, AP-33, December 1985, pp. 1347-1353.
- [46] H. Sasazawa, Y. Oshima, K. Sakurai, M. Ando, and N. Goto, "Slot Coupling in a Radial Line Slot Antenna for 12GHz Band Satellite TV Reception," *IEEE Transactions on Antennas and Propagation*, AP-36, September 1988, pp. 1221-1225.
- [47] J. Hirokawa, M. Ando and N. Goto, "An Analysis of Slot Radiation on a Parallel Plate Waveguide for a Radial Line Slot Antenna," *IEEE Antennas and Propagation Society International Symposium Digests*, 1989, pp. 1452-1455.
- [48] J. Hirokawa, M. Ando and N. Goto, "Analysis of Slot Coupling in a Radial Line Slot Antenna for DBS Reception," *IEE Proceedings - Microwave, Antennas and Propagation*, Vol. 137, No. 5, October 1990, pp. 249-254.
- [49] M. Ando, M. Takahashi, J. Takada, and N. Goto, "A Slot Design for Uniform Aperture Field Distribution in Single-Layered Radial Line Slot Antennas," *IEEE Antennas and Propagation Society International Symposium Digests*, 1990, pp.

- 930-933.
- [50] M. Takahashi, J. Takada, M. Ando, and N. Goto, "A Slot Design for Uniform Aperture Field Distribution in Single-Layered Radial Line Slot Antennas," *IEEE Transactions on Antennas and Propagation*, AP-39, December 1991, pp. 954-959.
- [51] M. Takahashi, J. Takada, M. Ando, and N. Goto, "Characteristics of Small-Aperture, Single-Layered Radial Line Slot Antennas," *IEE Proceedings - Microwave, Antennas and Propagation*, Vol. 139, No. 1, February 1992, pp. 79-83.
- [52] A. Akiyama, T. Yamamoto, M. Ando, N. Goto, and E. Takeda, "Design of Radial Line Slot Antennas for Millimeter Wave Wireless LAN," *IEEE Antennas and Propagation Society International Symposium Digests*, 1997, pp. 2516-2519.
- [53] M. Ando, T. Numata, J. Takada, and N. Goto, "A Linearly Polarized Radial Line Slot Antenna," *IEEE Transactions on Antennas and Propagation*, AP-36, December 1988, pp. 1675-1680.
- [54] J. Takada, M. Ando, and N. Goto, "A Reflection Cancelling Slot Set in a Linearly Polarized Radial Line Slot Antenna," *IEEE Transactions on Antennas and Propagation*, AP-40, April 1992, pp. 433-438.
- [55] A. Akiyama, T. Yamamoto, M. Ando, and N. Goto, "Numerical Optimisation of Slot Parameters for a Concentric Array Radial Line Slot Antenna," *IEE Proceedings - Microwave, Antennas and Propagation*, Vol. 145, No. 2, April 1998, pp. 141-145.
- [56] P. W. Davis, and M. E. Bialkowski, "Comparing Beam Squinting and Reflection Cancelling Slot Methods for Return Loss Improvement in RLSA Antennas," *IEEE*

- Antennas and Propagation Society International Symposium Digests*, 1997, pp. 1938-1941.
- [57] P. W. Davis, and M. E. Bialkowski, "Experimental Investigation into a Linearly Polarized Radial Slot Antenna for DBS TV in Australia," *IEEE Transactions on Antennas and Propagation*, AP-45, July 1997, pp. 1123-1128.
- [58] P. W. Davis, and M. E. Bialkowski, "Linearly Polarized Radial-Line Slot-Array Antennas with Improved Return-Loss Performance," *IEEE Antennas and Propagation Magazine*, Vol. 41, No. 1, February 1999, pp. 52-61.
- [59] R. F. Harrington, "*Time-Harmonic Electromagnetic Fields*," McGraw-Hill Book Company, 1960, Chapter 5, 7.
- [60] I.N. Sneddon, "*Fourier Transforms*," Mc-Graw Hill Book Company, 1951.
- [61] G. Tyras, "*Radiation and Propagation of Electromagnetic Waves*," Academic Press, 1969.
- [62] A. K. Bhattacharyya, "*Electromagnetic Fields in Multilayered Structures, Theory and Applications*," Artech House, Boston, London, 1993, Chapter 3 and 4.
- [63] I.S. Gradshteyn, and I. N. Ryzhik, "*Table of Integrals, Series and Products*," NewYork Academic Press, 1980.
- [64] C. A. Balanis, "*Antenna Theory, Analysis and Design*," John Willy, Second Edition, 1997, Chapter 3.
- [65] M. Abramowitz, and I. A. Stegun, "*Handbook of Mathematical Functions with Formulas, Graphs and Mathematical Tables*," National Bureau of Standards, Applied Mathematics Series, 1964.

REFERENCES

- [66] L. Shafai, A. A. Kishk and H. Moheb, "Multiple formulation for solution verification in antenna analysis an design problem," *IEEE Antennas & Propag. Magazine*, vol. 33, No. 2, pp. 7-15, 1991.
- [67] IE3D Zeland Corp. Manual, Zeland Software, Inc. - 48890 Milmont Drive - Suite 105D, Fremont, CA 94538, www.zeland.com.
- [68] T Hsieh, and C. S. Lee, "Double-Layer High-Gain Microstrip Array Antenna," *IEEE Transactions on Antennas and Propagation*, AP-48, July 2000, pp. 1033-1035.